PSI-1245

TOXIC SUBSTANCES FROM COAL COMBUSTION -- A COMPREHENSIVE ASSESSMENT

Quarterly Report No. 6

Reporting Start Date: 1 January 1997
Reporting End Date: 31 March 1997

Dr. L.E. Bool III and Dr. C.L. Senior
Physical Sciences Inc.
20 New England Business Center
Andover, MA 01810-1077

Prof. F.Huggins, Prof. G.P. Huffman, Prof. N. Shah
University of Kentucky
Lexington, KY 40506-0059

Prof. J.O.L. Wendt and Mr. W. Seames
University of Arizona
Tucson, AZ 85721

Prof. A.F. Sarofim, Prof. I. Olmez, and Mr. Taofang Zeng
Massachusetts Institute of Technology
Cambridge, MA 02139

Ms. S.Crowley and Dr. R. Finkelman
U.S. Geological Survey
Reston, VA 22092

Prof. Joseph J. Helble
University of Connecticut
Storrs, CT

Prof. M.J. Wornat
Princeton University
Princeton, NJ

DOE Contract No. DE-AC22-95PC95101

U.S. DEPARTMENT OF ENERGY
Pittsburgh Energy Technology Center
P.O. Box 10940
Pittsburgh, PA 15236

IN-HOUSE COVER

April 1997

Report Title Page from Disk

This report was prepared as an account of work sponsored by an agency of the United States Government. Neither the United States Government nor any agency thereof, nor any of their employees, makes any warranty, express or implied, or assumes any legal liability or responsibility for the accuracy, completeness, or usefulness of any information, apparatus, product, or process disclosed, or represents that its use would not infringe on privately owned rights. Reference herein to any specific commercial product, process, or service by trade name, trademark, manufacturer, or otherwise does not necessarily constitute or imply its endorsement, recommendation, or favoring by the United States Government or any agent thereof. The views and opinions of authors expressed herein do not necessarily state or reflect those of the United States Government or any agency thereof.

ABSTRACT

The Clean Air Act Amendments of 1990 identify a number of hazardous air pollutants (HAPs) as candidates for regulation. Should regulations be imposed on HAP emissions from coal-fired power plants, a sound understanding of the fundamental principles controlling the formation and partitioning of toxic species during coal combustion will be needed. With support from the Federal Energy Technology Center (FETC), the Electric Power Research Institute, and VTT (Finland), Physical Sciences Inc. (PSI) has teamed with researchers from USGS, MIT, the University of Arizona (UA), the University of Kentucky (UKy), the University of Connecticut, and Princeton University to develop a broadly applicable emissions model useful to regulators and utility planners. The new Toxics Partitioning Engineering Model (ToPEM) will be applicable to *all* combustion conditions including new fuels and coal blends, low-NO_x combustion systems, and new power generation plants. Development of ToPEM will be based on PSI's existing Engineering Model for Ash Formation (EMAF). During the last quarter coal analysis was completed on the final program coal, from the Wyodak Seam of the Powder River Basin. Combustion testing continued, including data collected on the self-sustained combustor at UA. Data from PSI and MIT were used to identify the governing mechanisms for trace element vaporization from the program coals. Mercury speciation and measurements were continued. Review of the existing trace element and organics emissions literature was completed. And, model development was begun.

TABLE OF CONTENTS

LIST OF GRAPHICAL MATERIALS

LIST OF GRAPHICAL MATERIALS (Continued)

LIST OF TABLES

SECTION 1

EXECUTIVE SUMMARY

1. EXECUTIVE SUMMARY

The technical objectives of this project are:

a) To identify the effect of the mode-of-occurrence of toxic elements in coal on the partitioning of these elements among vapor, submicron fume, and fly ash during the combustion of pulverized coal,

b) To identify the mechanisms governing the post-vaporization interaction of toxic elements and major minerals or unburnt char,

c) To determine the effect of combustion environment (i.e., fuel rich or fuel lean) on the partitioning of trace elements between vapor, submicron fume, and fly ash during the combustion of pulverized coal,

d) To model the partitioning of toxic elements between various chemical species in the vapor phase and between the vapor phase and complex aluminosilicate melts,

e) To develop a frame work for incorporating the results of the program into the Engineering Model for Ash Formation (EMAF).

A description of the work plan for accomplishing these objectives is presented in Section 2.1 of this report.

The work discussed in this report highlights the accomplishments of the sixth quarter of this program. These accomplishments include completion of standard coal analysis on the final Phase I program coal. The selective leaching work, to determine the forms of occurrence of various trace elements, was completed for the three bituminous coals. Data from the combustion zone experiments at PSI and MIT were analyzed to explore the observed differences between the two facilities and to determine the dominant mechanisms for trace element vaporization. The review of the existing trace element and organics emissions data from power plants was completed. Two major combustion experiments were completed on the self-sustained reactor at UA. Finally, work was begun to identify the models, and model parameters, required for ToPEM development, and how these models can be incorporated into the existing Engineering Model for Ash Formation (EMAF)

Specifically, in the last quarter the trace element concentration analysis was completed for the Wyodak coal. This analysis indicated that the concentrations of trace elements in this coal are within the range of the bituminous coals in this program, with the exception of arsenic. The concentration of this element, and that of chromium, is much lower than was found in the other program coals. The CCSEM analysis of this coal are similar to most low-sulfur western subbituminous coals. It is also likely that there is significant organic calcium that is not measured by CCSEM.

Another major activity in the last quarter was analysis of the vaporization data obtained at MIT and PSI to determine the mechanisms governing trace element vaporization in the combustion zone. These data suggested that significant differences in the particle temperature between the two facilities rather than capture of pyrite by silicates during the combustion process, which was hypothesized earlier, caused the differences in trace element vaporization. These data also suggested that for almost all elements, vaporization occurs from included mineral particles. This is especially true for those elements that were found to be associated with the pyrite.

A number of kinetic calculations were performed at MIT to determine the partitioning of chlorine between HCl and Cl_2 at temperatures and cooling rates consistent with the backpass of a utility boiler. These indicate that a much smaller fraction is found in the as Cl_2 than would be predicted from equilibrium.

Trace element and organic species emissions data reported in the EPRI PISCES report and in the scientific literature (period 1995-1996) were examined to identify gaps in our understanding of trace element combustion chemistry. The results suggest that fundamental data on trace element chemistry in combustion systems is needed to extrapolate the emissions findings of the field studies noted above to a broader range of fuels and sources.

Experiments were performed at PSI to explore the effect of cooling rate on mercury speciation. The data from these experiments suggest that the cooling rates typical of the economizer region of a power plant are sufficient to 'freeze' the oxidation of mercury -- leading to a higher fraction of mercury in the elemental form than would be predicted from equilibrium. Additional data are required, however, to further substantiate this hypothesis.

A series of important experiments was completed at the self-sustained combustor at UA. These experiments suggest that there is little change in the fraction of the ash in the submicron sizes between the combustion zone and the convective sections. This is consistent with vaporization of bulk species (silica) that recondense in the combustion zone. Size segregated ash samples have been sent to MIT for analysis and will be presented in later reports.

Finally, the mechanisms obtained from analysis of the PSI and MIT vaporization data were used to determine the submodels required to develop ToPEM. In order to predict trace element partitioning a vaporization model must be coupled with the existing burnout model. Additional models must be developed or modified to described trace element condensation on the existing submicron ash.

SECTION 2

INTRODUCTION AND PROGRAM OVERVIEW

2. INTRODUCTION AND PROGRAM OVERVIEW

Before electric utilities can plan or implement emissions minimization strategies for hazardous pollutants, they must have an accurate and site-specific means of predicting emissions in all effluent streams for the broad range of fuels and operating conditions commonly utilized. Development of a broadly applicable emissions model useful to utility planners first requires a sound understanding of the fundamental principles controlling the formation and partitioning of toxic species during coal combustion (specifically in Phase I, As, Se, Cr, and possibly Hg). Physical Sciences Inc. (PSI) and its team members will achieve this objective through the development of an "Engineering Model" that accurately predicts the formation and partitioning of toxic species as a result of coal combustion. The "Toxics Partitioning Engineering Model" (ToPEM) will be applicable to all conditions including new fuels or blends, low-NO_x combustion systems, and new power systems being advanced by DOE in the Combustion 2000 program.

Based on a goal of developing and delivering this ToPEM model, a 5-year research program was proposed. This program is divided into a 2-year Phase I program and a 3-year Phase II program. The objective of the ongoing Phase I program is to develop an experimental and conceptual framework for the behavior of selected trace elements (arsenic, selenium, chromium, and mercury) in combustion systems. This Phase I objective will be achieved by a team of researchers from MIT, the University of Arizona (UA), the University of Kentucky (UKy), Princeton University, the University of Connecticut, and PSI. Model development and commercialization will be carried out by PSI.

Our general approach to the development of the ToPEM model is to break the process for toxic formation into sub-processes, each of which will be addressed by team members who are experts in the area. Ultimately, this will result in new sub-models which will be added to the existing Engineering Model for Ash Formation (EMAF) to create ToPEM. Figure 2-1 illustrates the relationship between the elements of the Phase I Work Breakdown Structure and the sub-processes. Each of the areas identified in the figure will be addressed in the Phase I program as described below.

Program Overview

Forms of Occurrence of Trace Elements in Coal

One of the most important questions to be answered in the program as a whole is whether the form of a particular element in the coal affects its form of emission at the end of the process. The answer to this question will determine the shape of the sub-models that must be developed in this program. Thus, a detailed understanding of the forms of individual trace elements in coal provides a foundation for much of the rest of the program. Key issues that will be addressed in Phase I are the specific mineral associations of individual elements and the relationship between trace metal form and “standard” analyses.

Because of the importance of elemental form (e.g., sulfate versus silicate mineral) on partitioning, it is critical that coals representing a broad range of elemental forms be examined in

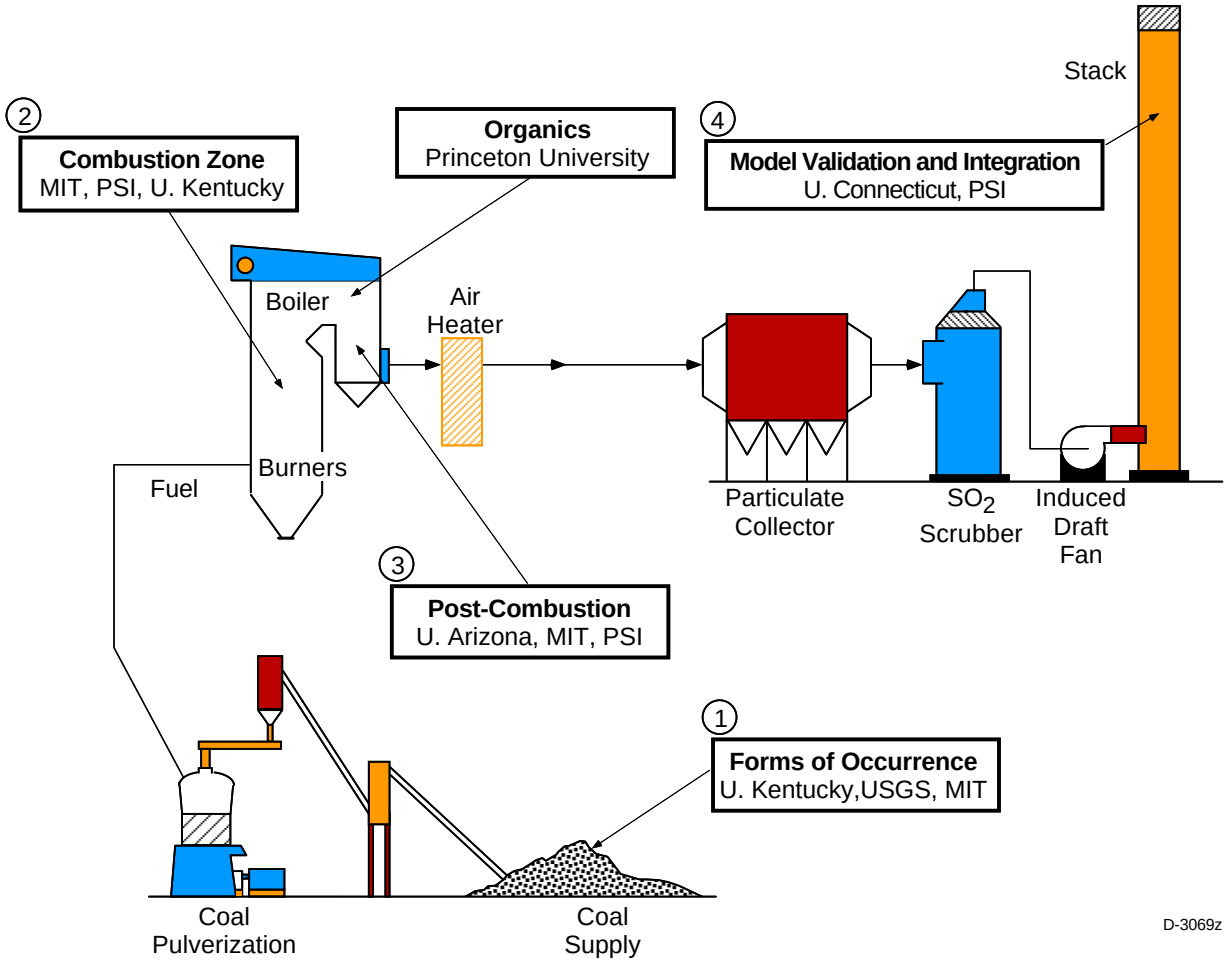

Figure 2-1. Project organization.

this program. In Task 2 we will select and acquire a total of four coals for study in this program. The coals chosen will (1) represent a broad range of elemental forms of occurrence; (2) represent the major coal ranks and commercial coal seams used for pulverized coal (PCS power generation in the US); and (3) include "future fuels" such as blends and beneficiated coals. Once selected fresh coal samples will be acquired and distributed to team members. These samples will be subjected to ultimate, proximate, and ASTM ash analysis. Coal samples will be analyzed for trace element concentrations by INAA at the MIT Nuclear Reactor Laboratory (Task 5).

Advanced analytical techniques such as Mössbauer spectroscopy and CCSEM will be used by UKy (Task 3) to determine the major mineral species present in the program coals and the combustion generated ash. This analysis will provide important insight on the minerals present in the coal, how they interact during the combustion process, and how this interaction may affect the partitioning of toxic elements.

Another important issue is the form-of-occurrence of the trace elements in the coal. In this task the mode of occurrence of As, Cr, and Se will be determined by combining XAFS and the Mössbauer/CCSEM derived data discussed above. Hg will also be evaluated. Other less critical trace elements (Mn, Ni, Zn, Pb, U, etc.) may also be evaluated, especially if their

abundance is unusually high in any of the program coals. In addition, the form-of-occurrence of Cl and S in coals and chars will be investigated.

As a complement to the time-intensive XAFS analysis mentioned above, a unique protocol developed by USGS will be used in Task 4 to analyze selected raw coal, and size and density segregated coal, samples for trace element forms of occurrence. This protocol combines low temperature (< 200°C) ashing, chemical analysis, x-ray diffraction, coal segregation via flotation, ammonium acetate and selected acid leaching, electron microbeam measurements, and low and moderate temperature heating tests to determine the forms of elements in coal. Because of the unique combination of existing testing and analytical facilities available at USGS, the work will be conducted at USGS laboratories. In addition, a relatively new technique, synchrotron radiation x-ray fluorescence microscopy (SRXFM), available at the National Synchrotron Light Source, will be tested for application in this area by UKy (Task 3). This technique uses x-ray fluorescence excited by a focussed synchrotron x-ray beam for imaging and compositional analysis. The x-ray yield obtained from a given element is orders of magnitude greater than that possible in an electron microscope or microprobe; hence, its sensitivity to trace element modes is much better, particularly for modes of occurrence involving highly dispersed elements

Combustion Zone Transformations

The effect of coal type and combustion conditions on the emission of the toxic trace elements will be investigated using the MIT laminar-flow drop tube reactor (Task 5). The fundamental mechanisms of toxic species formation and partitioning will be determined from careful examination of the ash formed under a variety of combustion conditions. Measurements will be made of the partitioning of the trace elements in the four coals as a function of temperature and equivalence ratio. These measurements will provide the baseline data on the fraction vaporized for the different elements to be studied in greater detail in Phase II of the program. Individual size-segregated ash samples (collected with a cascade impactor) will then be analyzed by INAA for total composition, Auger and STEM for surface composition, TEM and SEM for particle morphology, and possibly water washing and/or chemical leaching to determine the solubility of selected trace elements in the ash samples. Samples will also be submitted to UKy for chemical species analysis by XAFS and other techniques.

PSI will perform a detailed experimental study to determine the fundamental behavior of toxic species during combustion, including low NO_x conditions (Task 8). The work will use the PSI Entrained Flow Reactor (EFR) that has been used in many previous combustion studies on mineral matter transformations during pc combustion. This reactor is on a scale intermediate between the bench top apparatus to be used by other team members (UA, MIT) and the UA laboratory-scale combustor. Therefore the combustor will yield a better understanding of the overall behavior of toxic species while avoiding some of the confounding influences related to self-sustained combustion in the larger furnace. Utility-grind samples of the program coals will be burned under three different stoichiometric ratios, and two temperatures. Size segregated ash samples, and carbon filter samples will be collected. Ash samples collected during the combustion experiments will be analyzed by INAA and other techniques at MIT. By performing an elemental analysis on the size classified ash samples, we will identify the major mechanisms (e.g.,

vaporization and condensation) that govern the behavior of specific toxic species during the combustion process -- especially under reducing conditions.

Post-Combustion Transformations

The goal of this task is an increased understanding of the transformations of selected metals as the flue gases cool following the high temperature combustion zone. Experiments will be performed on two very different scales at UA. In addition, PSI will perform thermodynamic equilibrium calculations and make measurements of submicron aerosol size and composition from the large self-sustained combustor (Task 8 and 9).

At the small scale, UA will conduct experiments to explore the fundamental kinetics and mechanisms for metal vaporization and metal vapor-mineral interactions. Metal vapor-mineral interactions will be studied in this task using thermogravimetric analysis (TGA). The primary experimental parameters to be studied are temperature, gas composition (particularly the concentration of the metal species in the gas phase), the composition of the sorbent (char, silica, alumino-silicate, etc.), sorbent particle size and porosity, and exposure time (residence time). The primary properties that will be analyzed are the concentration of toxic trace metals in the particles as functions of time, the final chemical form of the trace metal, the leachability of the trace metal in the final particles, and if possible, the distribution of metal in the particles.

On a larger scale, UA will determine how both coal composition, detailed mineralogy and combustion conditions (including low NO_x conditions) govern the fate of toxic metals under practical time/temperature, self sustained, yet still aerodynamically well defined, pulverized coal combustion conditions. Other tasks focus, one at a time, on individual aspects of toxic metal partitioning. In this task, experiments are performed with time-temperature profiles similar to those in pc combustors. Therefore, the hypothesis derived from the smaller scale facilities can be tested under 'real world' conditions to determine the dominant mechanisms for trace element partitioning. Results from this portion of the project, together with the other portions, will lead to a quantitative model that will predict the fate of all toxic species as functions of coal quality and combustion configurations.

Select coals will be burned in the UA self-sustained combustor under premixed conditions where all the coal is mixed with all the air prior to combustion. The baseline tests will employ the naturally occurring temperature profile for each coal at a stoichiometric ratio of 1.2. Samples will be withdrawn at the exhaust port. Complete impactor samples will be collected and analyzed for each toxic metal (11 as listed in the CAAA plus U and Th) plus major elements. This will yield the particle size segregated toxic metal composition, which can be compared to data obtained form other tasks of this program. This data will then be examined to determine particle size dependence in order to infer possible mechanisms governing the fate of each metal.

Organic Emissions

Some organic emissions associated with coal combustors can have deleterious effects on the environment and/or human health. It is therefore very important (1) to know the identities, quantities, and toxicities of the organic species released from coal combustion systems and (2) to understand the chemical and physical processes that govern these species' formation, destruction, and release. Organic emissions data from the DOE Air Toxics and EPRI PISCES programs have the potential of benefitting the evaluation of the problem of organic emissions from coal combustion. In Task 7, Princeton University will conduct a critical review of the available field data, focusing on (1) the appropriateness, thoroughness, and reliability of the experimental techniques employed; (2) comparison with previously published emissions data; (3) the implications of the results; (4) similarly evaluating comparable data available from other countries, particularly Europe and Australia; review emerging technical literature on coal pyrolysis and combustion processes that affect organic emissions; (5) staying abreast of new results in the toxicity literature, relating to organic emissions from coal; and (6) communicating regularly with the other principal investigators of the air toxics team so that all will be cognizant of the ties between the organic and inorganic air toxics issues.

It is expected that the above efforts of analysis and literature review will lead to (1) comprehensive understanding of what is currently known about organic emissions from coal and (2) identification of the important questions that may still need to be addressed in future research.

Model Validation

Also under Task 7, the University of Connecticut will conduct a preliminary review of the relevant field data on inorganic emissions. In Phase I we will use the field data to focus the experimental program and to validate the models we will develop in Phase II. The Phase I effort focuses on data from the following sources:

- EPRI PISCES
- DOE Program
- VTT (Finland)
- KEMA (Netherlands).

Important issues to be addressed when reviewing these data include mass balance closure, methods of analysis and sample collection, effect of APCD, effect of bulk coal ash chemistry, particle size distribution, and speciation of Hg.

Model Development

PSI will use its silicate equilibrium model accounts for the *non-ideal* behavior of multi component silicate solutions in combination with its trace element database to calculate Cr and As partitioning. These results will be compared with laboratory data generated under Tasks 5.1, 6.1, 6.2, and 8, and inorganic species field data reviewed as part of Task 7. These calculations

may be repeated for Se and/or other elements if experimental data warrant interpretation of vaporization under conditions where silicate chemistry is dominant.

SECTION 3

RESULTS AND DISCUSSION

3. RESULTS AND DISCUSSION

3.1 Program Management (PSI)

During the last quarter PSI and ABB personnel met to discuss the data collected by ABB during their ESP testing experiments performed as part of another DoE-funded program. ABB burned the Wyodak coal, the same sample as used in this program, in their pilot scale combustor under a wide range of firing conditions. A series of size-segregated ash samples were collected with a Berner Low Pressure Impactor at the inlet and outlet of the pilot scale ESP. A number of these ash samples were selected for trace element analysis (NAA) to provide additional data on trace element partitioning during the combustion process. Analysis of these samples was begun in the last quarter and will be discussed in more detail in the next report.

3.2 Coal Characterization (UKy, USGS, PSI)

3.2.1 *Coal Mineralogy - Wyodak Coal*

The discrete mineralogy of the Wyodak coal has been determined using computer-controlled scanning electron microscopy (CCSEM). The data are summarized in Table 3-1. These data are not unlike data we have determined previously[3] for other low-sulfur western subbituminous coals. The mineral matter is richer in kaolinite than illite, has a low content of basic minerals (calcite, pyrite, siderite), and contains minor amounts of a Ca-Al phosphate mineral, which is most probably crandallite. This coal appears a little unusual in that the quartz content is quite high and is somewhat coarser in particle size than the other minerals. The illite content is also quite significant.

From both the CCSEM data as well as the Mössbauer data discussed below, it is clear that the iron-bearing minerals are relatively insignificant in this coal. The principal basic element in the coal is likely to be carboxyl-bound calcium, which is not detected in the Coal Minerals Analysis method.

Iron in the Wyodak coal has been investigated using both Mössbauer and XAFS spectroscopy. In comparison to the other three coals, the Mössbauer spectrum (Figure 3-1) of the Wyodak coal is comparable in intensity to that of the Elkhorn/Hazard coal, but significantly weaker than those of the Pittsburgh #8 and Illinois #6 coals. The Mössbauer spectrum of the Wyodak coal is complex; at least four different iron-bearing species appear to be present. Furthermore, the Mössbauer absorptions for jarosite and Fe^{2+}/clay are very broad, indicating additional complexity, such as the likely presence of further undefined contributions, such as the presence of FeOOH, or other sulfates or clay types. In view of such complexities, no attempt was made to analyze the Fe XAFS spectrum.

3.2.2 *Trace Element Concentrations*

The trace element analysis, by NAA, was completed for the Wyodak coal during the last quarter. These results, and the results from the other program coals, are shown in Table 3-2.

Table 3-1. CCSEM Analysis of Discrete Inorganic Minerals in Wyodak Coal

		AVERAGE SPECIES COMPOSITION											
#	MINERAL SPECIES	Na	Mg	Al	Si	P	S	Cl	K	Ca	Ti	Fe	Weight %
300	Quartz	0.	0.	0.	99.	0.	0.	0.	0.	0.	0.	0.	26.7
192	Kaolinite	0.	0.	47.	51.	0.	0.	0.	0.	1.	0.	0.	19.1
110	Illite	0.	0.	30.	54.	0.	0.	0.	10.	2.	1.	1.	8.0
3	K-Feldspar	0.	0.	15.	62.	0.	0.	0.	18.	2.	0.	2.	1.5
27	Montmorillonite	0.	0.	26.	62.	0.	2.	0.	0.	6.	2.	0.	2.2
301	Misc. Silicates	0.	0.	27.	61.	0.	2.	0.	3.	3.	1.	1.	29.0
4	Pyrite	0.	0.	0.	0.	0.	63.	0.	0.	0.	0.	35.	0.9
3	Ferrous Sulfate	0.	0.	0.	1.	0.	52.	0.	0.	2.	1.	43.	0.1
1	Chalcopyrite	0.	0.	0.	0.	0.	55.	0.	0.	0.	0.	22.	0.2
7	Misc. sulf.	0.	0.	0.	3.	0.	49.	0.	1.	6.	8.	31.	0.7
23	Misc. Phosphate	0.	0.	33.	2.	28.	0.	0.	0.	34.	1.	1.	2.5
5	Fe-rich	0.	0.	0.	0.	0.	1.	0.	0.	1.	0.	98.	0.4
1	Calcite	0.	0.	0.	0.	0.	0.	0.	0.	100.	0.	0.	0.1
5	Mixed Carbonate	0.	0.	2.	3.	6.	1.	1.	0.	32.	2.	53.	0.3
4	Ti oxide	0.	0.	0.	0.	0.	0.	0.	0.	6.	93.	0.	0.4
4	Ti-rich	0.	0.	4.	17.	0.	5.	0.	0.	13.	60.	0.	0.3
1	Sil-sulf	0.	0.	18.	44.	0.	20.	0.	0.	17.	0.	0.	0.1
1	Silicate-Pyrite	0.	0.	28.	28.	0.	23.	0.	0.	11.	0.	10.	0.1
1	Alumina-rich	0.	0.	100.	0.	0.	0.	0.	0.	0.	0.	0.	0.1
129	Misc. Mixed	0.	0.	29.	28.	7.	7.	1.	1.	23.	2.	0.	7.4
1122	GRAND TOTALS	0.	0.	23.	63.	1.	2.	0.	2.	4.	1.	2.	100.0

WEIGHT DISTRIBUTION

Size Ranges (Microns)

MINERAL SPECIES	WT. %	0.1	2.5	5.0	10.	20.	40.	80.
		2.5	5.0	10.0	20.	40.	80.	500.
Quartz	26.7	8.	21.	16.	23.	12.	10.	10.
Kaolinite	19.1	24.	33.	16.	21.	4.	1.	0.
Illite	8.0	11.	17.	23.	36.	8.	5.	0.
Misc. Silicates	29.0	38.	35.	12.	9.	5.	2.	0.
Misc. Mixed	7.4	56.	27.	12.	5.	0.	0.	0.
MINOR MINERALS	9.9	42.	29.	14.	9.	5.	1.	0.
GRAND TOTALS	100.0	27.	28.	15.	17.	7.	4.	3.

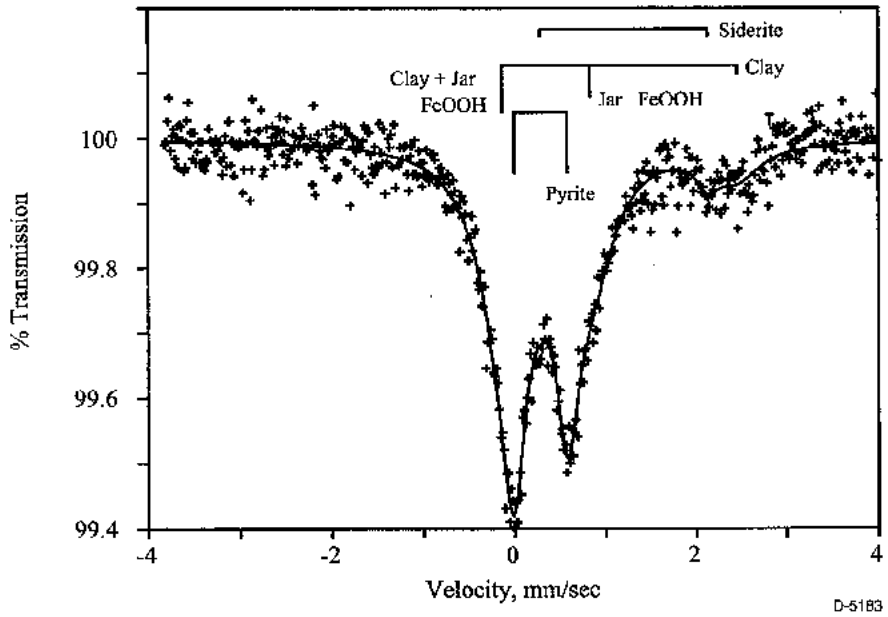

Figure 3-1. Mössbauer spectrum of the Wyodak coal.

As can be seen from this table, most of the trace element concentrations in the Wyodak coal are within the range shown by the bituminous coals. One important exception to this trend is the arsenic. The concentration of this element in the Wyodak is much lower than in the other program coals. The chromium content is also much lower.

3.2.3 *Trace Element Forms of Occurrence in the Wyodak Coal*

During the last quarter, new XANES data were obtained at both the Stanford Synchrotron Radiation Laboratory (SSRL), Palo Alto, CA, and the National Synchrotron Light Source (NSLS), Brookhaven National Laboratory, NY, on S, Cl, Cr, Fe, As, and Se in the Wyodak program coal. Attempts to prepare a density 2.88 sink fraction from this coal by flotation in bromoform were not successful as no appreciable amount of material settled to the bottom in bromoform. However, a float and tailings fraction were prepared from this coal using liquid of specific gravity 1.5. In this report, we have concentrated on data pertaining to elemental modes of occurrence in the raw coal.

(1) Sulfur:

Sulfur K-edge XANES data for the Wyodak coal were collected at NSLS over the energy range from 100 eV below the S K-edge at 2,472 eV to about 300 eV above the edge. In comparison to the other three program coals, the sulfur K-edge spectrum was rather weak, which reflects the low sulfur content (0.22 wt% as received) for this coal. However, the data were amenable to a least-squares fitting analysis (Figure 3-2), which showed that most (> 90%) of the sulfur was present in unoxidized forms (thiophene and thioether forms), except for a minor amount of organic sulfur as sulfone and inorganic sulfur as sulfate. Pyritic sulfur was not detected by this method.

Table 3-2. Trace Element Concentrations in Program Coals

Element	Pittsburgh Concentration (ppm)	Elkhorn/Hazard Concentration (ppm)	Illinois No. 6 Concentration (ppm)	Wyodak Concentration (ppm)
Na	600	340	400	710
Sc	1.8	3.9	2.2	1.8
Cr	13	20	14	7
Fe	8220	2970	13700	2700
Co	2.5	6.2	.6	1.7
Zn	17	18	70	33
As	4.1	4	2.7	1.3
Se	0.62	3.1	2.2	1.6
Br	17	25	3.7	2.4
Rb	8	5.1	13	3.6
Sr	160	120	ND	ND
Mo	0.85	4	4.9	1.7
Cd	0.06	0.31	0.15	0.30
Sb	0.26	1	0.38	0.23
Cs	0.55	0.45	0.99	0.26
Ba	110	130	52	370
La	4.5	14	4.7	4.9
Ce	8.8	27	9.3	8.7
Sm	0.78	2.5	0.9	0.71
Eu	0.2	0.37	0.19	0.18
Yb	0.38	1.4	0.032	0.35
Lu	0.063	0.24	0.0054	0.057
Hf	0.44	1.1	0.056	ND
Au (in ppb)	0.95	0.98	0.51	1.1
Hg	0.11	0.13	0.22	0.19
Th	1.2	4.3	0.095	1.7
U	0.31	1.9	ND	ND

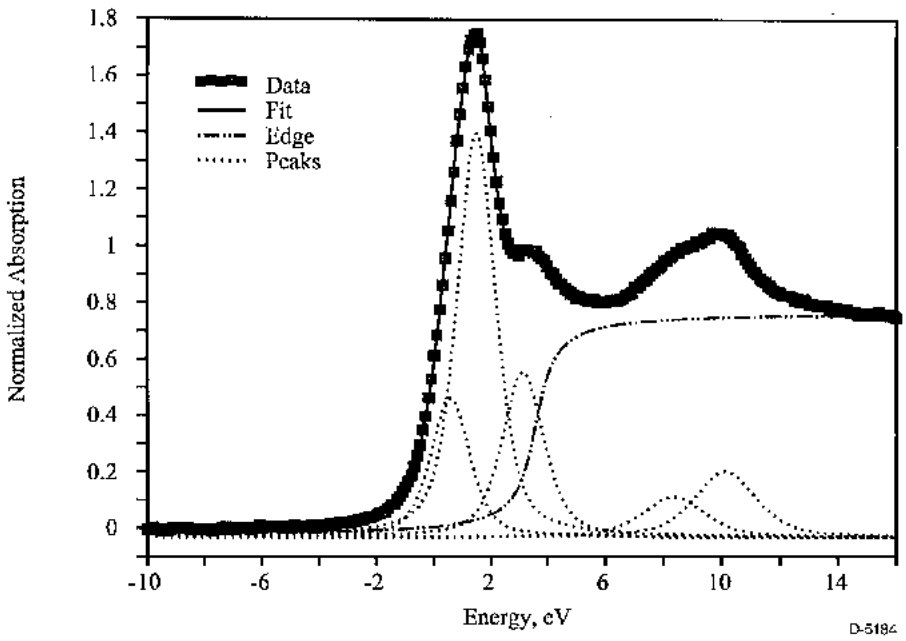

Figure 3-2. Least-squares fitted sulfur XANES spectrum of Raw Wyodak coal.

(2) Chlorine:

Chlorine K-edge XANES data for the Wyodak coal were collected at NSLS over the energy range from 100 eV below the Cl K-edge at 2,825 eV to about 300 eV above the edge. In comparison to the other three program coals, the chlorine XANES spectrum (not shown) was extremely weak, which indicates an extremely low chlorine content (estimated to be < 0.01 wt%) for this coal, and no useful fine structure could be discerned from the spectrum to assess the form of occurrence.

(3) Chromium:

The best chromium K-edge XANES data for the Wyodak coal were obtained at beam-line IV-3 at SSRL, but the data were of poor statistical quality in comparison to data obtained for chromium in the other program coals. We also attempted to get data at X-19A at NSLS, but the quality of the data were of even poorer quality. Hence, these data suggest that the chromium content of the Wyodak coal is quite low (estimated to be < 10 ppm). This is consistent with the 7 ppm concentration of chromium noted in Table 3-2. The Cr XANES spectrum (Figure 3-3) is also relatively broad and featureless, with just the hint of a small peak at the maximum. The spectrum suggests that at least one major form of occurrence of chromium in the Wyodak coal is not the same as those (principally CrOOH and Cr/illite) reported for the other three program coals. The features of the spectrum are more like those for a totally hydrated Cr^{3+} ion. The spectra of the Wyodak coal tailings and float fractions, measured at NSLS, showed little variation from that of the raw coal in either step-height or appearance. Our best interpretation of these data suggest that Cr is probably in solution as Cr^{3+} with only a weak connection to the coal matrix. Such an interpretation is compatible with isolated Cr^{3+} ions held at carboxyl sites on the coal matrix.

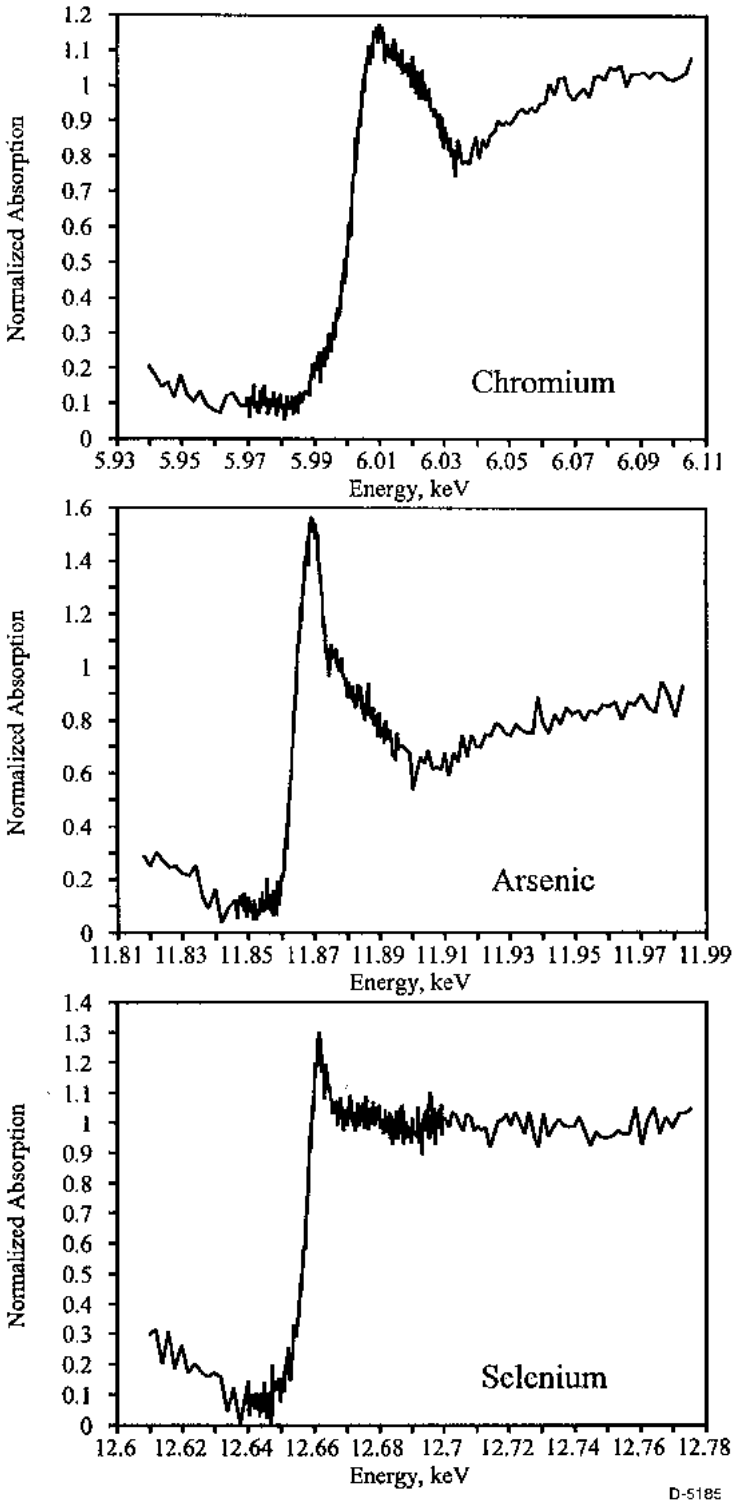

Figure 3-3. XANES spectra for chromium, arsenic, and selenium in Wyodak coal.

(4) Arsenic:

Arsenic data were obtained at both synchrotrons at beam-line X-18B at NSLS and at beam-line IV-3 at SSRL. The quality of the data were poor from both synchrotrons and hence indicate a low (< 3 ppm) concentration of arsenic in the Wyodak coal (again this is consistent with the concentration in Table 3-2). The spectra (Figure 3-3) resembled those of other low-arsenic subbituminous coals we have examined in the past,[3] and are compatible with the presence of significant As^{3+} in oxygen coordination (most probably, organically bound via carboxyl groups) and some As^{5+}, also in oxygen coordination as arsenate, formed by oxidation.

(5) Selenium:

The selenium XAFS data (Figure 3-3) for the Wyodak coal are of poorer quality (in part due to the fact that a less than desired number of scans were run) than that found for the relatively high selenium coals, Illinois #6 and Elkhorn/Hazard, examined previously. However, the data do indicate a content of Se that is comparable to the arsenic content in the coal and we estimate that there is perhaps as much as 2 ppm Se in this coal. Again, this estimate is consistent with the concentration shown in Table 3-2. The peak position is positive by about 1 eV with respect to an elemental Se standard. Owing to the poor quality of the spectrum, plus the fact that the spectra of the fractions have not been obtained, it is premature to make any conclusions at this time.

In summary, the XAFS data for the Wyodak coal indicate that the trace element concentrations are lower than those found for the other three coals. This observation, coupled with the fact that our XAFS database for low-rank coals is relatively meager, means that our conclusions on elemental modes of occurrence for the Wyodak coal are not nearly as firm as for the other three coals.

3.2.4 *Trace Element Forms of Occurrence in Coal - Summary of Data for Program Coals*

The forms of occurrence results for three trace elements are summarized below in Table 3-3. In almost all cases the results derived from XAFS (Kentucky) analysis are comparable to those from the leaching analysis (USGS). USGS data are not yet available for the Wyodak coal. Arsenic in the bituminous coals is primarily associated with the pyrite. The Elkhorn/Hazard coal contains an appreciable amount of oxidized arsenic. Preliminary XAFS results suggest that arsenic in the Wyodak coal is primarily organically associated. Selenium in all the bituminous coals is found in both the pyrite and organically associated forms. Chromium is found primarily as the hydrated form and in silicates for all coals.

3.3 Combustion Zone Transformations (PSI, MIT, UKy)

Work on the transformations of trace elements in the combustion zone is proceeding along two major fronts. In the first area investigators at PSI and UKy are working to determine how the oxidation state of pyrite and arsenic influence trace element vaporization in the combustion zone. As part of this area PSI is also addressing vaporization of trace elements under a wide

Table 3-3. Preliminary Forms of Occurrence for Program Coals

Coal	As	Se	Cr
Pittsburgh	**USGS: predominantly pyrite** **Kentucky: predominantly pyrite**	**USGS: pyrite or organics**	**USGS: silicates, carbonates or sulfides** **Kentucky: predominantly CrOOH, minor amount in illite**
Illinois 6	**USGS: predominantly pyrite** **Kentucky: predominantly pyrite**	**USGS: pyrite or organics** **Kentucky: pyrite and organics**	**USGS: silicates and possibly organic** **Kentucky: predominantly CrOOH, minor amount in illite**
Elkhorn/Hazard	**USGS: fine pyrites** **Kentucky: 60% pyrite; 40% arsenate**	**USGS: predominantly organic** **Kentucky: predominantly organic? not associated with pyrite, except "Heavy" fraction**	**USGS: silicates and possibly organic** **Kentucky: CrOOH, illite, minor amount chromite**
Wyodak	**Kentucky: organic, ions in carboxyl groups**		**Kentucky: CrOOH, ions in carboxyl sites**

range of combustion conditions. In the second area investigators at MIT are working with the size and density segregated coals and a droptube reactor to evaluate vaporization behavior of trace elements. This work is expanded upon at PSI where investigators are using the utility grind coal and the PSI entrained flow reactor (EFR) to determine the net vaporization of trace elements in the combustion zone.

3.3.1 *The Effect of Coal Oxidation on Trace Element Vaporization in the Combustion Zone*

One question to be addressed in this program is the effect of the form of occurrence of a given element on its partitioning between the vapor and condensed phases in the combustion zone. For example, arsenic has been reported to be quite variable in how it partitions between these phases during the combustion process. It has been proposed that the mode of occurrence of the arsenic in the coal causes the variability. To address this issue team members from PSI and UKy are evaluating the difference in the measured arsenic vaporization between a 'raw' coal and a weathered sample of that coal. Specifically, combustion tests were done with the PSI entrained flow reactor (EFR) to measure the vaporization of trace elements from the Illinois No. 6. As discussed in Table 3-3, arsenic in this coal is primarily substituted into the pyrite matrix. A sample of this coal was subsequently subjected to accelerated weathering as discussed in the last

Quarterly Report.[4] XAFS of the weathered sample indicated that the primary form of arsenic was as the oxide (arsenate).

To determine the degree of oxidation of both the pyrite and the arsenic, the weathered coal sample was analyzed by Mössbauer and XAFS. The Mössbauer data are summarized in Figure 3-4. The data show that about 45% of the pyritic iron has been oxidized to a mixture of iron sulfates (principally szomolnokite $FeSO_4.H_2O$, jarosite, and a minor amount of ferric sulfate). Further, there has been relatively little change in the iron forms of occurrence between the sample taken at the end of 60 days' oxidation and that taken after 90 days. This observation may indicate that a portion of the pyrite is relatively easily oxidized, whereas the remainder is much more resistant to oxidation.

The arsenic XAFS spectrum for the sample oxidized at 50°C for 90 days is shown in Figure 3-5. By means of a least-squares fitting routine, the amount of As in different forms can be determined with an experimental error of less than ±5%. For the spectral data shown in Figure 3-5, the least-squares fitting procedure indicated that about 57% of the arsenic was oxidized to arsenate, with the remaining 43% as unoxidized arsenical pyrite. This percentage of oxidized arsenic is greater than the percentage of oxidized iron (approximately 45%), estimated from the Mössbauer ratio of pyritic sulfur contents determined on unoxidized and 90 days' oxidized aliquots of the Illinois #6 coal. This observation would appear to support the hypothesis that the arsenic is largely associated with a fraction of the pyrite that is more susceptible to oxidation.

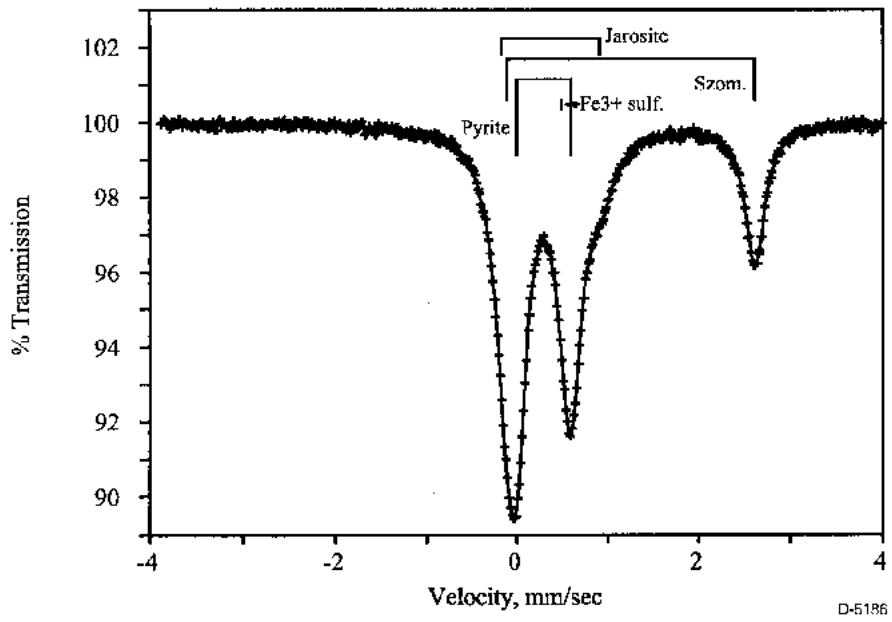

Figure 3-4. Mössbauer spectrum of Illinois #6 coal oxidized for 90 days.

Combustion tests with this coal were completed in the last quarter. The weathered coal was combusted in the PSI EFR at a stoichiometric ratio of 1.2, and a furnace setpoint of 1500 °C - identical to the baseline combustion tests performed with the unweathered coal.

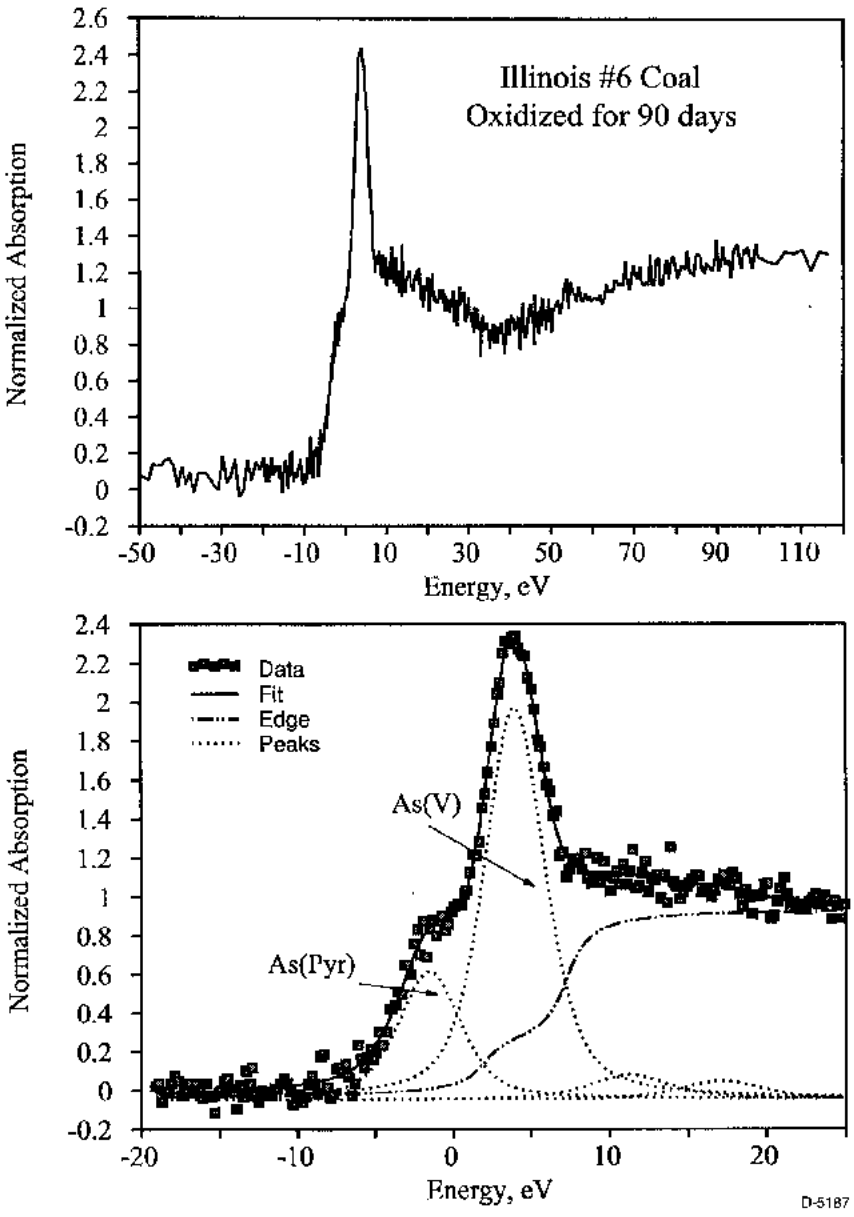

Figure 3-5. Arsenic XANES spectrum of Illinois #6 coal oxidized for 90 days (top). Least-squares fitted spectrum showing contributions due to As(V) and As(pyr) (bottom).

Ash samples were withdrawn from the furnace exit with the nitrogen quench probe and passed through the Mark III cascade impactor for size segregation and collection. These ash samples were sent to MIT for NAA, and will be discussed in more detail in the next quarterly report.

3.3.2 *XAFS Analysis of Char and Ash Samples*

During the last quarter, almost 4 weeks of synchrotron beam-time were made available to UKy personnel. As a result many new data have been obtained on the various samples generated

in the project. A listing of the new data obtained over during the quarter is shown in Table 3-4. Since much of this experimental time came towards the end of the quarter, there has not been sufficient time to analyze the data completely. However, most of the data have been at least cursorily examined and some of the conclusions pertaining to Hg in activated carbons are presented later in this report. Some additional findings on selected ash samples are also presented below.

Table 3-4. Sample Analyses Yet to be Completed at Kentucky

		XAFS DATA Obtained									
		Zn	As	Cr	Hg	Se	S	Cl	I	Ca	Mössbauer
(a) Samples from T. Zeng, MIT											
KYH4563	Stage 1	✓	✓	✓							
	Stage 2	✓	✓	✓							
	Presep.	✓	✓	✓	✓						
KYH90106	Stage 1	✓	✓	✓							
	Stage 5	✓	✓	✓							
	Presep.	✓	✓	✓							
KYL4563	Stage 1	✓	✓	✓							
	Stage 5	✓	✓	✓							
	Presep.	✓	✓	✓							
KYL90106	Stage 1	✓	✓	✓	✓						
	Stage 5	✓	✓	✓							
	Presep.	✓	✓	✓							
PTH90106	Stage 1	✓	✓								
	Stage 5	✓	✓								
	Presep.	✓	✓								
PTL90106	Stage 1	✓	✓								
	Stage 5	✓	✓								
	Presep.	✓	✓								
ILH90106	Stage 1	✓	✓								
	Stage 5	✓	✓								
	Presep.	✓	✓								
ILL90106	Stage 1	✓	✓								
	Stage 5	✓	✓								
	Presep.	✓	✓								

Table 3-4. (Continued) Sample Analyses Yet to be Completed

	XAFS DATA Obtained									
	Zn	As	Cr	Hg	Se	S	Cl	I	Ca	Mössbauer
In addition, the major minerals in six related samples are also being determined by the CCSEM method.										
(b) Ash samples from L. Bool, PSI										
EH-13	✓	✓	✓		✓					✓
I6-9	✓	✓	✓		✓					✓
P8-23	✓	✓	✓							✓
P8-44	✓	✓	✓							✓
(c) Char samples from L. Bool, PSI										
Pittsburgh #8		✓	✓							
Illinois #6		✓	✓							
Elkhorn/Hazard		✓	✓							
Sulfur XANES data reported for these samples in previous reports.[2]										
(d) Char samples from B. Wu, UA										
Pittsburgh #8				✓						
Illinois #6				✓						
Char samples from PSI that were treated in Hg-containing flue gas (see also narrative)										
(e) Char samples from G. Dunham, UNDEERC										
Char, LAC-1				✓		✓	✓	✓	✓	
Char, LAC-2				✓		✓	✓	✓	✓	
Char, LAC-3				✓		✓	✓	✓		
Char, LAC (-400)				✓						
Char, SAC-1				✓		✓		✓	✓	
Char, SAC-2				✓		✓		✓	✓	
Char, SAC (-400)				✓						

Table 3-4. (Continued) Sample Analyses Yet to be Completed

	XAFS DATA Obtained									
	Zn	As	Cr	Hg	Se	S	Cl	I	Ca	Mössbauer
Char, IAC-1				✓		✓		✓		
Char, IAC-2				✓		✓		✓		
Char, IAC (-400)				✓						
Char, LAC-5				✓						
Char, LAC-6				✓						
Char, LAC-7				✓						
Char, LAC-8				✓						
Fly-Ash-1				✓						
Fly-Ash-4				✓						
Fly-Ash-5				✓						
See also narrative.										

(f) Samples from Radian Corporation

In addition, the following ash and char sorbent samples from Radian Corporation were also examined at the Hg edge and/or at the S, As, or Ca edges. All of these samples showed either no evidence for the presence of mercury (estimated Hg content: < 2 ppm) or showed a very weak Hg edge that exhibited no discernable fine structure (estimated Hg content: 2 < 5 ppm) relative to the signal/noise ratio.

	Hg Response	Other Elements
PCARB-1	No signal	S, Ca, As (strong)
COMP-1A	No signal	S (weak), Ca
COMP-2A	Very weak signal	S (weak), Ca
PASH-1	No signal	S, Ca
PASH-2	---	S, Ca, As (strong)
PFLY-1	---	S, Ca, As
REAG-1A	---	S, Ca
REAG-2A	---	S, Ca
REAG-3A	---	S, Ca
U-I-A	No signal	
U-I-B	Weak signal	
U-I-C	Weak signal	

Table 3-4. (Continued) Sample Analyses Yet to be Completed

	XAFS DATA Obtained									
	Zn	As	Cr	Hg	Se	S	Cl	I	Ca	Mössbauer
U-II-A	Very weak signal									
U-II-B	Weak signal									
U-II-C	Weak signal									
U-II-D	Weak signal									

The Zn XAFS spectra (Figures 3-6 and 3-7) of ash from the Elkhorn/Hazard coal over the complete suite of size/density segregated samples from MIT have been examined and were found to show significant variation among the different types of samples, which no doubt reflects a wide variation in the zinc speciation in these ash samples. The ash samples were obtained using a cyclone preseparator followed by a cascade impactor at the outlet of MIT's drop tube furnace (DTF). The preseparator sample, therefore, contains the largest ash particles (approximately greater than 10 µm). Some of the spectra, such as that from the ash captured in the impactor preseparator when the high density, 90 to 106 µm, coal was burned (KYH90106 Presep), appear to arise from zinc sulfide. Other spectra, such as those from ash from the low density fractions of this coal (KYL4563 presep., KYL90106 presep.), appear to arise from zinc oxide. Spectra of samples from Stages 1 and 5 do not generally show these specific phases and further work is needed to explain the basis of their profiles. The Cr and As data do not appear to show such obvious changes.

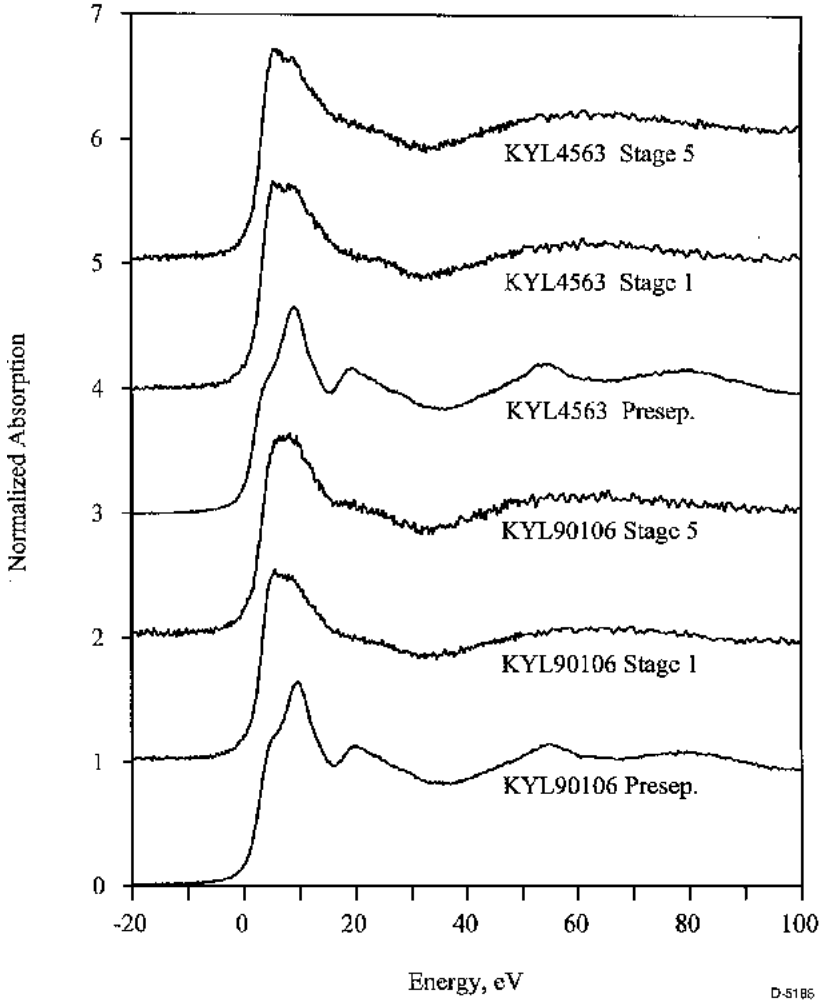

Figure 3-6. Zinc XANES spectra for low density Elkhorn/Hazard ash samples generated by MIT.

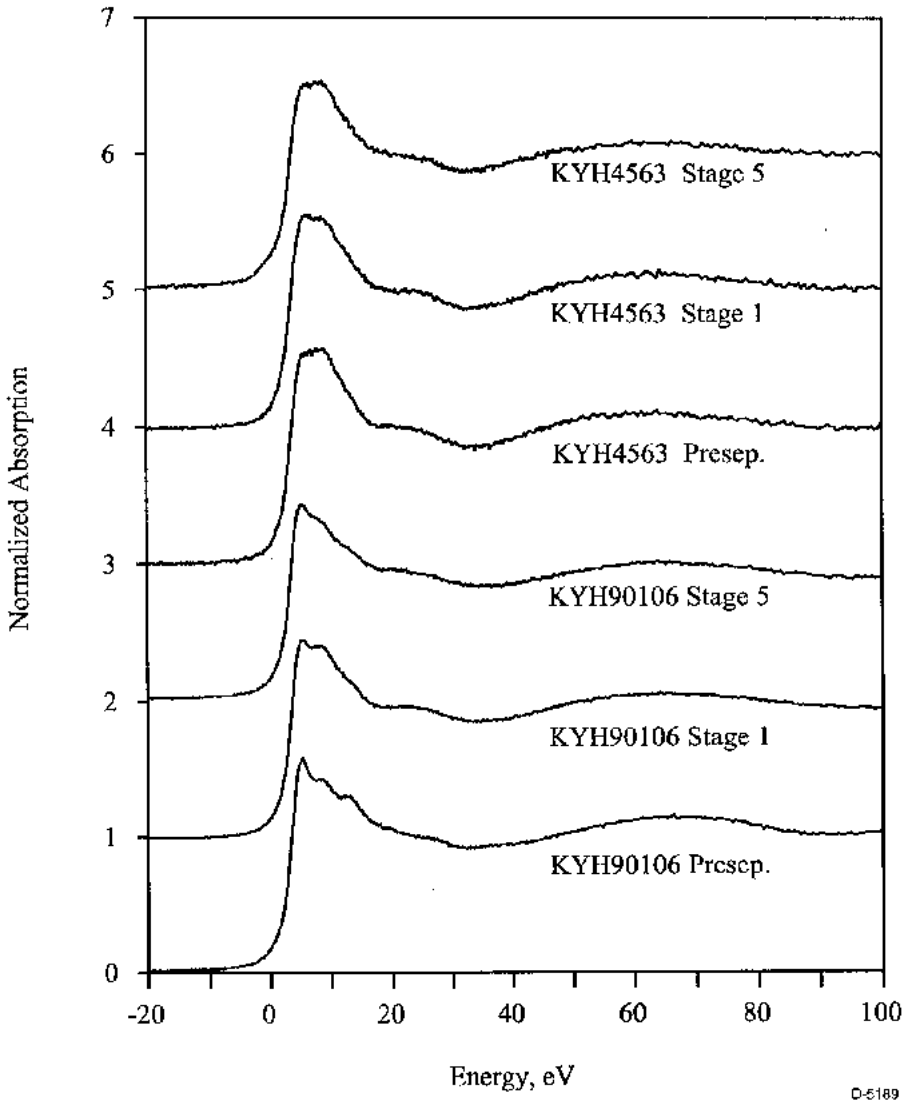

Figure 3-7. Zinc XANES spectra for high density Elkhorn/Hazard ash samples generated by MIT.

3.3.3 *Trace Element Vaporization in the Combustion Zone*

During the past quarter the data analysis was completed on the baseline Illinois No. 6 experiments performed at PSI (1500 °C furnace setpoint, stoichiometric ratio of 1.2). The NAA analysis and the particle size distribution shown in Figure 3-8 were used to calculate the fraction of each element that had vaporized during the combustion process. This fraction vaporized was defined as the mass smaller than or equal to 0.80 µm (Stage 6). Figure 3-9 shows the fractional vaporization for selected elements for the three bituminous coals under baseline conditions. In general, vaporization for all elements was lower in the Illinois No. 6 than in the other two program coals. This is interesting because several elements, specifically arsenic and selenium,

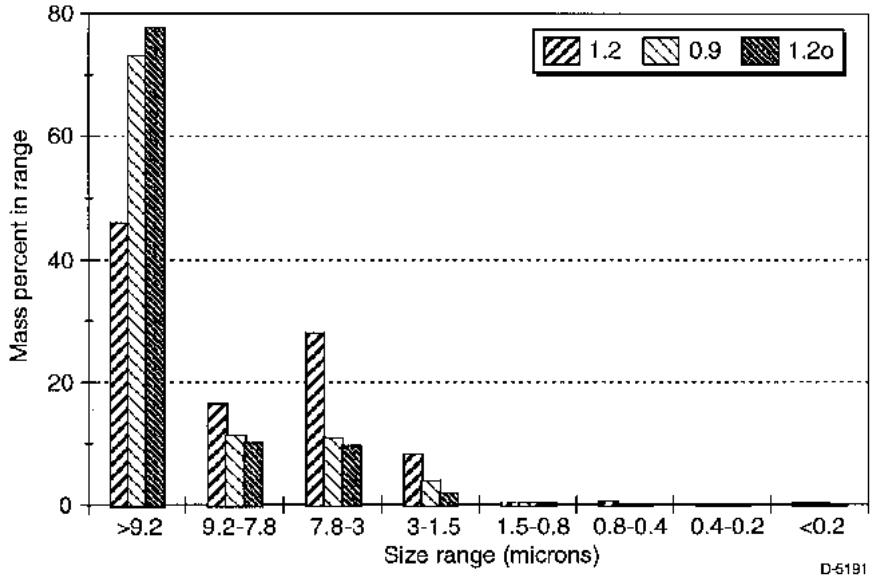

Figure 3-8. Measured ash particle size distributions for Illinois No. 6 (PSI EFR, 1500°C,SR=1.2).

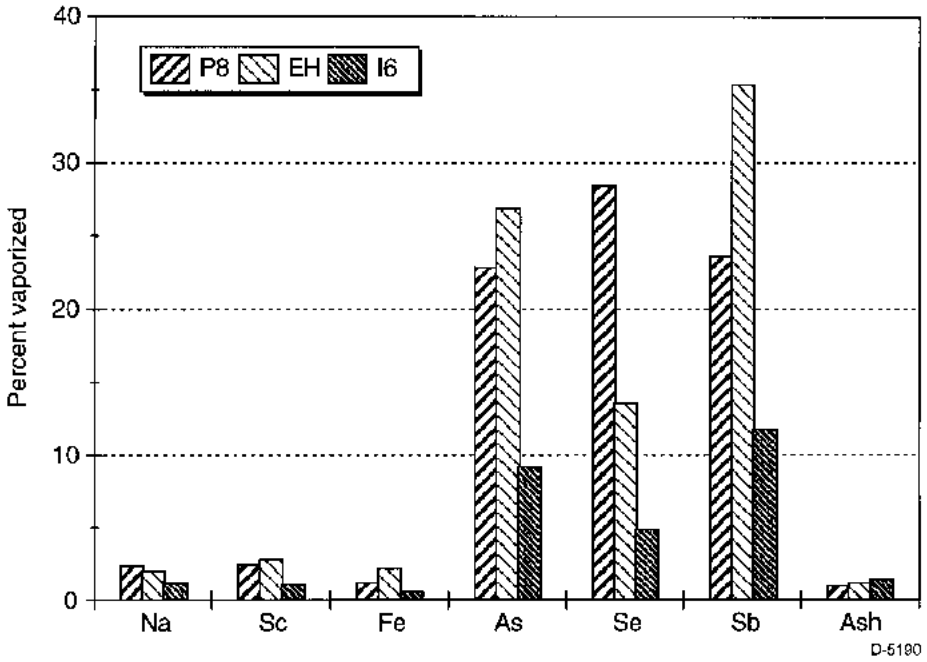

Figure 3-9. Fractional vaporization of trace elements from bituminous coals (furnace setpoint 1500°C, SR=1.2).

were shown to be associated with reactive minerals (pyrite) or organically associated in this coal. Thus one would expect these elements to be easily vaporized from this coal. More work is required to explain these results.

3.3.4 *Mechanisms for Trace Element Vaporization in the Combustion Zone*

In order to interpret the vaporization data collected in this program, it is useful to think about potential mechanisms for trace element vaporization during combustion. By performing 'thought experiments' for each mechanism, and comparing our predicted volatilization rates to those observed in the experiments, we can determine which mechanisms require further attention in Phase II and which mechanisms can be neglected.

There are several general mechanisms that may affect the volatilization of a given species during the combustion process. These mechanisms include:

1. Unconstrained vaporization (from excluded mineral particles)
2. Constrained vaporization (from included mineral particles)
3. Vaporization from included mineral particles that have been exposed as part of burnout
4. Capture of the reacting mineral (and associated trace elements) in glassy phases.

First we want to look at the effect of pyrite capture by silicates to form glassy phases on trace element vaporization. Many of the trace elements of interest have been shown to be associated with pyrite. If vaporization of these elements is delayed until the pyrite particle is exposed during char burnout, capture of the pyrite into a glassy melt may interfere with trace element vaporization. If, on the other hand, vaporization begins before the particle is exposed, this mechanism can be neglected. The relative importance of this mechanism can be estimated by comparing the observed vaporization rates from the two facilities, and the fraction of iron captured in the glassy phase. For example, since the MIT data show consistently higher vaporization rates than the PSI data for the same coal, we would expect a *lower* fraction of iron captured in the glassy phase (i.e., less interference from the glassy melt). A comparison of Mössbauer data collected during a previous DoE program is shown in Table 3-5. In one case a less than 75 µm size split of the Pittsburgh coal, from the same mine as the Pittsburgh coal in this program, was burned under at 20% oxygen in the MIT drop tube furnace (DTF). In the other case a utility grind sample of the same coal was burned in the PSI EFR at a stoichiometric ratio of 1.2. The MIT data show some unreacted pyrite in the ash, which may indicate that the residence time was too short to react all the pyrite. However, the PSI data show about the same

Table 3-5. Mössbauer Analysis of Ash Samples from Pittsburgh Coal
(% Iron in Each Phase)

Species	MIT DTF	PSI EFR
$Fe_{(1-x)}S$	9	0
Magnetite	27	44
Fe^{+2} glass	22	39
Fe^{+3} glass	42	17

amount of iron in the glassy phase as the MIT data. This would indicate that the coalescence of pyrite with other minerals to form a glassy phase proceeds at about the same rate in the two systems. Since the observed vaporization rates are so different, capture mechanism number 4 can be neglected. This, in turn, suggests that vaporization may begin much earlier in the char burnout process while the pyrite grains are still encapsulated by the char matrix.

Earlier work on the vaporization of inorganics from coal during combustion[1,2] has indicated that vaporization is strongly dependent on particle temperature. Based on this observation, a likely explanation for the differences in observed volatilities may be due to differences in particle temperatures between the two facilities. To evaluate this effect, an existing char burnout model was used to estimate the particle temperature as a function of time for different sized char particles in each facility. The Pittsburgh coal was used as a representative coal in these simulations. As can be seen from Figure 3-10 the peak particle temperatures in the MIT DTF are much higher than in the PSI EFR. This result suggests that the differences in observed trace element vaporization are related to the differences in temperature.

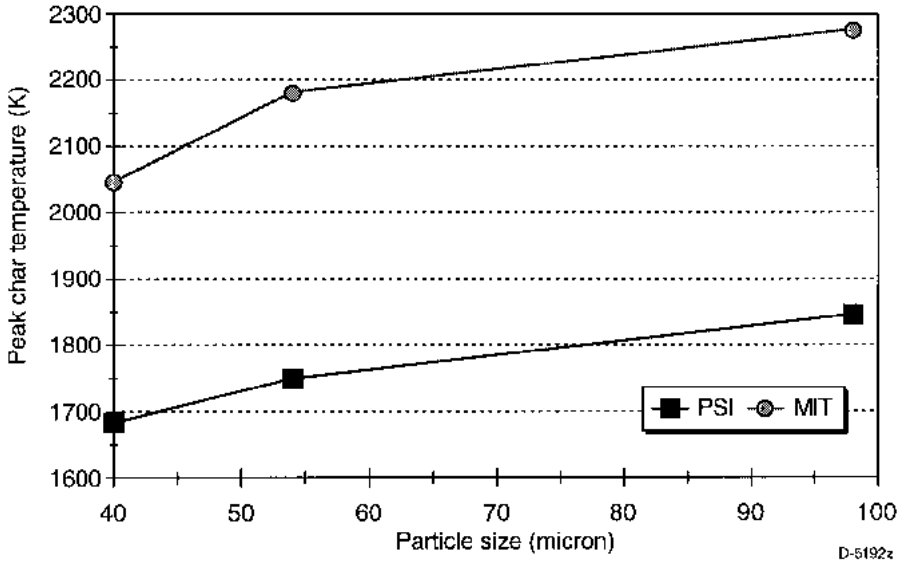

Figure 3-10. Predicted peak char temperatures (Pittsburgh coal).

Although these data indicate a strong temperature dependence on vaporization, the exact vaporization mechanism is still unclear. The lack of correlation between the fraction vaporized and the fraction of iron in the glass demonstrated above suggests that vaporization begins early in the char burnout process. Thus we would expect trace element vaporization from inclusions to be limited by diffusion through the pores in the char (internal diffusion control), or diffusion through the char boundary layer (external diffusion control). If internal diffusion is important, we might expect to see more vaporization from the high density fraction of the MIT coal samples than the low density fraction, because internal diffusion resistance might be higher for the low density coal particles. The plots shown in Figures 3-11 through 3-13 express the percentage of selected elements appearing in the submicron ash for the three bituminous coals. The MIT data are plotted next to the PSI data for SR=1.2 and SR=1.0 or 0.9. In general, the high density fraction does show a higher fraction vaporized than the low density fraction.

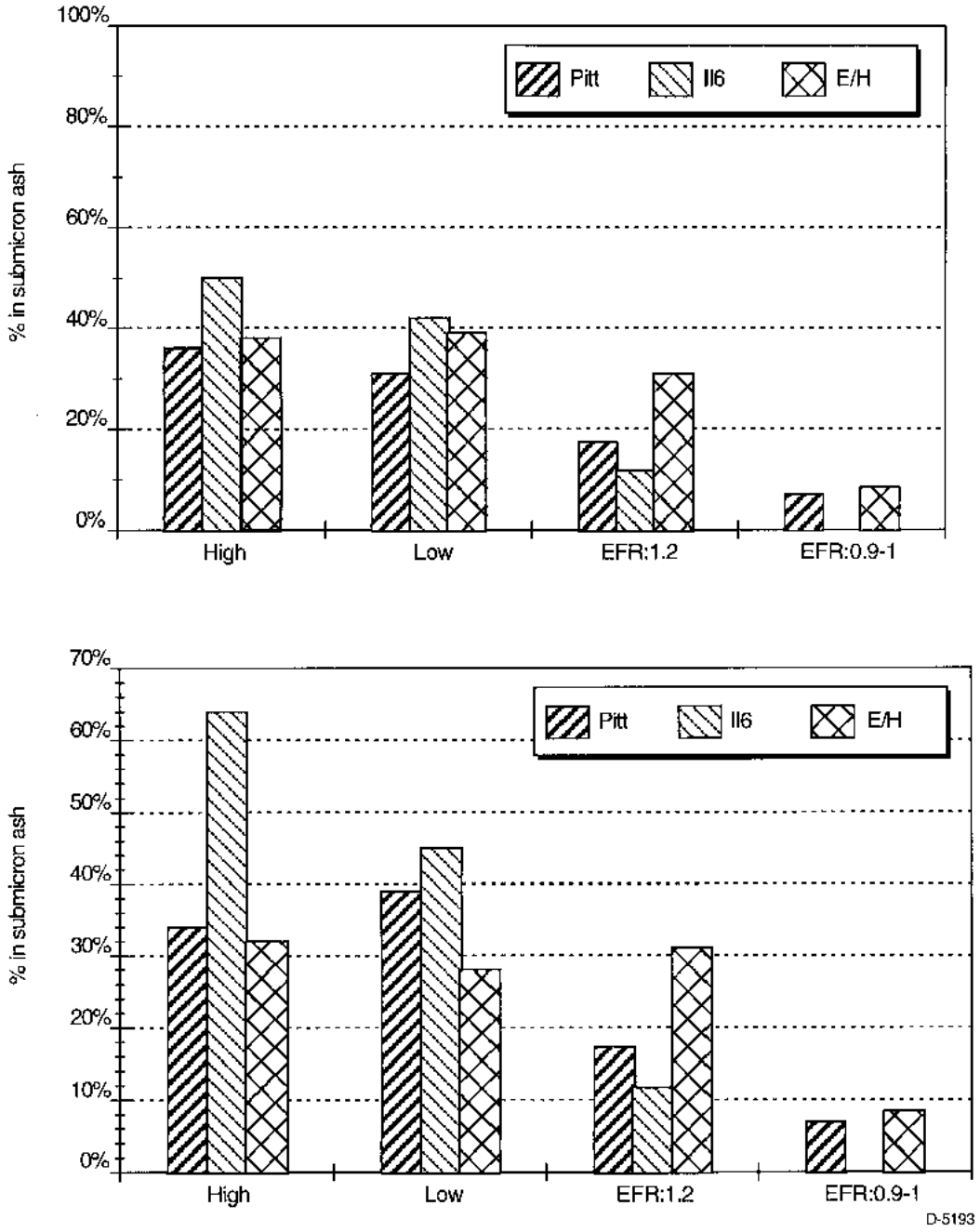

Figure 3-11. Fraction antimony in submicron ash; (top) 90 to 106 micron particles, (bottom) 45 to 63 micron particles.

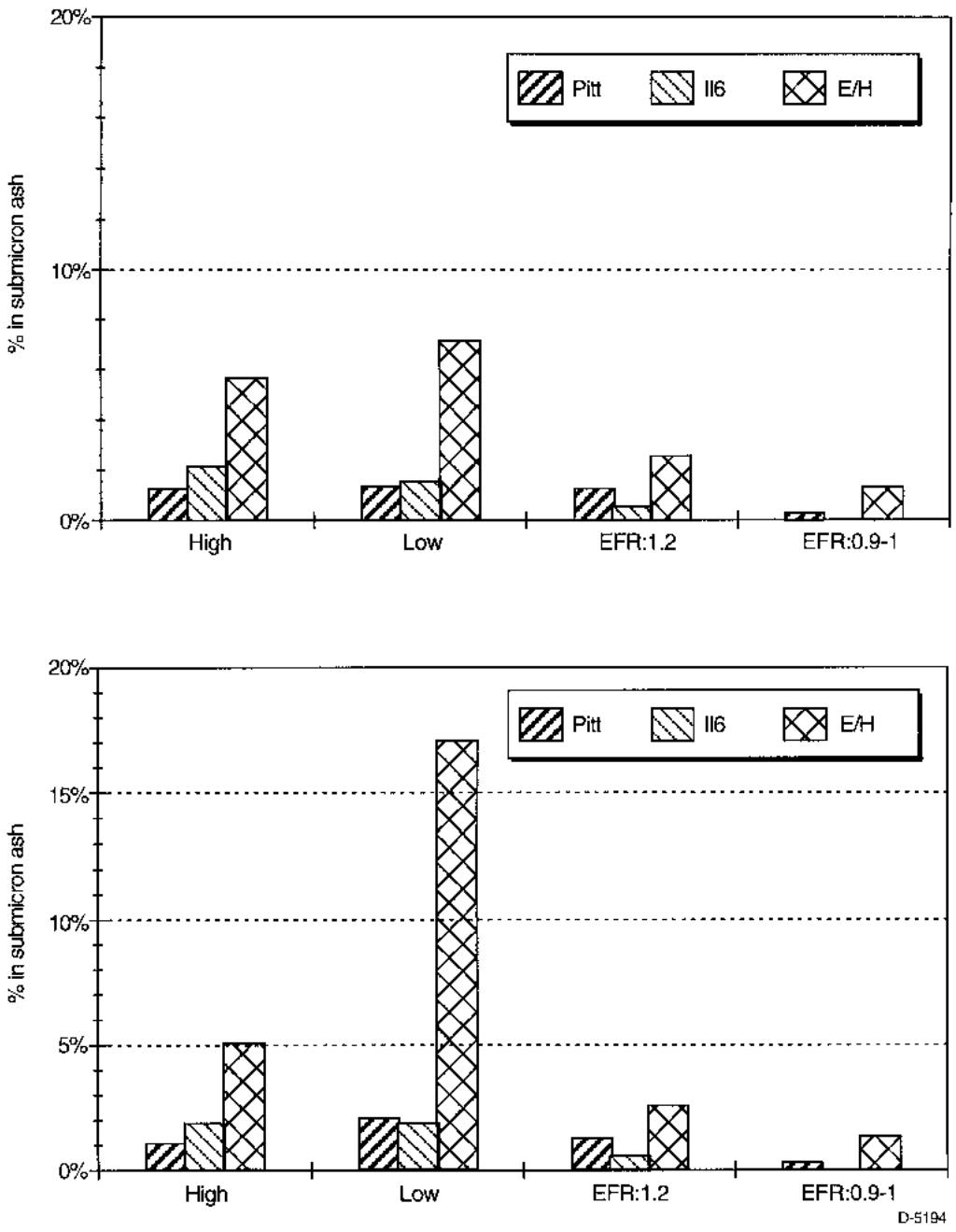

Figure 3-12. Fraction iron in submicron ash; (top) 90 to 106 micron particles, (bottom) 45 to 63 micron particles.

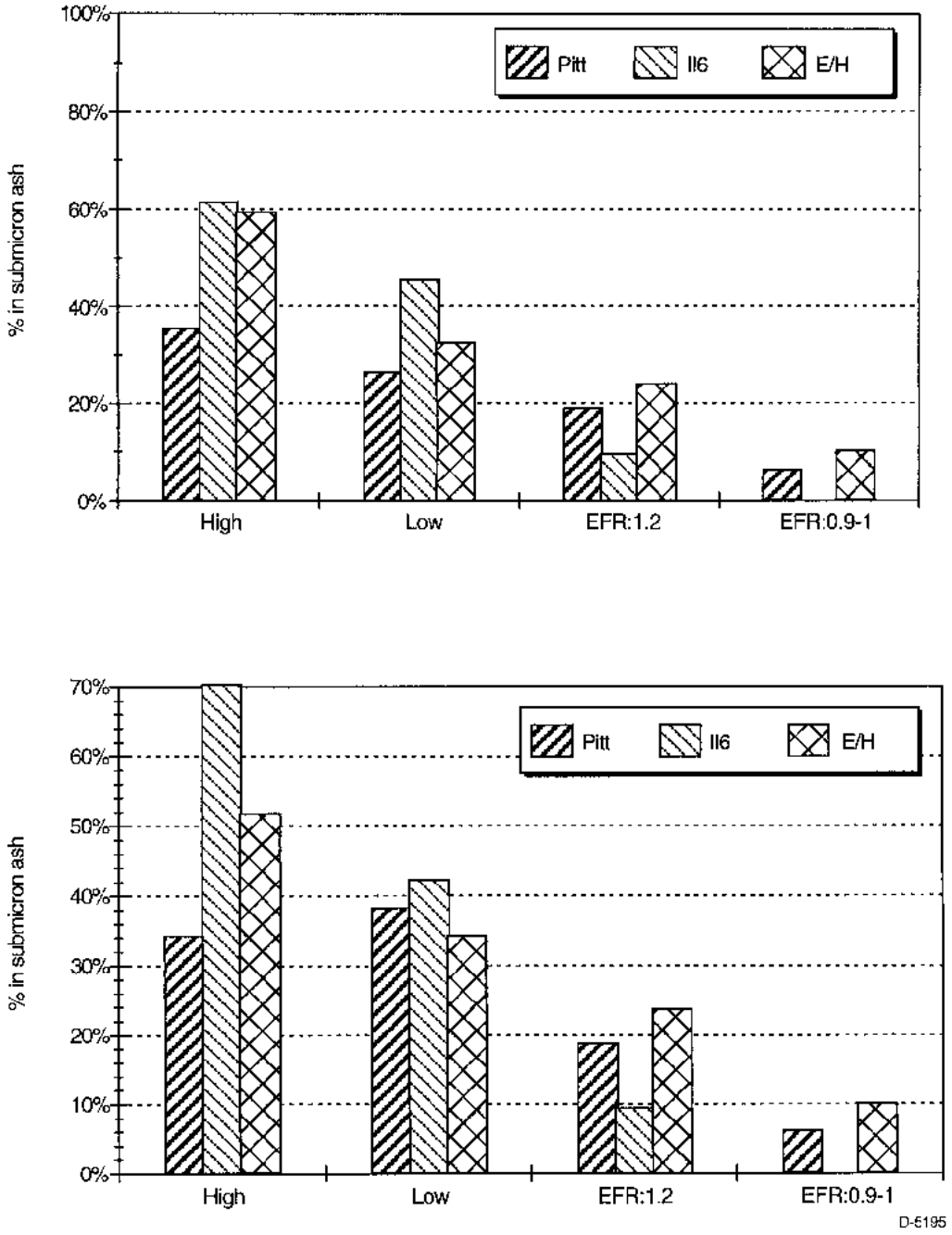

Figure 3-13. Fraction arsenic in submicron ash; (top) 90 to 106 micron particles, (bottom) 45 to 63 micron particles.

Another way to determine which mechanism might be controlling, external or internal diffusion control, is to look at the dependence of each mechanism on such parameters as char particle radius. Quann, in his doctoral thesis,[1] outlined several limiting cases for vaporization from a burning char particle. These cases, and their expected particle size dependence, are discussed in detail below.

For the case where we have vaporization from both internal inclusions and exposed inclusions on the char surface (see Figure 3-14), Quann[1] gives:

$$N_{t_b} = N_I^0 \; 4 \; \pi \; c \; r_i \; t_b \left[\frac{2}{5} \; D_e \; x_m^e + \frac{3}{5} \; D_m \; x_m^{es} \right] \tag{3-1}$$

and:

$$N_I^0 = \theta \; \frac{r_0^3}{r_i^3} \tag{3-2}$$

where:

N_{tb}	=	is the moles of metal vaporized per gram coal burned
N_I^0	=	number of inclusions in the char particle
c	=	molar concentration
r_i	=	inclusion radius
r_0	=	char radius
t_b	=	burnout time
D_e	=	effective diffusivity
D_m	=	metal diffusivity
x_m^e	=	equilibrium mole fraction metal at internal inclusion surface
x_m^{es}	=	equilibrium mole fraction metal at surface of exposed inclusion
θ	=	volume ratio of inclusions.

Based on these equations, the parameter derived by Mims et al.[2] can be derived (see Ref. 2 for derivation).

$$\frac{f_v}{t_b} = \frac{9 \; \pi \; \theta \; c}{r_i^2 \; C_o \; \rho_p} \left[\frac{r_i \; D_e \; x_m}{2 \; r_o \; (3\theta)^{1/2}} + \frac{D_m x_m^{es}}{5} \right] \tag{3-3}$$

where C_o is the concentration of the metal in the coal, ρ_p is the density of the char particle, and f_v is the fraction of the element vaporized during the combustion process. For vaporization from the external particles we assume $D_e << D_m$ then:

$$\frac{f_v}{t_b} \sim \frac{1}{r_i^2} \tag{3-4}$$

This indicates that the parameter is *independent* of char radius.

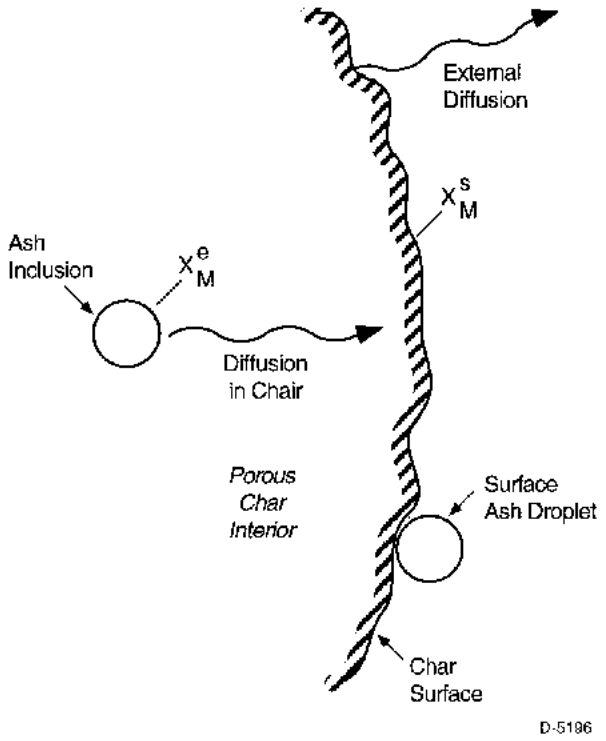

Figure 3-14. Schematic of trace element vaporization mechanisms.

For the limit where internal diffusion is limiting, the effective diffusivity term in Eq. (3-3) is much higher than the metal diffusion term. Thus:

$$\frac{f_v}{t_b} \sim \frac{1}{r_o} \tag{3-5}$$

For external diffusion control, as would occur with very fine inclusions or organically associated elements, we have:[2]

$$\frac{f_v}{t_b} = \frac{4\ D_m\ c\ x_s}{C_o\ r_o^2} \tag{3-6}$$

Thus, when external diffusion is controlling we would expect to see a $1/r_o^2$ dependence.

These equations suggest that if we can determine the effect of particle size on the fractional vaporization rate (f_v/t_b) we can begin to understand the mechanisms that drive trace element vaporization. In Figures 3-15 through 3-19 we plot the ratio of this parameter for two different particle sizes. f_v was calculated from the percentage of ash in submicron particles. t_b was estimated from calculated particle combustion histories. Also plotted is the behavior we would expect for either a $1/r_p$ or $1/r_p^2$ dependence. For example, the ratio of (f_v/t_b) for two different size ranges as measured by Mims[2] for several elements. These data have been corrected for the effect of particle temperature. As we can see, all of the elements measured by Mims et al. from a lignite coal demonstrated a $1/r_p^2$ dependence - suggesting that these elements either vaporized from very fine inclusions or from the carbon matrix. Unfortunately, the forms of occurrence of these elements in the coal were not measured in that program so we can not link the observed vaporization behavior with the forms of occurrence in the coal.

The data presented in Figures 3-16 and 3-17 were obtained by MIT in this program (20% oxygen, 1500°C). These data were corrected for the temperature difference due to differences in particle temperature (see Figure 3-10) using the temperature dependencies noted by Mims et al.[2] A $1/r_p$ dependence was noted for sodium in almost all cases. This finding is interesting as it suggests that sodium is vaporizing from discrete minerals contained within the char -- an unusual vaporization mechanism for this element. More forms of occurrence of this element in the coals is required to better understand these results. The data shown in Figures 3-16 and 3-17 also suggest that the dominant vaporization mechanism for iron vaporization is different between the two density classes. In the high density class there seems to be a $1/r_p^2$ dependence, whereas a $1/r_p$ was noted

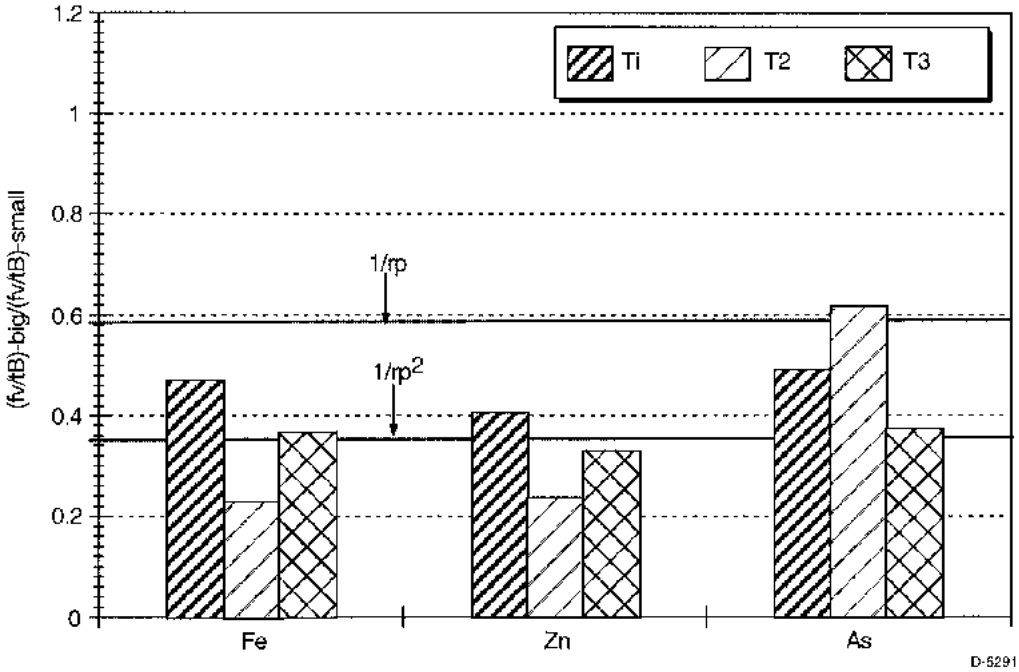

Figure 3-15. Ratio of functional vaporization rates - Mims et al.[2] data for Montana Lignite.

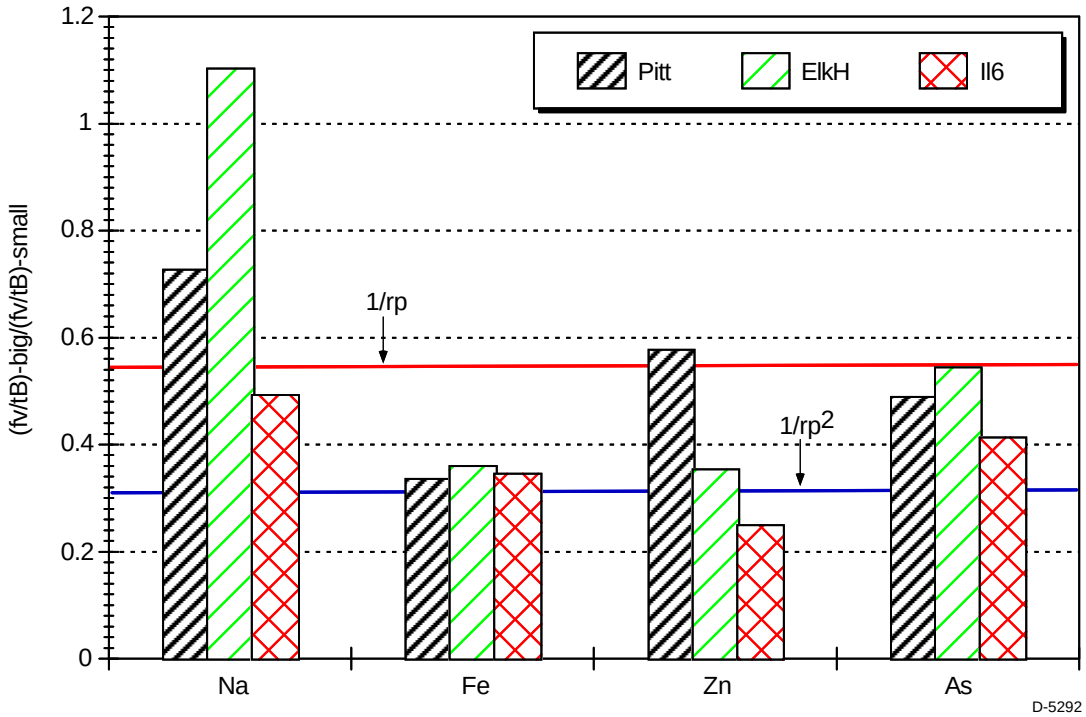

Figure 3-16. Ratio of fractional vaporization rates - high density cuts, temperature corrected (MIT DTF, 20% O_2, 1500°C).

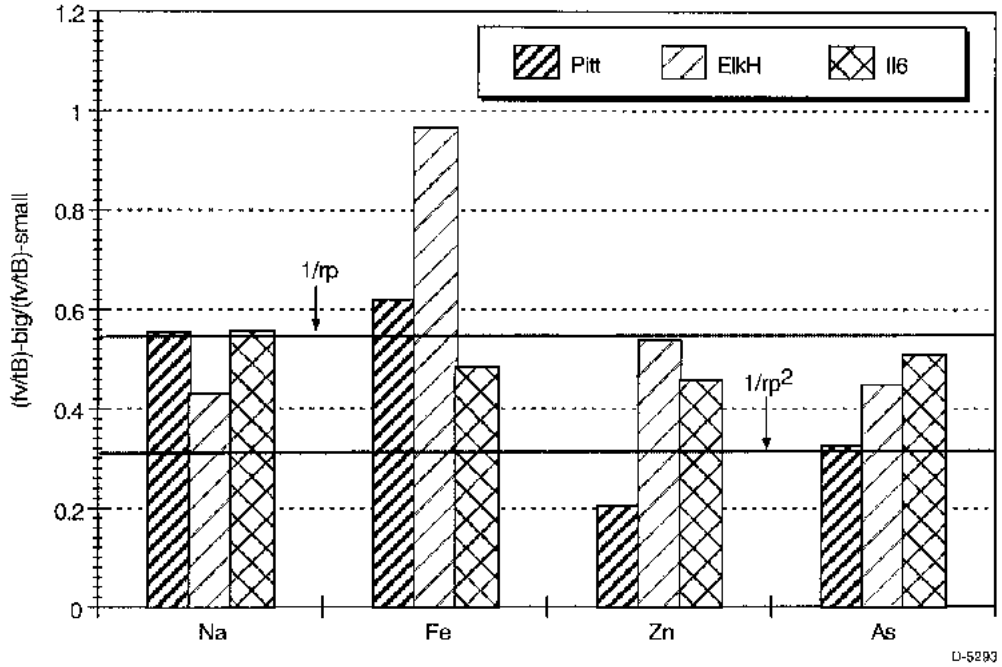

Figure 3-17. Ratio of fractional vaporization rates - low density cuts, temperature corrected (MIT DTF, 20% O_2, 1500°C).

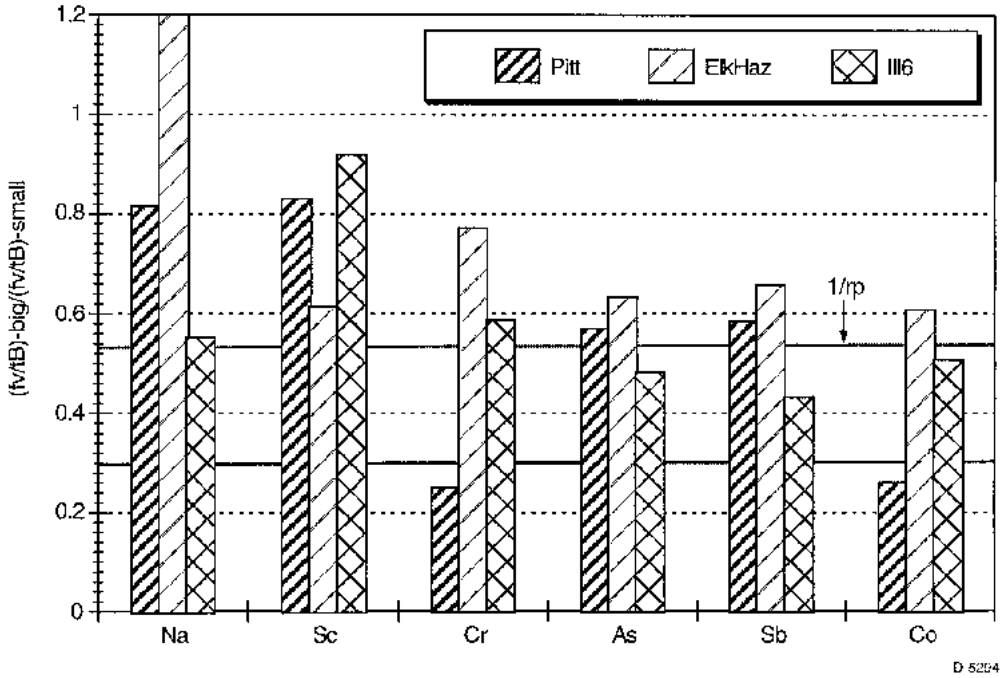

Figure 3-18. Ratio of fractional vaporization rates - high density cuts, not temperature corrected (MIT DTF, 20% O_2, 1500°C).

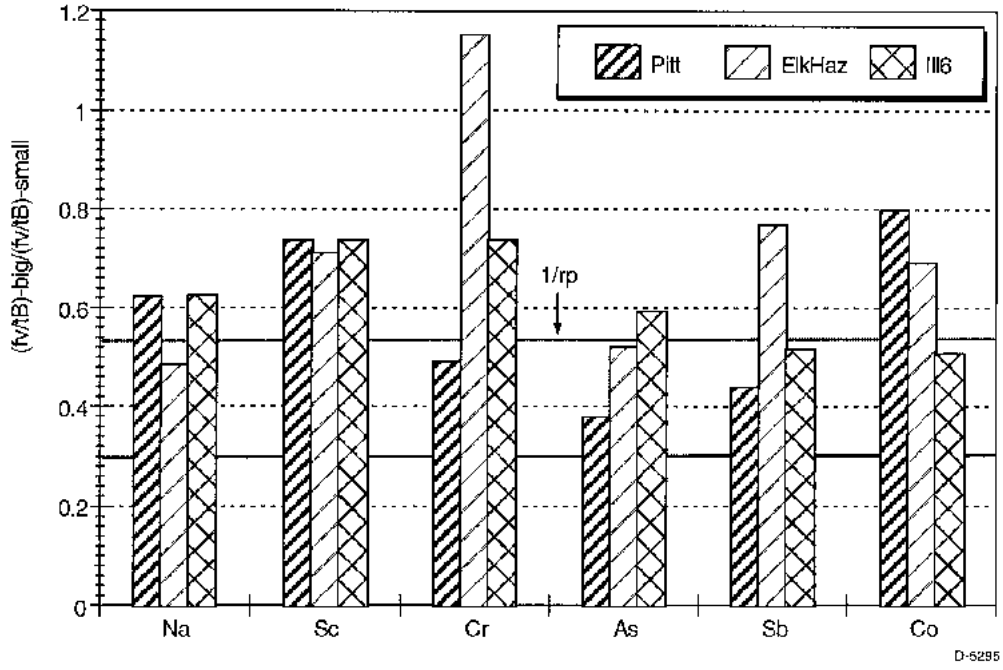

Figure 3-19. Ratio of fractional vaporization rates - low density cuts, not temperature corrected (MIT DTF, 20% O_2, 1500°C).

for the low density case. The $1/r_p^2$ dependence may be related to extraneous pyrite grains in the high density fraction -- vaporization from which would be limited by external diffusion. Iron may vaporize from the low density fraction by a reduction type mechanism noted by Quann.[1] The vaporization mechanism for zinc also seems to change between the different coals and density fractions, however more information on the forms of zinc in these fractions is required to explain these differences. In general, these data suggest that arsenic predominantly vaporizes from included pyrite. The only exception seems to be the low density fraction of the Pittsburgh coal. It is possible that the observed $1/r_p^2$ dependence for this sample may be caused by arsenic vaporization from fine pyrite grains in the coal. However, until the CCSEM analysis of this density split is complete, this mechanism is fairly speculative.

Figures 3-18 and 3-19 show the ratio of fractional vaporization rates for a number of elements. These data were not corrected for the difference in peak particle temperature associated with the particle size. These data suggest that most of the elements not discussed above, scandium, chromium, antimony, and cobalt also show a $1/r_p$ dependence, and therefore probably vaporize from discrete minerals.

3.4 Post-Combustion Transformations (UA, PSI, UKy)

Trace element transformations in the region between the furnace exit and the ESP play a critical role in determining the partitioning of that element between flyash captured in the ESP and vapors emitted from the stack. In this program we are investigating these post-combustion transformations on two different scales. Mercury capture by residual carbon, shown to be an important mechanism for mercury retention in the ash, is being evaluated in a small benchtop facility. Samples from other groups exploring mercury uptake by activated carbon were examined by XAFS to determine the forms of mercury that are retained in the char. Other interactions, such as condensation and reactive scavenging, between vaporized species and ash particles are being investigated using the larger self-sustained combustor at UA. Mercury speciation in flue gas is being evaluated in the PSI EFR. Finally, kinetic calculations are being performed at MIT to determine the partitioning of chlorine between HCL and Cl_2.

3.4.1 *XAFS Investigation of Hg Captured on Activated Carbons*

(1) UNDEERC Samples LAC-1,2,3, SAC-1,2, IAC-1,2:

The rationale for the investigation of these seven samples and preliminary Hg XAFS data obtained for this set of activated carbon samples provided by Grant Dunham of the University of North Dakota Energy and Environmental Research Center were described in the previous Quarterly Report.[4] In the current quarter, new XAFS data have been obtained for these samples at the S, Cl, Ca K edges and the I L_{III} edge. A brief discussion of the principal results is presented on an element by element basis. However, it should be noted that the analysis of these spectra has not yet been fully completed; hence, the conclusions presented here should be regarded as preliminary.

Iodine: As expected, XAFS spectroscopy showed that iodine was present only in the two IAC samples and absent in all other samples. The step-height for IAC-2 was about four to five times as large as that for IAC-1 sample exposed to the flue gas, perhaps indicating that iodine was partially volatilized during exposure to flue gas at a temperature of about 225°F. The closest match to the iodine L_{III}-edge XANES spectra of the IAC chars was exhibited by elemental iodine; however, the spectra were not identical.

Sulfur: Sulfur XAFS spectroscopy showed that sulfur was present in all samples, except for the two IAC samples. In the LAC samples, sulfur was found to be present predominantly as sulfate, whereas in the SAC samples, sulfur was present predominantly in elemental form. The data suggest that sulfur present in the flue gas is not significantly captured by the activated carbons.

Chlorine: Chlorine was present in significant amounts in the LAC samples exposed to the flue gas. On the basis of the chlorine K-edge step-height, the Cl contents are estimated to be as follows: LAC-1 > LAC-2 >> LAC-3. It should be noted that the IAC and SAC samples have yet to be examined at the chlorine edge. However, the Cl XANES data appear to suggest that chlorine can be captured efficiently from flue gas as HCl. Hence, reaction between Cl and Hg may occur readily at the char surface. Certainly, the Hg XAFS data for the LAC samples are compatible with Hg-Cl bonding; however, the discrimination between Hg-Cl and Hg-S bonding is quite subtle in XAFS spectroscopy and further work is needed to resolve this point.

Calcium: Calcium is present in significant amounts in both SAC and LAC samples; however, no IAC samples have been examined. Ca XANES spectra are different for the LAC and SAC sample sets. The Ca XANES spectra of the two LAC samples are closely similar and suggest Ca as Ca sulfate; those of the two SAC samples are also similar, but are more suggestive of Ca as carboxyl-bound species.

(2) Hg XAFS Spectroscopy of New UNDEERC Activated Carbon Samples:

During the quarter, Hg XAFS data were obtained for a number of new activated carbon samples from UNDEERC. These new samples included a set of three samples exposed to the simulated flue gas containing Hg in the form of mercurous chloride ($HgC\ell_2$), and a set of four LAC samples (LAC-5, 6, 7, 8) prepared under different conditions to the set of three samples (LAC-1, 2, 3) examined previously. Only a preliminary evaluation of the data will be given here as the analysis of the Hg XAFS data has only just commenced.

The Hg XANES spectra of the three samples [LAC (-400), SAC (-400), IAC (-400)] exposed to the flue gas containing mercurous chloride appear similar to the spectra obtained previously for the related samples (LAC-1, 2, SAC-1, IAC-1) exposed to the flue gas containing elemental Hg. Similar trends in the XANES data (e.g., separation of the two derivative peaks) to those seen previously have been noted for the current set of three samples.

Except, possibly for sample LAC-8, the Hg XANES spectra of the four new LAC samples are similar to the spectra of samples LAC-1 and LAC-2 examined previously. However, there is some significant variation in the step-height that will need to be evaluated.

(3) XAFS spectroscopy of Hg in Samples from UA:

The samples of PSI char exposed to mercury in experiments at UA have also been examined briefly. These spectra are not unlike those observed for the UNDEERC LAC-1,2 chars discussed in the previous Quarterly Report.[4] Further work will be performed on these samples.

3.4.2 *Mercury Capture by Residual Carbon*

During the last quarter mercury capture experiments were performed with chars from three of the program coals, the Illinois No. 6, the Pittsburgh, and the Wyodak. The samples were sent to a commercial laboratory for analysis. The results were obtained late in the last quarter, and are currently being analyzed. These will be discussed in detail in the next report.

3.4.3 *Mercury Speciation Measurements*

Mercury represents one of the most difficult trace elements to control in utility boilers. Although most researchers agree that mercury in coal vaporizes completely in the combustion zone of a boiler, predicting emissions of mercury has been problematic because the transformations of mercury in the post-combustion gases are not well understood. Mercury leaves the combustion zone in the form of elemental mercury in the gas phase. Some oxidation of mercury occurs as the flue gas cools. At the air heater exit, where the flue gas typically enters the pollution control train, mercury can be found in the gas phase as elemental mercury (Hg^0) or oxidized mercury species (Hg^{+2}) or in the particulate phase.

The efficiency of mercury removal by air pollution control devices (APCDs) such as electrostatic precipitators (ESPs) or flue gas desulfurization (FGD) units depends on the form (gas versus particulate) and speciation (Hg^0 versus Hg^{+2}). For example, oxidized mercury is more likely to be captured by residual carbon in ash or to be removed in an FGD unit, while elemental mercury is more likely to escape the air pollution control devices and be emitted to the atmosphere. Understanding the *speciation* of mercury in the post-combustion zone is critical to predicting its final form of emission (solid, liquid, or gaseous).

In Quarterly No. 4 from this program, we hypothesized that the oxidation of mercury is frozen in coal combustion flue gas is frozen below some temperature between 750 to 900 K (900 to 1200ºF). Equilibrium calculations suggest that mercury is entirely in the elemental form at the high temperatures associated with the combustion zone. As the gas cools equilibrium predicts that the mercury oxidizes. However, as discussed in Quarterly Report No. 4 some field data suggests that the mercury oxidation is 'frozen' at some temperature around 850 K. To test whether oxidation is indeed frozen at some temperature, a series of experiments were completed to measure the mercury speciation in real flue gas at a range of temperatures.

For these experiments the Illinois No. 6 coal was combusted under fuel lean conditions (stoichiometric ratio of 1.2). Flue gas was removed at the bottom of the reactor with either an unheated stainless steel tube or an unheated quartz tube. At the exit of the tube the sample was quenched with nitrogen. The temperature profile along the tube, including the quench point, was measured as part of the experimental protocol. Another set of experiments were performed using the standard nitrogen quench probe. By collecting data with the quench probe in the furnace, and at various other temperatures we hoped to test whether mercury speciation is, in fact, 'frozen' at some temperature. These mercury speciation measurements utilized the Ontario-Hydro method. This method was identified by a FETC-EPRI-UNDEERC team as one of the more reliable methods for measuring mercury speciation in flue gas.

Of the data collected, only two sets of samples yielded useable results. All of the samples using the quartz tube were found to have mercury concentrations in the impinger trains below the detection limit. The reason for this is unclear, as the duration of the runs was long enough to achieve concentrations several times higher than the detection limit. It is possible that leaks around the various metal-quartz seals may have caused dilution of the samples.

One sample yielded results, although with a low mass closure (32%). This sample was collected with the nitrogen quench probe and should represent the speciation in the furnace. Analysis of the particulate and the various impingers suggested that approximately 50% of the mercury was associated with the particulate. The gas phase mercury was approximately 66% elemental and 34% oxidized. The gas temperature at this location has been measured to be approximately 1300 K (1900°F) with the water-cooled probe installed.

The second sample that yielded good results was collected with a stainless steel tube. These data indicated that approximately 16% of the mercury was retained in the ash at 383 K. The measured cooling rate in this tube was approximately 200 k/s, which is comparable to the economizer in a power plant, where most of the mercury oxidation is predicted to occur. The vapor phase mercury was approximately 72% elemental mercury and 28% oxidized mercury. Mass closure for this experiment was approximately 100%.

Equilibrium predictions for this coal, shown in Figure 3-20, suggest that we should have found more elemental mercury at the high temperatures, and much less elemental mercury at the lower temperatures. Although the data at high temperatures should be considered preliminary, due to the low mass closure, the combination of the two data point suggest that the fraction of oxidized mercury is similar between the two samples -- contradicting the equilibrium predictions. Since the cooling rate of the low-temperature data is comparable to that found in the region of interest in a utility boiler, these data support the hypothesis that mercury oxidation is frozen due to kinetic effects.

Although these experiments provided some promising results, there exists the possibility that the sampling technique (i.e., the stainless steel tube) may have influenced the mercury speciation. In addition, much more work must be done to better understand the conditions required to 'freeze' mercury oxidation. These experiments are planned for Phase II of this program.

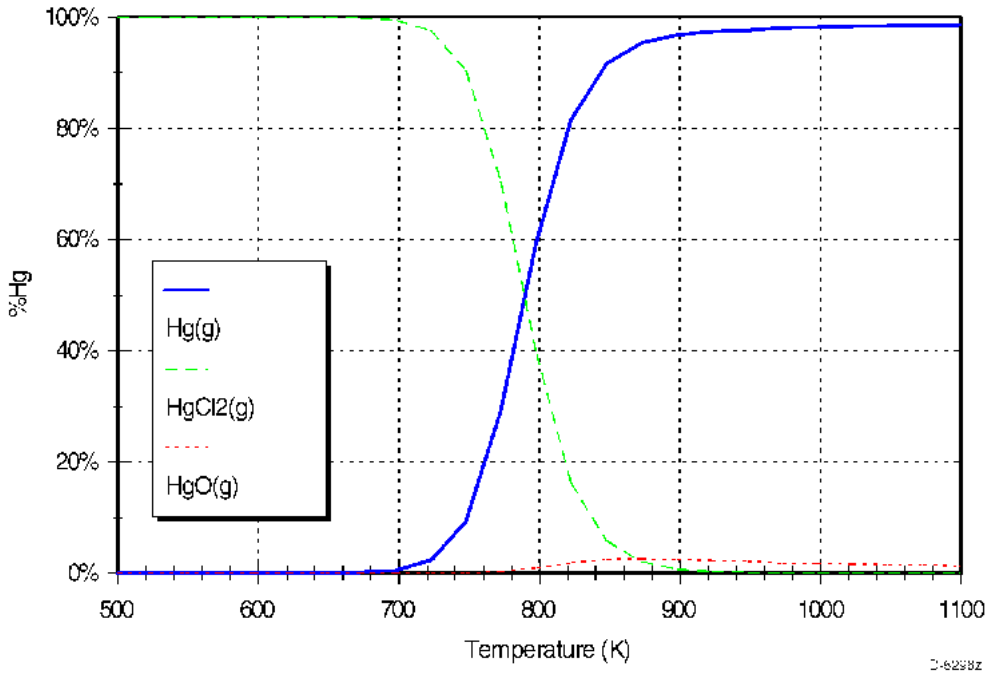

Figure 3-20. Equilibrium mercury speciation in flue gas as a function of temperature (Illinois No. 6 coal).

3.4.4 *Large Scale Combustion Experiments*

Laboratory Scale Combustor and Sampling Apparatus

The furnace used in these experiments is a 6 m (20 ft) long downfired combustor, with a 15 cm (6 in.) inner diameter. Sample ports are located at approximately 30.5 cm (1 ft) intervals along the length of the furnace. The furnace was designed to simulate the time/temperature histories and complex particle interactions of commercial-scale combustors while still providing a flow stream which is sufficiently well characterized to allow the mechanisms of trace element transformations and partitioning to be studied.

The combustor was fired with either natural gas or coal. Gas and particulate samples were collected along the length of the furnace using the systems described later in this section. When the particle laden flue gas exited the furnace it was routed through a baghouse to remove entrained particulate. The gas was then cooled to room temperature, combined with the purge air, chemically filtered, and discharged to the atmosphere. Condensed water was removed in a series of knockout pots. Gas flows through the system are controlled using two induced draft air blowers operating in series.

The temperature profile in the furnace was allowed to evolve naturally based on the coal feed rate, air feed rate, and pressure profile in the furnace. There are two fixed K-type thermo-couples installed in the furnace. The post-combustion thermocouple is located 320 cm below the burner. The exhaust-point thermocouple is located below the final sample port, roughly 600 cm below the burner (this thermocouple was inoperable during these experiments).

The temperature profile for the furnace was measured using a portable thermocouple probe. This probe consisted of a type R thermocouple encased in a ceramic shell. The thermocouple bead extended approximately 6 mm beyond the end of the ceramic shell and ended at the centerline of the furnace.

A portable gas sampling probe was used to measure the gas profile in the furnace. Flue gas was drawn through a water-cooled stainless steel tube from the centerline of the furnace. To remove entrained water and particulate, the gas was then routed through a series of filters plus a cooler and additional filters. The dry gas stream was analyzed for CO, CO_2, NO_x, and O_2. CO and CO_2 were analyzed using Beckman Model 864 nondispersive infrared analyzers. NO_x was determined using a Thermo Electron Model 10A chemiluminescent analyzer (a Model 300 molybdenum converter was utilized). Oxygen was analyzed using a Beckman Model F3 paramagnetic analyzer.

Particle sampling was carried out using a portable, water-cooled, stainless steel, aspirated isokinetic sampling probe. This probe was used to probe extract samples from the centerline of the furnace. Extracted samples were routed through a Berner Low Pressure Impactor (BLPI) using a metered dilution nitrogen stream and a vacuum pump. Isokinetic sampling was accomplished by adjusting the dilution flow rate at a near constant total flow rate. A slipstream of gas from the particulate sampling system was also routed to the NO_x analyzer to verify the dilution rate during particulate sampling.

The BLPI consists of 11 collection plates designed to collect particles of decreasing size on each plate. A listing of the size distribution for the BLPI plates is shown in Table 3-6. For accurate results, the BLPI must be utilized in two separate configurations. For collection of small particles, those below 0.337 microns, a cyclone is used on the inlet of the impactor to collect the larger particles. This allows the sampling time to be extended long enough to collect a significantly large sample of particulate. When large particles are to be collected, the cyclone is removed and a shorter sample time is used.

Table 3-6. Particle Cut-off Diameters for Berner Low Pressure Impactor

Impactor Plate Number	Cut-off Diameter (microns)
11	15.7
10	7.33
9	3.77
8	1.98
7	0.973
6	0.535
5	0.337
4	0.168
3	0.0926
2	0.0636
1	0.0324

The collection plates are lined with a 0.4 µm thick polycarbonate membrane (Poretics Products) coated with a high purity grease. When operating with the cyclone, Plates 1 to 6 contained membranes while Plates 7 to 11 were lined with grease-coated aluminum foil. Similarly, when the cyclone was not utilized, Plates 6 to 11 contained membranes while Plates 1 to 5 were lined with grease-coated aluminum foil.

Experimental Procedure

At the beginning of each experiment the furnace was preheated by burning natural gas for an extended period of time. The maximum sustainable gas feed rate was used in this preheat period. Typically, the furnace was allowed to warm up overnight and the temperature in the furnace at steady-state was related to the gas rate used in the preheat step. During preheat, exhaust gas was routed through a bypass line instead of through the baghouse. Once the preheat period was over, the baghouse was commissioned and allowed to warm-up until the gas temperature in the baghouse was approximately 100 ºC. This warm-up was normally accomplished in 15 min or less.

Once the furnace was hot enough to ignite the coal, the natural gas was turned off and the coal flow started. The temperature of the fixed post-combustion zone thermocouple was measured continuously during the coal feed warm-up period. The time that was required for furnace warm-up varied depending on how hot the furnace was at the time of switch over from gas to coal. A typical warm-up time was 1.5 to 3 h. During the coal feed warm-up period, the gas sampling and analysis system was commissioned. Each of the analyzers was calibrated with a certified calibration test prior to gas data collection.

After the gas sampling system was commissioned, the O_2 and CO_2 readings from Port 4b were then used to adjust the main air flow rate in order to set the stoichiometric ratio at 1.2. Port 4b is just below the combustion zone. It was our intention to adjust the exhaust gas blower speed to maintain a neutral pressure at Port 4b. It turns out that the exhaust blower speed was set to maximum throughout the experiment. Until slag buildup became significant, this speed corresponded to a near neutral pressure at Port 4b. Another reason for using Port 4b is that there is one appreciable crack in the furnace wall. It is located at the floor joint approximately 40 cm below Port 4b. Therefore readings from Port 5, which is below the floor joint, would not give a true reading of the excess oxygen content in the furnace.

In general, two sets of samples were obtained during each test run. Each set of samples consisted of a 'cyclone run' and a 'no-cyclone run.' The 'cyclone run' uses a cyclone in conjunction with the BLPI to allow more sample to be collected in the small size ranges. The 'no-cyclone run' is performed without the cyclone to measure the particle size distribution of the larger particles. Before sampling, the gas sampling probe was inserted into Port 4b and the main air rate was adjusted to insure stoichiometric combustion conditions. This final air flow rate was then used to calculate an isokinetic sampling rate at this port. The sampling rate was set at 90% of the maximum laminar gas velocity estimated in the furnace. A size segregated ash sample was then collected using the particle collection system described above.

When sampling was completed for each sampling run, the BLPI was unloaded. The polycarbonate membranes were folded and inserted in the sample vials. The combined vial/ash/membrane weight was obtained. Aluminum foil samples were weighed and stored in plastic Petri dishes. The cyclone catch, when collected, was emptied into a preweighed Petri dish. The dish containing the ash was weighed. The sample collection media for the next test run was weighed and loaded into the BLPI.

During the time period that the BLPI was being unloaded and reloaded, a gas profile of the furnace was obtained. All of the first floor sample ports below the combustion zone (Ports 4, 4b, and 4c) were sampled along with a representative sample of the ports on the basement floor (Ports 5 to 14). Once the BLPI was reloaded, the stoichiometry at Port 4b was reconfirmed with the gas sampling probe. The next sample test was then begun.

After the sampling was complete at the top of the furnace (1 set of samples), the gas sample probe was inserted into Port 12 to measure the difference in oxygen content between Ports 4b and 12. This difference is due to air leakage into the post-combustion section of the furnace which is under slightly negative pressure. Usually, the furnace has been operating on coal long enough that slag has built up over the crack at the floor joint and the isokinetic sampling rate at Port 12 is similar to the rate at Port 4b. However, during some of the runs, appreciable oxygen leakage was still detected. The difference in oxygen concentration was used to calculate a new, higher gas velocity in this section of the furnace, which was used in turn to determine an isokinetic sampling rate. The last set of samples, consisting of a 'cyclone' and 'no-cyclone' run, was then collected.

Results

A total of 11 sets of particulate samples were collected during six test runs for the Pittsburgh coal. For Illinois #6, seven sets of particulate samples were collected during four test runs. The sample sets and test runs are summarized in Table 3-7. Table 3-8 shows the sampling conditions for the most important sample sets.

Figures 3-21 and 3-22 show steady-state temperature profiles for the Pittsburgh and Illinois coals. The results are similar and no appreciable difference in the temperature profiles for the two coals can be discerned from this data. Note that the results for Run P8-1 shown in Figure 3-16 were obtained at the lower coal feed rate, 1.4 kg/h, compared to 2.0 kg/h for the other three sets of data. There is no discernable difference in the temperature profile based on these two coal feed rates.

Table 3-9 provides a summary of the mass fractions for the Pittsburgh sample sets 9 through 12. These represent the sample sets taken at a coal feed rate of 2.0 kg/h plus the extended sampling period (2 h with the cyclone and 6 min without the cyclone). Similarly, the mass fractions for the Illinois #6 sample sets are shown in Table 3-10. A more detailed compilation of the data, including the mass loading calculations used to generate these mass fractions is given in Appendix A. Using the mass fractions from each test, an average mass loading can be calculated for each coal type/coal feed/sample port combination. The resulting particle size distributions are shown in Figure 3-23.

These samples were then sent to MIT for INAA and will be discussed in more detail in the next report.

Table 3-7. A Summary of the Phase I Test Runs

Test Run #	Date	Coal Feed Rate	Sample Set #	Sample Port Used
P8-1	1/29/97	1.4 kg/h	97P8-1c 97P8-1 97P8-2c 97P8-2	12 12 12 13
P8-2	1/30/97	1.4 kg/h	97P8-3c 97P8-3 97P8-4c 97P8-4	4b 4b 4b 4b
P8-3	2/4/97	1.4 kg/h	97P8-5c 97P8-5 97P8-6c 97P8-6 97P8-7c 97P8-7	4b 4b 4b 4b 4b 4b
P8-5	2/18/97	2.0 kg/h	97P8-9c 97P8-9 97P8-10c 97P8-10	4b 4b 12 12
P8-6	2/20/97	2.0 kg/h	97P8-11c 97P8-11 97P8-12c 97P8-12	4b 4b 12 12
IL-1	2/25/97	2.0 kg/h	97IL-1c 97IL-1 97IL-2c 97IL-2	4b 4b 12 12
IL-2	2/27/97	2.0 kg/h	97IL-3c 97IL-3 97IL-4c 97IL-4	4b 4b 12 12
IL-3	3/3/97	2.0 kg/h	97IL-5c 97IL-5	4b 4b

IL-4	3/5/97	2.0 kg/h	97IL-6c 97IL-6 97-IL-7	12 12 12

Table 3-8. Conditions for Phase I Experiments

Sample Set # (Port Sampled)	Total Air Feed Rate (slpm)	Sampling Rate (slpm)	Sampling Temp. (°C at port where sample was taken)	Port 4b O_2 Conc (%)	Port 4b CO_2 Conc (%)	Port 12 O_2 Conc (%)	Port 12 CO_2 Conc (%)
97P8-9/9C (4b)	535	1.72	1167	3.3	18.6		
97P8-10/10c (12)	535	1.84	866	3.5	18.2	5.1	17.1
97P8-11/11c (4b)	535	1.72	1159	3.2	17.7		
97P8-12/12c (12)	535	1.72	---	3.0	17.3	3.0	16.2
97IL-1/1c (4b)	527	1.70	---	3.7	15.0		
97IL-2/2c (12)	527	1.70	---	3.6	15.0	3.8	15.0
97IL-3/3c (4b)	518	1.67	1170	3.4	15.2		
97IL-4/4c (12)	518	1.83	871	3.4	15.2	5.6	13.7
97IL-5/5c (4b)	547	1.70	1106	4.1	14.2		
97IL-6/6c (12)	540	2.10	842	3.9	16.1	7.0	12.2
97IL-7 (12)	540	1.96	842	3.6	15.6	6.8	11.9

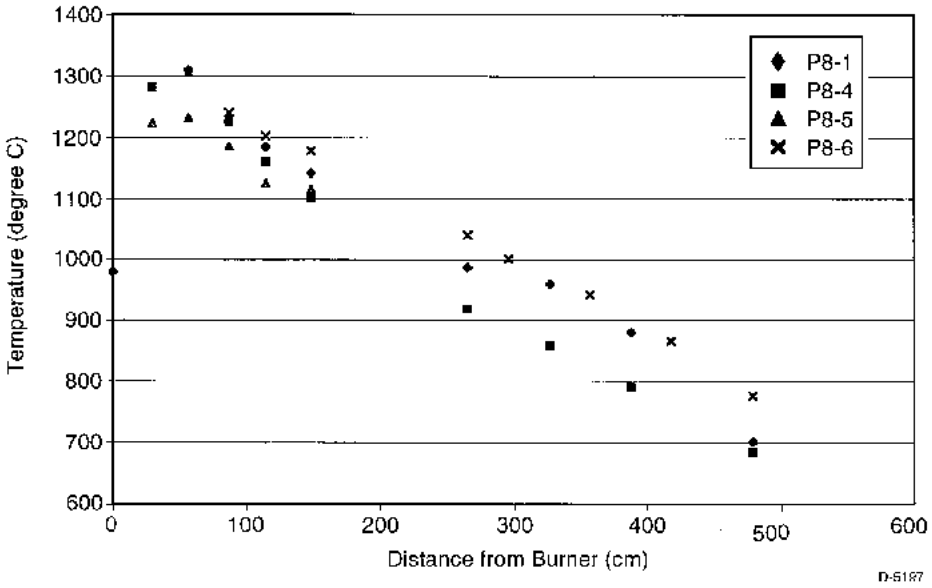

Figure 3-21. Steady state temperature profile for the Pittsburgh coal (UA laboratory combustor, SR=1.2).

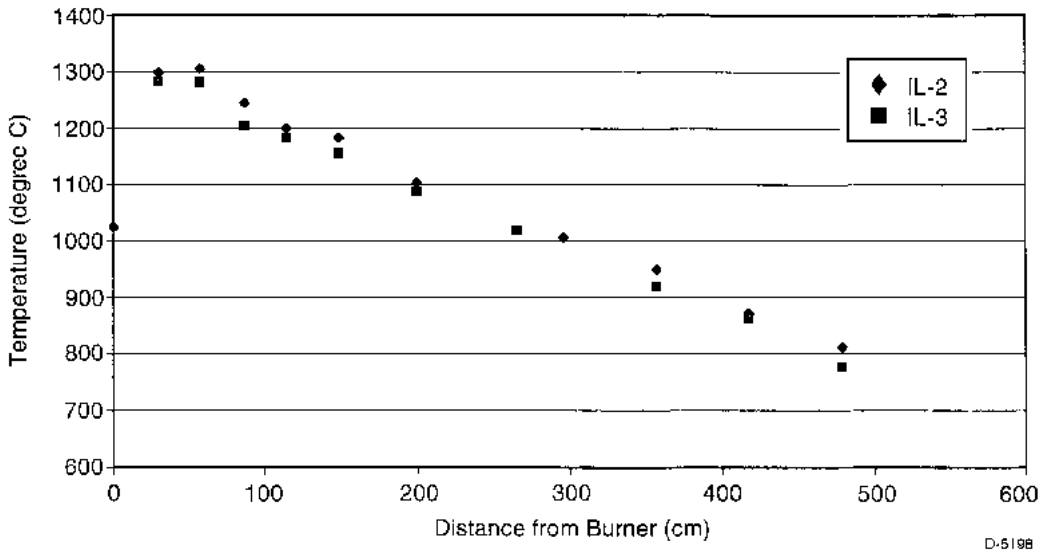

Figure 3-22. Steady state temperature profile for the Illinois No. 6 coal (UA laboratory combustor, SR=1.2).

Table 3-9. Summary of the Normalized Particle Size Distributions for Four Runs from Pittsburgh Coal (as Mass Fractions)

Impactor Stage	Run 9 (4b)	Run 11 (4b)	Average	Std Dev.	Run 10 (12)	Run 12 (12)	Average	Std Dev.
11	0.112174	0.064589	0.088381	0.033648	0.109563	0.042129	0.076	0.048
10	0.484779	0.389733	0.437256	0.067207	0.188224	0.67659	0.432	0.345
9	0.079228	0.137251	0.108239	0.041028	0.222872	0.071619	0.147	0.107
8	0.096485	0.25762	0.177053	0.11394	0.218189	0.039882	0.129	0.126
7	0.072168	0.086607	0.079388	0.01021	0.132974	0.048027	0.091	0.060
6	0.149565	0.049909	0.099737	0.070467	0.082406	0.046061	0.064	0.026
5	0.001712	0.005539	0.003625	0.002706	0.014544	0.023181	0.019	0.006
4	0.002594	0.004034	0.003314	0.001019	0.013689	0.010644	0.012	0.002
3	0.000415	0.002051	0.001233	0.001157	0.006844	0.012063	0.009	0.004
2	0.000882	0.001231	0.001056	0.000247	0.0077	0.019633	0.014	0.008
1	0	0.001436	0.000718	0.001015	0.002994	0.010171	0.007	0.005

Table 3-10. Summary of the Normalized Particle Size Distributions for Seven Runs from Illinois #6 Coal (as Mass Fractions)

Im-pactor Stage	Run 1 (4b)	Run 3 (4b)	Run 5 (4b)	Avg.	Std Dev.	Run 2 (12)	Run 4 (12)	Run 6 (12)	Run 7 (12)	Avg.	Std Dev.
11	0.146753	0.152064	0.234353	0.178	0.049	0.067051	0.070476	0.327818	0.121559	0.147	0.123
10	0.278192	0.332288	0.517822	0.376	0.126	0.244456	0.594528	0.375624	0.637671	0.463	0.185
9	0.165894	0.229035	0.087005	0.161	0.071	0.243059	0.075897	0.122932	0.071081	0.128	0.080
8	0.230976	0.086357	0.071569	0.130	0.088	0.12572	0.03072	0.044392	0.043267	0.061	0.044
7	0.104641	0.127659	0.054729	0.096	0.037	0.18439	0.128302	0.080247	0.066961	0.115	0.053
6	0.063806	0.060075	0.022453	0.049	0.023	0.079623	0.048791	0.030733	0.041207	0.050	0.021
5	0.005985	0.004729	0.003376	0.005	0.001	0.013246	0.019921	0.005241	0.005241	0.011	0.007
4	0.001948	0.005079	0.00647	0.004	0.002	0.012793	0.009325	0.002892	0.002892	0.007	0.005
3	0.000998	0.002715	0	0.001	0.001	0.006227	0.008477	0.003795	0.003795	0.006	0.002
2	0	0	0.001547	0.001	0.001	0.006453	0.009325	0.002711	0.002711	0.005	0.003
1	0.000808	0	0.000675	0.000	0.000	0.016982	0.004238	0.003615	0.003615	0.007	0.007

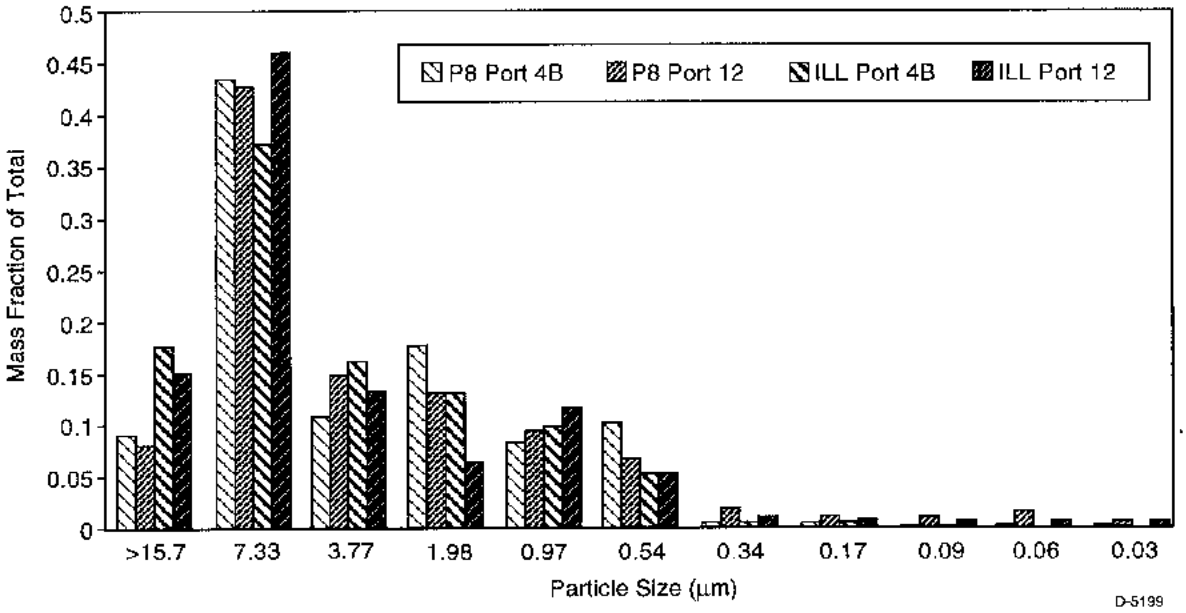

Figure 3-23. Ash particle size distributions for Illinois No. 6 and Pittsburgh coals (UA laboratory combustor, SR=1.2).

3.4.5 *Chlorine Partitioning*

Previous laboratory experiments can provide guidance on the most likely chemical pathways for gaseous elemental mercury as the flue gases in a coal-fired power plant cool. In a laboratory study,[5] a small continuous flow reactor was used for kinetic investigations of the reactions of gas-phase mercury with flue gas constituents. The results show that elemental mercury is oxidized by HCl and Cl_2, by NO_2, and by O_2 in the presence of activated carbon. Laboratory experiments have also demonstrated the reduction of oxidized mercury back to elemental mercury by reaction with SO_2 and CO as well as steel surfaces. At this point, it is impossible to say how important reduction reactions are in a full scale system.

The reaction of elemental mercury with HCl is fast above 700 K (800ºF) and seems to proceed slowly (if at all) below 600 K (600ºF). There is no obvious reaction pathway for the gas-phase oxidation of $Hg_{(g)}$ by HCl. The ones identified as candidates are complicated--they probably involve many elementary steps which are not known.[5] All this implies that attaining equilibrium when both HCl and Hg are present in trace concentrations may require a very long time. Indeed, there is evidence from laboratory and pilot data that the kinetics of Hg oxidation by HCl are slow at low temperatures. Based on pilot data, the addition of HCl to coal combustion flue gas at temperatures below 450 K (180°C) did not increase the amount of Hg^{+2} in coal combustion flue gas, indicating no reaction at those temperatures.[6]

On the other hand, the gas-phase reaction of Hg with Cl_2 is fast, even at 283 K (50°F). The reaction is probably a bimolecular reaction. In the continuous flow reactor previously cited,[5] as little as 2 ppm Cl_2 was sufficient to oxidize half the elemental Hg in about 1 s (starting with a mercury concentration of 0.012 ppm). At high concentrations of Cl_2 (>5 ppm), the Hg was

almost completely oxidized in 1 s at temperatures in the range of 493 to 973 K. The authors speculated that, at low temperatures, gas-solid reactions are important to the oxidation of Hg by Cl_2 because of some difficulties in getting reproducible results with their mercury measurement cell.

The formation of Cl_2 in the gas phase is thermodynamically favored at low temperatures. For example, the equilibrium calculations carried out in Quarterly Report No. 4 on the four program coals predict that 30 to 60% of the chlorine to be Cl_2 at 423 K. However, the formation of Cl_2 may be kinetically limited in the rapidly cooling flue gas which might reduce the gas-phase oxidation of elemental mercury relative to the equilibrium value.

Kinetic calculations were carried out using the CHEMKIN-II package using a typical time-temperature history from furnace exit to APCD inlet in a power plant. The effects of combustion stoichiometry and coal chlorine content were explored for a typical bituminous coal composition. A set of 264 reactions was used to model the chemical kinetics of major species containing the elements H, O, N, C, and Cl. Figure 3-24 shows the time-temperature history used in the calculations and the results for a coal with 2000 ppm chlorine and a stoichiometric ratio of 1.25. These calculations show that only about 1% of the chlorine is converted to Cl_2 at the APCD inlet. Thus, the conversion of HCl to the more reactive Cl_2 seems to be kinetically limited in a power plant flue gas.

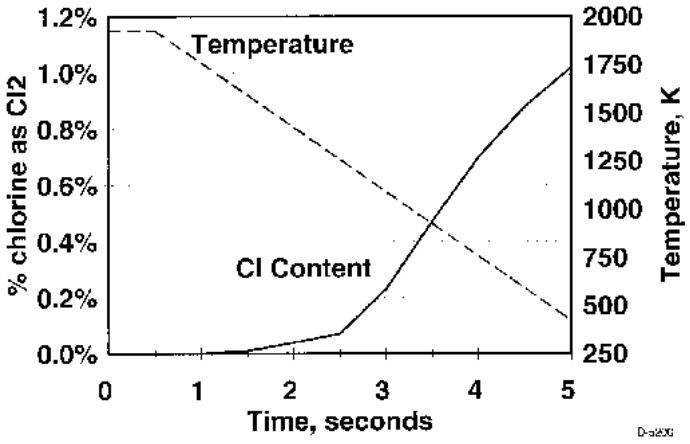

Figure 3-24. Gas temperature and predicted chlorine partitioning in a typical utility boiler.

As discussed above, thermochemical equilibrium is not reached in coal combustion flue gas. The flue gas in a coal-fired power plant cools rapidly as heat is transferred to water and steam. Since mercury is present in such trace amounts, mercury species may not have time to equilibrate as the gas cools, particularly because the major gas-phase oxidation reaction is with other trace species (HCl or Cl_2). Other trace species in the flue gas such as CO and SO_2 do not have time to equilibrate as the gas cools. For example, the oxidation of SO_2 to SO_3 in coal combustion flue gas does not proceed at a fast rate below about 1500 K[7] and thus the SO_3 concentration is effectively frozen below this temperature in the flue gas. Similarly for trace

species, present in ppm or ppb amounts, equilibrium may not be attained as the flue gas cools as demonstrated here by the results of kinetic calculations for chlorine in flue gas.

3.5 Literature Review (UConn, Princeton)

Under Task 7 of the program, field measurements of organic and trace element emissions from coal combustion are to be critically evaluated. The objective of this examination is the identification of areas in which our knowledge of trace element combustion chemistry is incomplete. In Phase I of this 5-year, two- phase program, the literature review and analysis will lead to (1) a comprehensive view of the state of knowledge obtainable from field measurements, and (2) identification of critical issues that need to be addressed in laboratory experimentation and modeling in the other program tasks. A subsequent extension of this task in Phase II will provide the basis for validation of the trace element transformation and emissions model being developed under Task 8 of this program. This section represents an interim summary of progress on Task 7 during the first year of the Phase I program.

3.5.1 *Review of the EPRI Field Study: Organic Emissions*

Summary of Report Findings

EPRI chose 16 substances for measurement in the field study, in accordance with two criteria: (1) the likelihood that the substances would be found in utility emissions (based on previous EPRI findings) and (2) the availability of toxicity factors. Of the chosen 16, the organic substances include: benzene, toluene, formaldehyde, polychlorinated dibenzodioxins and dibenzofurans (PCDD/PCDF), and polycyclic aromatic hydrocarbons (PAH).

As revealed in the EPRI Report,[8] the measured levels of each of these substances vary greatly from plant to plant, as illustrated in Figure 3-25 for benzene emissions from 22 coal-fired plants. Values range from 0.2 to 200 lb/10^{12} Btu, spanning 3 orders of magnitude. In the absence of any obvious correlation between emission level and plant type, the data are treated in statistical fashion. The geometric mean of 3.8 lb/10^{12} Btu is calculated, along with the 95% confidence interval, which lies between 1.6 and 8.8 lb/10^{12} Btu. It is important to realize that the "95% confidence interval" does not correspond to a range in which 95% of the measurements fall. As Figure 3-25 illustrates, 9 of the 22 measurements fall within the 95% confidence interval for benzene; six lie below, and seven lie above. The lowest measurement corresponds to approximately one-fifteenth of the geometric mean; the highest measurement, a factor of 40 times the geometric mean. It might be noted that a straight arithmetic mean of the benzene emissions measurements would yield a value of approximately 22 lb/10^{12} Btu, more than a factor of 5 higher than the geometric mean.

In the Report, the emissions measurements of each of the other organic substances are analyzed as in Figure 3-25, and the results are summarized in Table 3-11. PAH emissions and PCDD/PCDF emissions are reported as benzo[*a*]pyrene and *2,3,7,8*-tetrachloro-*p*-dioxin equivalents, respectively, after appropriate toxicity-based weightings were assigned to the various measured PAH and PCDD/PCDF species, as explained in the Report, Appendix B. As Table 3-11 reveals, the 95% confidence intervals for the other organics are at least as broad as that of benzene, so it follows that the measured levels of these substances also vary by orders of magnitude from plant to plant, though the values themselves are small.

The Report uses toxicity data and emissions factors (the geometric means of the emissions measurements) to calculate carcinogenic risks and noncarcinogenic inhalation hazards for maximally and reasonably exposed individuals (MEI and REI) living within 50 km of the 600 power plants. The risks and hazards due to all 16 selected emissions are summed, and the results for each plant type are illustrated in Figures 3-26 and 3-27. For all three types of coal plants — bituminous, subbituminous, and lignite — the contributions to carcinogenic risk (Figure 3-26) and to noncarcinogenic hazard (Figure 3-27) are included in the "other" category. As shown in these figures, organics are calculated to contribute < 2% of the total carcinogenic risk and < 5% of the total noncarcinogenic hazard of coal power plant emissions. The Report concludes that organic emissions from the 600 U.S. power plants do not constitute any health risks to

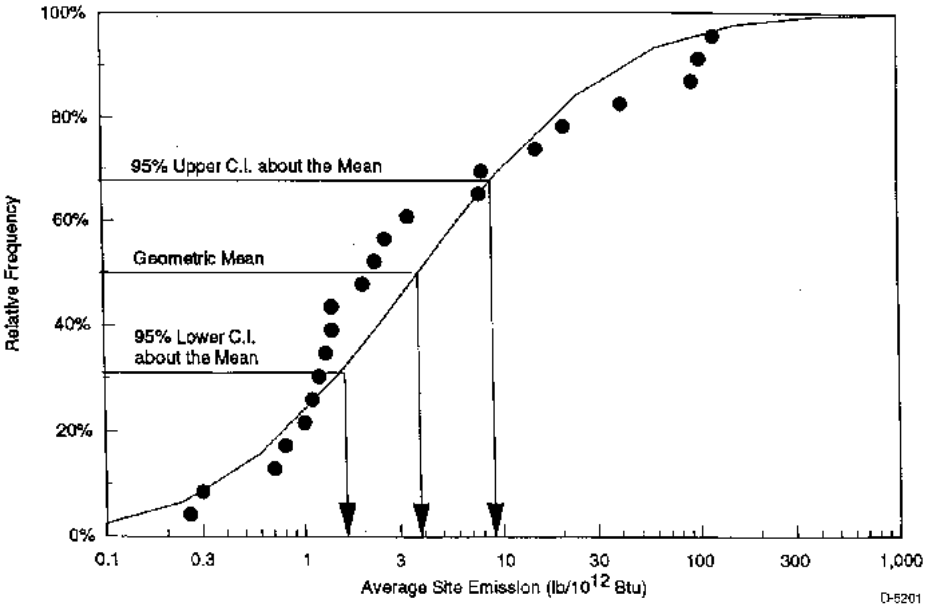

Figure 3-25. Distribution of benzene emissions factors for coal-fired units. (Figure B-17 from the Report)[1]

Table 3-11. Organic Substance Emission Factors for Coal-Fired Units, lb/10^{12} Btu (Table 3-5 from the Report[8])

Organic Substance/Class	Measurements	Geometric Mean	95% C.I.[a]
Benzene	23	3.8	1.6 to 8.8
Toluene	21	1.4	0.7 to 3
Formaldehyde	22	3	1.5 to 6
Benzo[*a*]pyrene equivalent	11	0.0018	0.0004 to 0.0082
2,3,7,8-tetrachloro-*p*-dioxin equivalent	9	2×10^{-6}	$(4 - 100) \times 10^{-7}$

[a] 95% confidence interval is about the geometric mean, not about all the data

humans: "Although uncertainty in organic compound emission factors is relatively high, neither carcinogenic inhalation risk estimates nor hazard index estimates are sensitive to these uncertainties for any plant type, due to the small contribution of organic compounds to cancer risk estimates and hazard index estimates." (EPRI Report,[8] p. 7-24).

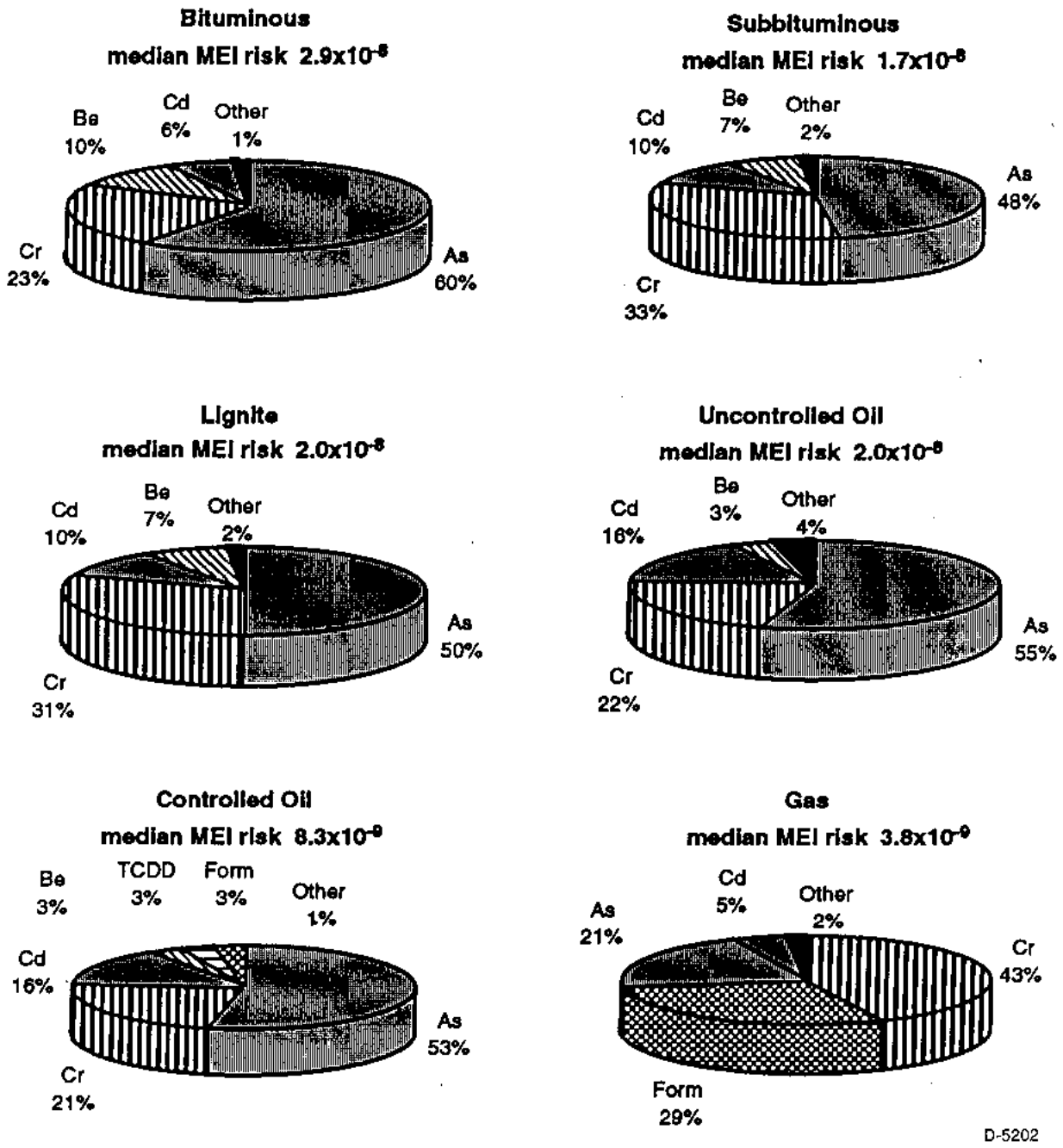

Figure 3-26. Contributions by individual substances to MEI inhalation carcinogenic risk, median plant by fuel type (Figure 7-4 from the Report).[8]

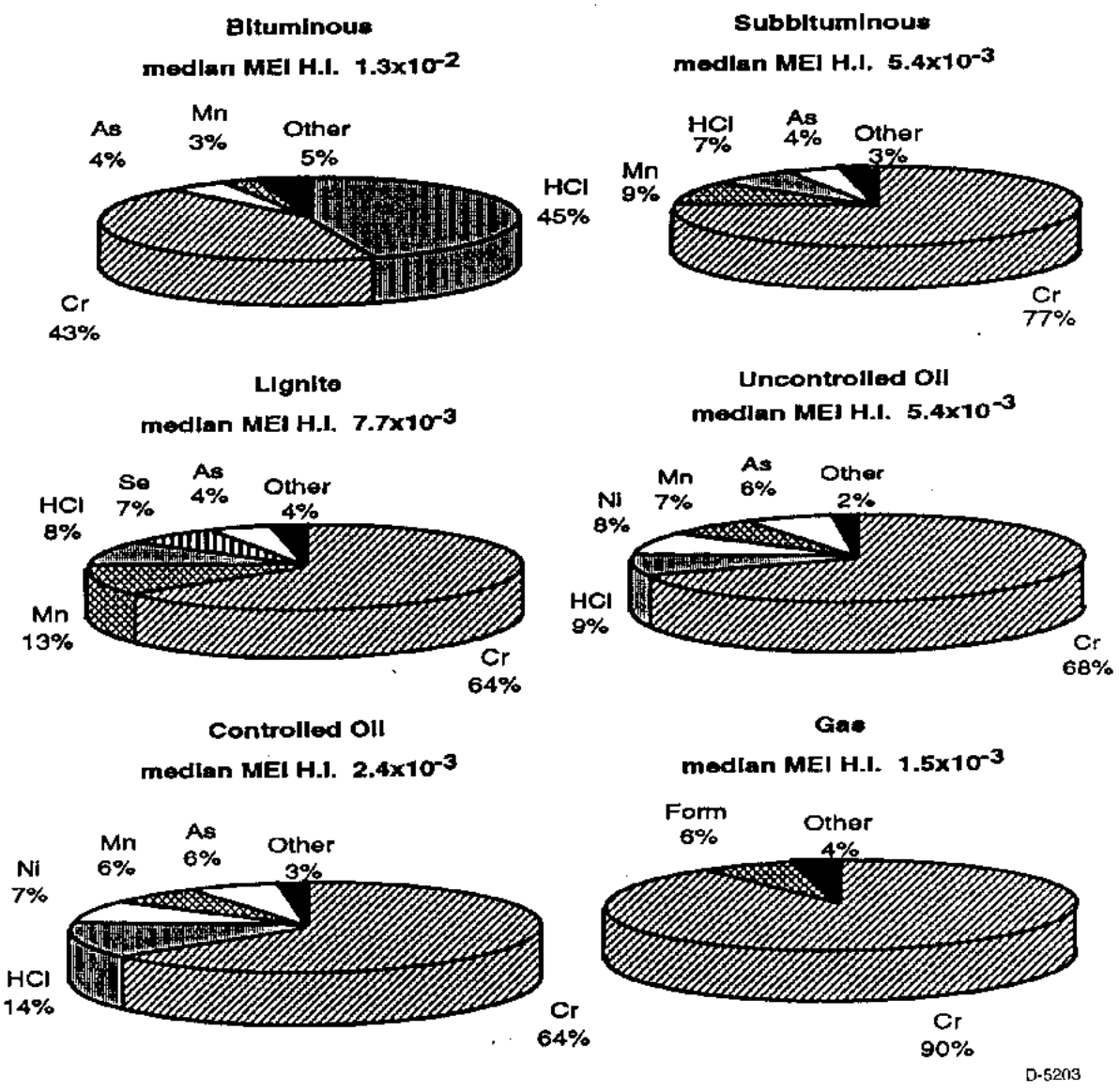

Figure 3-27. Contributions of individual substances to MEI inhalation hazard index (Figure 7-8 from the Report).[8]

Evaluation of Findings

In examining the results presented in the Report, it is necessary to consider the types of methods used in the emissions measurements. Aldehydes were collected by EPA Method 0011, converted to stable forms by treatment with dinitrophenylhydrazine, and the derivatives analyzed by high pressure liquid chromatography (HPLC). Volatile organics, including benzene and toluene, were sampled with an EPA Method 0030 sampling train, trapped by Tenax and charcoal sorbents, and analyzed by gas chromatography-mass spectrometry (GC-MS) with EPA Method 5041. PCDD/PCDF were sampled by a method similar to EPA Method 0011 and analyzed by EPA Method 23 with GC and high resolution MS. Semi-volatile organics, including PAH, were collected by EPA Method 0010 with a Modified Method 5 sampling train, trapped with a particulate filter and XAD-2 resin, and analyzed by GC-MS according to EPA Method 8270. Except for the aldehydes, therefore, all of the organics were analyzed by GC-MS.

In the following, we assess several aspects of the Report's results of organic emissions measurements: sample collection, analytical methods, species not included, and health effects. At the outset it should be noted that the power plant emissions testing program is an extremely ambitious undertaking, one of immense difficulty, particularly in view of the non-laboratory-like setting of the measurements. The proceeding comments, therefore, are not to be taken as criticisms but as guidelines for understanding the limitations of the reported measurements.

Sample Collection. First of all, it should be acknowledged that nine contracting companies participated in the plant measurements: Radian, SRI, Battelle, Weston, KVB, Acurex, Clean Air Engineering, Interpol, and Carnot. Even though the large scope of the field testing project may have necessitated the use of many contractors, it should be borne in mind that the multitude of contractors lends some variability to the data. Second, as stated in the Report (p. 2-1), the contractors employed the EPA-recommended methods for sampling, but some of the methods had not yet been validated for power plant streams, and others were being pushed to or beyond their limits. In several cases, low levels of organic species necessitated modification of collection techniques at the site so that detectable amounts of sample could be collected. The difficulty of obtaining quantifiable samples from extremely dilute streams is not to be overlooked. Third, errors can be introduced by the use of sorbents (e.g., Tenax) and resins (e.g., XAD-2) during sampling — either by irreversible retention of components or by the introduction of contaminants. Macroreticular resins used for sorption of PAH are particularly notorious for introducing artifacts.[9] Therefore, even though many species can be collected by the EPA methods used, other species may have escaped detection.

Methods of Analysis. The derivatization, extraction, and HPLC analysis procedure used for the measurement of the aldehydes appears to be sound. GC-MS — the method used for analyzing volatile organics, PCDD/PCDF, and semi-volatile organics — is an excellent method for the volatile organics such as benzene and toluene. It is limited in application for semi-volatile organics such as PAH, however, for three primary reasons: (1) Sample components have to be vaporized in the injector of the GC before they can get onto the GC column for separation. Some components, particularly less-volatile ones, can be trapped in the injector so that they are never put onto the GC column or detected among the separated products. (2) Some components,

particularly polar compounds, can be irreversibly retained by the GC column so that they too are never detected. (3) Differentiation of PAH isomers is very important since some are carcinogenic and others are not (e.g., benzo[*a*]pyrene and benzo[*e*]pyrene). In GC-MS, a compound is identified by its retention time and mass spectrum. For PAH, each family of isomers (e.g., $C_{20}H_{12}$) has the same mass spectrum, so identification of a particular isomer requires a unique retention time. This requirement is not that serious for PAH of less than five rings because the number of isomers is manageable and reference standards are available to enable one to determine the retention time of all isomers. However, GC-MS is not very reliable for analysis of PAH of greater than five fused rings since: (1) the number of isomers goes up exponentially with the number of rings comprising the PAH, and the availability of reference standards of these isomers goes way down and (2) PAH of > five rings are also not easily vaporized at the temperatures used in most GC injectors. Because of these various problems of GC analysis — injector trapping, irreversible retention on the column, indistinguishability between mass spectra of isomeric PAH, and lack of component vaporizability — sample components can either be missed or misidentified. It is thus extremely important to report mass balances on GC analyses: *What proportion of the mass of material injected into the gas chromatograph is actually accounted for in the identified products?*

Species Not Included. The Report gives emissions measurements of nine PAH — benz[*a*]anthracene, chrysene, benzo[*b*]fluoranthene, benzo[*j*]fluoranthene, benzo[*k*]fluoranthene, benzo[*a*]pyrene, dibenz[*a,h*]anthracene, indeno[*1,2,3-cd*]pyrene, and benzo[*ghi*]perylene — all of which are four-, five-, and six-ring species. Surprisingly absent are phenanthrene, fluoranthene, and pyrene, the three-and-four-ring species observed to be among the most abundant PAH measured from coal-burning power plants.[10-12] Early EPRI studies,[12, 13] however, had found these species to be associated with particulate matter, so in later work the EPRI contractors may not have looked for these compounds in the gas phase, if they has not been aware of the more recent work[14,15] linking these species with the gas phase. Since PAH emissions from coal are the products of pyrolysis reactions, it is reasonable to compare the identified nine PAH with PAH products from coal pyrolysis. Years of experience[16-20] in this field tell us that it is most unusual to have the nine specified PAH without a host of other product species in the sample as well. Figure 3-28, for example, shows an HPLC chromatogram of PAH from the pyrolysis of a low-rank coal.[20] In addition to the nine PAH identified in the Report, this chromatogram displays 41 other PAH — some of which have greater than five rings, partially hydrogenated rings, alkyl substituents, carbonyl groups, or cyclopenta-fused rings. It should be noted that some of the species identified in Figure 3-28 — *e.g.*,benzo[*ghi*]fluoranthene, cyclopenta[*cd*]pyrene, and naphtho[*2,1-a*]pyrene — have mutagenicities significantly greater than that of benzo[*a*]pyrene,[21,22] so omission of such species can lead to incomplete or misleading conclusions about health effects. The fact that the Report gives measurements of only nine PAH—none of which have greater than six rings, substituent groups, or cyclopenta-fused rings — is most probably a consequence of the GC-MS analytical methods used. Once again underlined is the importance of knowing what proportion of the sample mass is accounted for in the products measured by GC-MS.

It should also be noted that aromatic compounds having nitro substituent groups; N, S, or O ring heteroatoms; and oxygen-containing functionalities are also not included in the Report's

results. If present, these species — particularly the highly mutagenic nitro-PAH[23-31] and PAH with ring nitrogen[32-39] — could also have impact on the health effects assessment. Nitro-PAH have been measured from other coal combustors.[10,26,40] Other coal-derived "organics" not mentioned in the Report are soot and unburned carbon associated with fly ash.

Health Effects. The Report assesses the health effects of organic emissions from power plants, using toxicity information and measured emissions levels of aldehydes, benzene, toluene, PCDD/PCDF, and nine particular PAH. A number of other organic species that could be present, however, are never mentioned. Since it is the objective of the Report to evaluate health effects of plant emissions, it is most important that there be an accounting of the strongly biologically active compounds such as nitro-PAH, PAH with ring nitrogen, and species such as cyclopenta[*cd*]pyrene and naphtho[*2,1-a*]pyrene, which are more mutagenic than benzo[*a*]pyrene. If these species have been specifically searched for by appropriate analytical techniques, then the documentation of the tests confirming the absence of these compounds needs to be presented. If it is the case, however, that steps have not been taken to measure these biologically active species, then it remains indeterminate whether the organic emissions from power plants do or do not pose a health concern. Of critical importance are mass balances on the sample collection and sample analysis processes: *What percentage of the organics produced are collected, and what percentage of the mass collected is accounted for in the identified products?*

Key Questions

In order to address some of the uncertainties that the above evaluation raises, we have formulated the set of questions listed below.

1. In the sampling from the power plants, what tests were conducted to ensure that the sampling methods did indeed pick up all the organic emissions and that none could get by the sampling system without being trapped?

2. Of the total organic mass that was collected during the sampling from the plants, what proportion is actually accounted for by the particular organic products whose identities and quantities are given in the reports? The EPRI Synthesis Report gives measurements of benzene, toluene, formaldehyde, nine particular PAH, and a number of PCDD/PCDF. Is there documentation that verifies that these particular organic compounds account for the whole of the organic samples collected? If so, what methods were used to make the determination? Were these methods capable of detecting and quantifying classes of organic compounds other than the particular ones reported? If these particular species do not account for the whole of the organic mass collected, on what basis were other organics excluded from consideration?

3. Apparently in the EPRI study, some early "screening" runs were conducted to establish which organic species were measurable and which were below detection limits. Were these results or similar ones used as screening guidelines in the DOE study, and if so, are

the results from these screening runs available? What methods were used to determine which species would be targeted and which would be below detection limits?

4. During the gas chromatographic analyses of the organic samples, were mass balances conducted to show (1) that all mass injected was in fact vaporized in the injector so that it could all get onto the GC column for analysis and (2) that there were no peaks in the chromatograms corresponding to species other than those identified and quantified in the Report? Are the actual chromatograms available for examination?

These questions have been shared with EPRI and DOE, who sponsored the field emissions studies, and both organizations have responded very helpfully by sharing additional reports and providing access to further data and information. We will be working together in the coming period of time to answer the above questions and others that may arise on organic emissions.

3.5.2 *Field Data Review: Inorganic Species Emissions (Trace Elements)*

Approach for Analysis of Trace Element Data in Literature

The data being considered under this task are measurements of the following parameters made at operating full scale coal-fired power stations. The term 'full scale' is meant to include any central station electric power generation facility burning pulverized coal.

a) Trace element concentrations in the fly ash as a function of ash particle size.
b) Corresponding data for trace element concentration in the parent coals.
c) Trace element emissions for different types of air pollution control equipment.

At the start of the program in November 1995, two major sources of such data were identified. The first was the Electric Utility Trace Substances Synthesis Report,[8] published by the Electric Power Research Institute (EPRI) of Palo Alto, CA, in November 1994. The emissions data described in the EPRI report were obtained during the EPRI program Power Plant Integrated Systems: Chemical Emissions Study (PISCES). In the remainder of this report, the terms 'PISCES' and 'PISCES data' are used to identify the Synthesis Report. The other major source of trace element field data was a recently completed Department of Energy (DOE) led study of eight different US power plants. Although the DOE Summary Report was not yet available at the start of work on Task 7 (January 1996), the individual contractor reports for each facility were available.

Additional data identified at the outset of this program were those published by the utility KEMA in the Netherlands describing a measurements made in their boilers, and data available from the VTT Aerosol Technology Group of Espoo, Finland for several different European boilers. Subsequent to the start of our work, additional data from a British power station and a Spanish power station were published in the open literature.

Work described in this interim report includes an assessment of the EPRI PISCES data, preliminary evaluation of the DOE data, and evaluation of the recent British and Spanish data.

Summary of Results

The PISCES dataset provides a comprehensive examination of trace element chemistry at over 40 U.S. sites. In the PISCES study, coal rank, ash content, sulfur content, trace element concentrations, coal higher heating value, trace element emissions rate, and particulate matter emissions rate were all determined. From this dataset, the operating efficiency of air pollution control devices, both in collecting particulate matter and in removing trace elements from the stack gases can be determined. By calculating both of these parameters, it is possible to determine whether an individual trace element is collected more efficiently than the particulate matter, less efficiently than the particulate matter, or with the same efficiency as the particulate matter. This calculation was undertaken as the first task in the review of the PISCES dataset.

The particulate collection efficiency of an air pollution control device is defined as

$$\eta = \frac{PM_{in} - PM_{out}}{PM_{in}} \tag{3-7}$$

where PM_{in} is the particulate matter concentration at the inlet of the air pollution control device (mass per unit energy content of the as-fired fuel, e.g. [lb/MBtu]) and PM_{out}, the particulate matter concentration at the device outlet (same units). This can be rearranged to

$$PM_{out} = PM_{in} (1 - \eta) = \frac{f_a (1 - \eta)}{H} \tag{3-8}$$

where f_a is the ash content of the coal on an as-fired basis (mass/mass, e.g. [lb/lb]) and H is the higher heating value of the coal (energy content per unit mass, e.g., [Btu/lb]).

For any trace element *I* present in the coal, the emissions E_i (mass per unit energy content of the as-fired fuel, e.g., [lb *I* / MBtu]) can be determined from

$$E_i = A_{i,in} (1 - \eta_i) = \frac{C_i (1 - \eta_i)}{H} \tag{3-9}$$

where $A_{i,in}$ is the concentration of the trace element in the gas stream entering the air pollution control device (mass per unit energy content of the as-fired fuel), C_i is the concentration of the trace element in the coal (mass/mass), and η_i is the capture efficiency of trace element *I* in the air pollution control device, defined by an expression analogous to Eq. (3-1). Combining Eqs. (3-2) and (3-3), an expression for trace element emissions as a function of coal parameters and air pollution control device efficiency is obtained,

$$E_i = \frac{C_i \, PM_{out} \, (1 - \eta_i)}{f_a \, (1 - \eta)} \qquad (3\text{-}10)$$

Measurements of E_i, C_i, PM_{out}, and f_a were all made as part of the PISCES data sets. A plot of E_i v. ($C_i \, PM_{out} / f_a$) should therefore pass through the origin and be linear with slope equal to $(1 - \eta_i) / (1 - \eta)$. For trace elements that are captured with greater efficiency than the corresponding fly ash, the slope will be less than one, a result of η_i being greater than η. If the efficiency of trace element capture is identical to the efficiency of particulate capture, the slope will equal one.

The above analysis implicitly assumes that the relationship between trace element capture efficiency and particulate capture efficiency is not dependent upon the type of air pollution control equipment. Analysis of trace element emissions data grouped by type of air pollution control equipment can be used to test this assertion. Further, if the partitioning of trace elements among the vapor phase and fly ash particles of different sizes is *not* consistent from furnace to furnace, then poor correlations (Eq. (3-10)) would be obtained for any grouping of data. Under this latter scenario, the emissions from any facility are dependent upon the fate of the trace element during combustion. A poor correlation (Eq. (3-10)) is therefore indicative of poorly understood trace element combustion transformations. This reasoning is summarized in Table 3-12.

Table 3-12. Data Interpretation

Slope (Eq. (4))	R^2	Interpretation
1	Close to 1	Trace element capture equal to particulate capture
> 1	Close to 1	Trace element capture less than particulate capture
< 1	Close to 1	Trace element capture greater than particulate capture
–	Close to 1 when identical APCD considered	Type of APCD affects trace element capture
–	Far from 1	Trace element capture cannot be predicted from particulate capture. Concentration of trace element in vapor and in ash as f(dp) dependent upon mineralogical and combustion parameters

In the original analysis of the PISCES data, an equation of the form

$$E_i \approx a_i \left[\frac{C_i\ PM}{f_a}\right]^b \qquad (3\text{-}11)$$

was used in correlating the emissions data.[8] This is identical to Eq. (3-10) when the exponent b_i is equal to 1.

The results of using Eqs.(3-10) and (3-11) to fit the PISCES data are summarized in Table 3-13. In generating Table 3-13, the entire set of available data was used for each element. For some elements, the database can be expanded by including those points for which the concentration of the element in the coal, C_i, was the only missing parameter. For those samples, an estimated concentration C_i can be determined from the rank average value of the concentration for that element in coal of the indicated rank, using only those values less than the reported detection limit for the site in question. These additional points expanded the database for several elements as indicated in Table 3-13. Regardless of the size of the database, Eq. (3-11) provided a better fit to the data than did Eq. (3-10) for 10 of the 11 elements considered. This is further reflected in the values of the exponent b_i not equaling 1 as shown in the table, suggesting that the combustion transformations of trace elements are dependent upon mineralogical and combustion parameters.

Based on the results of the field data analysis, recommendations regarding bench-scale fundamental study of the combustion transformations and capture of individual elements were made. The resulting prioritization is shown in Table 3-14.

Element-Specific Discussion

Antimony (Sb)

No correlation was noted between the stack concentration Ei of antimony and the parameter (C_iPM/f_a) (Eq. (3-10)). The corresponding value of r^2 was determined to be 0.15 for the nine sites for which complete datasets were available. When the database is expanded to include sites for which the antimony concentration in the coal was estimated, four additional sites can be added (Table 3-15). Addition of these datasets does not change the lack of correlation with the group (C_iPM/f_a), however. In Figure 3-28, antimony emissions data (including the four additional points) are broadly scattered, with no trends apparent. Using the empirical approach described in the original analysis of the data (Eq. (3-11)), an r^2 correlation coefficient of 0.65 was reported by EPRI. Data from these nine sites plus the four others for which coal antimony concentrations were estimated are plotted in Figure 3-29.

Table 3-13. Data Correlation with Eqs. (3-10) and (3-11)

Element	R^2 (Eq.(3-10))	Slope (Eq. (3-10))	Intercept	Data Pairs	R^2 (Eq. (3-11))	a_i	b_i	N#
Sb	0.15 0.05	0.15 0.11	1.00 1.06	9 13	0.65	0.92	0.63	8
As	0.20 0.20	3.53 3.50	11.6 11.0	36 34	0.72	3.1	0.85	34
Be	0.74	1.23	0.116	17	0.83	1.2	1.1	17
Cd	0.02 0.01	-0.09 0.07	2.59 1.43	11 30	0.78	3.3	0.5	9
Cr	0.26	0.95	5.84	37	0.57	3.7	0.58	38
Co	0.28 0.28	0.80 0.80	2.09 2.14	18 20	0.57	1.7	0.69	20
Pb	0.80 0.80	5.54 5.50	-3.77 -3.13	33 34	0.62	3.4	0.80	33
Mn	0.38 0.38	1.04 1.27	1.80 1.80	37 38	0.57	3.8	0.60	37
Hg	0.003 0.004	3.94 4.77	6.18 6.02	32 34	---	---	---	---
Ni	0.073 0.079	16.6 14.0	1.42 1.41	27 35	0.51	4.4	0.48	25
Se	0.05 0.05	14.9 14.4	75.4 78.5	29 34				

Table 3-14. Conclusions Regarding Relative Need for Bench-Scale Investigations

High Priority	Middle Priority	Low Priority
As Hg Se	Cd Sb Cr Ni Pb	Be Mn Co

Table 3-15. Number of Datasets per Element

Element	Number of Datasets	Number of Datasets when Coal Concentration Non-detect Replaced with Rank Average Value
Sb	9	13
As	34	36
Be	17	17
Cd	11	30
Cr	37	37
Co	18	20
Pb	33	34
Mn	37	38
Hg	32	34
Ni	27	35
Se	29	34

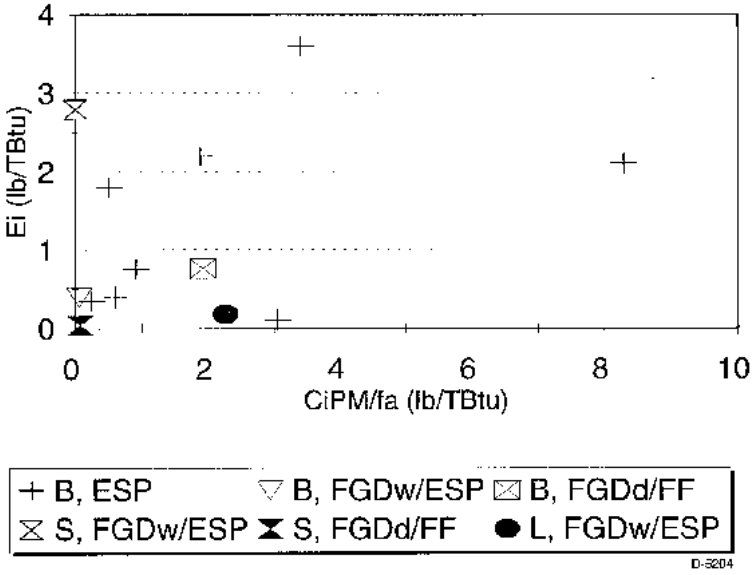

Figure 3-28. Antimony emissions data versus C_iPM/f_a.

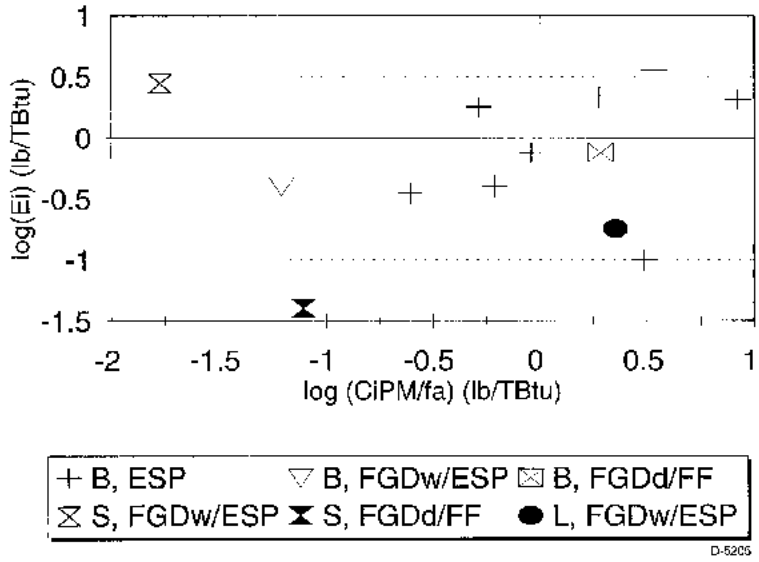

Figure 3-29. Antimony emissions data plotted on log-log coordinates (empirical fit).

Because of the small number of datasets (nine sites) and the large amount of scatter in the data, caution must be exercised in extrapolating these results for the purpose of estimating emissions at other sites or with other coals. The large amount of scatter also suggests that the partitioning of antimony among ash particles of different size classes is highly variable. The lack of apparent trends with coal rank or antimony concentration suggest that antimony transformations and partitioning in a combustion environment are not well understood. It is therefore recommended that antimony transformations under combustion conditions be further studied at the bench scale (see Table 3-14).

The complete tabulation of the antimony data used in preparing these figures is provided in Appendix B.

Arsenic

No correlation was noted between the stack concentration E_i of arsenic and the parameter (C_iPM/f_a) (Eq. (3-10)). The corresponding value of r^2 was determined to be 0.20 for the 36 sites contained in the database (including three for which the rank average value of the concentration of arsenic in the coal was used). In Figure 3-30, arsenic emissions data (including the three additional points) are scattered, although there is clustering of the data near the origin of the plot. Using the empirical approach described in Eq. (3-11), an r^2 correlation coefficient of 0.72 was reported by EPRI (34 datasets). In all cases, the intercept (concentration at which E_i equal to zero) was calculated from the regression analysis.

The database for arsenic is sufficiently large to permit consideration of subsets containing data for specific coal rank or type of air pollution control device. These trends are reported in Table 3-16. A strong correlation is seen for the seven sites employing fabric filtration as the method of air pollution control. A speculative explanation for this observation is that certain size

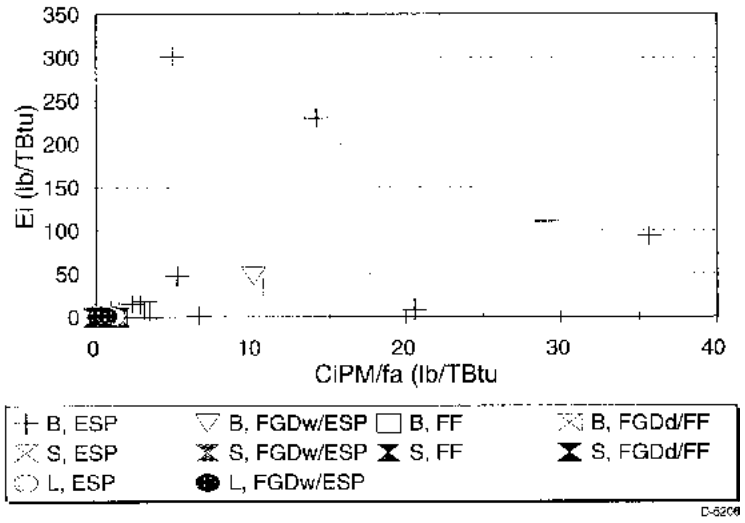

Figure 3-30. Arsenic emissions data versus C_iPM/f_a.

Table 3-16. Correlation of Arsenic Datasets Using Eq. (3-10)

Dataset	r^2	Slope	Intercept	# Sites
All data	0.20	3.53	11.0	36
Bituminous	0.14	3.04	20.8	23
Sub-bituminous	0.07	0.56	0.58	9
Lignite	0.14	1.26	0.89	4
ESP, ESP/FGD_w	0.18	3.35	14.9	29
FF, FF/FGD_d	0.92	2.65	-0.17	7

classes of ash particles are enriched in arsenic; further, these size classes are more effectively captured by systems using fabric filtration. This is consistent with observed high particulate capture efficiency for fabric filters (average of 0.999 for the 11 sites reporting data in this study) and potential enrichment of arsenic in the smallest particulate, a phenomenon which has been documented in field and laboratory measurements.[41-43] These results suggest that bench scale study of the combustion transformations of arsenic be accorded a high priority in the remainder of this program.

The complete tabulation of the arsenic data used in preparing these figures is provided in Appendix B.

Beryllium

Beryllium emissions data were linearly correlated with (C_iPM/f_a) with a correlation coefficient of 0.74 obtained for the full group of 17 sites. There were no sites for which the coal concentration was reported below the detection limit. This compares favorably with the regression coefficient of 0.83 reported by EPRI in its analysis of the data using the empirical relation of Eq. (3-11). These trends are shown in Figures 3-31 through 3-33. From these results, it can be concluded that beryllium is not enriched in smaller particles which may be more difficult to capture. Rather, the correspondence between beryllium capture and particulate capture, and the lack of any trend with coal rank or air pollution control device (see Appendix B) suggests that beryllium is concentrated in ash particles greater than 1 or 2 µm in size. Because of this, it is recommended that fundamental study of beryllium be accorded a relatively low priority in the remainder of this fundamental program. The complete tabulation of beryllium data used in preparing these figures is provided in the Appendix B.

Cadmium

As shown in Figures 3-34 and 3-35, no correlation was noted between the stack concentration E_i of cadmium and the parameter (C_iPM/f_a) (Eq. (3-10)). The corresponding value of r^2 was determined to be 0.02 for the 11 sites contained in the database. Addition of the 19 sites for which the rank average value of the concentration of cadmium in the coal was used did not improve the correlation. In Figure 3-32, cadmium emissions data (including the additional points) are scattered, with most of the data clustered near the origin. Using Eq. (3-11) as described in the original analysis of the data, an r^2 correlation coefficient of 0.78 was reported by EPRI (nine datasets); it is unclear which two datasets included here were not included in the

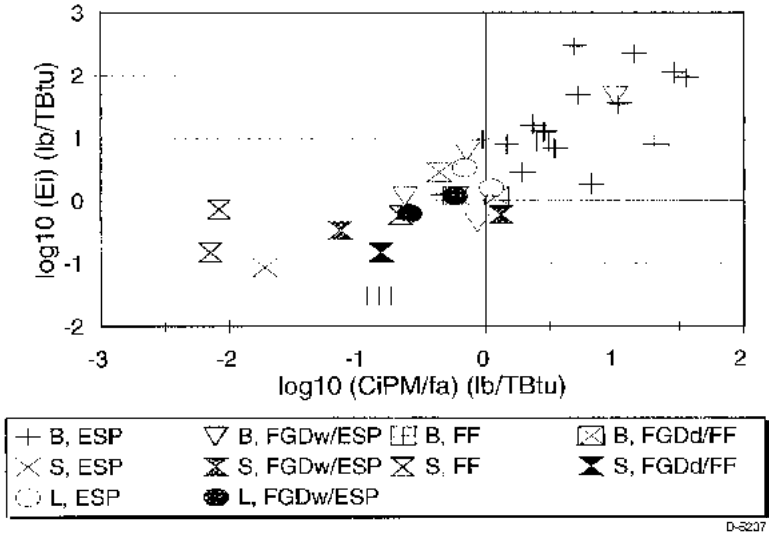

Figure 3-31. Arsenic emisions data plotted on log-log coordinates (empirical fit).

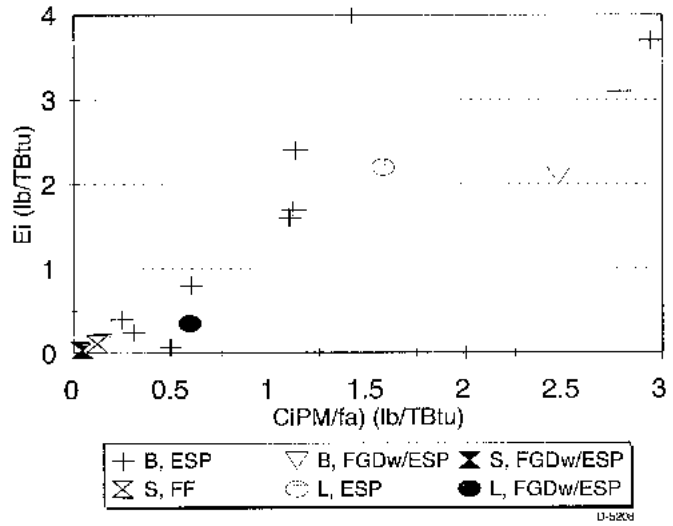

Figure 3-32. Beryllium emissions data versus C_iPM/f_a.

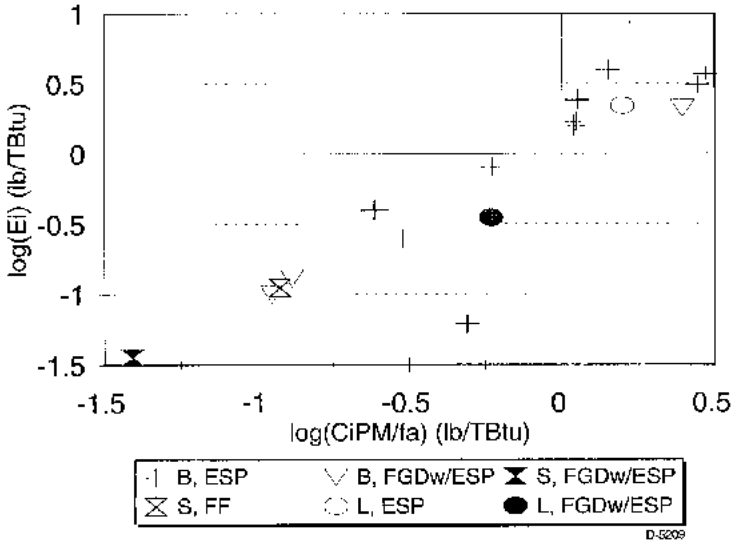

Figure 3-33. Beryllium emissions data plotted on log-log coordinates (empirical fit).

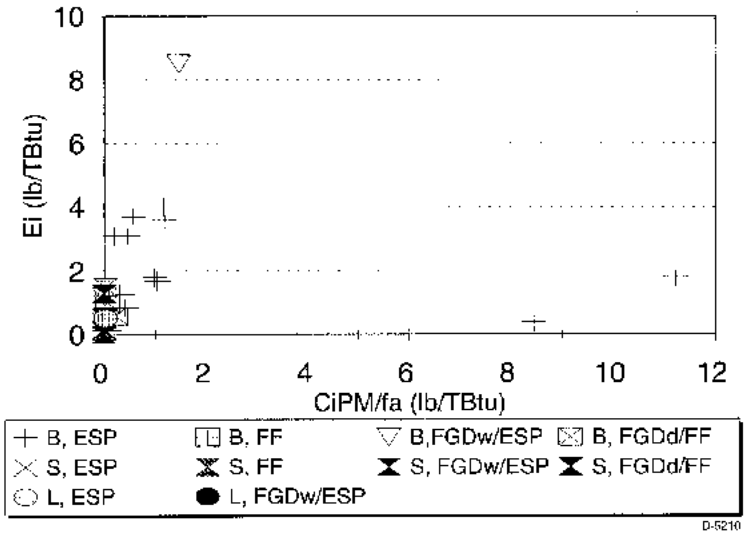

Figure 3-34. Cadmium emissions data versus C_iPM/f_a.

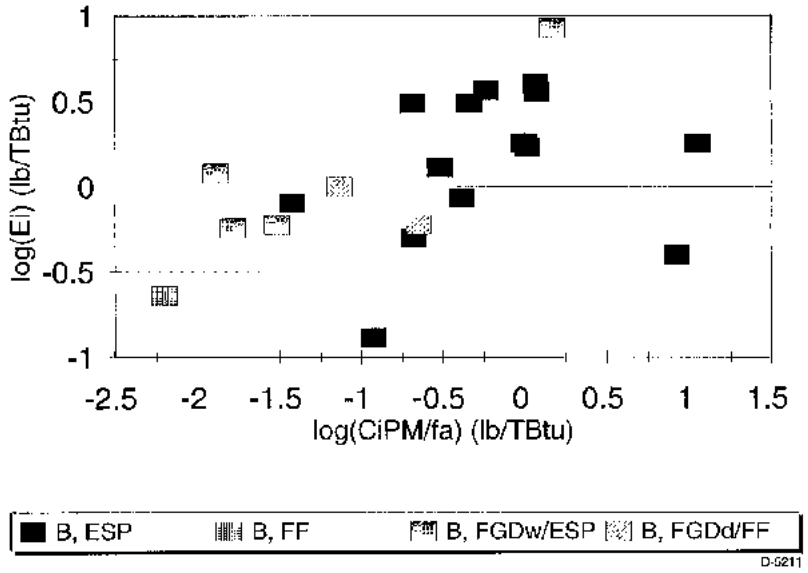

Figure 3-35. Cadmium emissions data plotted on log-log coordinates (empirical fit).

EPRI analysis. Association of cadmium with calcium in the ash of a sub-bituminous coal has been reported in another field study;[41] no evidence for enhanced capture of cadmium by calcium rich sub-bituminous coal ash was seen in the PISCES data. The Querol et al. findings do suggest that ash chemistry may have some effect on cadmium emissions; for this reason, it is recommended that examination of cadmium be accorded a middle priority in the remainder of this program.

The complete tabulation of the cadmium data used in preparing these figures is provided in Appendix B.

Chromium

Chromium emissions were uniformly low, falling well below 40 lb/TBtu for most sites. No correlation was noted, however, between the stack concentration E_i of chromium and the parameter (C_iPM/f_a) (Eq. (3-10)). The corresponding value of r^2 was determined to be 0.26 for the 37 sites contained in the database. The scatter in chromium emissions data can be seen more clearly in Figures 3-36 and 3-37, with Figure 3-36 presenting the data as a function of (C_iPM/f_a), sorted according to coal rank and air pollution control device type, and Figure 3-38 presenting the same data sorted only according to coal rank. Using Eq. (3-11), an r^2 correlation coefficient of 0.57 was reported by EPRI. High capture efficiencies noted for chromium (0.99 average) indicate that fractional chromium emissions will be low relative to the fractional emissions of other trace elements; issues associated with oxidation state-specific toxicity (Cr (VI)) warrant further study, however. It is therefore recommended that further study of chromium transformations focus on speciation, and be afforded a middle range prioritization. The complete tabulation of the chromium data is provided in Appendix B.

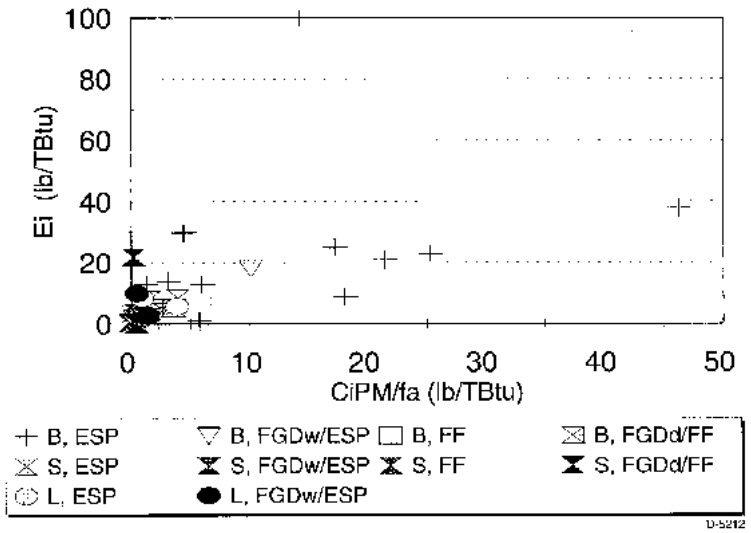

Figure 3-36. Chromium emissions versus C_iPM/f_a sorted according to rank and APCD types.

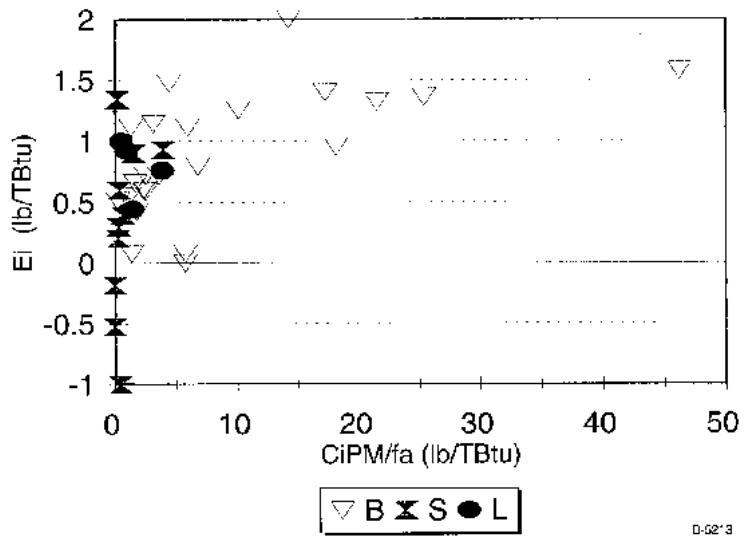

Figure 3-37. Chromium emissions data versus C_iPM/f_a sorted according to coal rank.

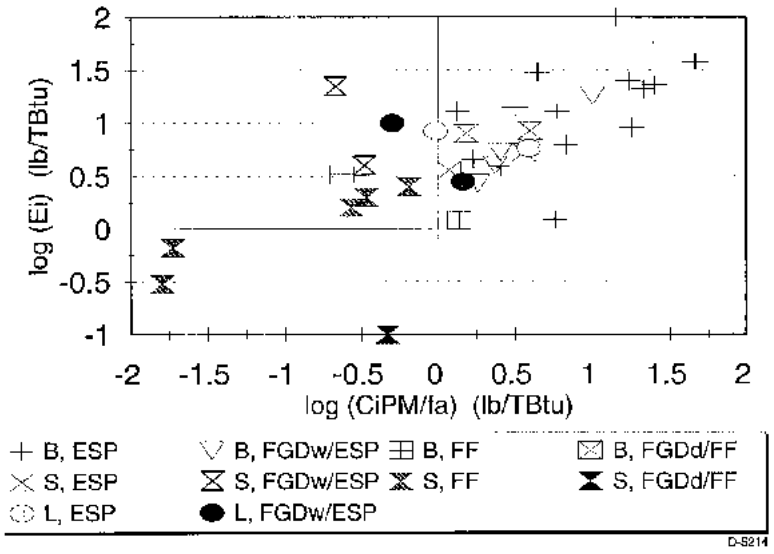

Figure 3-38. Chromium emissions data plotted on log-log coordinates (empirical fit).

Cobalt

Cobalt emissions were also uniformly low, falling well below 10 lb/10^{12} Btu for most sites. No correlation was noted between the stack concentration E_i of cobalt and the parameter (C_iPM/f_a) (Eq. (3-10)). The corresponding value of r^2 was determined to be 0.28 for the 20 sites contained in the database. The scatter in cobalt emissions data can be seen more clearly in Figure 3-39, which presents emissions data as a function of the term (C_iPM/f_a). Using Eq. (3-11), an r^2 correlation coefficient of 0.57 was reported by EPRI. In a recent field study, Querol et al.[41] presented cobalt concentration data that correlated with $1/d_p^2$, suggesting a mechanism of vaporization and surface condensation.[44] Because of the low levels of emissions observed in the EPRI data, however, it is recommended at this time that further study of cobalt be afforded a relatively low priority.

The complete tabulation of the cobalt data is provided in Appendix B.

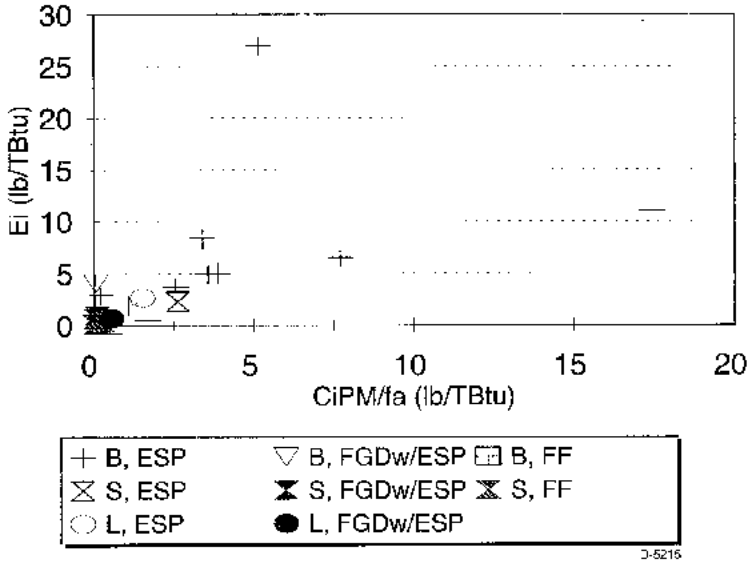

Figure 3-39. Cobalt emissions data versus C_iPM/f_a.

Lead

Lead emissions were correlated with the parameter (C_iPM/f_a) (Eq. (3-10)) with an r^2 value of 0.80 (34 datasets) (Figures 3-40 and 3-41). This compares with a value of 0.62 reported by EPRI in the original analysis of the data using Eq. (3-11) (Figure 3-42). This suggests that lead emissions may be predictable from knowledge of coal parameters alone. These data further suggest that the transformations of lead under combustion conditions are not dependent upon coal rank, coal mineralogy, or ash particle size. In recently published field studies, however, Querol et al.[41] and Martinez-Tarazona and Spears[42] reported that lead was enriched in the smallest fly ash particles, suggesting possible vaporization and surface enrichment. Because of this, it is recommended that lead be identified as a middle priority candidate for further fundamental study under this program. A complete tabulation of the lead data is provided in Appendix B.

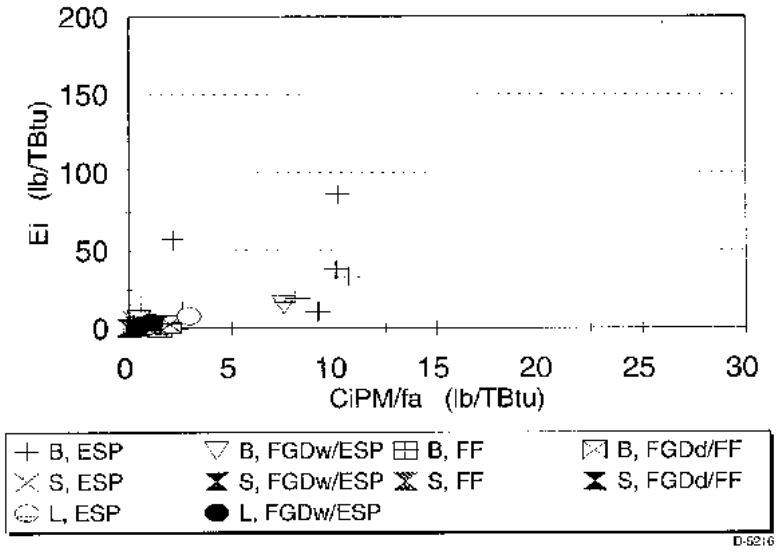

Figure 3-40. Lead emissions data versus C_iPM/f_a (full range of data).

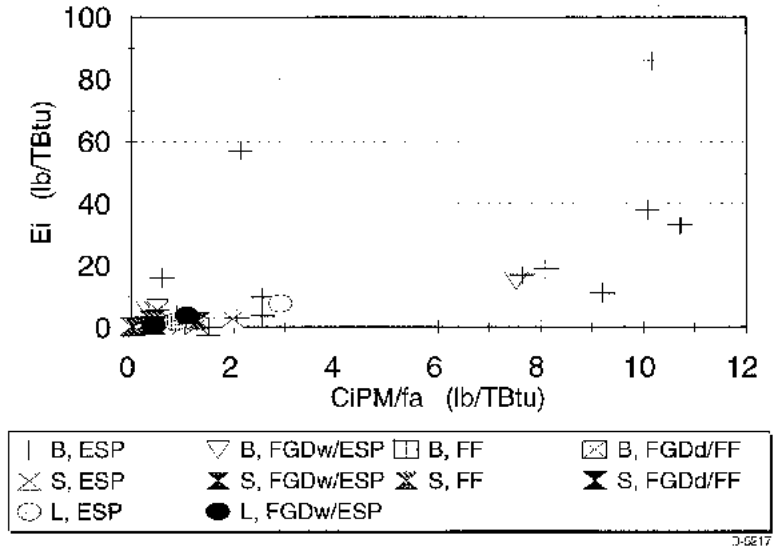

Figure 3-41. Lead emissions data versus C_iPM/f_a (partial range of data).

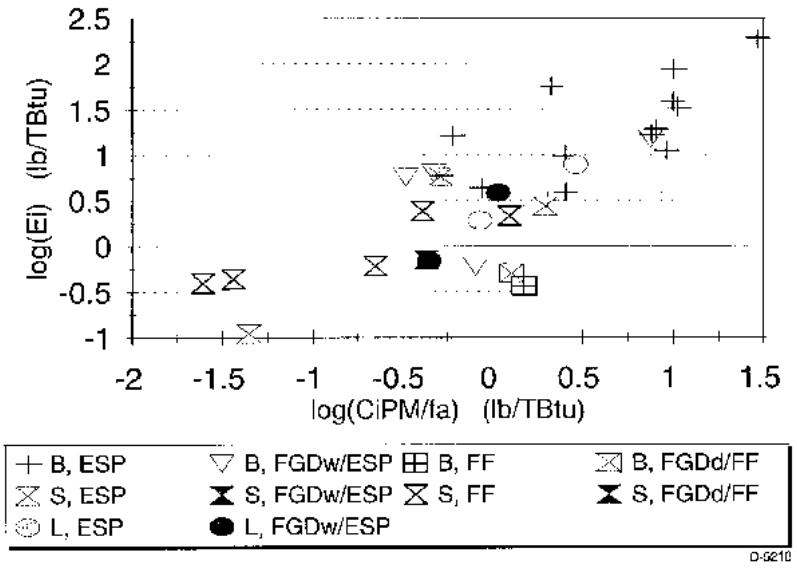

Figure 3-42. Lead emissions data plotted on log-log coordinates (empirical fit).

Manganese

Manganese emissions correlated with the parameter (C_iPM/f_a) (Eq. (3-10)) with an r^2 value of 0.38 (38 datasets, including one for which a rank average coal concentration value was used) (Figure 3-43). This compares with a value of 0.57 reported by EPRI in the original analysis of the data using the empirical approach described earlier (Figure 3-44). Despite this poor correlation, an average manganese capture efficiency of 0.99 suggests that manganese emissions are minimal and are less than particulate emissions (on a capture efficiency basis). Manganese is generally depleted in the smallest ash particles and enriched in the largest particles and in the bottom ash, suggesting that it can be managed through effective particulate control. Manganese is therefore a low priority element for further study in this program.

A complete tabulation of the manganese data is provided in Appendix B.

Mercury

Mercury emissions showed no correlation with either C_iPM/f_a ($r^2 = 0.004$) or with the logarithm of the same term ($r^2 = 0.15$). The scatter inherent in the mercury emissions data can be seen in Figures 3-45 and 3-46. A better correlation was obtained when the concentration of mercury in coal, C_i, was used as the independent variable (Figure 3-47). A correlation coefficient of 0.56 was obtained for the 34 datasets used to produce this plot. This trend is consistent with the expected complete vaporization of highly volatile mercury.

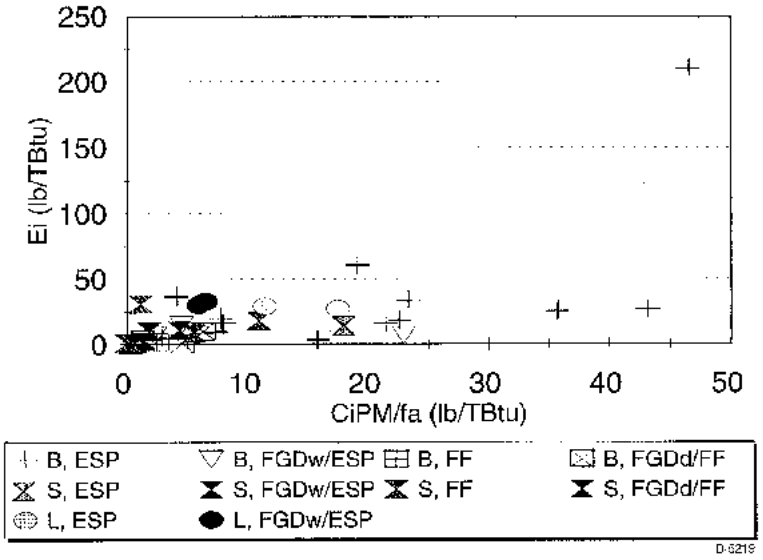

Figure 3-43. Managanese emissions data versus C_iPM/f_a.

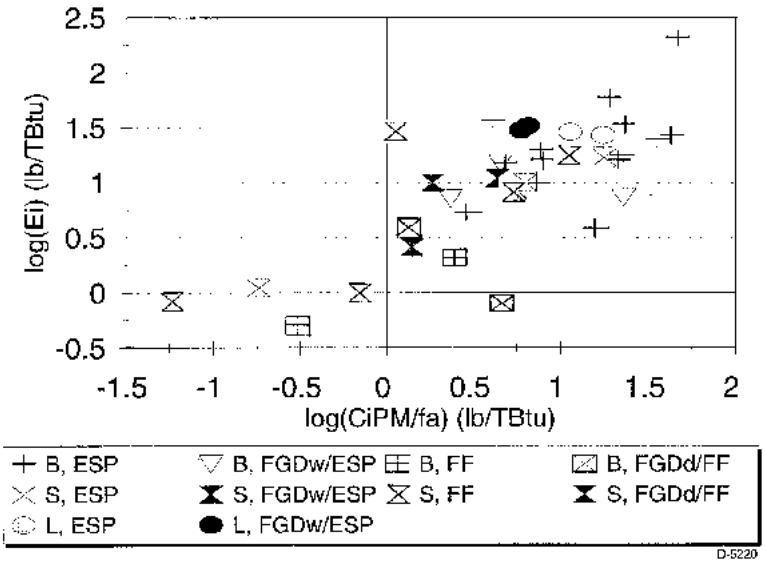

Figure 3-44. Manganese emissions data plotted on log-log coordinates (empirical fit).

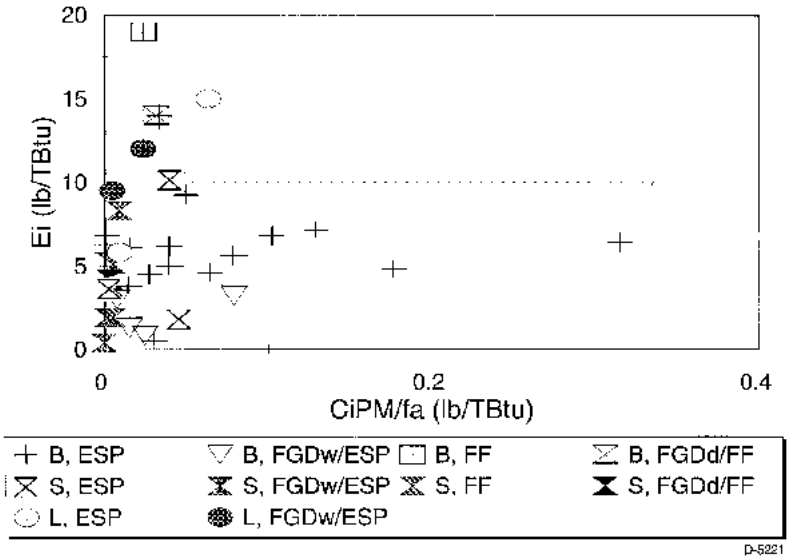

Figure 3-45. Mercury emissions data versus C_iPM/f_a.

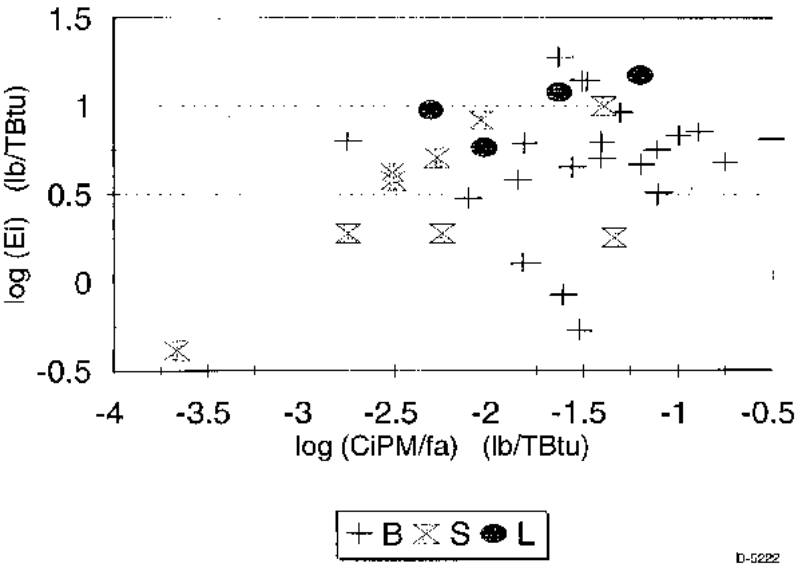

Figure 3-46. Mercury emissions data plotted on log-log coordinates (empirical fit).

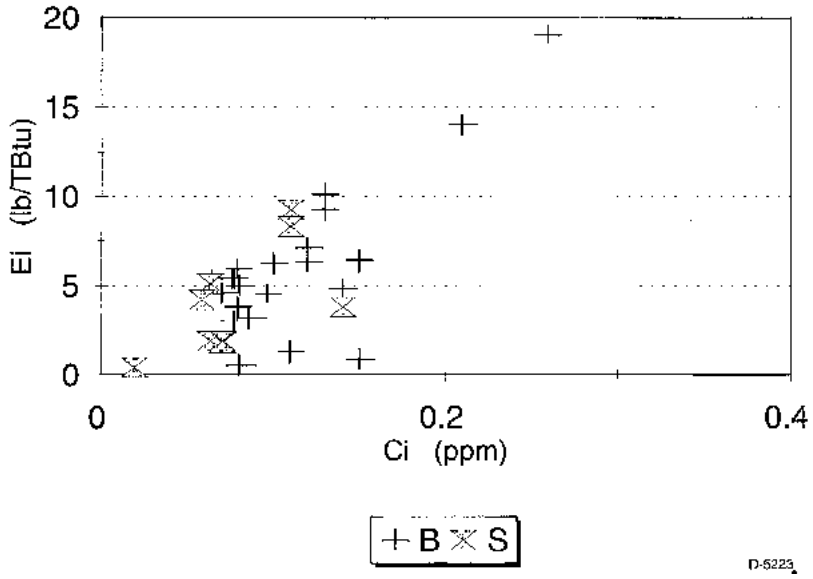

Figure 3-47. Mercury emissions data versus C_i.

Although mercury is expected to vaporize completely under combustion conditions, the stack emissions of the resulting vapor are not readily predicted. Mercury capture efficiencies ranged from 0 to 97%, indicating highly variable removal. Rank-dependence was also noted, with average capture efficiencies of 0.31 measured for lignitic and bituminous coals, and 0.45 for sub-bituminous coals. Both the speciation of mercury (oxidized versus elemental forms) and the presence of residual carbon in the fly ash are believed to contribute to mercury removal from flue gases. Firm conclusions regarding mechanisms or trends cannot be drawn from the field data, however, because of the large degree of uncertainty in reported data, due in part to the difficulty of measuring small concentrations of mercury. Laboratory study of the speciation of mercury, and the interaction of mercury with carbon in ash, should therefore remain high priorities within this program. A complete tabulation of the mercury data is provided in Appendix B.

Nickel

Nickel emissions data are plotted in Figures 3-48 and 3-49. Eight data points for which rank-average data were used for the concentration of nickel in the coal are included. No correlation analysis was performed for the nickel data.

Laboratory studies have shown nickel to be generally non-volatile; field data indicating a high degree of capture (average nickel removal efficiency of 0.98) are consistent with this reported trend. Querol et al.[41] recently reported nickel enrichment in small ash particles produced from combustion of a sub-bituminous coal, however. It is therefore recommended that further laboratory study of nickel be accorded middle priority in this program. Nickel data are tabulated in Appendix B.

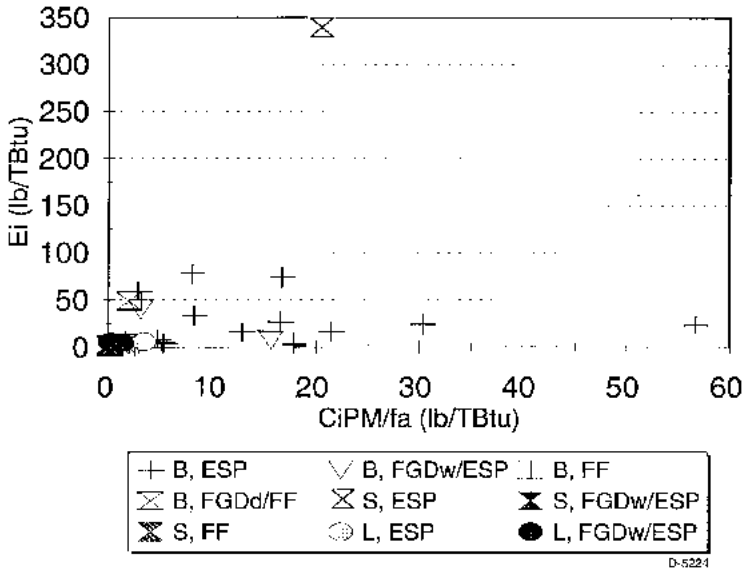

Figure 3-48. Nickel emissions data versus C_iPM/f_a.

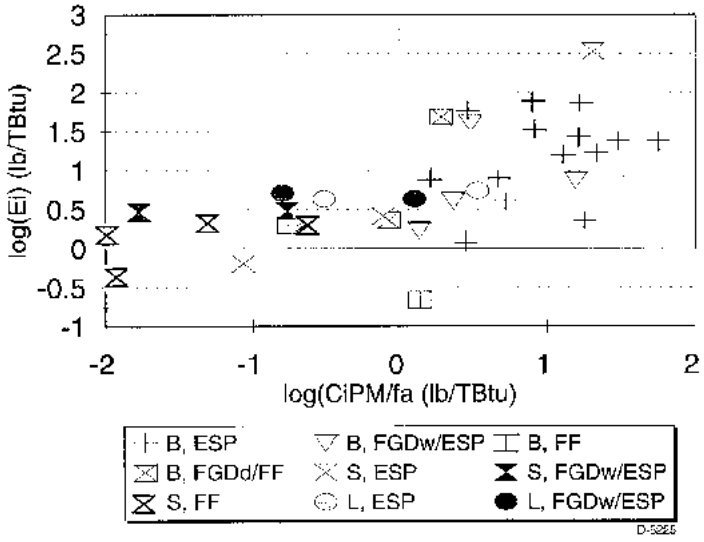

Figure 3-49. Nickel emissions data plotted on log-log coordinates (empirical fit).

Selenium

Selenium emissions showed no correlation with either C_iPM/f_a ($r^2 = 0.05$ for the 29 complete datasets; $r^2 = 0.05$ for 34 datasets including five for which rank-average values of selenium concentrations in coal were used). Correlations with the empirical equation were better ($r^2 = 0.49$ for 34 datasets including five for which rank-average values of selenium concentrations in coal were used). No correlation with concentration of selenium in the coal was noted (Figures 3-50 through 3-52; $r^2 = 0.03$ for 34 datasets). Selenium capture efficiencies ranged from 0 to 99%, indicating highly variable removal. Rank-dependence was also noted, with average capture efficiencies of 0.44, 0.98, and 0.63 determined for bituminous, sub-bituminous, and lignitic coals, respectively. This rank dependence, and particularly the high capture efficiencies noted for facilities burning sub-bituminous coals, indicates that ash chemistry, especially the presence of calcium on particle surfaces, may be important in determining selenium emissions. Querol et al.,[41] in a published study of density separated ash obtained from a 1050 MW station burning sub-bituminous coal, also noted an association between selenium and calcium in the ash. Further study of this element at the bench scale should be accorded a high priority in the remainder of this program. A complete tabulation of the selenium data is provided in Appendix B.

3.6 Toxics Partitioning Engineering Model (ToPEM) Development (PSI)

The primary objective of this program is to develop a fundamentally-based predictive model to allow utility operators to predict trace element emissions from their plants. This Toxics Partitioning Engineering Model (ToPEM) will be applicable to *all* combustion conditions including new fuels and coal blends, low-NO_x combustion systems, and new power generation plants. Development of ToPEM will be based on PSI's existing Engineering Model for Ash Formation (EMAF).

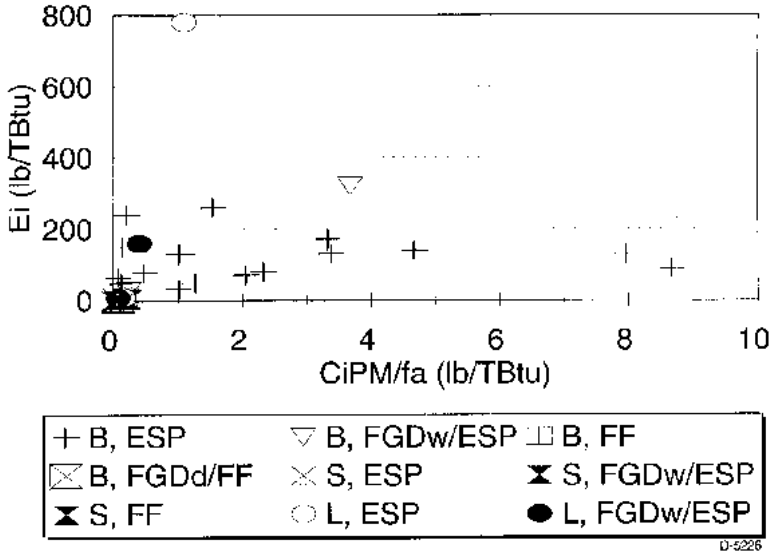

Figure 3-50. Selenium emissions data versus C_iPM/f_a.

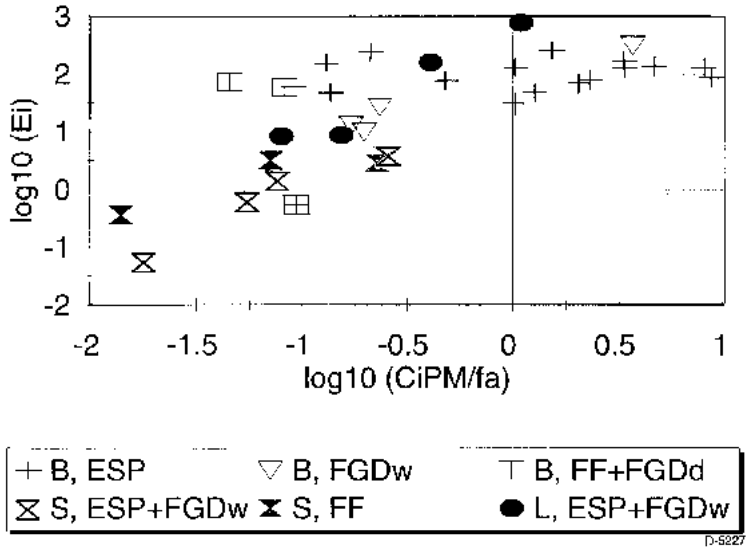

Figure 3-51. Selenium emissions data plotted on log-log coordinates (empirical fit).

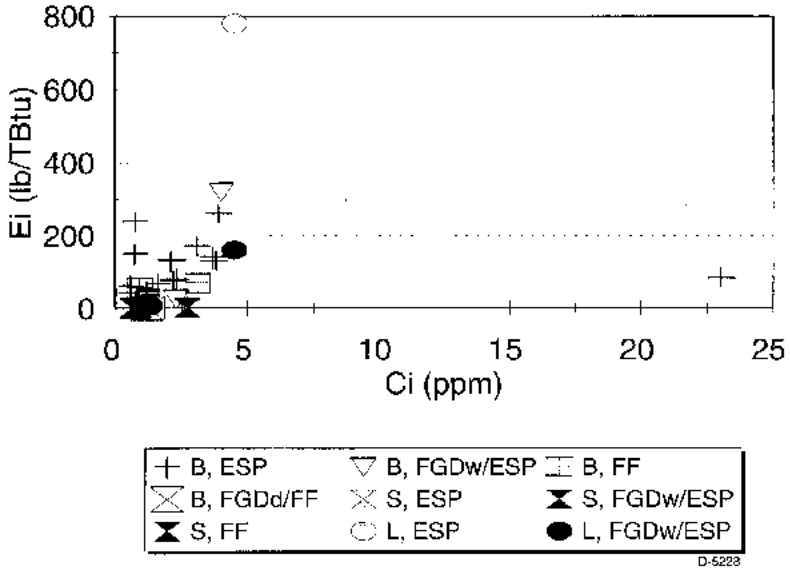

Figure 3-52. Selenium emissions data versus C_i.

The work discussed earlier on the major mechanisms governing trace element partitioning in the combustion zone allows us to determine which sub-models must be further developed, and to determine how these sub-models might be incorporated into the Engineering Model for Ash Formation. In the following subsections the major components of the ToPEM model, and how they will be integrated, are discussed. Critical parameters to be examined as part of the Phase II program will also be identified.

3.6.1 *Description of Engineering Model for Ash Formation (EMAF)*

A simplified flowchart of the Engineering Model for Ash Formation (EMAF) is shown in Figure 3-53. Also shown (in the broken boxes) are the proposed modifications for the development of the ToPEM. The EMAF is discussed in detail elsewhere[45] and will, therefore, only be discussed in here in general terms.

The model starts by reading in the appropriate input parameters from the data file. These parameters include information on the coal psd, mineral psd and composition (from CCSEM), and parameters controlling the modes of interactions between minerals during burnout. These data are then used to generate a virtual assembly of 'empty' coal particles with the appropriate size distribution. The mineral particles are then distributed among the virtual particles until the average volume fraction of ash in any given size range of coal particles equals the volume fraction of ash in the entire coal.

At this point the model has created a group of particles, both mineral-containing coal particles and excluded minerals, that simulate the size and composition distribution in the coal. In order to simulate the fly ash resulting from complete char combustion, and neglecting vaporization, the model jumps to the mineral interaction routine described later in this section. To simulate vaporization, or combustion under reducing conditions (resulting in incomplete char combustion), additional steps are required. Specifically, ToPEM needs to be modified to include the effect of the combustion environment on the time-temperature, and burnout, history of particles in the combustion zone.

In order to simulate the char burnout and trace element vaporization a new submodel must be developed. The existing EMAF contains a kinetic submodel that calculates the fractional burnout and the particle temperatures during the combustion process. This submodel is similar to that discussed elsewhere.[46] In the kinetic submodel, the fractional burnout of char in a given size range is calculated by simultaneously solving for the burnout of all the size ranges present in the coal. For example, a coal with a particle size distribution ranging from 10 to 120 μm is divided into 12 size bins. The kinetic submodel then simultaneously solves the 12 rate equations describing burnout in the individual size bins, 12 heat balances on the particles in these bins (to determine particle temperature), and the bulk oxygen, carbon monoxide, and carbon dioxide concentrations. Using these relations the submodel predicts which particles burn out first, and as a result predicts the degree of burnout for all size ranges.

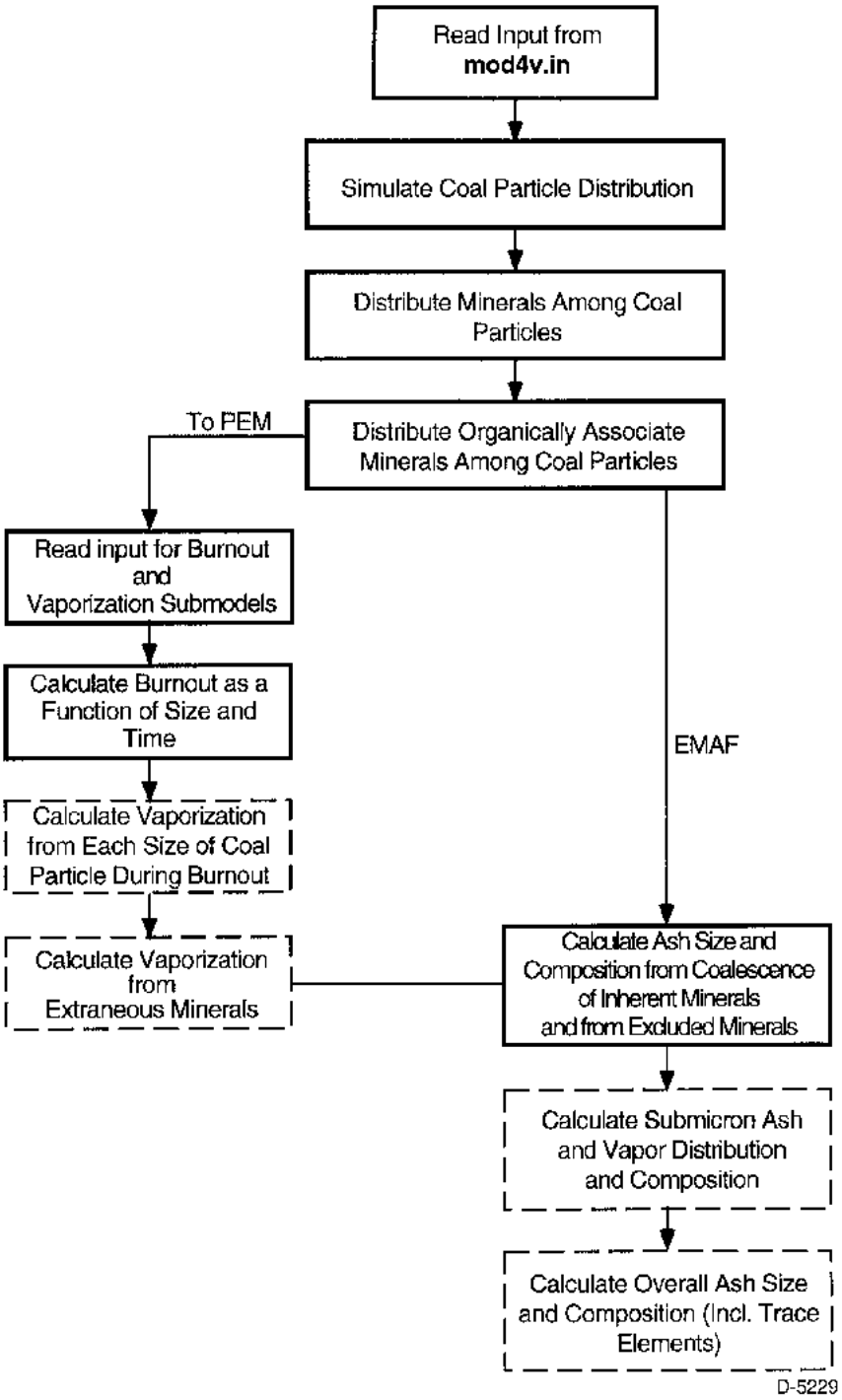

Figure 3-53. Flow diagram of EMAF including planned submodels for ToPEM.

The kinetic submodel required to predict trace element vaporization will be incorporated into the existing char combustion model. As discussed elsewhere in this report (Section 3.3.3) trace element vaporization is probably dominated by thermal effects and intraparticle transport effects. Therefore a model that takes these effects into account, such as that proposed by Quann will be used to calculate the fraction of a given element that vaporizes from coal particles (including extraneous minerals) in a given size range during the burnout process. By integrating these results over the entire size range of coal particles we can predict the net vaporization from the coal. The proposed vaporization submodel is discussed in more detail in Section 3.6.2.

In the current EMAF the output of this burnout submodel is used to define the fraction of minerals in each simulated coal particle that is **not** exposed to the outer char particle surface during the combustion process. These minerals will generally maintain the same size and composition, since they cannot interact with other minerals. The remaining minerals are assumed to coalesce and interact with other minerals. Based on these mechanisms, the model predicts the size and composition distributions of the bulk ash.

At this point the model has predicted the size and composition of the supermicron ash, and the existing EMAF writes the results to output files and ends. ToPEM, however, will also include a submodel to predict the size and composition of the submicron ash, including the trace elements. This model has been developed for bulk ash constituents as part of an earlier DoE funded program (Contract Number DE-FG02-92ER81376). In Phase II the model, discussed in Section 3.6.3, will be modified to include condensation of trace elements and incorporated into ToPEM code. ToPEM will then combine the supermicron and submicron distributions to describe the entire ash particle size distribution and composition distribution. This tool will provide an important starting point for the development of a commercial, user friendly, software package to predict slagging and trace element emissions from boilers, similar to PSI's Slagging Advisor™ program.

3.6.2 *Proposed Vaporization Model*

Although development of the vaporization model will be accomplished in Phase II, some of the Phase I results and some existing vaporization models can be used to generate a general framework for the vaporization model. As discussed earlier (Section 3.3.3) several mechanisms have been proposed that may control vaporization of trace elements during burnout. These mechanisms include capture of the reactive mineral (i.e., pyrite) into a glassy phase which may inhibit reaction, pore diffusion control, vaporization from minerals exposed during burnout, and film diffusion control. Of these mechanisms, the data collected to date in this program, and those data collected by earlier researchers at MIT[1,2] suggest that internal pore and external film diffusion control are the most important, and will therefore form the basis of the vaporization model.

The model we will use in ToPEM is based largely on earlier work by Quann.[1] He proposed that for the conditions we proposed here (internal or external diffusion control) the vaporization rate of an element (V_c) can be given by:

$$V_c = \eta N_I V_I^{ni} \quad (3\text{-}12)$$

where:

η = the effectiveness factor that takes into account internal and external diffusion control
N_I = the number of inclusions that have not been exposed
V_I^{ni} = the vaporization rate from a single non-interacting inclusion.

The effectiveness factor is given by:

$$\eta = \frac{3}{\phi_i}\left[\frac{1}{\tanh\phi_i} - \frac{1}{\phi_i}\right]\left[1 + \frac{D_e}{\alpha_i D_{O2}}\left(\frac{\phi_V}{\tanh\phi_V} - 1\right)\right]^{-1} \quad (3\text{-}13)$$

where:

ϕi = Thiele modulus
D_e = effective diffusivity of element
D_{o2} = diffusivity of oxygen
α_1 = Stephan flow parameter.

The number of inclusions that have not been exposed is related to the initial volume fraction of minerals in the char and the volume of char that has been burned away. Vaporization of the element from a single non-interacting inclusion is given by:

$$V_c^{ni} = 4\ \pi\ c\ D_e\ r_i\ x_m^e \quad (3\text{-}14)$$

where:

c = molar concentration
r_i = radius of the inclusion
x_m^e = equilibrium mole fraction of element at the inclusion surface.

Although this model has been shown to work fairly well for major species (such as silicon) it has not been tested for vaporization of trace elements. Mims et al.[2] used a similar model, however, to describe vaporization of arsenic from a Montana Lignite with good results. All of the model parameters are readily available, or can be easily estimated, with the exception of the equilibrium mole fraction of the element at the inclusion surface. Current equilibrium data do not exit to allow this parameter to be calculated. Therefore, the kinetics of vaporization is a major issue that must be addressed in the Phase II.

One major mechanism that has not been discussed here is reactive scavenging of vapor phase species by minerals. For example, sodium vapors have been shown to react with silicate minerals,[47] thereby reducing the amount of sodium present in the submicron ash. If specific interactions are identified for trace elements (e.g., reaction of arsenic and calcium) a sink term will have to be incorporated. This situation requires detailed information about the mechanisms leading to the reactive scavenging and the kinetics of the scavenging process. These issues, among others, will be addressed in Phase II of this program.

3.6.3 *Submicron Ash Formation Submodel*

One of the goals of this work is to incorporate an aerosol formation submodel into the engineering model for ash formation (EMAF). Development of this model was completed under separate DoE funding as part of the program "Advanced Analytical Methods for Selection of Coal and Coal Blends," Contract Number DE-FG02-92ER81376. Modifications to the model to include description of trace element behavior will take place in Phase II of this program.

Many investigators have measured two distinct modes in the submicron ash,[48,49] ultrafine and intermediate. The ultrafine mode is primarily derived from vaporization and condensation of inorganics during the combustion process. The intermediate mode is primarily derived from submicron minerals present in the coal. The model addresses these modes separately.

Ultrafine Ash Mode

In the submicron ash formation submodel the mass of the major species that vaporizes is estimated based on the work from Quann.[1] In his work the general vaporization equation described in the preceding subsection is simplified to address two specific modes of vaporization; internal diffusion control (vaporization from inclusions), and external diffusion control (vaporization of organically associated minerals). The required equilibrium vapor pressure is derived from a reduction reaction at the surface of the inclusion. Thus, the mass of major species vaporized during the combustion process can be predicted with a reasonable degree of accuracy. And, as these species form the bulk of the submicron aerosol, the particle size distribution can be calculated from the mass of the major species that vaporize, the mass of the trace elements is neglected.

The self-preserving aerosol model can be used to calculate the size distribution.[50] Initially, let us neglect scavenging of small particles by large (supermicron particles). The total volume of the aerosol is constant and equal to the amount of material vaporized:

$$V = f_v M_{ash} \tag{3-15}$$

where M_{ash} is the ash loading in g/m^3. The initial number of particles is therefore

$$N(0) = \frac{6V}{\pi D_o^3} \tag{3-16}$$

where D_o is the initial particle diameter, which can be calculated from nucleation theory. The initial diameter can be estimated to be one or two molecules since the saturation ratio is generally large. The rate of decay of the number distribution is given by

$$\frac{dN}{dt} = -\frac{1}{2}\left[\frac{3}{4\pi}\right]^{1/6}\left[\frac{6kT}{\rho_p}\right]^{1/2}\left[\frac{p}{RT}\right]I_1 V^{1/6} N^{11/6} \tag{3-17}$$

The size distribution is calculated from N(t) and V as

$$n = \left[\frac{N^2}{V}\right]\Psi(\eta) \tag{3-18}$$

where $\eta = vN/V$. The function $\Psi(\eta)$ is tabulated by Friedlander.[51]

To make the calculation, we will assume that nucleation and coagulation happen on much faster time scales than those on which the gas temperature is changing. That is, we will impose a temperature-temperature history on the gas. For example, Flagan and Friedlander used the following temperature history to simulate the boiler: T = 1800 K for 0.5 s, T = 1800 to 1400 K over 1 s, and T = 1400 to 425 K over 2 s.

Intermediate Mode

Unfortunately, CCSEM analysis does not provide information on particles less than approximately 1 μm in the coal which may contribute to the submicron aerosol. This intermediate mode is significantly larger than the fine mode produced by the vaporization-condensation process. From measurements made by VTT[52] we believe that this mode does exist. The aerosol appears to consist of dense spheres which would suggest that the intermediate mode is not the product of a vaporization-condensation process. Instead, this mode may result from fine minerals in the coal. These have been observed via TEM[53] in sub-bituminous coals.

The approach taken here is somewhat simplified but does produce results that appear realistic. However, some refinement will be needed. The size distribution of minerals as measured by CCSEM from eleven coals of various rank were examined. When the mineral

distribution is calculated the largest number of minerals is found in the smallest size bin of approximately 1 to 2.5 µm in diameter.

The number of submicron minerals is approximated by assuming that the number distribution (on a log Dp basis) is symmetric about the 1 to 2.5 μm size range. The sizes chosen for the bins are 0.156 to 0.313, 0.313 to 0.625, and 0.625 to 1.25 μm. If the number distribution denoted by n(Dp) is the number of minerals between Dp and Dp + dDp then my assumption is equivalent to

$$\begin{aligned} n(0.625) &= n(1.25) \\ n(0.313) &= n(2.5) \\ n(0.156) &= n(5) \quad . \end{aligned} \tag{3-19}$$

The calculation was be performed for each mineral class and then summed over all mineral classes. The mass distribution, $n_m(Dp)$ is then calculated for each mineral class of the submicron mode as

$$n_m(Dp) = \rho(\pi/6) Dp^3 n(Dp) \quad . \tag{3-20}$$

The entire mass distribution is then renormalized.

Once the amount of submicron minerals has been predicted, we assume that some fraction of the ultrafine minerals are released from the char during devolatilization and char combustion. These minerals melt but do not otherwise interact. And, therefore, are assumed to form ash particles of the same size and composition as the original minerals. Recent visual evidence[54] suggests that ultrafine aluminosilicate minerals are ejected from coal particles during devolatilization.

3.6.4 *Phase II Research Needs*

As can be seen by the preceding discussion, the Engineering Model for Ash Formation and the Submicron Ash Formation Submodel are powerful tools for predicting the size and composition of the fly ash generated from burning a wide range of coals under various conditions. However, to modify these codes to include the trace element partitioning, there is still a great deal of work that must be done in the Phase II program. In short we need to:

- Explore trace element vaporization and partitioning for a wider range of coals and combustion conditions to further validate the transport limitations proposed from the Phase I data

- Perform a series of time resolved experiments under wide range of combustion conditions, using well characterized pyrite particles to derive the equilibrium vapor pressure of elements associated with pyrite

- If the oxidation state of pyrite is shown to play a major role in vaporization, as will be discussed in the next report, these experiments should be repeated to determine the effect of oxidation on the equilibrium vapor pressure of trace elements associated with the oxidized pyrite (including reducing conditions)

- Perform experiments to explore reactive scavenging by specific minerals (e.g., arsenic by calcium)

- Measure trace element partitioning in larger systems to test models and evaluate proposed condensation mechanisms.

SECTION 4

CONCLUSIONS

4. CONCLUSIONS

In the last quarter the trace element concentration analysis was completed for the Wyodak coal. This analysis indicated that the concentrations of trace elements in this coal are within the range of the bituminous coals in this program, with the exception of arsenic. The concentrations of this element, and that of chromium, are much lower than was found in the other program coals. The CCSEM analysis of this coal are similar to most low-sulfur western sub-bituminous coals. The mineral matter is richer in kaolinite than illite, has a low content of basic minerals (calcite, pyrite, siderite), and contains minor amounts of a Ca-Al phosphate mineral, which is most probably crandallite. This coal appears a little unusual in that the quartz content is quite high and is somewhat coarser in particle size than the other minerals. The illite content is also quite significant. It is also likely that there is significant organic calcium that is not measured by CCSEM.

Another major activity in the last quarter was analysis of the vaporization data obtained at MIT and PSI to determine the mechanisms governing trace element vaporization in the combustion zone. Significant differences in the particle temperature between the two facilities cause substantial differences in the amount of each element observed in the submicron ash. In addition, Mössbauer analysis of ash from these two facilities (from the same coal) indicated that the fraction of iron that was captured into the glass was essentially the same. Therefore, capture of pyrite by silicates during the combustion process, did not cause the difference in observed vaporization as was hypothesized earlier. It is more likely that the significant differences in the particle temperatures between these facilities caused the observed differences.

Based on earlier work by Quann,[1] and Mims et al,[2] relations were derived to determine the effect of measurable coal parameters, such as particle size, on vaporization from burning coal particles. If trace elements vaporized from inclusions (such as pyrite) that had been exposed during burnout, no coal particle size dependence would be expected. Vaporization from inclusions inside the char, limited by internal diffusion in the char, yields a $1/r_p$ dependence. For cases where vaporization is limited by external diffusion, such as vaporization from the char matrix or ultrafine inclusions, a $1/r_p^2$ dependence should be found. The fractional vaporization data obtained from combustion of the size and density segregated coal samples in the MIT droptube furnace (DTF) were examined to determine which of these trends were present. For almost all elements, the data suggest that vaporization occurs from included mineral particles. This is especially true for those elements that were found to be associated with the pyrite.

A number of kinetic calculations were performed at MIT to determine the partitioning of chlorine between HCl and Cl_2 at temperatures consistent with the backpass of a utility boiler. Although equilibrium predictions suggest that a high fraction of the chlorine is present as Cl_2, which may enhance oxidation of vapor phase mercury, the kinetic calculations indicate that the reaction is actually kinetically limited. In fact, only 1% of the chlorine was predicted to be present at Cl_2 at the APCD outlet.

A review has been conducted of the organic emissions parts of the four-volume EPRI Report TR-104614, "Electric Utility Trace Substances Synthesis Report." In evaluating the

results, some key questions have arisen pertaining to species screening procedures, mass balances on sampling and analytical procedures, and the inclusion/exclusion of other organic species not mentioned in the Report. We are now working with representatives of EPRI, DOE, and the contracting companies who performed the field emission studies to address these key questions and others that may arise.

Trace element emissions data reported in the EPRI PISCES report and in the scientific literature (period 1995-1996) were examined to identify gaps in our understanding of trace element combustion chemistry. A comparison of trace element emissions with particulate emissions indicated that emissions of most coal-derived trace elements, while generally low, did not correlate with a parameter incorporating particulate emissions and trace element concentrations in the coals. This was particularly true of the elements mercury, selenium, and arsenic. A correlation would be expected for all elements if trace element capture efficiencies were only dependent on particulate capture efficiencies. This finding suggests that fundamental data on trace element chemistry in combustion systems is needed to extrapolate the emissions findings of the field studies noted above to a broader range of fuels and sources.

Experiments were performed at PSI to explore the effect of cooling rate on mercury speciation. These experiments suggest that the cooling rates typical of the economizer region of a power plant are sufficient to 'freeze' the oxidation of mercury -- leading to a higher fraction of mercury in the elemental form than would be predicted from equilibrium. Additional data are required, however, to further substantiate this hypothesis.

A series of important experiments was completed at the self-sustained combustor at UA. These experiments suggest that there is little change in the fraction of the ash in the submicron sizes between the combustion zone and the convective sections. This is consistent with vaporization of bulk species (silica) that recondense in the combustion zone. Size segregated ash samples have been sent to MIT for analysis and will be presented in later reports.

Finally, the mechanisms obtained from analysis of the PSI and MIT vaporization data were used to determine the submodels required to develop ToPEM. Specifically, the framework of the existing Engineering Model for Ash Formation (EMAF) was reviewed to determine which models were required, and how these models should be incorporated. EMAF currently allows the user to calculate the supermicron ash composition and size distribution based on the coal properties and mineralogy, from CCSEM. Included in this model is a submodel to calculate the burnout and temperature of coal particles in each size class. In order to predict trace element partitioning a vaporization model must be coupled with the burnout model. This combination will provide the amount of each trace element in the vapor phase at the exit of the flame zone. This information will then be fed into a model to predict the submicron ash composition and distribution. The fundamental submicron ash model has already been developed, but must be modified to include condensation of the vapor phase trace elements, particularly to determine what fraction of the trace element remains in the vapor phase.

SECTION 5

REFERENCES

5. REFERENCES

1. Quann, R.J.,Sc.D. Thesis, Massachusetts Institute of Technology, 1992.

2. Mims, C.A., Neville, M., Quann, R.J., and Sarofim, A.F., “Laboratory Studies of Trace Element Transformations During Coal Combustion”, 87th AIChE Meeting, Boston, MA, August 1979

3. G. P. Huffman, and F. E. Huggins in: "The Chemistry of Low-Rank Coals", ed. H. H. Schobert, ACS Symposium Series, Vol. 264, pp. 159-174, 1984.

4. Bool, III, L.E., Senior, C.L., Huggins,F., Huffman, G.P., Shah, N., Wendt, J.O.L., Sarofim, A., Olmez, I., and Zeng, T., “Toxic Substances from Coal Combustion -- A Comprehensive Assessment”, Quarterly Report No. 5 prepared for Department of Energy, PETC, under Contract No. DE-AC22-95PC95101, PSIT-1245, January, 1996

5. Nordin, A., Schager, P., Hall, B., “Mercury Speciation in Flue Gases: A Comparison of Results from Equilibrium Calculations with Results from Laboratory Experiments,” presented at Swedish-Finnish Flames Days, Turku, Finland, September, 1990.

6. Galbreath, K.C and Zygarlicke, C.J. “Mercury Speciation in Coal Combustion and Gasification Flue Gases,” *Env.Sci.Tech.,* **1996**, *30*, 2421-2426.

7. Flagan, R.C and Seinfeld, J. H *Fundamentals of Air Pollution Engineering*, Prentice Hall: Englewood Cliffs, NJ, 1988

8. EPRI Report TR-104614, "Electric Utility Trace Substances Synthesis Report," Project 3081, November, 1994.

9. W. H. Griest and J. E. Caton, "Extraction of Polycyclic Aromatic Hydrocarbons for Quantitative Analysis," Chapter 3 in *Handbook of Polycyclic Aromatic Hydrocarbons*, ed. by A. Bjorseth. New York: Marcel Dekker (1983), pp. 95-148.

10. G. M. Sverdrup, J. C. Chuang, L. Slivon, A. R. McFarland, J. A. Cooper, R. W. Garber, and B. S. Smith, "Comparison of Chemical Composition of Fly Ash Particles Collected in the Plume and Stack of a Coal-Fired Power Plant," presented at Workshop on Managing Hazardous Air Pollutants: State of the Art, Washington D. C., 1991.

11. KVB, Inc., "Measurements of POM Emissions from Coal-Fired Utility Boilers," EPRI REport CS-2885, Project 1075-1, Final Report, February, 1983.

12. Oak Ridge National Laboratory, "Identification and Quantification of Polynuclear Organic Matter (POM) on Particulates from a Coal-Fired Power Plant," EPRI Report EA-1092, Project 1057-1, Interim Report, June, 1979.

13. Southern Research Institute, "Planning Studies for Measurement of Chemical Emissions in Stack Gases of Coal-Fired Power Plants," EPRI Report EA-2892, Project 1776-1, Final Report, March, 1983.

14. Szpunar, C.B.,"Air Toxics Emissions from the Combustion of Coal: Identifying and Quantifying Hazardous Air Pollutants from U.S. Coals," Argonne National Laboratory Report ANL/EAIS/TM-83, September, 1992.

15. Sloss, L.L., and Smith, I.M., "Organic Compounds from Coal Utilisation," International Energy Agency Coal Research Report IEACR/63, October, 1993

16. Warnot, M.J., Sarofim, A.F., J.P., Longwell, "Changes in the Degree of Substitution of Polycyclic Aromatic Compounds from Pyrolysis of a High-Volatile Bituminous Coal," *Energy & Fuels*, 1987

17. Warnot, M.J., Sarofim, A.F., J.P., Longwell, "Pyrolysis-Induced Changes in the Ring Number Composition of Polycyclic Aromatic Compounds from a High Volatile Bituminous Coal, "*Twenty-Second Symposium (International) on Combustion*, Pittsburgh, 1988

18. Grimmer, G., Jacob, J., Dettbarn, G., and Naujack, K.W., "Determination of Polycyclic Aromatic Hydrocarbons, Azaarenes, and Tiaarenes Emitted from Coal-Fired Residential Furnaces by Gas Chromatography/Mass Spectrometry," *Fesnius Zeitschrift fur Analytische Chemie*, 1985

19. Vernaglia, B.A., Warnot, M.J., Li, C.Z., and Nelson, P.F., "The Effects of Pyrolysis Temperature and Ion-Exchanged Metals on the Composition of Brown Coal Tars Produced in a Fluidized Bed Reactor," *Twenty-Sixth Symposium (International) on Combustion*, The Combustion Institute, 1996

20. Vernaglia, B. A., Wornat, M. J., Lafleur, A. L., Plummer, E. F., Nelson, P. F., and Li, C.-Z., in preparation, 1997.

21. Durant, J. L., Busby, W. F., Lafleur, A. L., Penman, B. W., and Crespi, C. L. , "Human Cell Mutagenicity of Oxygenated, Nitrated, and Unsubstituted Polycyclic Aromatic Hydrocarbons Associated with Urban Air," *Mutation Research 371:* 123-157 (1996).

22. A. L. Lafleur, J. P. Longwell, J. A. Marr, P. A. Monchamp, E. F. Plummer, W. G. Thilly, P. P. Y. Mulder, B. B. Boere, J. Cornelisse, and J. Lugtenburg, "Bacterial and Human Cell Mutagenicity Study of Some $C_{18}H_{10}$ Cyclopenta-Fused Polycyclic Aromatic Hydrocarbons Associated with Fossil Fuels Combustion," *Environmental Health Perspectives 101:* 146-153 (1993).

23. S. C. Ruckmick, R. J. Hurtubise, *Journal of Chromatography 321:* 343-352 (1985).

24. E. J. Calabreese and E. M. Kenyon, *Air Toxics and Risk Assessment.* Chelsea, Michigan: Lewis Publishers (1991).

25. J. Lewtas and M. G. Nishioka, "Nitroarenes: Their Detection, Mutagenicity and Occurrence in the Environment," in *Nitroarenes*, ed. by P. C. Howard, S. S. Hecht, and F. A. Beland. New York: Plenum Press (1990), pp. 61-72.

26. C. Wei, O. G. Raabe, L. S. Rosenblatt, *Environmental Mutagenesis 4:* 249 (1982).

27. H. Tokiwa and Y. Ohnishi, "Mutagenicity and Carcinogenicity of Nitroarenes and Their Sources in the Environment," *CRC Critical Reviews in Toxicology 17:* 23-60 (1986).

28. P. A. Andrews, D. Bryant, S. Vitakunas, M. Gouin, G. Anderson, B. E. McGarry, M. A. Quilliam, and D. R. McCalla, in *Polynuclear Aromatic Hydrocarbons: Formation, Metabolism, and Measurement,* ed. by M. Cooke and A. J. Dennis. Colombus, Ohio: Battelle Press (1983), p. 89.

29. S. S. Hecht and K. El-Bayoumy, "The Possible Role of Nitroararenes in Human Cancer," in *Nitroarenes*, ed. by P. C. Howard, S. S. Hecht, and F. A. Beland. New York: Plenum Press (1990), pp. 309-316.

30. M. R. Plasterer, G. M. Booth, M. L. Lee, W. R. West, P. Smith, M. L. Tedjamulia, Y. Tominaga, and R. N. Castle, "Comparative Mutagenicity of Analogous Amino- and Nitropolycyclic Aromatic Hydrocarbons," in *Health and Environmental Research on Complex Organic Mixtures*, ed. by R. H. Gray, E. K. Chess, P. J. Mellinger, R. G. Riley, and D. L. Springer. Springfield, Virginia: National Technical Information Service (1987), pp. 251-258.

31. R. Mermelstein, H. S. Rosenkranz, and E. C. McCoy, "The Microbial Mutagenicity of Nitroarenes," in *Genetic Effects of Airborne Agents*, ed. by R. R. Tice, D. L. Costa, and K. M. Schiach. New York: Plenum Press (1982), pp. 369-396.

32. D. W. Later, M. L. Lee, K. D. Bartle, R. C. Kong, and D. L. Vassilaros, *Analytical Chemistry 53:* 1612-1620 (1981).

33. D. W. Later, M. L. Lee, R. A. Pelroy, and B. W. Wilson, in *Polynuclear Aromatic Hydrocarbons: Physical and Biological Chemistry*, ed. by M. Coole. A. J. Dennis, G. L. Fisher. Colombus, Ohio: Battelle Press (1982), pp. 427-438.

34. D. A. Haugen, V. C. Stamoudis, M. J. Peak, A. S. Bopari, in *Polynuclear Aromatic Hydrocarbons: Physical and Biological Chemistry*, ed. by M. Coole. A. J. Dennis, G. L. Fisher. Colombus, Ohio: Battelle Press (1982), pp. 347-356.

35. M. Nishioka, P. A. Smith, G. M. Booth, M. L. Lee, H. Kudo, D. R. Muchiri, R. N. Castle, and L. H. Klemm, *Preprints of Papers—American Chemical Society, Division of Fuel Chemistry 30* (4): 93-98 (1985).

36. C.-h. Ho, B. R. Clark, M. R. Buerin, B. D. Barkenbus, T. K. Rao, and J. L. Epler, *Mutation Research 85:* 335-345 (1981).

37. M. Dong, I. Schmeltz, E. Lavoie, and D. Hoffmann, in *Carcinogenesis—A Comprehensive Survey, Vol. 3. Polynuclear Aromatic Hydrocarbons,* ed. by P. W. Jones and R. I. Freudenthal. New York: Raven Press (1978), pp. 97-108.

38. P. Burchill and A. A. Herod, *Fuel 62:* 20-29 (1983).

39. C. E. Ostman, A. L. Colmsjo, *Fuel 67:* 396-400 (1988).

40. R. L. Hanson, T. R. Henderson, C. H. Hobbs, C. R. Clark, R. L. Carpenter, J. S. Dutcher, "Detection of Nitroaromatic Compounds on Coal Combustion Particles," *Journal of Toxicological and Environmental Health 11:* 791-800 (1983).

41. Querol, X., Fernandez-Turiel, J.L., and Lopez-Soler, A., *Fuel* **74**, 1994

42. Martinez-Tarazona, M.R., and Spears, D.A., *Fuel Processing Technology*, **47**, 1996

43. Quann, R.J., Neville, M., and Sarofim, A.F., *Combustion Science and Technology*, **74**, 1990

44. Neville, M., and Sarofim, A.F., *Fuel*, **64**, 1984

45. Bool, III, L.E., Helble, J.J., Shah, N., Shah, A., Huffman, G.P., Huggins, F.E., Rao, K.R.P.M., Sarofim, A., Zeng, T., Reschke, R., Gallien, D., and Peterson, T.W., "Fundamental Study of Ash Formation and Deposition: Effect of Reducing Stoichiometry," Final Report prepared for Department of Energy, PETC, under Contract No. DE-AC22-93PC92190, PSIT-1178/TR-1407, September 1995.

46. Bool, L.E., Peterson, T.W., Wendt, J.O.L, "The Partitioning of Iron During the Combustion of Pulverized Coal.", *Comb. and Flame*, **99**, 1995

47. Boni, A. et al., "Transformations of Inorganic Coal Constituents in Combustion Systems", Phase I Final Report, U.S. DoE Contract No. DE-AC22-86PC90751, 1991

48. Schmidt, E.W., Gieseke, J.A., and Allen, J.M., "Size Distribution of Fine Particulate Emissions from a Coal-Fired Power Plant," *Atm.Env*. **10**, 1976.

49. McElroy, M.W., Carr, R.C., Ensor, D.S., and Markowski, G.R., "Size Distribution of Fine Particles from Coal Combustion," *Science* **215**, 13-19, 1982.

50 Flagan, R.C. and Friedlander, S.K., Recent Developments in Aerosol Science, J. Davis ed., John Wiley and Sons, N.Y., p.25, 1978.

51. Freidlander, S.K., Smoke, Dust and Haze, John Wiley and Sons, NY, 1977.

52. Joutensaari, J., Kauppinen, E.I., Jokiniemi, J.K., and Helble, J.J., "Studies on ash vaporization in power plant scale pulverized coal combustion," paper presented at the Engineering Foundation Conference on The Impact of Ash Deposition on Coal Fired Power Plants, Solihull, UK, 20-25 June, 1993.

53. Hurley, J.P., and Shobert, H.H., "Ash Formation During Pulverized Subbituminous Coal Combustion, 1. Characterization of Coals, Inorganic Transformations during Early Stages of Burnout", *Energy & Fuels*, **6**, 1992

54. Lunden, M., "Impact of Mineral Matter on Char Reactivity", presented at IEA Workshop on Emerging Issues in Coal Combustion, Livermore, CA, April 15-17, 1997

APPENDIX A

Experimental Particle Size Distribution Data

Pittsburgh #8 Runs 9-12

Illinois #6 Runs 1-7

Particule Size Distribution Calculations
Test: 97P8-9
NOCYCLONE

Greased Filter Weights

STAGE	1st	2nd	3rd	Average
11.00000	0.00676	0.00678		0.00677
10.00000		0.03103	0.03105	0.03104
9.00000	0.03047	0.03045		0.03046
8.00000	0.03166	0.03163		0.03165
7.00000	0.03121		0.03122	0.03122
6.00000	0.02966		0.02963	0.02965
5.00000		0.13730	0.13732	0.13731
4.00000		0.13663	0.13665	0.13664
3.00000	0.14072		0.14078	0.14075
2.00000	0.13705	0.13718	0.13710	0.13711
1.00000	0.13809	0.13806		0.13808

Empty vial Weights

STAGE	1st	2nd	3rd	Average
11.00000	0.96736	0.96737		0.96737
10.00000	0.96660	0.96664		0.96662
9.00000		0.96978	0.96979	0.96979
8.00000	0.97348	0.97352		0.97350
7.00000	0.97178	0.97180		0.97179
6.00000	0.97559	0.97349	0.97552	0.97487
5.00000				
4.00000				
3.00000				
2.00000				
1.00000				

Filter+Ash+Vial

STAGE	1st	2nd	3rd	Average
11.00000	0.97486		0.97484	0.97485
10.00000	1.00078		1.00072	1.00075
9.00000	1.00078		1.00072	1.00075
8.00000		1.00577	1.00575	1.00576
7.00000		1.00348	1.00345	1.00347
6.00000		1.00546	1.00547	1.00547
5.00000	0.13737	0.13740		0.13739
4.00000	0.13676	0.13683	0.13681	0.13680
3.00000	0.14065	0.14063		0.14064
2.00000	0.13714	0.13708	0.13709	0.13710
1.00000	0.13810	0.13809		0.13810

Filter

Vial Average	Filter+Ash+Vial
0.96737	0.97485
0.96662	1.00075
0.96979	1.00075
0.97350	1.00576
0.97179	1.00347
0.97487	1.00547
0.00000	0.13739
0.00000	0.13680
0.00000	0.14064
0.00000	0.13710
0.00000	0.13810

Net Mass Collected

STAGE	MASS (no cyclone)	Mass Fraction (no cyclone)	Mass Fraction (cyclone)	Normalized Mass
11.00000	0.00071	0.11281	0.00441	0.11217
10.00000	0.00309	0.48751	0.00669	0.48478
9.00000	0.00051	0.07967	0.01261	0.07923
8.00000	0.00061	0.09703	0.01774	0.09649
7.00000	0.00046	0.07257	0.01307	0.07217
6.00000	0.00095	0.15041	0.00472	0.14956
5.00000	0.00007		0.00171	0.00171
4.00000	0.00016		0.00259	0.00259
3.00000	0.00000		0.00042	0.00042
2.00000	0.00000		0.00068	0.00068
1.00000	0.00002		0.00000	0.00000
Cyclone			0.93516	
TOTAL MASS	0.00634	1.00000	1.00000	1.00000
		>0.337	0.99440	
		<0.337	0.00560	

STAGE	Normalized Distribution (wt %)
11.00000	11.21737
10.00000	48.47786
9.00000	7.92276
8.00000	9.64851
7.00000	7.21677
6.00000	14.95649
5.00000	0.17119
4.00000	0.25938
3.00000	0.04150
2.00000	0.06819
1.00000	0.00000
Cyclone TOTAL MASS	100.00000

Particule Size Distribution Calculations
Test: 97P8-9
WITH CYCLONE

Greased Filter Weights

STAGE	1st	2nd	3rd	Average
11.00000	0.02533	0.02536		0.02535
10.00000	0.14146	0.14145		0.14146
9.00000	0.13717	0.13703	0.13724	0.13707
8.00000	0.1396	0.13963	0.13960	0.13961
7.00000		0.13242	0.13246	0.13244
6.00000	0.03256		0.03256	0.03256
5.00000	0.03114	0.03111		0.03113
4.00000	0.02747	0.02746		0.02747
3.00000	0.03071	0.03071	0.03077	0.03073
2.00000	0.03202	0.03205		0.03204
1.00000		0.02940	0.02904	0.02922
Cyclone				
4th wt on plate 9:		0.13684		

Empty vial Weights

STAGE	1st	2nd	3rd	Average
11.00000				
10.00000				
9.00000				
8.00000				
7.00000				
6.00000	0.96675	0.96671		0.96673
5.00000		0.96298	0.96299	0.96299
4.00000	0.96705	0.96707		0.96706
3.00000	0.96371	0.96368		0.96370
2.00000	0.97118	0.9712		0.97119
1.00000	0.97472	0.97469		0.97471
Cyclone	2.59258	2.62715		2.60987

Filter+Ash+Vial

STAGE	1st	2nd	3rd	Average
11.00000	0.02578		0.02576	0.02577
10.00000	0.14211	0.14209		0.14210
9.00000	0.13830	0.13827		0.13829
8.00000	0.14131	0.14133		0.14132
7.00000	0.13371	0.13369		0.13370
6.00000	0.99874	0.99975		0.99975
5.00000	0.99427	0.99428		0.99428
4.00000	0.99476	0.99479		0.99478
3.00000	0.99447	0.99446		0.99447
2.00000	1.00328	1.00335	1.00330	1.00331
1.00000	1.00383	1.00381		1.00382
Cyclone		2.76050	2.63950	2.70000

Filter

Vial Average	Filter+Ash+Vial
0.00000	0.02577
0.00000	0.14210
0.00000	0.13829
0.00000	0.14132
0.00000	0.13370
0.00000	0.99975
0.96673	0.99428
0.96299	0.99478
0.96706	0.99447
0.96370	0.99447
0.97119	1.00331
0.97471	1.00382
2.60987	2.70000

Net Mass Collected

STAGE	MASS	MASS FRACTION
11.00000	0.00043	0.00441
10.00000	0.00065	0.00669
9.00000	0.00121	0.01261
8.00000	0.00171	0.01774
7.00000	0.00126	0.01307
6.00000	0.00046	0.00472
5.00000	0.00017	0.00171
4.00000	0.00025	0.00259
3.00000	0.00004	0.00042
2.00000	0.00008	0.00088
1.00000	0.00000	0.00000
Cyclone	0.09014	0.93516
TOTAL MASS	0.09639	1.00000

Particule Size Distribution Calculations
Test: 97P8-10
NOCYCLONE

Greased Filter Weights

STAGE	1st	2nd	3rd	Average
11.00000	0.00590	0.00590		0.00590
10.00000	0.02931	0.02923	0.02925	0.02926
9.00000	0.03050		0.03060	0.03055
8.00000	0.02909	0.02908		0.02909
7.00000	0.03039	0.03034		0.03037
6.00000	0.03123	0.03121		0.03122
5.00000	0.14159	0.14153		0.14156
4.00000	0.14048	0.14048		0.14048
3.00000	0.13821		0.13817	0.13819
2.00000	0.13615	0.13613		0.13614
1.00000	0.14120		0.14123	0.14122

Empty vial Weights

STAGE	1st	2nd	3rd	Average
11.00000	0.96437		0.96441	0.96439
10.00000	0.96948		0.96953	0.96951
9.00000	0.96258	0.96252	0.96267	0.96259
8.00000	0.98191	0.98187		0.98189
7.00000	0.97033		0.97028	0.97031
6.00000	0.97106		0.97102	0.97104
5.00000				
4.00000				
3.00000				
2.00000				
1.00000				

Filter+Ash+Vial

STAGE	1st	2nd	3rd	Average
11.00000	0.97048		0.97049	0.97049
10.00000	0.99906	0.99916	0.99909	0.99910
9.00000	0.99346	0.99362	0.99354	0.99354
8.00000	1.01131	1.01143	1.01135	1.01136
7.00000	1.00086	1.00096	1.00088	1.00091
6.00000	1.00237	1.00246	1.00239	1.00241
5.00000	0.14138	0.14131	0.14136	0.14135
4.00000	0.14028	0.14019	0.14025	0.14024
3.00000	0.13812	0.13803	0.13809	0.13808
2.00000	0.13600	0.13591	0.13596	0.13596
1.00000	0.14121		0.14119	0.14120

Filter

Vial Average	Filter+Ash+Vial
0.96439	0.97049
0.96951	0.99910
0.96259	0.99354
0.98189	1.01136
0.97031	1.00091
0.97104	1.00241
0.00000	0.14135
0.00000	0.14024
0.00000	0.13808
0.00000	0.13596
0.00000	0.14120

Net Mass Collected

STAGE	MASS (no cyclone)	Mass Fraction (no cyclone)	Mass Fraction (cyclone)	Normalized Mass
11.00000	0.00020	0.11482	0.01312	0.10956
10.00000	0.00033	0.19725	0.02353	0.18822
9.00000	0.00040	0.23356	0.01041	0.22287
8.00000	0.00039	0.22866	0.02695	0.21819
7.00000	0.00024	0.13935	0.02781	0.13297
6.00000	0.00015	0.08636	0.02736	0.06241
5.00000	0.00000		0.01454	0.01454
4.00000	0.00000		0.01369	0.01369
3.00000	0.00000		0.00684	0.00684
2.00000	0.00000		0.00770	0.00770
1.00000	0.00000		0.00299	0.00299
Cyclone			0.82504	
TOTAL MASS	0.00170	1.00000	1.00000	1.00000
		>0.337	0.95423	
		<0.337	0.04577	

STAGE	Normalized Distribution (wt %)
11.00000	10.95630
10.00000	18.82236
9.00000	22.28717
8.00000	21.81895
7.00000	13.29739
6.00000	6.24063
5.00000	1.45444
4.00000	1.36889
3.00000	0.68444
2.00000	0.77000
1.00000	0.29944
Cyclone TOTAL MASS	100.00000

Particule Size Distribution Calculations
Test: 97P8-10
WITH CYCLONE

Greased Filter Weights

STAGE	1st	2nd	3rd	Average
11.00000	0.02754	0.02748	0.02750	0.02751
10.00000		0.13722	0.13720	0.13721
9.00000	0.14216	0.14211	0.14213	0.14213
8.00000	0.13676	0.13675		0.13676
7.00000	0.13501	0.13499		0.13500
6.00000	0.03154		0.03152	0.03153
5.00000	0.03125		0.03124	0.03125
4.00000	0.03319	0.03320		0.03320
3.00000	0.03322	0.03323		0.03323
2.00000	0.03004	0.03004		0.03004
1.00000	0.02719	0.02716		0.02718
Cyclone				8.00552

Empty vial Weights

STAGE	1st	2nd	3rd	Average
11.00000				
10.00000				
9.00000				
8.00000				
7.00000				
6.00000	0.96416	0.96417		0.96417
5.00000	0.96467	0.96472		0.96470
4.00000	0.96062	0.96064		0.96063
3.00000	0.96019	0.96022		0.96021
2.00000	0.97365	0.97385	0.97351	0.97367
1.00000	0.97573		0.97572	0.97573
Cyclone	8.00734	8.00345	8.00577	8.00552

Filter+Ash+Vial

STAGE	1st	2nd	3rd	Average
11.00000	0.02767		0.02765	0.02766
10.00000		0.1375	0.13747	0.13749
9.00000	0.14226		0.14225	0.14226
8.00000	0.13706	0.13708		0.13707
7.00000	0.13531	0.13534		0.13533
6.00000	0.99602	0.99601		0.99602
5.00000	0.99612	0.99610		0.99611
4.00000	0.99400	0.99397		0.99399
3.00000	0.99351	0.99351		0.99351
2.00000	1.00382	1.00378		1.00380
1.00000	1.00295	1.00292		1.00294

Filter

Vial Average	Filter+Ash+Vial
0.00000	0.02766
0.00000	0.13749
0.00000	0.14226
0.00000	0.13707
0.00000	0.13533
0.96417	0.99602
0.96470	0.99611
0.96063	0.99399
0.96021	0.99351
0.97367	1.00380
0.97573	1.00294
8.00552	8.01516

Net Mass Collected

STAGE	MASS	MASS FRACTION
11.00000	0.00015	0.01312
10.00000	0.00028	0.02353
9.00000	0.00012	0.01041
8.00000	0.00031	0.02695
7.00000	0.00032	0.02781
6.00000	0.00032	0.02738
5.00000	0.00017	0.01454
4.00000	0.00016	0.01369
3.00000	0.00008	0.00684
2.00000	0.00009	0.00770
1.00000	0.00003	0.00299
Cyclone	0.00964	0.82504
TOTAL MASS	0.01169	1.00000

Particule Size Distribution Calculations
Test: 97P8-11
NOCYCLONE

Greased Filter Weights

STAGE	1st	2nd	3rd	Average
11.00000	0.00597	0.00590	0.00607	0.00598
10.00000	0.02757		0.02763	0.02760
9.00000	0.02816		0.02813	0.02815
8.00000		0.03191	0.03194	0.03193
7.00000		0.02854	0.02855	0.02855
6.00000	0.03161		0.03165	0.03163
5.00000	0.13819		0.13820	0.13820
4.00000	0.12475		0.12475	0.12475
3.00000	0.13651		0.13650	0.13651
2.00000	0.14208		0.14205	0.14207
1.00000	0.13923	0.13925		0.13924

Empty vial Weights

STAGE	1st	2nd	3rd	Average
11.00000	0.67944	0.67942		0.67943
10.00000	0.67545	0.67542		0.67544
9.00000	0.67792	0.67791		0.67792
8.00000	0.67725	0.67923		0.67824
7.00000	0.67090	0.67089		0.67090
6.00000	0.67270	0.67267		0.67269
5.00000				
4.00000				
3.00000				
2.00000				
1.00000				

Filter+Ash+Vial

STAGE	1st	2nd	3rd	Average
11.00000	0.68584	0.68586		0.68585
10.00000	0.70569	0.70569		0.70569
9.00000	0.70700	0.70699		0.70700
8.00000	0.71193	0.71191		0.71192
7.00000	0.70004	0.70002		0.70003
6.00000	0.70466		0.70465	0.70466
5.00000	0.13824	0.13827		0.13826
4.00000	0.12477	0.12480		0.12478
3.00000	0.13652	0.13655		0.13654
2.00000	0.14160	0.14164		0.14162
1.00000	0.13920	0.13922		0.13921

Filter

Vial Average	Filter+Ash+Vial
0.67943	0.68585
0.67544	0.70569
0.67792	0.70700
0.67824	0.71192
0.67090	0.70003
0.67269	0.70466
0.00000	0.13826
0.00000	0.12479
0.00000	0.13654
0.00000	0.14162
0.00000	0.13921

Net Mass Collected

STAGE	MASS (no cyclone)	Mass Fraction (no cyclone)	Mass Fraction (cyclone)	Normalized Mass
11.00000	0.00044	0.06552	0.02038	0.06459
10.00000	0.00266	0.39538	0.03720	0.38973
9.00000	0.00093	0.13924	0.02585	0.13725
8.00000	0.00176	0.26136	0.02161	0.25762
7.00000	0.00059	0.08786	0.00814	0.08661
6.00000	0.00034	0.05063	0.00485	0.04991
5.00000	0.00006		0.00554	0.00554
4.00000	0.00004		0.00403	0.00403
3.00000	0.00003		0.00205	0.00205
2.00000	0.00000		0.00123	0.00123
1.00000	0.00000		0.00144	0.00144
Cyclone			0.86769	
TOTAL MASS	0.00672	1.00000	1.00000	1.00000
		>0.337	0.98571	
		<0.337	0.01429	

STAGE	Normalized Distribution (wt %)
11.00000	6.45685
10.00000	38.97329
9.00000	13.72506
8.00000	25.76201
7.00000	8.66073
6.00000	4.99083
5.00000	0.55387
4.00000	0.40344
3.00000	0.20514
2.00000	0.12308
1.00000	0.14360
Cyclone TOTAL MASS	100.00000

Particule Size Distribution Calculations
Test: 97P8-11
WITH CYCLONE

Greased Filter Weights

STAGE	1st	2nd	3rd	Average
11.00000	0.02973	0.02975		0.02974
10.00000	0.13991	0.13990		0.13991
9.00000	0.14106	0.14105		0.14106
8.00000		0.13827	0.13827	0.13827
7.00000	0.14094	0.14094		0.14094
6.00000		0.03010	0.03009	0.03010
5.00000	0.03118	0.03116		0.03117
4.00000	0.03076	0.03079		0.03078
3.00000	0.02978	0.02981		0.02980
2.00000	0.03138	0.03138		0.03138
1.00000	0.03102	0.03102		0.03102
Cyclone				

Filter

Vial Average	Filter+Ash+Vial
0.00000	0.03123
0.00000	0.14263
0.00000	0.14295
0.00000	0.13985
0.00000	0.14154
0.67486	0.70531
0.67772	0.70929
0.67282	0.70389
0.67622	0.70617
0.67551	0.70698
0.67534	0.70647
7.75880	7.82225

Net Mass Collected

STAGE	MASS	MASS FRACTION
11.00000	0.00149	0.02038
10.00000	0.00272	0.03720
9.00000	0.00189	0.02585
8.00000	0.00158	0.02161
7.00000	0.00059	0.00814
6.00000	0.00035	0.00485
5.00000	0.00040	0.00554
4.00000	0.00030	0.00403
3.00000	0.00015	0.00205
2.00000	0.00009	0.00123
1.00000	0.00010	0.00144
Cyclone	0.06345	0.86789
TOTAL MASS	0.07312	1.00000

STAGE	1st	2nd	3rd	Average
11.00000				
10.00000				
9.00000				
8.00000				
7.00000				
6.00000	0.67486	0.67486		0.67486
5.00000	0.67772	0.67771		0.67772
4.00000	0.67282	0.67281		0.67282
3.00000	0.67623	0.67621		0.67622
2.00000	0.6755	0.67551		0.67551
1.00000	0.67535	0.67533		0.67534
Cyclone	7.75883	7.75883	7.75874	7.75880

Filter+Ash+Vial

STAGE	1st	2nd	3rd	Average
11.00000	0.03124		0.03122	0.03123
10.00000	0.14263		0.14262	0.14263
9.00000	0.14295		0.14294	0.14295
8.00000	0.13990	0.13979	0.13986	0.13985
7.00000		0.14153	0.14154	0.14154
6.00000		0.70529	0.70533	0.70531
5.00000		0.70930	0.70928	0.70929
4.00000		0.70388	0.70389	0.70389
3.00000		0.70616	0.70617	0.70617
2.00000		0.70697	0.70698	0.70698
1.00000		0.70647	0.70646	0.70647
Cyclone	7.82216	7.82232	7.82226	7.82225

Particule Size Distribution Calculations
Test: 97P6-12
NOCYCLONE

Greased Filter Weights

STAGE	1st	2nd	3rd	Average
11.00000	0.00669	0.00667		0.00668
10.00000	0.02958	0.02954		0.02956
9.00000	0.03181	0.03186		0.03184
8.00000	0.02938	0.02939		0.02939
7.00000	0.02886	0.02888		0.02887
6.00000	0.02804	0.02803		0.02804
5.00000	0.13993	0.13994		0.13994
4.00000	0.13746	0.13746		0.13746
3.00000	0.13913	0.13912		0.13913
2.00000	0.13560	0.13561		0.13561
1.00000	0.14313	0.14315		0.14314

Empty vial Weights

STAGE	1st	2nd	3rd	Average
11.00000	0.67453	0.67452		0.67453
10.00000	0.67445	0.67442		0.67444
9.00000		0.67380	0.67377	0.67379
8.00000	0.68729	0.68703	0.68687	0.68706
7.00000	0.67629	0.67630		0.67630
6.00000	0.68256	0.68261	0.68253	0.68257
5.00000				
4.00000				
3.00000				
2.00000				
1.00000				

Filter+Ash+Vial

STAGE	1st	2nd	3rd	Average
11.00000		0.68145	0.68146	0.68146
10.00000	0.70799	0.70803		0.70801
9.00000	0.70604		0.70605	0.70605
8.00000		0.71669	0.71668	0.71669
7.00000	0.70543	0.70547		0.70545
6.00000	0.71086		0.71089	0.71088
5.00000	0.13998	0.13994		0.13996
4.00000	0.13753	0.13749		0.13751
3.00000	0.13908	0.13906		0.13907
2.00000		0.13562	0.13563	0.13563
1.00000	0.14314	0.14315		0.14315

Filter

Vial Average	Filter+Ash+Vial
0.67453	0.68146
0.67444	0.70801
0.67379	0.70605
0.68706	0.71669
0.67630	0.70545
0.68257	0.71088
0.00000	0.13996
0.00000	0.13751
0.00000	0.13907
0.00000	0.13563
0.00000	0.14315

Net Mass Collected

STAGE	MASS (no cyclone)	Mass Fraction (no cyclone)	Mass Fraction (cyclone)	Normalized Mass
11.00000	0.00025	0.04558	0.01490	0.04213
10.00000	0.00402	0.73200	0.07522	0.67658
9.00000	0.00043	0.07748	0.03241	0.07162
8.00000	0.00024	0.04315	0.01892	0.03988
7.00000	0.00029	0.05196	0.00323	0.04803
6.00000	0.00027	0.04963	0.02673	0.04606
5.00000	0.00002		0.02318	0.02318
4.00000	0.00005		0.01064	0.01064
3.00000	0.00000		0.01206	0.01206
2.00000	0.00002		0.01963	0.01963
1.00000	0.00001		0.01017	0.01017
Cyclone			0.75290	
TOTAL MASS	0.00549	1.00000	1.00000	1.00000
		>0.337	0.92431	
		<0.337	0.07569	

STAGE	Normalized Distribution (wt %)
11.00000	4.21289
10.00000	67.65902
9.00000	7.16191
8.00000	3.98820
7.00000	4.80269
6.00000	4.60609
5.00000	2.31806
4.00000	1.06442
3.00000	1.20634
2.00000	1.96326
1.00000	1.01711
Cyclone TOTAL MASS	100.00000

Particule Size Distribution Calculations
Test: 97P8-12
WITH CYCLONE

Greased Filter Weights

STAGE	1st	2nd	3rd	Average
11.00000	0.02988	0.02984		0.02986
10.00000	0.13897	0.13893		0.13895
9.00000	0.14163	0.14154	0.14157	0.14158
8.00000	0.13934	0.13930		0.13932
7.00000	0.14158	0.14145	0.14152	0.14152
6.00000	0.03231	0.03230		0.03231
5.00000	0.03017	0.03016		0.03017
4.00000	0.03120	0.03119		0.03120
3.00000	0.03127	0.03127		0.03127
2.00000	0.03214	0.03212		0.03213
1.00000	0.03250	0.03250		0.03250
Cyclone				

Empty vial Weights

STAGE	1st	2nd	3rd	Average
11.00000				
10.00000				
9.00000				
8.00000				
7.00000				
6.00000	0.67173		0.67169	0.67171
5.00000	0.67704		0.67701	0.67703
4.00000	0.68179	0.68183		0.68181
3.00000	0.67504	0.67507		0.67506
2.00000	0.68442	0.68446		0.68444
1.00000	0.68065	0.68067		0.68066
Cyclone	7.64603	7.64600		7.64602

Filter+Ash+Vial

STAGE	1st	2nd	3rd	Average
11.00000	0.03017		0.03018	0.03018
10.00000	0.14053	0.14055		0.14054
9.00000	0.14226	0.14227		0.14227
8.00000		0.13973	0.13971	0.13972
7.00000		0.14159	0.14158	0.14159
6.00000	0.70458	0.70458		0.70458
5.00000	0.70769	0.70767		0.70768
4.00000	0.71323	0.71323		0.71323
3.00000	0.70659	0.70657		0.70658
2.00000	0.71699	0.71698		0.71699
1.00000	0.71338	0.71337		0.71338
Cyclone	7.66191	7.66195		7.66193

Filter

Vial Average	Filter+Ash+Vial
0.00000	0.03018
0.00000	0.14054
0.00000	0.14227
0.00000	0.13972
0.00000	0.14159
0.67171	0.70458
0.67703	0.70768
0.68181	0.71323
0.67506	0.70658
0.68444	0.71699
0.68066	0.71338
7.64602	7.66193

Net Mass Collected

STAGE	MASS	MASS FRACTION
11.00000	0.00032	0.01490
10.00000	0.00159	0.07522
9.00000	0.00068	0.03241
8.00000	0.00040	0.01892
7.00000	0.00007	0.00323
6.00000	0.00056	0.02673
5.00000	0.00049	0.02318
4.00000	0.00023	0.01064
3.00000	0.00026	0.01206
2.00000	0.00042	0.01963
1.00000	0.00021	0.01017
Cyclone	0.01591	0.75290
TOTAL MASS	0.02114	1.00000

Particle Size Distribution Calculations
Test: 97IL1
NOCYCLONE

Greased Filter Weights

STAGE	1st	2nd	3rd	Average
11.00000	0.00680	0.00679		0.00680
10.00000	0.03249	0.03246		0.03248
9.00000	0.03515		0.03515	0.03515
8.00000	0.03046	0.03044		0.03045
7.00000	0.02945	0.02941		0.02943
6.00000	0.02945	0.02945		0.02945
5.00000	0.14073	0.14077		0.14075
4.00000	0.14145	0.14146		0.14146
3.00000	0.14096	0.14100		0.14098
2.00000	0.14067	0.14069		0.14068
1.00000	0.14086	0.14089		0.14088

Empty vial Weights

STAGE	1st	2nd	3rd	Average
11.00000	0.96575	0.96574		0.96575
10.00000	0.96718	0.96717		0.96718
9.00000	0.97370	0.97367		0.97369
8.00000	0.95980	0.95977		0.95979
7.00000	0.97146	0.97145		0.97146
6.00000	0.97471	0.97468		0.97470
5.00000				
4.00000				
3.00000				
2.00000				
1.00000				

Filter+Ash+Vial

STAGE	1st	2nd	3rd	Average
11.00000	0.97312	0.97311		0.97312
10.00000	1.00074	1.00074		1.00074
9.00000	1.00950	1.00947		1.00949
8.00000	0.99115	0.99113		0.99114
7.00000	1.00131	1.00128		1.00130
6.00000	1.00441	1.00438		1.00440
5.00000	0.14088	0.14092		0.14090
4.00000	0.14145	0.14149		0.14147
3.00000	0.14097	0.14101		0.14099
2.00000	0.14044	0.14044		0.14044

Filter

Average	Vial Average	Filter+Ash+Vial
0.00680	0.96575	0.97312
0.03248	0.96718	1.00074
0.03515	0.97369	1.00949
0.03045	0.95979	0.99114
0.02943	0.97146	1.00130
0.02945	0.97470	1.00440
0.14075	0.00000	0.14090
0.14146	0.00000	0.14147
0.14098	0.00000	0.14099
0.14068	0.00000	0.14044
0.14088	0.00000	0.14082

Net Mass Collected

STAGE	MASS (NO Cyclone)	MASS FRACTION (No Cyclone)	MASS FRACTION (Cyclone)	Normalized Mass	STAGE	Normalized Distribution (wt %)
11.00000	0.00057	0.14820	0.00000	0.14863	11.00000	14.66347
10.00000	0.00109	0.28093	0.06678	0.27797	10.00000	27.79684
9.00000	0.00065	0.16753	0.04324	0.16576	9.00000	16.57610
8.00000	0.00090	0.23325	0.02680	0.23079	8.00000	23.07903
7.00000	0.00041	0.10567	0.01131	0.10456	7.00000	10.45569
6.00000	0.00025	0.06443	0.00303	0.06375	6.00000	6.37542
5.00000	0.00015		0.00647	0.00647	5.00000	0.64748
4.00000	0.00001		0.00211	0.00211	4.00000	0.21069
3.00000	0.00001		0.00108	0.00108	3.00000	0.10791
2.00000	0.00000		0.00000	0.00000	2.00000	0.00000
1.00000	0.00000		0.00087	0.00087	1.00000	0.08736
Cyclone			0.83930			
TOTAL MASS	0.00388	1.00000	1.00000	1.00000	TOTAL MASS	100.00000
		>0.337	0.98947			
		<0.337	0.01053			

Particle Size Distribution Calculations
Test: 97IL1
WITH CYCLONE

Greased Filter Weights

STAGE	1st	2nd	3rd	Average
11.00000	0.03007	0.03009		0.03008
10.00000	0.13897	0.13897		0.13897
9.00000	0.13862	0.13862		0.13862
8.00000	0.13779	0.13779		0.13779
7.00000	0.13859	0.13859		0.13859
6.00000	0.03146	0.03147		0.03147
5.00000	0.02865	0.02866		0.02866
4.00000	0.03131	0.03133		0.03132
3.00000	0.02849		0.02847	0.02848
2.00000	0.03274	0.32700		0.17987
1.00000	0.02908	0.02911		0.02910

Empty vial Weights

STAGE	1st	2nd	3rd	Average
11.00000	8.33489	8.33479		8.33484
10.00000				
9.00000				
8.00000				
7.00000				
6.00000	0.97128	0.97127		0.97128
5.00000	0.96737	0.96374		0.96556
4.00000	0.96692	0.96689		0.96691
3.00000	0.96332	0.96330		0.96331
2.00000	0.96048	0.96048		0.96048
1.00000	0.96236	0.96235		0.96236
Cyclone	7.96359	7.96176	7.96018	7.96201
	7.96463	7.95991		

Filter+Ash+Vial

STAGE	1st	2nd	3rd	Average
11.00000	0.03673	0.03672		0.03673
10.00000	0.16498	0.16494		0.16496
9.00000	0.15543	0.15547		0.15545
8.00000	0.14821		0.14823	0.14822
7.00000	0.14294	0.14304	0.14300	0.14299
6.00000	1.00390	1.00394		1.00392
5.00000	0.99672	0.99674		0.99673
4.00000	0.99904	0.99905		0.99905
3.00000	0.99220	0.99222		0.99221
2.00000	0.9935	0.99352		0.99351
1.00000	1.01178		1.01180	1.01179
Cyclone	8.28823	8.28832	8.28829	8.28828

Net Mass Collected

Vial Average	Filter+Ash+Vial	STAGE	MASS	Mass Fraction
8.33484	0.03673	11.00000	0.00000	0.00000
0.00000	0.16496	10.00000	0.02599	0.06678
0.00000	0.15545	9.00000	0.01683	0.04324
0.00000	0.14822	8.00000	0.01043	0.02680
0.00000	0.14299	7.00000	0.00440	0.01131
0.97128	1.00392	6.00000	0.00116	0.00303
0.96556	0.99673	5.00000	0.00252	0.00647
0.96691	0.99905	4.00000	0.00082	0.00211
0.96331	0.99221	3.00000	0.00042	0.00108
0.96048	0.99351	2.00000	0.00000	0.00000
0.98236	1.01179	1.00000	0.00034	0.00087
7.96201	8.28828	Cyclone	0.32627	0.83830
		TOTAL MASS	0.38920	1.00000

Particle Size Distribution Calculations
Test: 97IL2
NOCYCLONE

Greased Filter Weights

STAGE	1st	2nd	3rd	Average
11.00000	0.00733	0.00734		0.00734
10.00000	0.03101	0.03100		0.03101
9.00000	0.03294	0.03294		0.03294
8.00000	0.03169	0.03168		0.03169
7.00000	0.03019	0.03018		0.03019
6.00000	0.02986	0.02982		0.02984
5.00000	0.14042	0.14044		0.14043
4.00000	0.13945	0.13946		0.13946
3.00000	0.13760	0.13761		0.13761
2.00000	0.13854	0.13855		0.13855
1.00000	0.14221	0.14224		0.14223

Empty vial Weights

STAGE	1st	2nd	3rd	Average
11.00000	0.97576	0.97572		0.97574
10.00000	0.97144	0.97140		0.97142
9.00000	0.97304	0.97301		0.97303
8.00000	0.96647	0.96645		0.96646
7.00000	0.97507	0.97503		0.97505
6.00000	0.96742	0.96742		0.96742
5.00000				
4.00000				
3.00000				
2.00000				
1.00000				

Filter+Ash+Vial

STAGE	1st	2nd	3rd	Average
11.00000	0.98315	0.98316		0.98316
10.00000	1.00269	1.00270	1.00276	1.00272
9.00000	1.00623	1.00628		1.00626
8.00000	0.99826	0.99831		0.99830
7.00000	1.00544	1.00547		1.00546
6.00000	1.01733	1.01738		1.01736
5.00000	0.14021	0.14015		0.14018
4.00000	0.13940	0.13945		0.13943
3.00000	0.13752	0.13757		0.13755
2.00000	0.13854	0.13858		0.13856
1.00000	0.14206	0.14209		0.14208

Filter

Vial Average	Filter+Ash+Vial
0.97574	0.98316
0.97142	1.00272
0.97303	1.00626
0.96646	0.99830
0.97505	1.00546
0.98742	1.01736
0.00000	0.14018
0.00000	0.13943
0.00000	0.13755
0.00000	0.13856
0.00000	0.14208

Net Mass Collected

STAGE	MASS (NO Cyclone)	MASS FRACTION (No Cyclone)	MASS FRACTION (Cyclone)	Normalized Mass	STAGE	Normalized Distribution (wt %)
11.00000	0.00008	0.07101	0.00702	0.06705	11.00000	6.70509
10.00000	0.00029	0.25888	0.00577	0.24446	10.00000	24.44563
9.00000	0.00029	0.25740	0.01042	0.24306	9.00000	24.30594
8.00000	0.00015	0.13314	0.04766	0.12572	8.00000	12.57204
7.00000	0.00022	0.19527	0.05174	0.18439	7.00000	18.43899
6.00000	0.00010	0.08432	0.02343	0.07962	6.00000	7.96229
5.00000	0.00000		0.01325	0.01325	5.00000	1.32458
4.00000	0.00000		0.01279	0.01279	4.00000	1.27929
3.00000	0.00000		0.00623	0.00623	3.00000	0.62267
2.00000	0.00002		0.00645	0.00645	2.00000	0.64531
1.00000	0.00000		0.01698	0.01698	1.00000	1.69818
Cyclone			0.79826			
TOTAL MASS	0.00113	1.00000	1.00000	1.00000	TOTAL MASS	100.00000
		>0.337	0.94430			
		<0.337	0.05570			

Particle Size Distribution Calculations
Test: 97IL2
WITH CYCLONE

Greased Filter Weights

STAGE	1st	2nd	3rd	Average
11.00000	0.03049	0.03049		0.03049
10.00000	0.13860	0.13862		0.13861
9.00000	0.14192	0.14192		0.14192
8.00000	0.13778	0.13779		0.13779
7.00000	0.13733	0.13732		0.13733
6.00000		0.03250	0.03250	0.03250
5.00000		0.03046	0.03044	0.03045
4.00000		0.03146	0.03144	0.03145
3.00000	0.03056	0.03058		0.03057
2.00000	0.03214	0.03218		0.03216
1.00000	0.03097	0.03010		0.03054

Empty vial Weights

STAGE	1st	2nd	3rd	Average
11.00000				
10.00000				
9.00000				
8.00000				
7.00000				
6.00000	0.96711	0.96710		0.96711
5.00000	0.96779	0.96776		0.96778
4.00000	0.96696	0.96694		0.96695
3.00000	0.96822	0.96821		0.96822
2.00000	0.97385	0.97383		0.97384
1.00000	0.96617	0.96616		0.96617
Cyclone	7.72191		7.72191	7.72191

Filter+Ash+Vial

STAGE	1st	2nd	3rd	Average
11.00000	0.03079	0.03081		0.03080
10.00000		0.13885	0.13888	0.13887
9.00000		0.14237	0.14239	0.14238
8.00000		0.13988	0.13990	0.13989
7.00000		0.13960	0.13962	0.13961
6.00000	1.00063	1.00065		1.00064
5.00000	0.99880	0.99882		0.99881
4.00000	0.99895	0.99898		0.99897
3.00000	0.99905	0.99906		0.99906
2.00000	1.00631	1.00626		1.00629
1.00000	0.99744	0.99746		0.99745
Cyclone	7.75717	7.75716		7.75717

Filter

Vial Average	Filter+Ash+Vial
0.00000	0.03080
0.00000	0.13887
0.00000	0.14238
0.00000	0.13989
0.00000	0.13961
0.96711	1.00064
0.96778	0.99881
0.96695	0.99897
0.96822	0.99906
0.97384	1.00629
0.96617	0.99745
7.72191	7.75717

Net Mass Collected

STAGE	MASS	Mass Fraction
11.00000	0.00031	0.00702
10.00000	0.00026	0.00577
9.00000	0.00046	0.01042
8.00000	0.00211	0.04766
7.00000	0.00229	0.05174
6.00000	0.00103	0.02343
5.00000	0.00058	0.01325
4.00000	0.00057	0.01279
3.00000	0.00027	0.00623
2.00000	0.00029	0.00645
1.00000	0.00075	0.01698
Cyclone	0.03526	0.79826
TOTAL MASS	0.04417	1.00000

Particle Size Distribution Calculations
Test: 97IL3
NOCYCLONE

Greased Filter Weights

STAGE	1st	2nd	3rd	Average
11.00000	0.00620	0.00624		0.00622
10.00000	0.02991	0.02995		0.02993
9.00000	0.03088	0.03088		0.03088
8.00000	0.03024	0.03027		0.03026
7.00000	0.02960	0.02964		0.02962
6.00000	0.02930	0.02934		0.02932
5.00000	0.14300	0.14130		0.14215
4.00000	0.14216	0.14217		0.14217
3.00000	0.14387	0.14388		0.14388
2.00000	0.14178	0.14177		0.14178
1.00000	0.14399	0.14399		0.14399

Empty vial Weights

STAGE	1st	2nd	3rd	Average
11.00000		0.68466	0.68464	0.68465
10.00000	0.68237	0.68234		0.68236
9.00000	0.67961	0.67959		0.67960
8.00000		0.67655	0.67647	0.67651
7.00000	0.67772	0.67769		0.67771
6.00000	0.67240	0.67239		0.67240
5.00000				
4.00000				
3.00000				
2.00000				
1.00000				

Filter+Ash+Vial

STAGE	1st	2nd	3rd	Average
11.00000	0.69126	0.69129		0.69128
10.00000	0.71316	0.71318		0.71317
9.00000	0.71108	0.71110		0.71109
8.00000	0.70699	0.70700		0.70700
7.00000	0.70766	0.70767		0.70767
6.00000	0.70187	0.70188		0.70188
5.00000	0.14137	0.14138		0.14138
4.00000	0.14215	0.14215		0.14215
3.00000	0.14386	0.14385		0.14386
2.00000	0.14170	0.14169		0.14170
1.00000	0.14389	0.14387		0.14388

Filter

Vial Average	Filter+Ash+Vial
0.68465	0.69128
0.68236	0.71317
0.67960	0.71109
0.67651	0.70700
0.67771	0.70767
0.67240	0.70188
0.00000	0.14138
0.00000	0.14215
0.00000	0.14386
0.00000	0.14170
0.00000	0.14388

Net Mass Collected

STAGE	MASS (NO Cyclone)	MASS FRACTION (No Cyclone)	MASS FRACTION (Cyclone)	Normalized Mass	STAGE	Normalized Distribution (wt %)
11.00000	0.00040	0.15399	0.00525	0.15206	11.00000	15.20640
10.00000	0.00069	0.33650	0.00219	0.33229	10.00000	33.22880
9.00000	0.00061	0.23194	0.01743	0.22903	9.00000	22.90346
8.00000	0.00023	0.08745	0.02794	0.08636	8.00000	8.63573
7.00000	0.00034	0.12928	0.01541	0.12766	7.00000	12.76586
6.00000	0.00016	0.06084	0.01016	0.06007	6.00000	6.00747
5.00000	0.00000		0.00473	0.00473	5.00000	0.47289
4.00000	0.00000		0.00508	0.00508	4.00000	0.50792
3.00000	0.00000		0.00271	0.00271	3.00000	0.27147
2.00000	0.00000		0.00000	0.00000	2.00000	0.00000
1.00000	0.00000		0.00000	0.00000	1.00000	0.00000
Cyclone			0.90910			
TOTAL MASS	0.00263	1.00000	1.00000	1.00000	TOTAL MASS	100.00000
		>0.337	0.98748			
		<0.337	0.01252			

Particle Size Distribution Calculations
Test: 97IL3
WITH CYCLONE

Greased Filter Weights

STAGE	1st	2nd	3rd	Average
11.00000	0.02999	0.03000		0.03000
10.00000	0.14125	0.14125		0.14125
9.00000	0.14174	0.14175		0.14175
8.00000	0.14041	0.14041		0.14041
7.00000	0.14587	0.14588		0.14588
6.00000	0.03164	0.03165		0.03165
5.00000	0.03461	0.03461		0.03461
4.00000	0.03041	0.03042		0.03042
3.00000	0.02906	0.02907		0.02907
2.00000	0.02873		0.02875	0.02874
1.00000	0.03046	0.03047		0.03047

Empty vial Weights

STAGE	1st	2nd	3rd	Average
11.00000				
10.00000				
9.00000				
8.00000				
7.00000				
6.00000	0.67944	0.67945		0.67945
5.00000	0.67306	0.67307		0.67307
4.00000	0.68198	0.68197		0.68198
3.00000	0.67002	0.67006		0.67004
2.00000		0.67126	0.69125	0.68126
1.00000	0.68516		0.67514	0.68015
Cyclone	7.95789	7.95727	7.95670	7.95729

Filter+Ash+Vial

STAGE	1st	2nd	3rd	Average
11.00000	0.03029	0.03030		0.03030
10.00000	0.14137	0.14136		0.14136
9.00000	0.14274	0.14274		0.14274
8.00000	0.14200	0.14201		0.14201
7.00000	0.14675	0.14676		0.14676
6.00000	0.71167	0.71167		0.71167
5.00000	0.70794	0.70795		0.70795
4.00000	0.71269	0.71267		0.71268
3.00000	0.69926	0.69926		0.69926
2.00000	0.70022	0.70022		0.70022
1.00000	0.70576	0.70577		0.70577
Cyclone	8.00931	8.00900	8.00857	8.00919
	8.00989			

Filter

Vial Average	Filter+Ash+Vial
0.00000	0.03030
0.00000	0.14138
0.00000	0.14274
0.00000	0.14201
0.00000	0.14676
0.67945	0.71167
0.67307	0.70795
0.68198	0.71268
0.67004	0.69926
0.68126	0.70022
0.68015	0.70577
7.95729	8.00919

Net Mass Collected

STAGE	MASS	Mass Fraction
11.00000	0.00030	0.00525
10.00000	0.00013	0.00219
9.00000	0.00099	0.01743
8.00000	0.00159	0.02794
7.00000	0.00088	0.01541
6.00000	0.00058	0.01016
5.00000	0.00027	0.00473
4.00000	0.00029	0.00508
3.00000	0.00016	0.00271
2.00000	0.00000	0.00000
1.00000	0.00000	0.00000
Cyclone	0.05191	0.90910
TOTAL MASS	0.05710	1.00000

Particle Size Distribution Calculations
Test: 97IL4
NOCYCLONE

Greased Filter Weights

STAGE	1st	2nd	3rd	Average
11.00000	0.00660	0.00660		0.00660
10.00000	0.02984	0.02986		0.02985
9.00000	0.03016	0.03015		0.03016
8.00000		0.03008	0.03009	0.03009
7.00000	0.03152	0.03151		0.03152
6.00000	0.03042	0.03042		0.03042
5.00000		0.14097	0.14097	0.14097
4.00000		0.14158	0.14157	0.14158
3.00000		0.14266	0.14264	0.14265
2.00000	0.14099	0.14103		0.14101
1.00000	0.13921	0.13924		0.13923

Empty vial Weights

STAGE	1st	2nd	3rd	Average
11.00000	0.68198		0.68198	0.68198
10.00000	0.68057	0.68058		0.68058
9.00000	0.67535	0.67536		0.67536
8.00000	0.68778	0.68778		0.68778
7.00000	0.67397	0.67396		0.67397
6.00000	0.67599	0.67600		0.67600
5.00000				
4.00000				
3.00000				
2.00000				
1.00000				

Filter+Ash+Vial

STAGE	1st	2nd	3rd	Average
11.00000	0.68877	0.68878		0.68878
10.00000	0.71207	0.71207		0.71207
9.00000	0.70571	0.70573		0.70572
8.00000	0.71794	0.71796		0.71795
7.00000	0.70583	0.70584		0.70584
6.00000	0.70655	0.70655		0.70655
5.00000	0.14101	0.14102		0.14102
4.00000	0.14156	0.14155		0.14156
3.00000	0.14253	0.14254		0.14254
2.00000	0.14092	0.14094		0.14093
1.00000	0.13922	0.13922		0.13922

Filter

Vial Average	Filter+Ash+Vial
0.68198	0.68878
0.68058	0.71207
0.67536	0.70572
0.68778	0.71795
0.67397	0.70584
0.67600	0.70655
0.00000	0.14102
0.00000	0.14156
0.00000	0.14254
0.00000	0.14093
0.00000	0.13922

Net Mass Collected

STAGE	MASS (NO Cyclone)	MASS FRACTION (No Cyclone)	MASS FRACTION (Cyclone)	Normalized Mass
11.00000	0.00019	0.07429	0.03009	0.07048
10.00000	0.00165	0.62667	0.04860	0.59453
9.00000	0.00021	0.08000	0.01314	0.07590
8.00000	0.00009	0.03238	0.01695	0.03072
7.00000	0.00036	0.13524	0.00212	0.12830
6.00000	0.00014	0.05143	0.02246	0.04879
5.00000	0.00004		0.01992	0.01992
4.00000	0.00000		0.00932	0.00932
3.00000	0.00000		0.00848	0.00848
2.00000	0.00000		0.00932	0.00932
1.00000	0.00000		0.00424	0.00424
Cyclone			0.81534	
TOTAL MASS	0.00263	1.00000	1.00000	1.00000
		>0.337	0.94871	
		<0.337	0.05129	

STAGE	Normalized Distribution (wt %)
11.00000	7.04759
10.00000	59.45276
9.00000	7.58971
8.00000	3.07203
7.00000	12.83023
6.00000	4.87910
5.00000	1.99209
4.00000	0.93247
3.00000	0.84770
2.00000	0.93247
1.00000	0.42385
TOTAL MASS	100.00000

Particle Size Distribution Calculations
Test: 97IL4
WITH CYCLONE

Greased Filter Weights

STAGE	1st	2nd	3rd	Average
11.00000	0.02988	0.02988		0.02988
10.00000	0.14237	0.14237	0.14236	0.14237
9.00000	0.14173	0.14173		0.14173
8.00000		0.14446	0.14445	0.14446
7.00000	0.14494	0.14494		0.14494
6.00000	0.02934	0.02933		0.02934
5.00000	0.03031	0.03030		0.03031
4.00000	0.03102	0.03099		0.03101
3.00000	0.03224	0.03222		0.03223
2.00000	0.03134	0.03133		0.03134
1.00000		0.03449	0.03449	0.03449

Empty vial Weights

STAGE	1st	2nd	3rd	Average
11.00000				
10.00000				
9.00000				
8.00000				
7.00000				
6.00000		0.67722	0.67722	0.67722
5.00000	0.67617	0.67616		0.67617
4.00000		0.68391	0.68386	0.68389
3.00000	0.67447	0.67446		0.67447
2.00000	0.68754	0.68751		0.68753
1.00000	0.67952	0.67951		0.67952
Cyclone	7.94434		7.94343	7.94389

Filter+Ash+Vial

STAGE	1st	2nd	3rd	Average
11.00000	0.03023	0.03024		0.03024
10.00000	0.14294	0.14294		0.14294
9.00000	0.14188	0.14189		0.14189
8.00000	0.14465	0.14466		0.14466
7.00000	0.14497	0.14496		0.14497
6.00000	0.70681	0.70683		0.70682
5.00000	0.70669	0.70672		0.70671
4.00000	0.71499	0.71501		0.71500
3.00000	0.70679	0.70680		0.70680
2.00000	0.71896	0.71898		0.71897
1.00000	0.71406	0.71405		0.71406
Cyclone	7.95355	7.95336	7.9536	7.95350

Filter

Vial Average	Filter+Ash+Vial
0.00000	0.03024
0.00000	0.14294
0.00000	0.14189
0.00000	0.14466
0.00000	0.14497
0.67722	0.70682
0.67617	0.70671
0.68389	0.71500
0.67447	0.70680
0.68753	0.71897
0.67952	0.71406
7.94389	7.95350

Net Mass Collected

STAGE	MASS	Mass Fraction
11.00000	0.00035	0.03009
10.00000	0.00057	0.04860
9.00000	0.00015	0.01314
8.00000	0.00020	0.01695
7.00000	0.00002	0.00212
6.00000	0.00026	0.02246
5.00000	0.00024	0.01992
4.00000	0.00011	0.00932
3.00000	0.00010	0.00848
2.00000	0.00011	0.00932
1.00000	0.00005	0.00424
Cyclone	0.00962	0.81534
TOTAL MASS	0.01180	1.00000

Particle Size Distribution Calculations
Test: 97IL5
NOCYCLONE

Greased Filter Weights

STAGE	1st	2nd	3rd	Average
11.00000	0.00654	0.00654		0.00654
10.00000	0.02951	0.02950		0.02951
9.00000	0.02906	0.02902		0.02904
8.00000	0.03021	0.03024		0.03023
7.00000	0.02921	0.02921		0.02921
6.00000	0.02959	0.02957		0.02958
5.00000		0.14031	0.14033	0.14032
4.00000	0.14126	0.14126		0.14127
3.00000	0.14025	0.14024		0.14025
2.00000	0.13976	0.13975		0.13976
1.00000	0.14026	0.14026		0.14026

Empty vial Weights

STAGE	1st	2nd	3rd	Average
11.00000	0.68849	0.68848		0.68849
10.00000	0.67271	0.67272		0.67272
9.00000	0.67821	0.67822		0.67822
8.00000	0.67059	0.67059		0.67059
7.00000	0.67216	0.67217		0.67217
6.00000	0.67780	0.67779		0.67780
5.00000				
4.00000				
3.00000				
2.00000				
1.00000				

Filter+Ash+Vial

STAGE	1st	2nd	3rd	Average
11.00000	0.69586	0.69586		0.69586
10.00000	0.70407	0.70406		0.70407
9.00000	0.70757	0.70756		0.70757
8.00000	0.70107	0.70107		0.70107
7.00000	0.70157	0.70157		0.70157
6.00000	0.70745	0.70746		0.70746
5.00000	0.14024	0.14027		0.14026
4.00000	0.14119	0.14121		0.14120
3.00000	0.14021	0.14021		0.14021
2.00000	0.13972	0.13973		0.13973

Filter

Vial Average	Filter+Ash+Vial
0.68849	0.69586
0.67272	0.70407
0.67822	0.70757
0.67059	0.70107
0.67217	0.70157
0.67780	0.70746
0.00000	0.14026
0.00000	0.14120
0.00000	0.14021
0.00000	0.13973
0.00000	0.14026

Net Mass Collected

STAGE	MASS (NO Cyclone)	MASS FRACTION (No Cyclone)	MASS FRACTION (Cyclone)	Normalized Mass
11.00000	0.00084	0.23722	0.00515	0.23435
10.00000	0.00184	0.52415	0.00250	0.51782
9.00000	0.00031	0.08807	0.01364	0.08701
8.00000	0.00025	0.07244	0.02045	0.07157
7.00000	0.00020	0.05540	0.01587	0.05473
6.00000	0.00008	0.02273	0.00554	0.02245
5.00000	0.00000		0.00338	0.00338
4.00000	0.00000		0.00647	0.00647
3.00000	0.00000		0.00000	0.00000
2.00000	0.00000		0.00155	0.00155
1.00000	0.00000		0.00068	0.00068
Cyclone			0.92477	
TOTAL MASS	0.00352	1.00000	1.00000	1.00000
		>0.337	0.98793	
		<0.337	0.01207	

STAGE	Normalized Distribution (wt %)
11.00000	23.43530
10.00000	51.78219
9.00000	8.70053
8.00000	7.15689
7.00000	5.47291
6.00000	2.24530
5.00000	0.33759
4.00000	0.64705
3.00000	0.00000
2.00000	0.15473
1.00000	0.06752
TOTAL MASS	100.00000

Particle Size Distribution Calculations
Test: 97IL5
WITH CYCLONE

Greased Filter Weights

STAGE	1st	2nd	3rd	Average
11.00000	0.02890	0.02887		0.02889
10.00000	0.14316	0.14313		0.14315
9.00000	0.14150	0.14150		0.14150
8.00000	0.14478	0.14477		0.14478
7.00000	0.13956	0.13956		0.13956
6.00000	0.02931	0.02931		0.02931
5.00000	0.03003	0.02999		0.03001
4.00000	0.02868	0.02867		0.02868
3.00000	0.02823	0.02822		0.02823
2.00000	0.03001	0.03001		0.03001
1.00000	0.02986	0.02984		0.02985

Empty vial Weights

STAGE	1st	2nd	3rd	Average
11.00000				
10.00000				
9.00000				
8.00000				
7.00000				
6.00000	0.67352	0.67354		0.67353
5.00000	0.68568	0.68570		0.68569
4.00000	0.67255	0.67258		0.67257
3.00000	0.67596	0.67600		0.67598
2.00000	0.68353	0.68355		0.68354
1.00000	0.67425	0.67428		0.67427
Cyclone		7.99590	7.99586	7.99588

Filter+Ash+Vial

STAGE	1st	2nd	3rd	Average
11.00000	0.02980	0.02980		0.02980
10.00000	0.14359	0.14358		0.14359
9.00000	0.14393	0.14392		0.14393
8.00000	0.14841	0.14841		0.14841
7.00000	0.14238	0.14238		0.14238
6.00000	0.70382	0.70383		0.70383
5.00000	0.71629	0.71631		0.71630
4.00000	0.70238	0.70240		0.70239
3.00000	0.70484	0.70240		0.70362
2.00000	0.71383	0.71382		0.71383
1.00000	0.70424	0.70423		0.70424
Cyclone	8.16023	8.16025		8.16024

Filter

Vial Average	Filter+Ash+Vial
0.00000	0.02980
0.00000	0.14359
0.00000	0.14393
0.00000	0.14841
0.00000	0.14238
0.67353	0.70383
0.68569	0.71630
0.67257	0.70239
0.67598	0.70362
0.68354	0.71383
0.67427	0.70424
7.99588	8.16024

Net Mass Collected

STAGE	MASS	Mass Fraction
11.00000	0.00091	0.00515
10.00000	0.00044	0.00250
9.00000	0.00243	0.01364
8.00000	0.00364	0.02045
7.00000	0.00282	0.01587
6.00000	0.00098	0.00554
5.00000	0.00060	0.00338
4.00000	0.00115	0.00647
3.00000	0.00000	0.00000
2.00000	0.00027	0.00155
1.00000	0.00012	0.00068
Cyclone	0.16436	0.92477
TOTAL MASS	0.17773	1.00000

Particle Size Distribution Calculations
Test: 97IL6
NOCYCLONE

Greased Filter Weights

STAGE	1st	2nd	3rd	Average
11.00000	0.00678	0.00677		0.00678
10.00000	0.02834	0.02832		0.02833
9.00000	0.02856	0.02855		0.02856
8.00000	0.02888	0.02888		0.02888
7.00000	0.02918	0.02919		0.02919
6.00000	0.02925	0.02926		0.02926
5.00000	0.14136	0.14135		0.14136
4.00000	0.13968	0.13966		0.13967
3.00000	0.13934	0.13934		0.13934
2.00000	0.13974	0.13974		0.13974
1.00000	0.14039	0.14039		0.14039

Empty vial Weights

STAGE	1st	2nd	3rd	Average
11.00000	0.67185	0.67187		0.67186
10.00000	0.68479	0.68477		0.68478
9.00000	0.67515	0.67516		0.67516
8.00000	0.67479	0.67483		0.67481
7.00000	0.67700	0.67702		0.67701
6.00000	0.67707	0.67710		0.67709
5.00000				
4.00000				
3.00000				
2.00000				
1.00000				

Filter+Ash+Vial

STAGE	1st	2nd	3rd	Average
11.00000	0.67958	0.67961		0.67960
10.00000	0.71421	0.71421		0.71421
9.00000	0.70406	0.70408		0.70407
8.00000	0.70382	0.70382		0.70382
7.00000	0.70641	0.70645		0.70643
6.00000	0.70641	0.70645		0.70643
5.00000	0.14131	0.14127		0.14129
4.00000	0.13958	0.13955		0.13957
3.00000	0.13927	0.13927		0.13927
2.00000	0.13963	0.13961		0.13962
1.00000	0.14038	0.14036		0.14037

Filter

Vial Average	Filter+Ash+Vial
0.67186	0.67960
0.68478	0.71421
0.67516	0.70407
0.67481	0.70382
0.67701	0.70643
0.67709	0.70643
0.00000	0.14129
0.00000	0.13957
0.00000	0.13927
0.00000	0.13962
0.00000	0.14037

Net Mass Collected

STAGE	MASS (NO Cyclone)	MASS FRACTION (No Cyclone)	MASS FRACTION (Cyclone)	Normalized Mass	STAGE	Normalized Distribution (wt %)
11.00000	0.00096	0.33391	0.00940	0.32782	11.00000	32.78176
10.00000	0.00110	0.38261	0.01229	0.37562	10.00000	37.56244
9.00000	0.00036	0.12522	0.00940	0.12293	9.00000	12.29316
8.00000	0.00013	0.04522	0.00813	0.04439	8.00000	4.43920
7.00000	0.00023	0.08174	0.00289	0.08025	7.00000	8.02470
6.00000	0.00009	0.03130	0.00904	0.03073	6.00000	3.07329
5.00000	0.00000		0.00524	0.00524	5.00000	0.52414
4.00000	0.00000		0.00289	0.00289	4.00000	0.28918
3.00000	0.00000		0.00380	0.00380	3.00000	0.37955
2.00000	0.00000		0.00271	0.00271	2.00000	0.27111
1.00000	0.00000		0.00361	0.00361	1.00000	0.36148
		Cyclone	0.93060			
					TOTAL	
	TOTAL MASS	0.00288	1.00000	1.00000	MASS	100.00000
		>0.337	0.98175			
		<0.337	0.01825			

Particle Size Distribution Calculations
Test: 97IL6
WITH CYCLONE

Greased Filter Weights

STAGE	1st	2nd	3rd	Average
11.00000	0.02911	0.02912		0.02912
10.00000	0.14313	0.14312		0.14313
9.00000	0.14385	0.14384		0.14385
8.00000	0.14219	0.14219		0.14219
7.00000	0.14505	0.14504		0.14505
6.00000	0.03024	0.03027		0.03026
5.00000	0.02969	0.02969		0.02969
4.00000	0.03471	0.03471		0.03471
3.00000	0.03059	0.03059		0.03059
2.00000	0.02941	0.02942		0.02942
1.00000	0.03067	0.03067		0.03067

Empty vial Weights

STAGE	1st	2nd	3rd	Average
11.00000				
10.00000				
9.00000				
8.00000				
7.00000				
6.00000	0.67567	0.67568		0.67568
5.00000	0.67979	0.67978		0.67979
4.00000	0.66902	0.66902		0.66902
3.00000	0.67438	0.67440		0.67439
2.00000	0.66992	0.66993		0.66993
1.00000	0.67428	0.67428		0.67428
Cyclone	7.53077	7.53079		7.53078

Filter+Ash+Vial

STAGE	1st	2nd	3rd	Average
11.00000	0.02938	0.02937		0.02938
10.00000		0.14347	0.14346	0.14347
9.00000	0.14409	0.14412		0.14411
8.00000	0.14241	0.14242		0.14242
7.00000	0.14512	0.14513		0.14513
6.00000	0.70618	0.70618		0.70618
5.00000	0.70963	0.70961		0.70962
4.00000	0.70382	0.70380		0.70381
3.00000	0.70509	0.70506		0.70509
2.00000	0.69942	0.69941		0.69942
1.00000	0.70525	0.70525		0.70525
Cyclone	7.55381	7.55476	7.56135	7.55652
	7.55900	7.55370		

Filter

Vial Average	Filter+Ash+Vial
0.00000	0.02938
0.00000	0.14347
0.00000	0.14411
0.00000	0.14242
0.00000	0.14513
0.67568	0.70618
0.67979	0.70962
0.66902	0.70381
0.67439	0.70509
0.66993	0.69942
0.67428	0.70525
7.53078	7.55652

Net Mass Collected

STAGE	MASS	Mass Fraction
11.00000	0.00026	0.00940
10.00000	0.00034	0.01229
9.00000	0.00026	0.00940
8.00000	0.00023	0.00813
7.00000	0.00008	0.00289
6.00000	0.00025	0.00904
5.00000	0.00014	0.00524
4.00000	0.00008	0.00289
3.00000	0.00010	0.00360
2.00000	0.00008	0.00271
1.00000	0.00010	0.00361
Cyclone	0.02574	0.93060
TOTAL MASS	0.02766	1.00000

Particle Size Distribution Calculations
Test: 97IL7 Using Run 6 cyclone data & run 7 no cyclone data
NOCYCLONE

Greased Filter Weights

STAGE	1st	2nd	3rd	Average
11.00000	0.00650	0.00651		0.00651
10.00000	0.02997	0.02999		0.02998
9.00000	0.03052	0.03054		0.03053
8.00000	0.03018	0.03020		0.03019
7.00000	0.02997	0.02999		0.02998
6.00000	0.02879	0.02880		0.02880
5.00000	0.13597	0.13595		0.13596
4.00000	0.13684	0.13681		0.13683
3.00000	0.13742	0.13739		0.13741
2.00000	0.13804	0.13801		0.13803
1.00000	0.13579	0.13576		0.13578

Empty vial Weights

STAGE	1st	2nd	3rd	Average
11.00000		0.96397	0.96396	0.96397
10.00000	0.96057	0.96058		0.96058
9.00000	0.96699	0.96700		0.96700
8.00000	0.96883	0.96883		0.96883
7.00000	0.96066	0.96064		0.96065
6.00000	0.95998	0.95997		0.95998
5.00000				
4.00000				
3.00000				
2.00000				
1.00000				

Filter+Ash+Vial

STAGE	1st	2nd	3rd	Average
11.00000		0.97107	0.97105	0.97106
10.00000	0.99364	0.99366		0.99365
9.00000	0.99788	0.99786		0.99787
8.00000	0.99925	0.99921		0.99923
7.00000	0.99097	0.99094		0.99096
6.00000	0.98898	0.98896		0.98897
5.00000	0.13602	0.13602		0.13602
4.00000	0.13686	0.13684		0.13685
3.00000	0.13743	0.13742		0.13743
2.00000	0.13798	0.13799		0.13799
1.00000	0.13576	0.13579		0.13578

Net Mass Collected

Filter

Vial Average	Filter+Ash+Vial
0.96397	0.97106
0.96058	0.99365
0.96700	0.99787
0.96883	0.99923
0.96065	0.99096
0.95998	0.96897
0.00000	0.13602
0.00000	0.13685
0.00000	0.13743
0.00000	0.13799
0.00000	0.13578

STAGE	MASS (NO Cyclone)	MASS FRACTION (No Cyclone)	MASS FRACTION (Cyclone)	Normalized Mass	STAGE	Normalized Distribution (wt %)
11.00000	0.00059	0.12382	0.00840	0.12156	11.00000	12.15593
10.00000	0.00309	0.64953	0.01229	0.63767	10.00000	63.76710
9.00000	0.00034	0.07240	0.00940	0.07106	9.00000	7.10613
8.00000	0.00021	0.04407	0.00813	0.04327	8.00000	4.32669
7.00000	0.00033	0.06821	0.00289	0.06696	7.00000	6.69606
6.00000	0.00020	0.04197	0.00904	0.04121	6.00000	4.12065
5.00000	0.00006		0.00524	0.00524	5.00000	0.52414
4.00000	0.00003		0.00289	0.00289	4.00000	0.28918
3.00000	0.00002		0.00380	0.00380	3.00000	0.37955
2.00000	0.00000		0.00271	0.00271	2.00000	0.27111
1.00000	0.00000		0.00361	0.00361	1.00000	0.36148
Cyclone			0.93060			
TOTAL MASS	0.00477	1.00000	1.00000	1.00000	TOTAL MASS	100.00000
		>0.337	0.98175			
		<0.337	0.01825			

APPENDIX B

Data from PISCES Study Used to Determine Trace Element Capture Efficiencies

Antimony (Sb) 6/24/96
EPRI data
D: EI < DL set = rank avg of values < DL and EI < DL datasets not used

Rank	Control Device	Unit ID	Modified Ei (lb/TBtu)	Actual Ei (lb/TBtu)	Modified Ci (coal) (ppm)	Actual C (coal) (ppm)	Pi/out (lb/MBtu)	Inlet	HHV (MBtu)	PMpen (lb/MBtu)	Control Device	n	EI (lb/TBtu)	CI*PM/a	CI*PM/a *(1-n)	nl	r/n
D	ESP	DOE 3	1.8	1.8	0.67	0.67	0.1	0.12	12,300	9.30	ESP	98.818	1.8	0.5225	44.186	95.926	0.971
E	ESP	DOE 4	0.4	0.4	0.61	0.61	0.14	0.138	14,300	9.65	ESP	98.549	0.4	0.6188	42.667	99.082	1.005
E	ESP	19	0.35	0.35	0.03	0.03	0.036	0.091	13,500	6.74	ESP	99.466	0.35	0.2402	46.667	99.960	0.998
E	ESP	18	0.76	0.76	0.85	0.85	0.14	0.19	13,400	9.70	ESP	90.557	0.76	0.9154	83.433	90.802	1.002
E	ESP	116	0.1	0.1	0.654	< 1		0.046	0.12	12,300	9.30	ESP	99.506	0.1	0.2507	50.698	99.809	1.003
E	ESP	16 L	2.2	2.2	1.5		1.5	0.12	0.095	13,300	6.88	ESP	98.257	2.2	1.6947	108.696	97.976	0.997
E	ESP	110 L	3.6	3.6	0.795	< 4		0.041	0.089	12,100	6.86	ESP	99.402	3.6	0.3927	65.702	99.621	0.951
E	ESP	DOE 5	2.1	2.1	22		22	0.043	0.114	10,000	3.26	ESP	99.479	2.1	8.2588	1594.203	99.868	1.004
E	FGDw	DOE 1	0.4	0.4	0.61		0.61	0.014	0.138	14,300	9.65	FGDw	99.855	0.4	0.0618	42.667	99.002	0.992
E	FGDd	SNRS116	0.76	0.76	0.654	< 1		0.029	0.12	12,900	9.30	FGDd	99.688	0.76	0.1581	50.698	98.501	0.988
S	FGDw	101	2.8	2.8	0.6		0.6	0.007	0.05	10,000	25.00	FGDw	99.972	2.8	0.0156	60.000	95.335	0.954
S	FGDd	DOE 7	0.04	0.04	1.5		1.5	0.012	0.229	10,500	21.67	FGDd	99.946	0.04	0.0786	142.857	99.072	1.000
L	FGDw	DOE 6	0.18	0.18	37	< 37		0.0104	0.17	9,970	17.05	FGDw	99.999	0.18	2.2606	8711.100	99.995	1.001

Averages	nl	r/n	# points	Max r/n	Min r/n
overall	98.313	0.999	13	1.005	0.951
bituminous	99.077	0.991	10	1.005	0.951
sub-bitum	97.653	0.977	2	1.000	0.954
lignite	99.995	1.001	1	-	-
ESP	98.151	0.991	8	1.005	0.951
FGDw	98.570	0.987	5	1.001	0.954
FF	-	-	0	-	
FGDd	-	-	0	-	
ESP+FGDw	98.318	0.999	13		
ESP+FGDd	-	-	0		
bituminous coal					
ESP	98.151	0.991	8	1.005	0.951
FGDw	98.782	0.990	2	0.992	0.988
FF			0	-	-
FGDd	-	-	0	-	
ESP+FGDw	98.277	0.991	10		
FF+FGDd			0		
subbituminous coal					
ESP	-	-	0	-	-
FGDw	97.653	0.977	2	1.000	0.954
FF	-	-	0	-	-
FGDd			0	-	-
ESP+FGDw	97.653	0.977	2		
FF+FGDd	-	-	0		
lignite coal					
ESP	-	-	0		
FGDw	99.995	1.001	1	-	-
FF	-	-	0	-	-
FGDd	-	-	0	-	-
ESP+FGDw	99.995	1.001	1		
FF+FGDd	-	-	0		
ESP					
bitum	98.151	0.991	8		
sub-bit		-	0		
lig	-	-	0		
FGDw					
bitum	98.782	0.990	2		
sub-bit	97.653	0.977	2		
lig	99.995	1.001	1		
FF					
bitum	-	-	0		
sub-bit	-	-	0		
lig	-	-	0		
FGDd	bitum	-	-	0	
	sub-bit	-	-	0	
	lig	-	-	0	

Arsenic 6/18/96
EPRI data
E: CI < DL set equal to rank average of data < DL and E: < DL data not used

Rank	Control Device	Unit ID	Modified EI (lb/TBtu)	Actual EI (lb/TBtu)	Modified CI (coal) (ppm)	Actual CI (coal) (ppm)	PMout (lb/MBtu)	fash	HHV (Btu/lb)	PMycn (lb/MBtu)	Control Device	n	EI (lb/TBtu)	CI*PM / (a *(1-n)	ni	nVn
B	ESP	116B	1.30	1.30	1.90	1.90	0.022	0.090	11,900	7.56	ESP	99.77	1.30	0.4495	159.964	99.19	0.9947
B	ESP	110L	9.50	9.50	1.90	<2.3	0.041	0.083	12,100	8.88	ESP	99.40	9.50	0.9386	157.025	93.95	0.9451
B	ESP	DOE 4	16.00	16.00	2.30	2.30	0.140	0.138	11,350	9.65	ESP	98.55	16.00	2.3933	160.839	90.05	0.9138
B	ESP	DOE 3	13.00	13.00	3.10	3.10	0.110	0.120	12,900	9.30	ESP	98.82	13.00	2.8417	240.310	94.69	0.9572
B	ESP	116	2.90	2.90	5.50	5.50	0.046	0.120	12,900	9.30	ESP	99.51	2.90	1.9167	387.587	99.25	0.9975
B	ESP	19	7.90	7.90	5.70	5.70	0.038	0.010	13,500	0.74	ESP	90.14	7.90	20.2600	492.222	98.13	1.0014
B	ESP	12	1.90	1.90	6.20	6.20	0.100	0.094	13,750	8.88	ESP	98.54	1.90	6.5957	452.555	99.53	1.0035
B	ESP	114R	8.00	8.00	8.10	8.10	0.016	0.089	13,350	8.69	ESP	99.76	8.00	1.4562	609.023	98.69	0.9892
B	ESP	18	36.00	36.00	10.00	10.00	0.140	0.130	13,400	9.70	ESP	98.56	36.00	10.7692	746.268	95.18	0.9657
B	ESP	122	230.00	230.00	11.00	11.00	0.120	0.093	13,370	8.86	ESP	98.27	230.00	14.1935	822.737	72.04	0.7331
B	ESP	114B	7.00	7.00	12.00	12.00	0.095	0.007	13,500	0.44	ESP	99.61	7.00	3.4483	666.666	99.21	0.9960
B	ESP	DOE 5	301.00	301.00	13.00	15.00	0.043	0.114	13,850	8.26	ESP	99.46	301.00	4.9035	942.029	98.66	0.9840
B	ESP	15	13.00	13.00	13.00	15.00	0.028	0.127	13,000	9.77	ESP	99.71	13.00	2.8661	1000.000	98.70	0.9898
B	ESP	16	94.00	94.00	17.00	17.00	0.210	0.100	13,730	7.30	ESP	97.12	94.00	35.7000	1240.875	92.42	0.9515
B	ESP	161	110.00	110.00	20.00	25.00	0.120	0.095	13,800	8.88	ESP	98.26	110.00	20.0526	1666.667	93.40	0.9526
B	ESP	DOE 2	48.00	48.00	33.00	35.00	0.019	0.120	12,900	9.00	ESP	99.89	48.00	5.2250	2556.140	98.12	0.9832
B	FGDw	DOE 4	1.20	1.20	2.30	2.30	0.014	0.138	14,300	9.65	FGDw	99.85	1.20	0.2333	180.839	99.25	0.9940
B	FGDw	21	6.20	6.20	4.30	4.30	0.011	0.057	14,000	4.79	FGDw	98.77	6.20	0.7060	307.143	97.88	0.9821
B	FGDw	12	0.45	0.45	5.20	5.20	0.013	0.094	13,700	6.86	FGDw	99.81	0.45	0.8674	452.555	99.00	1.0000
B	FGDw	125	48.00	48.00	11.00	11.00	0.090	0.096	11,343	7.61	FGDw	98.80	48.00	10.1020	843.384	94.31	0.9545
B	FF	18 FF	5.03	5.03	10.00	10.00	0.002	0.130	13,400	9.70	FF	99.98	0.18	0.1462	746.268	100.00	1.0002
B	FF	DOE 2 FF	8.80	8.80	34.00	34.00	0.011	0.120	12,900	9.23	FF	99.88	8.80	3.1187	2815.385	99.86	0.9978
B	FGDd	SNRB116	1.20	1.20	5.00	5.00	0.029	0.120	12,900	9.30	FGDd	99.69	1.20	1.2083	387.597	99.69	1.0000
S	ESP	22	0.0870	0.0870	0.05	0.05	0.002	0.068	11,980	5.68	ESP	99.97	0.09	0.0188	70.952	99.88	0.9990
S	ESP	102	2.9000	2.9000	0.68	<1.3	0.058	0.088	12,200	7.21	ESP	99.20	2.90	0.4020	53.825	94.81	0.9533
S	ESP	11	1.2000	1.2000	1.60	1.60	0.023	0.082	11,300	5.21	ESP	99.56	1.20	0.5835	134.454	99.11	0.9955
S	FGDw	11	0.6000	0.6000	1.60	1.60	0.051	0.062	11,900	5.21	FGDw	99.02	0.60	1.3161	134.454	99.55	1.0054
S	FGDw	101	0.3400	0.3400	2.60	2.60	0.007	0.250	10,300	25.00	FGDw	99.97	0.34	0.0728	260.000	99.87	0.9990
S	FF	115	0.75	0.75	0.48	0.48	0.002	0.112	12,565	5.91	FF	99.98	0.75	0.0981	98.201	98.04	0.9905
S	FF	115L	0.15	0.15	0.84	0.84	0.001	0.105	12,638	5.91	FF	99.99	0.15	0.0070	50.641	99.70	0.9972
S	FF	101	0.59	0.59	2.60	2.60	0.021	0.250	10,300	25.00	FF	99.92	0.59	0.2184	260.000	99.77	0.9988
S	FGDd	DOE 7	0.15	0.15	2.00	2.00	0.012	0.229	10,500	21.81	FGDd	99.94	0.15	0.1520	276.190	99.95	1.0000
L	ESP	20	3.40	3.40	2.00	2.00	0.054	0.210	10,000	21.00	ESP	99.76	3.40	0.6800	280.000	98.79	0.9903
L	ESP	DOE 6	1.60	1.60	9.40	9.40	0.020	0.170	9,970	17.05	ESP	99.66	1.60	1.1059	942.828	99.83	0.9995
L	FGDw	20	0.65	0.65	2.80	2.80	0.019	0.210	10,000	21.00	FGDw	99.81	0.89	0.2595	280.000	99.78	0.9987
L	FGDw	DOE 5	1.20	1.20	9.40	9.40	0.010	0.170	9,970	17.05	FGDw	99.94	1.20	0.5751	942.828	99.87	0.9993

	Averages	ei	nVn	# points	Max nVn	Min nVn
	overall	98.39	0.9705	36	1.0014	0.6840
	bituminous	94.84	0.9576	29	1.0014	0.6840
	sub-bitum	99.04	0.9921	9	1.0054	0.9538
	lignite	99.57	0.9969	4	0.9995	0.9903
	ESP	94.42	0.9539	21	1.0014	0.6840
	FGDw	95.81	0.9817	8	1.0054	0.9545
	FF	99.43	0.9949	6	1.0002	0.9808
	FGDd	99.82	1.0000	2	1.0000	1.0000
	ESP+FGDw	95.00	0.9640	29		
	FF+FGDd	99.54	0.9983	7		
bituminous coal						
	ESP	93.16	0.9439	16	1.0014	0.6840
	FGDw	97.90	0.9329	4	1.0009	0.9545
	FF	99.85	0.9990	2	1.0002	0.9978
	FGDd	99.68	1.0000	1		
	ESP+FGDw	94.10	0.9513	20		
	FF+FGDd	99.76	0.9993	3		
subbituminous coal						
	ESP	97.07	0.9828	3	0.9890	0.9538
	FGDw	99.71	1.0022	2	1.0054	0.9890
	FF	99.17	0.9921	3	0.9986	0.9808
	FGDd	99.96	1.0000	1	-	-
	ESP+FGDw	98.60	0.9905	5		
	FF+FGDd	99.90	0.9941	4		
lignite coal						
	ESP	99.31	0.9948	2	0.9995	0.9903
	FGDw	99.82	0.9990	2	0.9998	0.9987
	FF					
	FGDd					
	ESP+FGDw	99.57	0.9969	4		
	FF+FGDd					
ESP						
	bitum	93.16	0.9433	16		
	sub-bit	97.87	0.9828	3		
	lig	99.31	0.9949	2		
FGDw						
	bitum	97.85	0.9829	4		
	sub-bit	99.71	1.0022	2		
	lig	99.82	0.9990	2		
FF						
	bitum	99.83	0.9990	2		
	sub-bit	99.17	0.9921	3		
	lig					

Beryllium (Be) 6/6/06
D: EI < DL ignored

Rank	Control Device	Unit ID	Modified EI (lb/TBtu)	Actual EI (lb/TBtu)	Modified CI (coal) (ppm)	Actual CI (coal) (ppm)	PMcal (lb/MBtu)	fuel	HHV (lb/MBtu)	PM(cal) (lb/MBtu)	Control Device	n	Modified EI (lb/TBtu)	CIPM/lb	CIPM / lb *(1-n)	n	n/n
B	ESP	DOE 4	1.7	1.7	1.1	1.1	0.14	0.139	14,000	9.65	ESP	98.5493	1.7	1.1159	76.923	97.7900	0.9923
B	ESP	122	4	4	1.1	1.1	0.12	0.093	13,370	8.96	ESP	98.2748	4	1.4194	82.274	95.1382	0.9861
B	ESP	15	0.4	0.4	1.1	1.1	0.028	0.127	13,000	9.77	ESP	99.7194	0.4	0.2425	84.615	99.5273	0.9981
B	ESP	DOE 3	1.6	1.6	1.2	1.2	0.11	0.12	12,900	9.30	ESP	98.8175	1.6	1.1000	93.023	98.2800	0.9948
B	ESP	DOE 5	0.062	0.062	1.3	1.3	0.043	0.114	13,800	8.26	ESP	99.4795	0.062	0.4604	94.203	99.9342	1.0046
B	ESP	18	3.7	3.7	1.4	1.4	0.91	0.1	13,700	7.30	ESP	97.1290	3.7	2.9400	102.190	96.3793	0.9923
B	ESP	DOE 2	0.25	0.25	1.9	1.9	0.019	0.12	12,900	9.30	ESP	99.7958	0.25	0.3008	147.287	99.8303	1.0003
B	ESP	16 L	3.1	3.1	2.2	2.2	0.12	0.095	13,800	0.89	ESP	98.2568	3.1	2.7709	159.420	98.0555	0.9980
B	ESP	114 B	0.8	0.8	3.3	3.3	0.016	0.089	13,300	8.68	ESP	99.7809	0.8	0.5933	248.120	99.6778	0.9992
B	ESP	114 B	2.4	2.4	3.6	3.6	0.025	0.08	13,500	5.08	ESP	99.5781	2.4	1.1250	268.667	99.1000	0.9952
D	FGDw	21	0.19	0.19	0.79	0.79	0.017	0.067	14,000	4.70	FGDw	99.7701	0.13	0.1297	66.429	99.7698	1.0000
B	FGDw	DOE 4	0.1	0.1	1.1	1.1	0.014	0.138	14,000	9.65	FGDw	99.8549	0.1	0.1116	76.923	99.8700	1.0002
B	FGDw	125	2.1	2.1	2.2	2.2	0.09	0.09	13,943	0.18	FGDw	98.5827	2.1	2.4750	168.673	98.7559	1.0023
S	FGDw	101	0.036	0.036	1.4	1.4	0.007	0.25	10,900	25.00	FGDw	99.9720	0.036	0.0392	140.000	99.9743	1.0000
S	FF	101	0.11	0.11	1.4	1.4	0.021	0.25	10,900	25.00	FF	99.9169	0.11	0.1176	140.000	99.9214	1.0001
L	ESP	20	2.2	2.2	6.5	6.5	0.051	0.21	10,900	21.00	ESP	99.7571	2.2	1.5789	650.000	99.6615	0.9990
L	FGDw	20	0.35	0.35	6.5	6.5	0.019	0.21	10,900	21.00	FGDw	99.9095	0.35	0.5881	650.000	99.9462	1.0004

Averages	ni	n/n	# points	*Max* n/n	*Min* n/n
overall	98.9183	0.9967	17	1.0046	0.9861
bituminous	98.6236	0.9958	15	1.0046	0.9861
sub-bitum	99.9479	1.0009	2	1.0021	1.0000
lignite	99.8039	0.9997	2	1.0004	0.9990
ESP	98.4885	0.9947	11	1.0046	0.9861
FGDw	99.6630	1.0006	5	1.0021	1.0000
FF	99.9214	1.0001	1	1.0001	1.0001
FGDd	-	-	0	-	-

Cadmium (Cd) 6/18/96
EPRI data
F: Cl < DL set equal to rank avg of values < DL and El < DL data NOT USED

Rank	Control Device	Unit ID	Modified El (lb/TBtu)	Actual E (lb/TBtu)	Modified Cl (coal) (ppm)	Actual C (coal) (ppm)	PMout (lb/MBtu)	fash	HHV (btu/MBtu)	PMgas (lb/MBtu)	Control Device	n	El (lb/TBtu)	CIPM/Mb	CIPM/ lb *(1-n)	nl	n/n
B	ESP	18	0.5	0.5	0.1	<0.11	0.2	0.1	13,700	7.30	ESP	97.1200	0.5	0.2100	7.298	93.1500	0.9594
B	ESP	DOE 5	0.8	0.8	0.1	<0.13	0.043	0.114	13,000	8.85	ESP	99.4795	0.8	0.0377	7.248	99.9600	0.9943
B	ESP	DOE 4	1.3	1.3	0.3	0.3	0.14	0.138	14,300	9.65	ESP	98.5490	1.3	0.3043	25.979	99.8000	0.9618
B	ESP	19	0.13	0.13	0.3	<0.4	0.036	0.091	13,800	6.74	ESP	99.4659	0.13	0.1187	22.232	99.4150	0.9905
B	ESP	18	3.1	3.1	0.43	0.43	0.14	0.13	10,400	9.76	ESP	96.5569	3.1	0.4631	32.090	90.3395	0.9166
B	ESP	DOE 3	3.7	3.7	0.63	0.63	0.11	0.12	12,900	9.30	ESP	98.8175	3.7	0.5775	46.837	92.4238	0.9359
B	ESP	122	4	4	0.9	0.9	0.12	0.093	13,970	6.96	ESP	99.2748	4	1.1613	67.315	94.0578	0.9571
B	ESP	110 B	0.86	0.86	1.7	1.7	0.022	0.081	11,900	7.65	ESP	99.7123	0.86	0.4110	142.857	99.3080	0.9968
B	ESP	110 L	1.7	1.7	2.1	2.1	0.041	0.083	12,100	6.86	ESP	99.4023	1.7	1.0373	173.554	99.0206	0.9962
B	ESP	18 L	3.6	3.6	0.93	<2.0	0.12	0.045	13,800	6.62	ESP	98.2568	3.6	1.1775	67.552	94.6708	0.9636
B	ESP	12	1.8	1.8	0.93	<34	0.1	0.094	13,700	6.86	ESP	98.5496	1.8	0.9917	68.045	97.3547	0.9870
B	ESP	15	3.1	3.1	0.99	<8	0.028	0.127	13,000	9.77	ESP	99.7134	3.1	0.2055	71.709	95.8770	0.9995
B	ESP	114 B	1.8	1.8	39	39	0.025	0.087	13,500	6.44	ESP	99.6121	1.8	1.2005	2889.089	99.9377	1.0030
B	ESP	114 R	0.4	0.4	47	47	0.016	0.089	13,300	6.69	ESP	99.7609	0.4	8.4494	3533.835	99.8887	1.0023
B	FF	18 FF	0.23	0.23	0.43	0.43	0.0019	0.13	13,400	9.70	FF	99.9804	0.23	0.0065	32.090	99.2838	0.9930
B	FGDw	21	0.57	0.57	0.1	<0.1	0.011	0.067	14,000	4.79	FGDw	99.7701	0.57	0.0184	7.143	92.0200	0.9223
B	FGDw	DOE 4	0.6	0.6	0.9	0.9	0.014	0.130	14,300	9.65	FGDw	99.8548	0.6	0.0304	23.979	97.1400	0.9728
B	FGDw	15	8.5	8.5	1.6	1.6	0.09	0.088	13,043	7.61	FGDw	98.8022	8.5	1.4694	122.671	93.0709	0.9420
B	FGDw	12	1.2	1.2	0.93	<3.4	0.013	0.94	13,700	68.61	FGDw	99.9811	1.2	0.0126	68.045	98.2365	0.9826
B	FGDd	SNRD11B	0.6	0.6	0.99	<0.9	0.009	0.12	12,000	8.50	FGDd	99.6883	0.6	0.2253	72.265	99.1697	0.9918
B	FGDd	14	1	1	0.99	<3	0.0073	0.093	13,700	6.79	FGDd	99.8925	1	0.0732	68.045	99.5304	0.9954
S	ESP	22	0.16	0.16	0.08	<0.1	0.0016	0.068	11,980	6.68	ESP	99.8736	0.16	0.0016	6.675	97.6040	0.9768
S	ESP	11	1.5	1.5	0.08	< 2	0.023	0.052	11,900	6.21	ESP	99.5585	1.5	0.0297	6.723	77.6675	0.7803
S	FF	115	0.12	0.12	0.08	< 0.05	0.0019	0.112	12,565	8.51	FF	99.9787	0.12	0.0014	6.367	98.1153	0.9814
S	FF	101	0.53	0.53	0.08	<0.1	0.021	0.25	10,000	25.00	FF	99.9180	0.53	0.0067	8.000	93.3750	0.9345
S	FGDw	101	0.4	0.4	0.08	<0.1	0.007	0.25	10,000	25.00	FGDw	99.9720	0.4	0.0022	8.000	95.0000	0.9503
S	FGDw	11	1.3	1.3	0.08	< 2	0.0051	0.062	11,900	6.21	FGDw	99.8027	1.3	0.0205	8.723	90.5625	0.9074
S	FGDd	UOE 7	0.026	0.026	0.08	< 0.05	0.012	0.229	10,500	21.81	FGDd	99.9450	0.026	0.0042	7.619	99.8588	0.9971
L	ESP	20	0.52	0.52	0.14	<0.14	0.051	0.21	10,000	21.00	ESP	99.7571	0.52	0.0340	14.000	96.2857	0.9652
L	FGDw	20	0.7	0.7	0.14	<0.14	0.019	0.21	10,000	21.00	FGDw	99.9095	0.7	0.0127	14.000	95.0000	0.9509

		nl	n/n	# points	Max n/n	Min n/n
Averages	overall	94.9679	0.9553	30	1.0033	0.7803
	bituminous	95.9838	0.9675	21	1.0033	0.8943
	sub-bitum	91.7290	0.9182	7	0.9971	0.7803
	lignite	95.6429	0.9580	2	0.9852	0.9509
	ESP	94.6826	0.9556	17	1.0033	0.7803
	FGDw	93.9186	0.9896	7	ERR	0.8074
	FF	98.5245	0.9896	3	0.9930	0.9345
	FGDd	99.1196	0.9926	3	0.9971	0.9864
	ESP+FGDw	94.2042	0.9489	24		
	FF+FGDd	98.0021	0.9919	6		
bituminous coal						
	ESP	95.5855	0.9659	14	1.0033	0.8943
	FGDw	95.1188	0.9649	4	0.9826	0.9223
	FF	99.2853	0.9980	1		
	FGDd	98.8501	0.9906	2	0.9948	0.9864
	ESP+FGDw	95.4813	0.9636	18		
	FF+FGDd	99.9945	0.9914	3		
subbituminous coal						
	ESP	87.0458	0.8785	2	0.9769	0.7803
	FGDw	87.8513	0.8786	2	0.9503	0.8074
	FF	95.7451	0.9579	2	0.9814	0.9345
	FGDd	99.6588	0.9971	1		
	ESP+FGDw	87.7355	0.8786	4		
	FF+FGDd	97.0497	0.9710	3		
lignite coal						
	ESP	95.2857	0.9652	1		
	FGDw	95.0000	0.9509	1		
	FF					
	FGDd					
	ESP+FGDw	95.6429	0.9580	2		
	FF+FGDd					
ESP						
	bitum	95.5855	0.9659	14		
	sub bit	87.6458	0.8783	2		
	lig	95.2857	0.9652	1		
FGDw						
	bitum	95.1188	0.9649	4		
	sub-bit	87.8513	0.8786	2		
	lig	95.0000	0.9509	1		
FF						
	bitum	99.2853	0.9930	1		
	sub-bit	95.7451	0.9579	2		
	lig					
FGDd	bitum	98.8501	0.9906	2		
	sub-bit	99.6588	0.9971	1		
	lig					

Chromium (Cr) 6/13/96
EPRI data
E: only data sets with Cl, Ei > DL used

Rank	Control Device	Unit ID	Modified Ei (lb/TBtu)	Actual Ei (lb/TBtu)	Modified Cl (coal) (ppm)	Actual Cl (coal) (ppm)	PMout (lb/MBtu)	fash	+HV (lb/MBtu)	PMgen (lb/MBtu)	Control Device	n	Ei (lb/TBtu)	CIPM/s	CIPM / *a *(1-e)	ni	m/n
B	ESP	110 B	13	13	5.5	5.5	0.022	0.091	11,900	7.65	ESP	99.7123	13	1.3297	462.185	97.1873	0.9747
B	ESP	110 L	30	30	9	9	0.041	0.093	12,100	8.86	ESP	99.4023	30	4.4456	743.902	95.9867	0.9654
B	ESP	114 B	4.6	4.6	9.4	9.4	0.016	0.089	13,900	8.69	ESP	99.7526	4.6	1.6889	706.767	98.9491	0.9959
B	ESP	114 B	14	14	11	11	0.025	0.087	13,500	8.44	ESP	99.8121	14	3.1698	814.815	99.2618	0.9986
B	ESP	122	100	100	11	11	0.12	0.093	13,370	8.96	ESP	98.2748	100	14.1995	822.797	87.8455	0.8839
B	ESP	18	25	25	16	16	0.14	0.13	13,400	9.70	ESP	98.5569	25	17.2308	1194.030	97.9063	0.9934
B	ESP	DOE 2	3.0	3.0	16	16	0.019	0.12	12,800	9.30	ESP	99.7958	3.0	2.5333	1240.310	99.6656	0.9969
B	ESP	16 L	21	21	17	17	0.19	0.095	13,800	6.66	ESP	99.2668	21	21.4737	1231.884	98.2953	1.0004
B	ESP	110	1	1	15	15	0.046	0.12	12,900	9.30	ESP	99.5355	1	5.7500	1167.791	99.9746	1.0041
B	ESP	19	13	13	15	15	0.030	0.091	13,600	6.74	ESP	99.4659	13	5.9341	1111.111	98.8200	0.9936
B	ESP	12	9	9	17	17	0.1	0.094	13,700	6.86	ESP	99.5426	9	10.0051	1240.876	99.2747	1.0004
B	ESP	DOE 5	6.2	6.2	18	18	0.043	0.114	13,800	8.28	ESP	99.4795	6.2	8.7595	1304.348	99.5247	1.0005
B	ESP	16	38	38	22	22	0.21	0.1	13,700	7.30	ESP	97.1230	38	46.2000	1635.839	97.6236	1.0053
B	ESP	DOE 4	29	29	25	25	0.14	0.138	14,000	9.65	ESP	98.5403	29	25.3623	1748.252	98.6844	1.0014
B	ESP	15	1.2	1.2	26	26	0.028	0.127	13,000	9.77	ESP	99.7134	1.2	5.7500	2090.000	99.9466	1.0008
B	FGDw	125	18	18	11	11	0.09	0.090	13,043	7.51	FGDw	99.6562	18	10.1020	843.364	97.8657	0.9905
B	FGDw	21	2.7	2.7	11	11	0.011	0.057	14,000	4.79	FGDw	99.7701	2.7	1.8000	785.714	99.6464	0.9969
B	FGDw	12	4	4	17	17	0.013	0.094	13,700	6.68	FGDw	99.8105	4	2.3511	1240.876	99.5776	0.9957
B	FGDw	DOE 4	5.3	5.3	25	25	0.014	0.138	14,000	9.65	FGDw	99.8548	5.3	2.5362	1748.252	99.8968	0.9964
B	FF	DOE 2 FF	1.2	1.2	15	15	0.011	0.12	13,000	9.23	FF	99.8608	1.2	1.3760	1153.846	99.8660	1.0002
B	FF	15 FF	3.3	3.3	16	16	0.0019	0.13	13,400	9.70	FF	99.9604	3.3	0.2398	1194.030	99.7236	0.9974
B	FGDd	SNRB116	5.3	5.3	15	15	0.029	0.12	12,800	9.00	FGDd	99.6660	5.3	3.6250	1162.791	99.5442	0.9986
B	FGDd	14	3.6	3.6	15	15	0.0073	0.093	13,700	6.78	FGDd	99.8925	3.6	1.1724	1094.891	99.8212	0.9978
S	ESP	11	8	8	4.1	4.1	0.023	0.062	11,800	5.21	ESP	99.5535	8	1.5210	344.086	97.6780	0.9817
S	ESP	102	8.5	8.5	6	6	0.058	0.088	12,200	7.21	ESP	99.1559	8.5	3.9545	431.893	98.2717	0.9907
S	FGDw	101	22	22	7.7	7.7	0.007	0.25	10,000	25.00	FGDw	99.9720	22	0.2156	770.000	97.1429	0.9717
S	FGDw	11	4	4	4	4	0.0051	0.062	11,900	5.21	FGDw	99.9021	4	0.9290	336.134	99.8100	0.9981
S	FF	DOE 8	2	2	4.2	4.2	0.009	0.112	11,700	9.57	FF	99.9080	2	0.3375	358.974	99.4429	0.9954
S	FF	10	1.6	1.6	7.1	7.1	0.008	0.21	11,000	18.09	FF	99.9581	1.6	0.2705	645.455	99.7521	0.9979
S	FF	101	2.5	2.5	7.7	7.7	0.021	0.25	10,000	25.00	FF	99.8160	2.5	0.6468	770.000	99.0753	0.9876
S	FF	115	0.66	0.66	1.1	1.1	0.0019	0.112	12,565	8.81	FF	99.9737	0.66	0.0187	57.545	99.2461	0.9927
S	FF	115 U	0.3	0.3	1.4	1.4	0.0012	0.105	12,038	8.01	FF	99.9856	0.3	0.0160	113.777	99.7292	0.9974
S	FGDd	DOE 7	0.1	0.1	9.9	9.9	0.012	0.229	10,500	21.81	FGDd	99.9450	0.1	0.4664	847.619	99.9482	1.0004
L	ESP	DOE 6	8.4	8.4	8.2	8.2	0.03	0.17	9,870	17.05	ESP	99.6827	8.4	0.9047	822.467	98.9787	0.9909
L	ESP	20	5.8	5.8	16	16	0.051	0.21	10,000	21.00	ESP	99.7571	5.8	3.8657	1600.000	98.6375	0.9888
L	FGDw	DOE 6	10	10	8.2	8.2	0.0104	0.17	9,870	17.05	FGDw	99.9390	10	0.5018	822.467	98.7641	0.9884
L	FGDw	20	2.8	2.8	16	16	0.019	0.21	10,000	21.00	FGDw	99.9016	2.8	1.4476	1600.000	98.8260	0.9892

		ni	m/n	# points	Max m/n	Min m/n
	Averages					
	overall	98.6760	0.9918	37	1.0074	0.9839
	bituminous	98.4370	0.9915	23	1.0074	0.9839
	sub-bitum	98.9736	0.9914	10	1.0004	0.9717
	lignite	99.3403	0.9943	4	0.9992	0.9884
	ESP	98.0466	0.9887	19	1.0074	0.9839
	FGDw	98.9323	0.9919	8	0.9992	0.9717
	FF	98.6379	0.9869	7	1.0002	0.9927
	FGDd	99.7246	0.9989	3	1.0004	0.9975
	ESP+FGDw	99.3690	0.9896	27		
	FF+FGDd	99.6669	0.9970	10		
bituminous coal						
	ESP	97.8878	0.9882	15	1.0074	0.9839
	FGDw	99.2241	0.9966	4	0.9989	0.9905
	FF	98.6258	0.9868	2	1.0002	0.9974
	FGDd	99.6677	0.9982	2	0.9986	0.9975
	ESP+FGDw	98.1682	0.9900	19		
	FF+FGDd	99.7008	0.9965	4		
subbituminous coal						
	ESP	97.9749	0.9869	2	0.9907	0.9831
	FGDw	97.9764	0.9804	2	0.9991	0.9717
	FF	98.5691	0.9862	5	0.9979	0.9927
	FGDd	99.9882	1.0004	-	-	-
	ESP+FGDw	97.9726	0.9831	4		
	FF+FGDd	99.8596	0.9969	8		
lignite coal						
	ESP	99.3081	0.9949	2	0.9988	0.9909
	FGDw	99.3046	0.9938	2	0.9992	0.9884
	FF					
	FGDd					
	ESP+FGDw	99.3063	0.9943	4		
	FF+FGDd					
ESP						
	bitum	97.8878	0.9882	15		
	sub-bit	97.9749	0.9869	2		
	lig	99.3081	0.9949	2		
FGDw						
	bitum	99.2241	0.9966	4		
	sub-bit	97.9764	0.9804	2		
	lig	99.3046	0.9938	2		
FF						
	bitum	98.6090	0.9866	2		
	sub-bit	99.5691	0.9962	5		
	lig					
FGDd						
	bitum	98.6077	0.9982	2		
	sub-bit	99.9552	0.9988	1		
	lig					

Cobalt (Co) 8/18/98
EPRI data
F: CI < DL set equal to DL (two points only - 21 & 110L) and EI < DL data NOT USED

Rank	Control Device	Unit ID	Modified EI (lb/TBtu)	Actual EI (lb/TBtu)	Modified CI (coal) (ppm)	Actual CI (coal) (ppm)	PMout (lb/MBtu)	fash	HHV (lb/MBtu)	HMgen (lb/MBtu)	Control Device	n	EI (lb/TBtu)	CIPM/a	CIPM/ (a *(1-n)	nl	min
B	ESP	110 L	3	3	0.5 < 0.5		0.041	0.083	12,100	6.86	ESP	99.4333	3	0.2470	41,322	93.7400	0.9330
B	ESP	DOE 4	5	5	3.5	3.5	0.11	0.138	14,300	9.65	ESP	98.5493	5	0.5507	244.755	97.9671	0.9940
B	ESP	DOE 3	8.4	8.4	3.7	3.7	0.11	0.12	12,900	9.30	ESP	98.8175	8.4	0.9017	986.899	97.0714	0.9823
B	ESP	122	27	27	4	4	0.12	0.093	13,570	6.98	ESP	98.2748	27	5.1613	299.177	90.9753	0.9257
B	ESP	DOE 5	0.55	0.55	4.5	4.5	0.043	0.114	13,000	8.26	ESP	99.4795	0.55	1.6974	326.087	98.8315	1.0035
B	ESP	15	2	2	5	5	0.028	0.127	13,000	9.77	ESP	99.7134	2	1.1024	384.615	98.4600	0.9977
B	ESP	16 L	6.5	6.5	6.1	6.1	0.12	0.095	13,800	6.88	ESP	98.2568	6.5	7.7053	142.029	88.5285	1.0026
B	ESP	10	3.7	3.7	6.4	6.4	0.036	0.081	13,500	6.74	ESP	99.4559	3.7	2.6319	474.074	99.2195	0.9975
B	ESP	16	11	11	8.3	8.3	0.21	0.1	13,700	7.39	ESP	97.1290	11	17.4300	505.839	98.1843	1.0109
B	ESP	110 B	5	5	16	16	0.022	0.091	11,900	7.85	ESP	99.7123	5	5.0685	1544.538	99.6281	0.9992
B	FGDw	DOE 4	0.7	0.7	3.5	3.5	0.014	0.138	14,300	9.65	FGDw	99.8549	0.7	0.3551	244.755	99.7440	0.9988
B	FGDw	21	4.1	4.1	0.5	0.5	0.011	0.067	14,000	4.79	FGDw	99.7701	4.1	0.0821	35.714	88.5200	0.8572
B	FF	DOE 2FF	0.15	0.15	6.4	6.4	0.011	0.12	13,000	9.23	FF	99.8308	0.15	0.4950	415.385	99.9639	1.0008
S	ESP	102	2.4	2.4	4	4	0.058	0.088	12,200	7.21	ESP	99.1959	2.4	2.6304	327.869	99.2680	1.0007
S	FGDw	11	1	1	1.5	1.5	0.0061	0.052	11,900	5.21	FGDw	99.9021	1	0.1234	126.050	99.2067	0.9930
S	FGDw	101	0.13	0.13	3.1	3.1	0.027	0.25	10,000	25.30	FGDw	99.9720	0.13	0.0868	310.000	99.9587	0.9989
S	FF	101	0.32	0.32	3.1	3.1	0.021	0.25	10,000	25.30	FF	99.9160	0.32	0.2604	310.000	99.8968	0.9988
S	FF	DOE 8	0.7	0.7	1.4	1.4	0.009	0.112	11,700	8.57	FF	99.9060	0.7	0.1125	119.658	99.4150	0.9951
-	ESP	20	2.7	2.7	6.3	6.3	0.051	0.21	10,000	21.30	ESP	99.7071	2.7	1.0300	630.000	99.0774	0.9981
-	FGDw	20	0.69	0.69	6.3	6.3	0.013	0.21	10,000	21.30	FGDw	99.9095	0.69	0.5700	630.000	99.8905	0.9998

		n	r^n	# points	Max r^n	Min r^n
	Averages					
	overall	97.9519	0.9880	20	1.0109	0.887
	bituminous	97.0627	0.9795	13	1.0109	0.887
	sub-bitum	99.5489	0.9977	5	1.0007	0.993
	lignite	99.7310	0.9990	2	0.9998	0.998
	ESP	97.7047	0.9871	12	1.0109	0.9257
	FGDw	97.4578	0.9757	5	0.9999	
	FF	99.7568	0.9986	3	1.0008	
	FGDd	-	-	0	-	
	ESP+FGDw	97.6321	0.9838	17		
	FF+FGDd	99.7586	0.9985	3		
bituminous coal						
	ESP	97.0617	0.9847	10	1.0109	0.926
	FGDw	94.1170	0.9429	2	0.9998	0.887
	FF	99.9639	1.0008	1	-	-
	FGDd	-	-	0	-	-
	ESP+FGDw	96.8209	0.9777	12		
	FF+FGDd	99.9639	1.0008	1		
subbituminous coal						
	ESP	99.2680	1.0007	1	-	
	FGDw	99.5824	0.9964	2	0.9999	0.993
	FF	99.6559	0.9974	2	0.9999	0.996
	FGDd	-	-	0	-	
	ESP+FGDw	99.4776	0.9979	3		
	FF+FGDd	99.6559	0.9974	2		
lignite coal						
	ESP	99.5714	0.9981	1	-	
	FGDw	99.8905	0.9999	1	-	
	FF					
	FGDd					
	ESP+FGDw	99.7310	0.9999	2		
	FF+FGDd	-	-	-		
ESP						
	bitum	97.0617	0.9847	10		
	sub-bit	99.2680	1.0007	1		
	lig	99.5714	0.9981	1		
FGDw						
	bitum	94.1170	0.9429	2		
	sub-bit	99.5824	0.9964	2		
	lig	99.8905	0.9999	1		
FF						
	bitum	99.9639	1.0008	1		
	sub-bit	99.6559	0.9974	2		
	lig			0		
FGDd	bitum	-	-	0		
	sub-bit	-	-	0		
	lig	-	-	0		

Lead (Pb) 5/18/96
EPRI data
n: CI < DL set = rank avg of data < DL and EI < DL data NOT USED

Rank	Control Device	Unit ID	Modified Ei (lb/TBtu)	Actual Ei (lb/TBtu)	Modified Ci (coal) (ppm)	Actual Ci (coal) (ppm)	Pb/Ash (lb/MBtu)	Ash	HHV (Btu/lb)	PVgen (lb/MBtu)	Control Device	n	EI (lb/TBtu)	CIPM/fa	CIPM/ fa*(1-n)	ei	ei/n
B	ESP	11	5.8	5.8	1.4	1.4	0.023	0.062	11,900	5.21	ESP	99.5585	5.8	0.5194	117.647	95.0700	0.95
B	ESP	12	9.7	9.7	2.4	2.4	0.1	0.064	13,700	6.06	ESP	88.5426	8.7	2.5532	775.182	94.4829	0.96
B	ESP	15	4.3	4.3	4	4	0.026	0.127	13,000	9.77	ESP	99.7134	4.3	0.0819	307.692	98.6026	0.99
B	ESP	116 B	16	16	2.516667	< b		0.029	0.061	11,900	7.65	ESP	99.7123	<5	0.6084	2111.485	92.4344	0.93
B	ESP	16	33	33	5.1	5.1	0.21	0.1	19,700	7.56	ESP	97.1240	33	10.7100	379.205	90.1053	0.94
B	ESP	DOE 5	3.6	3.6	6.8	6.8	0.043	0.114	13,900	8.26	ESP	99.4795	3.6	2.5849	492.754	99.2286	1.00
B	ESP	18 L	11	11	7.3	7.3	0.12	0.086	13,800	6.68	ESP	98.2568	11	9.2211	529.986	97.8235	1.00
B	ESP	DOE 4	19	19	8	8	0.14	0.138	14,300	5.65	ESP	96.8493	19	8.1159	559.441	98.8038	0.98
B	ESP	DOE 3	38	38	11	11	0.11	0.12	12,900	9.50	ESP	88.8175	38	10.0833	852.713	95.5436	0.97
B	ESP	DOE 2	3.1	3.1	13	13	0.019	0.12	13,000	9.23	ESP	99.7942	3.1	2.0585	1000.000	99.8500	1.00
B	ESP	114 R	57	57	16	16	0.016	0.12	12,900	9.50	ESP	99.0280	57	2.1333	1240.310	95.4044	0.96
B	ESP	110 L	17	17	17	17	0.041	0.091	13,500	6.74	ESP	99.3918	17	7.0595	1259.259	98.8500	0.99
B	ESP	122	190	190	25	25	0.12	0.1	13,700	7.30	ESP	98.3560	190	30.0000	1824.818	89.5880	0.91
B	ESP	114 B	86	86	37	37	0.025	0.041	11,900	7.65	ESP	98.6731	86	10.1646	3109.244	97.2341	0.98
B	FGDw	12	5.7	5.7	2.4	2.4	0.013	0.064	13,700	6.06	FGDw	99.8105	5.7	0.3319	775.182	95.7465	0.97
B	FGDw	21	6.3	6.3	2.9	2.9	0.011	0.067	14,000	4.79	FGDw	99.7701	6.3	0.4751	207.145	95.9586	0.97
B	FGDw	DOE 4	0.6	0.6	8	8	0.014	0.138	14,300	9.65	FGDw	99.8649	0.6	0.0910	559.441	99.0926	1.00
B	FGDw	125	15	15	8.2	8.2	0.09	0.008	13,048	7.61	FGDw	98.8022	<5	7.5305	628.859	97.8141	0.99
B	FF	DOE 2 FF	0.36	0.36	19	13	0.011	0.085	13,800	6.68	FF	99.8402	0.36	1.5053	942.029	99.0618	1.00
B	FGDd	SNRB116	0.5	0.5	5.3	5.3	0.029	0.12	12,900	9.50	FGDd	99.6869	0.5	1.2808	410.853	99.8763	1.00
S	ESP	11	5.8	5.8	1.4	1.4	0.023	0.062	11,800	5.21	ESP	99.5585	5.8	0.5194	117.647	95.0700	0.95
S	ESP	22	0.11	0.11	2	2	0.0015	0.068	11,980	5.68	ESP	99.9736	0.11	0.0441	166.945	99.9341	1.00
S	ESP	102	2.7	2.7	3	3	0.038	0.090	12,200	7.81	ESP	99.1959	2.7	1.9773	245.902	98.9020	1.00
S	FGDw	101	0.72	0.72	19	13	0.057	0.21	10,000	21.00	FGDw	99.9867	0.72	0.4333	1000.000	99.9446	1.00
S	FF	115	0.44	0.44	3.1	2.1	0.0018	0.112	12,565	8.91	FF	99.9787	0.44	0.0355	167.151	99.7357	1.00
S	FF	115 U	0.4	0.4	2.2	2.2	0.0012	0.105	12,638	8.31	FF	99.9858	0.4	0.0251	174.078	99.7708	1.00
S	FF	10	0.6	0.6	6.1	6.1	0.008	0.21	11,000	10.00	FF	99.9581	0.6	0.2324	554.545	99.8918	1.00
S	FF	DOE 8	2.4	2.4	5.2	5.2	0.009	0.112	11,700	9.57	FF	99.8060	2.4	0.4179	444.444	99.4600	1.00
S	FF	101	2.2	2.2	19	13	0.021	0.21	10,000	21.00	FF	99.9000	2.2	1.3000	1000.000	99.8836	1.00
S	FGDd	DOE 7	0.7	0.7	8.2	8.2	0.012	0.229	10,500	21.61	FGDd	99.9450	0.7	0.4297	783.952	99.9104	1.00
L	ESP	DOE 6	1.9	1.9	7.3	7.3	0.02	0.17	9,970	17.05	ESP	99.8827	1.9	0.8686	732.197	99.7405	1.00
L	ESP	20	7.7	7.7	12	12	0.051	0.21	10,000	21.00	ESP	98.7571	7.7	2.9143	1200.000	99.3583	1.00
L	FGDw	DOE 8	0.69	0.69	7.9	7.3	0.0104	0.17	9,970	17.05	FGDw	99.9300	0.69	0.4466	732.197	99.8056	1.00
L	FGDw	20	3.8	3.8	12	12	0.019	0.21	10,000	21.00	FGDw	99.9095	3.8	1.0857	1200.000	99.8835	1.00

		ei	ei/n	# points	Max ei/n	Min ei/n
Averages	overall	97.7576	0.9826	34	1.0019	0.911
	bituminous	96.8310	0.9738	30	1.0019	0.911
	sub-bitum	99.2451	0.9941	10	0.9998	0.955
	lignite	99.0720	0.9980	4	0.9997	0.996
	ESP	96.5585	0.9731	19	0.9998	0.9109
	FGDw	98.6778	0.9885	7	1.0004	0.9693
	FF	99.7752	0.9985	6	1.0012	0.996
	FGDd	99.0843	1.0000	2	1.0019	1.002
	ESP+FGDw	97.1276	0.9775	26		
	FF+FGDd	99.8050	0.9990	8		
bituminous coal						
	ESP	95.8285	0.9679	14	0.9990	0.911
	FGDw	97.8029	0.9824	4	1.0004	0.969
	FF	99.9618	1.0012	1	-	-
	FGDd	99.8785	1.0019	1	-	-
	ESP+FGDw	95.2656	0.9707	18		
	FF+FGDd	99.9200	1.0016	2		
sub-bituminous coal						
	ESP	97.9607	0.9909	3	0.9996	0.955
	FGDw	99.9445	0.9998	1	-	-
	FF	99.7379	0.9979	5	0.9993	0.996
	FGDd	99.9104	0.9997	1	-	-
	ESP+FGDw	98.4627	0.9878	4		
	FF+FGDd	99.7886	0.9982	6		
gritte coal						
	ESP	99.5494	0.9973	2	-	
	FGDw	99.7945	0.9997	2	-	
	FF					
	FGDd					
	ESP+FGDw	88.6723	0.9983	4		
	FF+FGDd	-	-			
ESP						
	bitum	95.0283	0.9679	14		
	sub-bit	97.9687	0.9839	3		
	lig	99.5494	0.9973	2		
FGDw						
	bitum	97.8029	0.9824	4		
	sub-bit	99.9445	0.9998	1		
	lig	99.7945	0.9997	2		
FF						
	bitum	99.9618	1.0012	1		
	sub-bit	99.7379	0.9979	5		
	lig	-	-	0		
FGDd	bitum	-	1.0019	1		
	sub-bit	99.9104	0.9997	1		
	lig	-	-	0		

Manganese (Mn) 6/24/96
EPRI data
C: CI < DL (one point) set = rank avg of other values and EI < DL NOT USED

Rank	Control Device	Unit ID	Modified EI (lb/TBtu)	Actual EI (lb/TBtu)	Modified CI (coal) (ppm)	Actual CI (coal) (ppm)	PMout (lb/MBtu)	fash	HHV (btu/lb)	PMgen (lb/MBtu)	Control Device	n	EI (lb/TBtu)	CIPM/fa	CIPM / fa*(1-n)	nl	1-n
B	ESP	19	5.4	5.4	7.3	7.3	0.036	0.09	12,500	6.74	ESP	99.4659	5.4	2.8879	540 741	99.0014	1.00
B	ESP	18 L	21	21	14	14	0.12	0.195	11,000	6.88	ESP	98.2566	21	17.6842	1214.493	97.8300	1.00
B	ESP	110 L	16	16	16	16	0.041	0.083	12,400	6.88	ESP	99.4029	16	7.9006	1322 314	98.7900	0.99
B	ESP	16	25	25	17	17	0.21	0.1	13,700	7.33	ESP	97.1230	25	35.7000	1249 876	97.9853	1.01
B	ESP	110 B	37	37	17	17	0.022	0.091	11,900	7.65	ESP	99.7123	37	4.1099	1423.571	97.4100	0.93
B	ESP	12	60	60	18	18	0.1	0.094	13,700	6.86	ESP	98.5426	60	19.1489	1313 869	95.4333	0.97
B	ESP	116	10	10	19	19	0.046	0.12	12,900	9.30	ESP	99.5056	10	7.2833	1472 868	99.3211	1.00
B	ESP	18	18	18	21	21	0.14	0.13	13,400	9.70	ESP	98.5569	18	22.6154	1557 164	98.8614	1.00
B	ESP	DOE 4	34	34	23	23	0.14	0.138	14,300	9.65	ESP	98.5493	34	23.3333	1508 392	97.6867	0.99
B	ESP	114 B	20	20	27	27	0.025	0.087	13,500	6.44	ESP	99.6121	20	7.7586	2330 000	99.0000	0.99
B	ESP	114 R	15	15	27	27	0.016	0.089	13,300	6.69	ESP	99.7609	15	4.8539	2330 075	99.2617	0.99
B	ESP	15	8.6	8.6	28	28	0.026	0.127	13,000	9.77	ESP	99.7134	8.6	6.1702	2153 946	99.6007	1.00
B	ESP	122	210	210	36	36	0.12	0.093	13,370	6.98	ESP	98.2748	210	46.4516	2092 595	92.2008	0.94
B	ESP	DOE 3	27	27	47	47	0.11	0.12	12,900	9.30	ESP	98.8176	27	43.0833	3843.411	99.2589	1.00
B	ESP	DOE 5	16	16	57	57	0.045	0.114	13,800	8.26	ESP	99.4795	16	21.5000	4130 435	99.6128	1.00
B	ESP	DOE 2	3.9	3.9	100	100	0.019	0.12	12,900	9.30	ESP	99.7958	3.9	16.8333	7751 958	99.8497	1.00
B	FGDw	21	15	15	27.65909	-	0.011	0.057	14,000	4.79	FGDw	99.7701	15	4.5246	1368.506	99.2380	0.99
B	FGDw	DOE 4	7.2	7.2	23	23	0.014	0.138	14,300	9.65	FGDw	99.8549	7.2	2.9388	1638 392	99.5593	1.00
B	FGDw	125	7.3	7.3	25	25	0.09	0.098	13,043	7.51	FGDw	98.8022	7.3	22.9592	1916 737	99.819	1.01
B	FF	18 FF	0.51	0.51	21	21	0.0019	0.13	13,400	9.70	FF	99.9804	0.51	0.3069	1557 164	99.9675	1.00
B	FF	DOE 2 FF	2.1	2.1	27	27	0.011	0.12	13,000	9.23	FF	99.8808	2.1	2.4750	2079 923	99.8989	1.00
B	FGDd	SNIT8118	0.8	0.8	19	19	0.029	0.12	12,900	9.30	FGDd	99.6883	0.8	4.5917	1472 568	99.9457	1.00
B	FGDd	14	3.9	3.9	17	17	0.0073	0.093	13,700	6.79	FGDd	99.8926	3.9	1.3344	1240 876	99.6857	1.00
S	ESP	22	1.1	1.1	8.3	8.3	0.0015	0.068	11,900	5.63	ESP	99.9738	1.1	0.1831	602 521	99.8412	1.00
S	ESP	11	10	10	17	17	0.023	0.062	11,900	5.21	ESP	99.5685	10	3.3065	1428 571	99.3000	1.00
S	ESP	109	17	17	27	27	0.058	0.088	12,200	7.21	ESP	99.1959	17	17.7955	2213 115	99.0319	1.00
S	FGDw	11	2.6	2.6	17	17	0.0051	0.062	11,900	5.21	FGDw	99.9021	2.6	1.3984	1428.571	99.8480	1.00
S	FGDw	101	10	10	66	66	0.007	0.25	10,000	25.00	FGDw	99.9720	10	1.8480	6600.000	99.8485	1.00
S	FF	115	1	1	4.2	4.2	0.019	0.112	12,565	8.91	FF	99.7868	1	0.7125	334 262	99.7008	1.00
S	FF	115 U	0.89	0.89	5.2	5.2	0.0012	0.105	12,538	8.31	FF	99.9856	0.89	0.0684	411 458	99.7837	1.00
S	FF	10	31	31	30	30	0.006	0.21	11,000	19.09	FF	99.9561	31	1.1429	2727 273	98.8633	0.00
S	FF	101	8.5	8.5	66	66	0.021	0.25	10,000	25.00	FF	99.9160	8.5	5.5440	6600 000	99.8712	1.00
S	FF	DOE 8	18	18	156	156	0.009	0.112	11,700	9.57	FF	99.9080	18	10.9286	11623 93	99.845	1.00
S	FGDd	DOE 7	11	11	83	83	0.012	0.229	10,500	21.81	FGDd	99.9450	11	4.3480	7904 762	99.8808	1.00
L	ESP	20	27	27	72	72	0.051	0.21	10,000	21.00	ESP	99.7571	27	17.4857	7200 000	99.8250	1.00
L	ESP	DOE 6	29	29	97	97	0.02	0.07	9,970	17.05	ESP	99.8827	29	11.4118	9728 188	99.7019	1.00
L	FGDw	20	33	33	72	72	0.019	0.21	10,000	21.00	FGDw	99.9095	33	6.5143	7200 000	99.5417	1.00
L	FGDw	DOE 6	30	30	97	97	0.0104	0.07	9,970	17.05	FGDw	99.9390	30	5.9041	9728 188	99.8816	1.00

	Averages	nl	n1n	# points	Max nl/n	Min nl/n
	overall	99.0506	0.9857	38	1.0009	0.9382
	bituminous	98.6698	0.9943	23	1.0089	0.9382
	sub-bitum	99.533	0.9981	11	1.0004	0.9890
	lignite	99.640	0.9977	4	0.9987	0.9963
	ESP	98.5330	0.9934	21	1.0089	0.9382
	FGDw	99.0156	0.9968	7	1.0083	0.9947
	FF	99.7044	0.9979	7	1.0002	0.9890
	FGDd	99.8307	0.9993	3	1.0026	0.9979
	ESP+FGDw	98.8038	0.9947	28		
	FF+FGDd	99.7423	0.9985	10		
bituminous coal						
	ESP	98.2183	0.9917	16	1.0089	0.9382
	FGDw	99.4089	1.0000	5	1.0083	0.9947
	FF	99.9332	1.0000	2	1.0002	0.9999
	FGDd	99.8157	1.0003	2	1.0026	0.9979
	ESP+FGDw	98.4159	0.9930	19		
	FF+FGDd	99.8744	1.0001	4		
subbituminous coal						
	ESP	99.4577	0.9983	5	1.0004	0.9974
	FGDw	99.8332	0.9990	2	0.9992	0.9988
	FF	99.6128	0.9979	5	0.9998	0.9890
	FGDd	99.8608	0.9992	1	-	-
	ESP+FGDw	99.6078	0.9989	5		
	FF+FGDd	99.6542	0.9974	6		
lignite coal						
	ESP	99.6635	0.9984	2	0.9987	0.9982
	FGDw	99.6167	0.9969	2	0.9975	0.9963
	FF					
	FGDd					
	ESP+FGDw	99.6401	0.9977	4		
	FF+FGDd					
ESP						
	bitum	98.2165	0.9917	16		
	sub-bit	99.4577	0.9983	5		
	lig	99.6635	0.9984	2		
FGDw						
	bitum	99.4089	1.0000	3		
	sub-bit	99.8332	0.9990	2		
	lig	99.6167	0.9969	2		
FF						
	bitum	99.9332	1.0000	2		
	sub-bit	99.6128	0.9979	5		
	lig					
FGDd						
	bitum	99.8157	1.0003	2		
	sub-bit	99.8608	0.9992	1		
	lig					

Mercury (Hg) 6/12/96
EPRI data
F: CI < DL set – avg of DL and EI < DL set NOT USED

Rank	Control Device	Unit ID	Modified EI (lb/TBtu)	Actual EI (lb/TBtu)	Modified CI (coal) (ppm)	Actual CI (coal) (ppm)	PMout (lb/MBtu)	fuel	HHV (lb/MBtu)	PMgen (lb/MBtu)	Control Device	n	EI (lb/TBtu)	CPM/kWh	CPM / (g * 11 n)	ni	n/n
B	ESP	DOE 5	0.53	0.53	0.08	0.08	0.048	0.114	10,800	0.26	ESP	99.4795	0.53	0.0002	5.797	90.8575	0.913
B	ESP	10 B	6.1	6.1	0.964	0.964	0.022	0.091	11,900	7.65	ESP	99.7123	6.1	0.0155	5.378	-13.4219	-0.135
B	ESP	DOE 3	4.6	4.6	0.07	0.07	0.11	0.12	12,900	8.30	ESP	98.8175	4.6	0.0042	5.426	15.2286	0.154
B	ESP	DOE 4	5.6	5.6	0.077	0.077	0.14	0.138	14,300	9.65	ESP	98.5493	5.6	0.0781	5.386	4.0000	0.041
B	ESP	122	6.8	6.8	0.078	0.078	0.12	0.093	13,170	8.96	ESP	98.2748	6.8	0.1018	5.909	-15.0835	-0.153
B	ESP	110 L	5	5	0.08	0.08	0.041	0.083	12,100	8.86	ESP	99.4033	5	0.0305	5.813	24.3750	0.245
B	ESP	19	6.2	6.2	0.1	0.1	0.036	0.091	13,500	8.74	ESP	99.4659	6.2	0.0389	7.407	19.3000	0.194
B	ESP	114 R	3.8	3.8	0.079228	< 0.11	0.016	0.089	13,300	8.69	ESP	99.7609	3.8	0.0142	5.957	38.2048	0.383
B	ESP	18	7.1	7.1	0.12	0.12	0.14	0.13	13,400	9.70	ESP	98.5569	7.1	0.1292	8.955	20.7167	0.210
B	ESP	114 B	4.5	4.5	0.096986	< 0.12	0.025	0.087	13,500	8.44	ESP	99.5121	4.5	0.0278	7.158	37.1355	0.373
B	ESP	116	9.2	9.2	0.13	0.13	0.046	0.12	12,900	9.80	ESP	99.5455	9.2	0.0408	10.078	8.7077	0.088
B	ESP	18 L	4.8	4.8	0.14	0.14	0.12	0.095	13,900	8.98	ESP	98.2568	4.8	0.1768	10.145	54.6667	0.548
B	ESP	16	6.4	6.4	0.15	0.15	0.21	0.1	13,700	7.90	ESP	97.1230	6.4	0.3150	10.949	41.5467	0.428
B	ESP	DOE 2	14	14	0.21	0.21	0.019	0.12	12,900	9.30	ESP	99.7958	14	0.0033	16.279	14.0000	0.140
B	FGDw	DOE 4	5	5	0.077	0.077	0.014	0.138	14,300	9.65	FGDw	99.8649	5	0.0078	5.385	44.2857	0.444
B	FGDw	125	3.2	3.2	0.086	0.086	0.09	0.098	13,043	7.61	FGDw	98.8022	3.2	0.0780	8.594	51.4679	0.521
B	FGDw	21	0.84	0.04	0.15	0.15	0.011	0.067	14,900	4.49	FGDw	99.7701	0.84	0.0048	10.714	92.1600	0.924
B	FGDw	12	1.3	1.3	0.11	0.11	0.013	0.094	13,700	0.89	FGDw	99.8105	1.3	0.0152	8.029	83.8091	0.840
B	FF	18 FF	6.3	6.3	0.12	0.12	0.0019	0.13	13,400	9.70	FF	99.8804	6.3	0.0018	8.955	29.6500	0.297
B	FF	DOE 2 FF	19	19	0.26	0.26	0.011	0.12	13,900	9.23	FF	99.8808	19	0.0038	20.000	5.0000	0.050
B	FGDd	SNRB116	14	14	0.19	0.19	0.009	0.12	12,900	9.30	FGDd	99.8883	14	0.0014	10.078	-38.9231	-0.390
S	ESP	102	1.8	1.8	0.07	0.07	0.058	0.066	12,200	7.21	ESP	99.1959	1.8	0.0461	5.738	68.8286	0.692
S	ESP	11	10	10	0.11	0.11	0.023	0.062	11,300	5.21	ESP	99.5585	10	0.0408	9.244	-8.1818	-0.082
S	ESP	22	3.6	3.6	0.14	0.14	0.0015	0.068	11,980	5.88	ESP	99.8736	3.6	0.0031	17.686	67.4829	0.675
S	FGDw	101	1.9	1.9	0.063	0.063	0.007	0.25	10,000	25.00	FGDw	99.9720	1.9	0.0018	5.300	59.8413	0.599
S	FGDw	11	8.3	8.3	0.11	0.11	0.0051	0.062	11,900	5.21	FGDw	99.9021	8.3	0.0000	9.244	-0.2000	0.002
S	FF	115 U	0.41	0.41	0.019	0.019	0.0012	0.105	12,838	8.51	FF	99.9856	0.41	0.0002	1.503	72.7205	0.727
S	FF	101	5.1	5.1	0.063	0.063	0.02	0.25	10,000	25.00	FF	99.9160	5.1	0.0053	5.300	19.0476	0.191
S	FF	DOE 8	1.9	1.9	0.07	0.07	0.009	0.112	11,700	9.67	FF	99.9060	1.9	0.0056	5.983	68.2429	0.683
S	FGDd	DOE 7	4.2	4.2	0.058	0.058	0.012	0.229	10,500	21.81	FGDd	99.9460	4.2	0.0030	5.524	23.9655	0.240
L	ESP	DOE 6	5.8	5.8	0.08	0.08	0.02	0.17	9,970	17.05	ESP	99.8027	5.8	0.0094	8.024	27.7175	0.278
L	ESP	20	15	15	0.26	0.26	0.051	0.21	10,000	21.00	ESP	99.7571	15	0.0691	26.000	42.9077	0.429
L	FGDw	DOE 8	9.5	9.5	0.09	0.09	0.0104	0.17	9,970	17.05	FGDw	99.9390	9.5	0.0049	8.024	-18.3937	-0.184
L	FGDw	20	12	12	0.26	0.26	0.019	0.21	10,000	21.00	FGDw	99.9095	12	0.0235	26.000	53.8462	0.539

	Averages	ni	n/n	# points	Max ni/n	Min n/n
	overall	32.0631	0.322	34	0.9237	-0.3904
	bituminous	28.2239	0.294	21	0.9237	-0.3904
	sub-bitum	43.6516	0.436	8	0.7274	-0.0822
	lignite	26.3694	0.264	4	0.5389	-0.1840
	ESP	27.5372	0.277	19	0.9199	-0.1535
	FGDw	48.4032	0.485	8	0.9237	-0.1840
	FF	38.8338	0.3895	5	0.7274	0.0501
	FGDd	7.470	-0.075	2	0.2388	-0.3904
	ESP+FGDw	33.7197	0.339	27		
	FF+FGDd	25.6731	0.2567	7		
bituminous coal						
	ESP	23.2020	0.235	14	0.9199	-0.1535
	FGDw	87.9307	0.882	4	0.9237	0.4435
	FF	17.3250	0.173	2	0.2388	0.0501
	FGDd	-38.9231	-0.390	1	-	-
	ESP+FGDw	33.1653	0.334	18		
	FF+FGDd	-1.4244	-0.015	3		
subbituminous coa						
	ESP	42.6432	0.426	3	0.5918	0.2750
	FGDw	40.0252	0.400	2	0.5936	0.1022
	FF	53.3397	0.5337	3	0.7274	0.1908
	FGDd	23.966	0.240	1	-	-
	ESP+FGDw	41.5660	0.417	5		
	FF+FGDd	45.9861	0.460	4		
lignite coa						
	ESP	35.0126	0.351	2	0.4241	0.2775
	FGDw	17.7262	0.177	2	0.5389	-0.1840
	FF					
	FGDd					
	ESP+FGDw	26.3694	0.264	4		
	FF+FGDd					
ESP						
	bitum	23.2020	0.235	14		
	sub-bit	42.6432	0.426	3		
	lig	35.0126	0.351	2		
FGDw						
	bitum	87.9307	0.882	4		
	sub-bit	40.0252	0.400	2		
	lig	17.7262	0.177	2		
FF						
	bitum	17.3250	0.173	2		
	sub-bit	53.3397	0.534	3		
	lig					
FGDd	bitum	-38.9231	-0.390	1		
	sub-bit	23.966	0.240	1		
	lig					

Mercury (Hg) 6/16/06
EPRI data
F=1; CI < DL set = avg of DI and EI < DL set NOT USED ***REPEAT with datasets having nI < 0 reset to nI = 0***

Rank	Control Device	Unit ID	Modified EI (lb/TBtu)	Actual EI (lb/TBtu)	Modified CI (coal) (ppm)	Actual CI (coal) (ppm)	PMout (lb/MBtu)	fash	HHV (lb/MBtu)	PMgen (lb/MBtu)	Control Device	n	EI (lb/TBtu)	CIPM/lb	CIPM / *a *(1-a)	r	n/n
B	ESP	DOE 5	0.53	0.53	0.08	0.08	0.043	0.114	13,800	8.26	ESP	99.4785	0.53	0.0302	5.797	90.8575	0.913
B	ESP	10 B	6.1	6.1	0.864	0.864	0.022	0.091	11,900	7.55	ESP	95.7123	6.1	0.0155	5.378	0.0000	0.000
B	ESP	DOE 3	4.6	4.6	0.67	0.67	0.11	0.12	12,900	9.30	ESP	96.8175	4.6	0.0242	5.426	15.2288	0.154
B	ESP	DOE 4	5.6	5.6	0.977	0.977	0.14	0.138	14,300	9.65	ESP	96.5493	5.6	0.0281	5.385	0.0000	0.000
B	ESP	122	6.8	6.8	0.979	0.979	0.12	0.093	13,370	8.98	ESP	96.2748	6.8	0.1019	5.909	0.0000	0.000
B	ESP	110 L	5	5	0.82	0.68	0.041	0.083	12,100	8.96	ESP	99.4093	5	0.0295	5.615	24.3759	0.245
B	ESP	19	6.2	6.2	0.1	0.1	0.036	0.091	13,500	8.74	ESP	99.4659	6.2	0.0396	7.467	16.3009	0.164
B	ESP	114 R	3.8	3.8	0.079222	< 0.1	0.016	0.089	13,300	8.89	ESP	99.7809	3.8	0.0142	5.957	36.2048	0.363
B	ESP	12	7.1	7.1	0.12	0.12	0.14	0.13	13,400	9.70	ESP	95.6569	7.1	0.1282	8.956	20.7167	0.210
B	ESP	114 0	4.5	4.5	0.095836	< 0.12	0.025	0.087	13,550	8.44	ESP	99.6121	4.5	0.0278	7.158	37.1355	0.373
B	ESP	110	9.2	9.2	0.19	0.19	0.046	0.12	12,990	9.90	ESP	99.5055	9.2	0.0498	10.678	8.7077	0.088
B	ESP	16 L	4.8	4.8	0.14	0.14	0.12	0.095	13,000	8.88	ESP	98.2568	4.8	0.1768	10.145	52.6857	0.536
B	ESP	16	6.4	6.4	0.15	0.15	0.21	0.1	13,750	7.90	ESP	97.1230	6.4	0.9150	10.949	41.5467	0.428
B	ESP	DOE 2	14	14	0.21	0.21	0.019	0.12	12,900	9.30	ESP	99.7858	14	0.0333	18.279	14.0000	0.140
B	FGDw	DOE 4	3	3	0.077	0.077	0.014	0.138	14,300	9.65	FGDw	99.8549	3	0.0078	5.386	44.2857	0.444
B	FGDw	125	3.2	3.2	0.086	0.086	0.09	0.098	13,043	7.51	FGDw	98.8022	3.2	0.0790	8.594	51.4679	0.521
B	FGDw	21	0.84	0.84	0.15	0.15	0.011	0.067	14,000	4.20	FGDw	99.7701	0.84	0.0248	10.714	98.1600	0.974
B	FGDw	12	1.3	1.3	0.11	0.11	0.013	0.094	13,700	8.98	FGDw	99.8105	1.3	0.0152	8.029	83.8991	0.843
B	FF	16 FF	6.3	6.3	0.12	0.12	0.0019	0.13	13,400	9.70	FF	99.9804	6.3	0.0016	8.955	29.6500	0.297
B	FF	DOE 2 FF	19	19	0.26	0.26	0.011	0.12	13,900	9.28	FF	99.8808	19	0.0238	20.000	5.0000	0.050
B	FGDd	SNHB116	14	14	0.19	0.19	0.039	0.12	12,900	9.30	FGDd	99.6883	14	0.0314	10.078	0.0000	0.000
S	ESP	102	1.8	1.8	0.07	0.07	0.008	0.088	12,200	7.21	ESP	99.1959	1.8	0.0461	5.738	66.6286	0.692
S	ESP	11	10	10	0.11	0.11	0.023	0.082	11,900	5.21	ESP	99.5585	10	0.0408	9.244	0.0000	0.000
S	ESP	22	3.6	3.6	0.14	0.14	0.0015	0.068	11,980	5.68	ESP	99.9736	3.6	0.0031	11.666	67.4629	0.975
S	FGDw	101	1.9	1.9	0.068	0.068	0.007	0.25	10,300	25.00	FGDw	99.9720	1.9	0.0018	5.300	69.8413	0.699
S	FGDw	11	8.0	8.0	0.11	0.11	0.0051	0.082	11,900	5.21	FGDw	99.9921	8.3	0.0000	9.242	10.2061	0.102
S	FF	115 U	0.41	0.41	0.019	0.019	0.0012	0.105	12,838	9.01	FF	99.9856	0.41	0.0002	1.509	72.7286	0.727
S	FF	101	5.1	5.1	0.063	0.063	0.021	0.25	10,300	25.00	FF	99.9169	5.1	0.0069	6.300	19.0476	0.191
S	FF	DOE 8	1.9	1.9	0.07	0.07	0.009	0.112	11,700	9.57	FF	99.9060	1.9	0.0056	5.983	68.2429	0.683
S	FGDd	DOE 7	4.2	4.2	0.058	0.058	0.012	0.229	10,500	21.81	FGDd	99.9450	4.2	0.0000	5.624	23.9656	0.240
L	ESP	DOE 6	5.8	5.8	0.09	0.09	0.02	0.17	8,970	17.06	ESP	99.5827	5.8	0.0094	8.024	27.7175	0.278
L	ESP	20	15	15	0.28	0.28	0.051	0.21	10,300	21.00	ESP	99.7571	15	0.0631	28.000	42.3077	0.424
L	FGDw	DOE 6	9.5	9.5	0.09	0.09	0.0104	0.17	8,970	17.06	FGDw	99.9399	9.5	0.0049	8.024	0.0000	0.000
L	FGDw	20	12	12	0.26	0.26	0.019	0.21	10,000	21.00	FGDw	99.9095	12	0.0036	26.000	53.8462	0.539

		nI	n/n	# points	Max n/n	Min n/n
Averages						
	overall	34.9455	0.351	34	0.9237	0.0000
	bituminous	31.6255	0.319	21	0.9237	0.0000
	sub-bitum	44.4607	0.446	9	0.7274	0.0000
	lignite	30.9870	0.310	4	0.5389	0.0000
	ESP	29.6787	0.299	19	0.9133	0.0000
	FGDw	50.7024	0.509	8	0.9237	0.0000
	FF	38.9338	0.3895	5	0.7274	0.0501
	FGDd	11.083	0.120	2	0.2308	0.0000
	ESP+FGDw	35.9079	0.351	27		
	FF+FGDd	31.2335	0.3125	7		
bituminous coal						
	ESP	25.5541	0.258	14	0.9133	0.0000
	FGDw	67.9307	0.682	4	0.9237	0.4435
	FF	17.3260	0.173	2	0.2966	0.0501
	FGDd	0.0000	0.000	1		-
	ESP+FGDw	34.9712	0.352	10		
	FF+FGDd	11.5500	0.118	9		
subbituminous coal						
	ESP	45.3705	0.456	3	0.6918	0.6750
	FGDw	40.0252	0.400	2	0.6986	0.1022
	FF	53.3387	0.5337	3	0.7274	0.1906
	FGDd	23.966	0.240	1	-	-
	ESP+FGDw	43.2324	0.434	5		
	FF+FGDd	45.9861	0.460	4		
lignite coal						
	ESP	35.0126	0.351	2	0.4241	0.2775
	FGDw	26.9231	0.269	2	0.5389	0.0000
	FF					
	FGDd					
	ESP+FGDw	30.9678	0.310	4		
	FF+FGDd					
ESP						
	bitum	25.5541	0.258	14		
	sub-bit	45.3705	0.456	3		
	lig	35.0126	0.351	2		
FGDw						
	bitum	67.9307	0.682	4		
	sub-bit	40.0252	0.400	2		
	lig	26.9231	0.269	2		
FF						
	bitum	17.3260	0.173	2		
	sub-bit	53.3387	0.534	3		
	lig					
FGDd	bitum	0.0000	0.000	1		
	sub-bit	23.966	0.240	1		
	lig					

Nickel (Ni) 6/24/98
EPRI data
0: CI < DL set = rank average of data < DL and EI < DL set = 0

Rank	Control Device	Unit ID	Modified EI (lb/TBtu)	Actual EI (lb/TBtu)	Modified CI (coal) (ppm)	Actual CI (coal) (ppm)	PMout (lb/MBtu)	fash	PMHV (lb/MBtu)	PMgen (lb/MBtu)	Control Device	n	EI (lb/TBtu)	CI/PM/a	Ca*PM/ fa*(1-n)	ni	n/n
B	ESP	110 B	7.7	7.7	6.7	6.7	0.022	0.091	11,800	7.65	ESP	99.712	7.7	1.6188	569.025	96.632	0.969
B	ESP	110 I	0 < 5.0		6.5	6.5	0.041	0.063	12,100	6.86	ESP	99.402	0	3.3590	561.983	100.000	1.006
D	ESP	116	0 < 16		8	8	0.046	0.12	12,900	9.30	ESP	99.505	0	3.6667	620.155	100.000	1.005
B	ESP	19	7.9	7.9	12	12	0.035	0.091	13,500	8.74	ESP	99.466	7.9	3.7478	868.889	99.111	0.996
B	ESP	18	16	16	12	12	0.14	0.13	13,400	9.70	ESP	98.557	15	12.9231	895.522	98.213	0.997
B	ESP	122	74	74	13	13	0.12	0.093	13,370	6.98	ESP	96.275	74	16.7742	972.326	92.389	0.940
B	ESP	DOE 5	4	4	14	14	0.043	0.114	13,800	8.26	ESP	99.479	4	5.2807	1014.493	99.836	1.001
B	ESP	16 L	17	17	17	17	0.12	0.096	13,800	6.88	ESP	98.257	17	21.4737	1231.884	98.620	1.004
B	ESP	DOE 2	1.2	1.2	12	18	0.010	0.10	12,900	9.30	ESP	99.796	1.2	2.8600	1395.349	99.914	1.001
B	ESP	DOE 3	27	27	18	18	0.11	0.12	12,900	9.30	ESP	98.818	27	16.6000	1395.349	98.965	0.999
B	ESP	15	59	5.9	12 38857	< 20	0.099	0.157	13,000	9.77	ESP	99.713	59	2.7308	952.821	93.908	0.941
B	ESP	16	24	24	27	27	0.21	0.1	13,700	7.30	ESP	97.129	24	66.7000	1970.803	98.782	1.017
B	ESP	114 B	78	78	28	28	0.025	0.087	13,500	8.44	ESP	99.612	78	8.6480	2074.074	96.239	0.966
B	ESP	DOE 4	24	24	30	30	0.14	0.138	14,300	9.65	ESP	88.549	24	30.4348	2097.902	98.856	1.003
B	ESP	12	2.3	2.3	15 85158	< 32	0.1	0.094	13,709	6.86	ESP	88.543	2.3	16.9421	1156.595	99.801	1.013
B	ESP	114 H	34	34	46	46	0.016	0.089	13,303	6.66	ESP	98.781	34	8.2697	3458.647	99.017	0.993
B	FGDw	21	1.7	1.7	8.3	8.3	0.011	0.067	14,000	4.76	FGDw	99.770	1.7	1.0667	592.857	99.713	0.999
B	FGDw	125	7.5	7.5	17	17	0.09	0.098	13,043	7.51	FGDw	98.802	7.5	15.6782	1304.981	98.495	1.006
B	FGDw	DOE 4	40	40	30	30	0.014	0.138	14,300	9.65	FGDw	99.855	40	3.0435	2097.902	98.993	0.992
B	FGDw	12	4	4	15 53158	< 32	0.013	0.094	13,709	6.86	FGDw	99.811	4	2.1695	1156.595	99.654	0.998
B	FF	116 FF	2	2	12	12	0.0010	0.13	13,400	9.70	FF	88.980	2	0.1754	895.522	99.777	0.998
B	FF	DOE 2 FF	0.22	0.22	1.5	1.5	0.011	0.12	13,000	9.35	FF	99.881	0.22	1.3750	1153.846	99.981	1.001
B	FGDd	SNRB116	49	49	8	8	0.029	0.13	12,900	9.30	FGDd	99.668	49	1.9333	620.155	92.099	0.924
B	FGDd	4	2.3	2.3	10.08	< 15	0.0073	0.093	13,709	6.79	FGDd	99.692	2.3	0.7912	735.765	99.637	0.998
S	ESP	22	0.64	0.64	3.0	3.9	0.0015	0.068	11,980	5.68	ESP	99.874	0.64	0.0860	326.543	99.308	0.990
S	ESP	11	2.6	2.6	2.075	< 10	0.023	0.062	11,999	5.21	ESP	99.559	2.6	0.7898	174.375	98.509	0.989
S	ESP	102	340	340	31	31	0.058	0.088	12,290	7.21	ESP	99.196	340	20.4318	2540.984	86.610	0.873
S	FGDw	101	2.9	2.9	0.8	< 1	0.007	0.25	10,000	25.00	FGDw	99.972	2.9	0.0168	60.000	95.167	0.952
S	FGDw	11	3	3	2.075	< 10	0.0051	0.062	11,999	5.21	FGDw	99.902	3	0.1707	174.375	98.280	0.984
S	FF	115	1.5	1.5	0.8	0.6	0.0018	0.112	12,565	8.91	FF	99.879	1.5	0.0102	47.752	96.359	0.969
S	FF	101	2	2	0.8	< 1	0.021	0.25	10,000	25.00	FF	99.916	2	0.0504	60.000	96.667	0.967
S	FF	115 U	0.45	0.45	1	1	0.0012	0.105	12,638	8.31	FF	99.886	0.45	0.0114	79.126	99.431	0.994
S	FF	DOE 8	2	2	2.8	2.8	0.008	0.112	11,700	8.57	FF	99.806	2	0.2250	239.316	99.164	0.993
S	FF	10	0 < 2.0		2.075	< 10	0.008	0.21	11,000	10.00	FF	99.958	0	0.0790	168.536	100.000	1.000
S	FGDd	DOE 7	0 < 0.30		0	5	0.012	0.229	10,530	21.81	FGDd	99.945	0	0.2680	476.190	100.000	1.001
S	FGDd	111	0 < 5.3		7 383333	< 120	0.041	0.14	10,020	13.97	FGDd	99.707	0	2.1623	730.86	100.000	1.003
L	ESP	DOE 6	4.3	4.3	2.6	2.6	0.02	0.17	8,979	17.65	ESP	99.693	4.3	0.3059	260.782	95.351	0.985
L	ESP	20	5.5	5.5	14	14	0.051	0.21	10,000	21.00	ESP	99.757	5.5	3.4000	1400.000	99.607	0.998
L	FGDw	DOE 6	5.1	5.1	2.6	2.6	0.0104	0.17	8,979	17.65	FGDw	99.939	5.1	0.1597	260.782	96.044	0.981
L	FGDw	20	4.3	4.3	14	14	0.019	0.21	10,000	21.00	FGDw	99.810	4.3	1.2667	1400.000	99.696	0.998

		ni	n/n	# points	Max n/n	Min n/n
	Averages					
	overall	96.142	0.986	40	1.0171	0.8732
	bituminous	98.312	0.990	24	1.0171	0.8239
	sub-bitum	97.642	0.977	12	1.0025	0.8732
	lignite	98.924	0.991	4	0.9985	0.9810
	ESP	97.307	0.986	21	1.0171	0.8732
	FGDw	98.509	0.988	8	1.0063	0.9519
	FF	98.340	0.989	7	1.0010	0.9675
	FGDd	97.947	0.981	4	1.0029	0.9239
	ESP+FGDw	96.000	0.987	29		
	FF+FGDd	98.515	0.986	11		
bituminous coal						
	ESP	98.191	0.982	16	1.0171	0.9401
	FGDw	99.221	0.997	4	1.0063	0.9824
	FF	99.879	0.999	2	1.0010	0.9401
	FGDd	95.893	0.961	2	0.9979	0.9239
	ESP+FGDw	98.397	0.993	20		
	FF+FGDd	97.986	0.980	4		
subbituminous coal						
	ESP	94.977	0.954	3	0.9883	0.8732
	FGDw	98.723	0.988	2	0.9939	0.9519
	FF	98.424	0.985	5	1.0004	0.9675
	FGDd	100.000	1.002	2	1.0029	1.0006
	ESP+FGDw	95.878	0.959	5		
	FF+FGDd	99.974	0.990	7		
lignite coal						
	ESP	98.979	0.992	2	0.9985	0.9847
	FGDw	98.859	0.989	2	0.9978	0.9810
	FF					
	FGDd					
	ESP+FGDw	98.924	0.991	4		
	FF+FGDd					
ESP						
	bitum	98.191	0.982	16		
	sub-bit	94.977	0.954	3		
	lig	98.979	0.992	2		
FGDw						
	bitum	99.221	0.997	4		
	sub-bit	96.723	0.965	2		
	lig	98.859	0.989	2		
FF						
	bitum	99.879	0.999	2		
	sub-bit	98.424	0.985	5		
	lig					
FGDd						
	bitum	95.893	0.961	2		
	sub-bit	100.000	1.002	2		
	lig					

Selenium (Se) 6/18/96
EPRI data
For Cl <DL set = avg of values < indicated D (rank-specific) and EI < DL datasets NOT USED

Rank	Control Device	Unit ID	Modified EI (lb/TBtu)	Actual EI (lb/TBtu)	Modified Cl (coal) (ppm)	Actual Cl (coal) (ppm)	PMout (lb/MBtu)	Ash	HHV (Btu/MBtu)	PMgen (lb/MBtu)	Control Device	n	EI (lb/TBtu)	CIPM/a	CIPPM / la *(1-n)	nl	nl/n
B	ESP	110 B	46	46	0.57	0.57	0.022	0.091	11,900	7.65	ESP	99.7123	46	0.1378	47.899	3.96	0.04
B	ESP	DOE 2	52	52	0.57	< 0.6	0.019	0.19	12,300	9.80	ESP	99.7958	52	0.0003	44.186	-0.32	-0.40
B	ESP	114 A	150	150	0.735	< 1.1	0.016	0.089	13,300	6.69	ESP	99.7609	150	0.1321	55.283	-1.42	-1.72
B	ESP	114 B	240	240	0.795	< 1.2	0.025	0.067	13,500	6.44	ESP	99.6121	240	0.2112	54.444	-3.92	-3.42
B	ESP	12	46	46	1.2	1.2	0.1	0.091	13,700	6.86	ESP	98.5428	46	1.2786	87.591	15.20	0.46
B	ESP	122	70	70	1.6	1.6	0.12	0.093	13,370	8.98	ESP	98.2748	70	2.0645	119.671	41.51	0.42
B	ESP	110 L	130	180	2.1	2.1	0.047	0.063	12,100	6.66	ESP	99.4023	130	1.0373	173.554	25.10	0.25
B	ESP	15	77	77	2.2	2.2	0.038	0.127	13,000	9.77	ESP	99.4134	77	0.4850	169.231	54.50	0.55
B	ESP	DOE 4	80	80	2.3	2.3	0.14	0.138	14,300	9.65	ESP	98.5493	80	2.2935	169.939	50.26	0.51
B	ESP	116	81	81	2.7	2.7	0.046	0.12	12,900	9.30	ESP	98.5066	81	1.0350	209.302	85.15	0.86
B	ESP	18	176	176	3.1	3.1	0.14	0.13	13,400	8.76	ESP	98.5569	170	3.3385	231.343	26.52	0.27
B	ESP	16 L	140	140	3.7	3.7	0.12	0.095	13,900	6.68	ESP	98.2568	140	4.6737	268.116	47.76	0.40
B	ESP	DOE 3	130	190	3.7	3.7	0.11	0.12	12,900	9.50	ESP	98.8175	130	3.3917	269.822	54.68	0.55
B	ESP	16	130	130	3.8	3.8	0.21	0.1	13,700	7.50	ESP	97.1230	130	7.9800	277.372	93.13	0.95
B	ESP	18	260	260	3.9	3.9	0.036	0.091	13,600	6.74	ESP	98.4659	260	1.5429	268.669	10.50	0.10
B	ESP	DOE 5	86	86	23	23	0.043	0.114	13,800	8.26	ESP	88.4785	86	8.5754	1666.67	94.84	0.96
B	FGDw	12	13	13	1.2	1.2	0.013	0.091	13,700	6.64	FGDw	99.8043	13	0.1714	87.591	85.16	0.85
B	FGDw	21	9.9	9.9	1.2	1.2	0.011	0.067	14,000	4.79	FGDw	99.7701	9.9	0.1970	85.714	86.45	0.89
B	FGDw	DOE 4	27	27	2.3	2.3	0.014	0.138	14,300	9.65	FGDw	99.8549	27	0.2333	169.939	93.21	0.96
B	FGDw	125	320	320	4	4	0.09	0.098	13,043	7.51	FGDw	98.8022	320	3.6735	306.875	-4.34	-0.04
B	FF	DOE 2 FF	56	56	0.9	0.9	0.011	0.12	13,000	9.23	FF	99.8592	56	0.0825	58.560	0.99	0.01
B	FF	18 HF	72	72	3.1	3.1	0.0019	0.13	13,400	9.70	FF	88.8804	72	0.0453	231.343	98.88	0.99
B	FGDd	14	0.55	0.55	1.2	1.2	0.0073	0.060	13,700	6.79	FGDd	99.8925	0.55	0.0942	87.591	99.57	0.99
S	ESP	11	3.8	3.8	0.67	0.67	0.023	0.062	11,900	5.21	ESP	99.5585	3.8	0.2465	58.303	99.25	0.94
S	ESP	22	0.053	0.053	0.78	0.78	0.0015	0.088	11,980	5.68	ESP	99.9736	0.053	0.0172	65.109	99.92	1.00
S	FGDw	11	0.55	0.55	0.67	0.67	0.0051	0.062	11,000	5.21	FGDw	99.8021	0.55	0.0551	66.303	98.86	0.99
S	FGDw	101	1.4	1.4	2.7	2.7	0.007	0.25	10,000	25.00	FGDw	99.9720	1.4	0.0756	270.000	99.46	1.00
S	FF	115	0.36	0.36	0.82	0.82	0.0019	0.112	12,565	8.91	FF	99.9767	0.36	0.0139	65.261	99.45	0.99
S	FF	DOE 8	3.2	3.2	0.88	0.88	0.009	0.112	11,700	9.57	FF	99.9060	3.2	0.0707	75.214	95.75	0.96
S	FF	101	2.9	2.9	2.7	2.7	0.021	0.25	10,000	25.00	FF	99.9160	2.9	0.2268	270.000	98.93	0.99
L	ESP	DOE 8	8.7	8.7	1.3	< 1.3	0.02	0.17	9,970	17.05	ESP	99.8827	8.7	0.1529	180.391	93.33	0.96
L	ESP	20	780	780	4.5	4.5	0.051	0.21	10,000	21.00	ESP	98.7571	780	1.0929	450.000	-71.33	-0.74
L	FGDw	DOE 5	8.3	8.3	1.3	< 1.3	0.0164	0.17	9,970	17.05	FGDw	99.9390	8.3	0.0795	180.391	99.53	0.99
L	FGDw	20	160	160	4.5	4.5	0.018	0.21	10,000	21.00	FGDw	99.9095	160	0.4071	450.000	64.44	0.85

		nl	nl/n	# points	Max nl/n	Min nl/n
	Averages					
	overall	38.9656	0.3917	84	0.9995	-0.4214
	bituminous	29.0791	0.2092	29	0.9948	-0.4214
	sub-bitum	97.9452	0.9805	7	0.9995	0.9366
	lignite	44.5184	0.4459	4	0.9369	-0.7351
	ESP	12.5633	0.1294	20	0.9995	-0.4214
	FGDw	76.1104	0.7620	8	0.9951	-0.0440
	FF	72.7974	0.7284	5	0.9947	0.0099
	FGDd	99.3721	0.9948	1	-	-
	ESP+FGDw	30.7911	0.3101	28		
	FF+FGDd	77.2255	0.7726	6		
bituminous coal						
	ESP	2.5084	0.0282	16	0.8534	-0.4214
	FGDw	83.1193	0.8323	4	0.8865	-0.0440
	FF	34.9337	0.3494	2	0.0099	0.0099
	FGDd	99.3721	0.9948	1	-	-
	ESP+FGDw	14.6296	0.1490	20		
	FF+FGDd	58.4131	0.5845	3		
subbituminous coal						
	ESP	98.5847	0.9860	2	0.9995	0.9366
	FGDw	99.1835	0.9923	2	0.9951	0.9894
	FF	98.0099	0.9810	3	0.9947	0.9584
	FGDd	-	-	0	-	-
	ESP+FGDw	97.8741	0.9802	4		
	FF+FGDd	99.0099	0.9910	3		
lignite coal						
	ESP	9.9972	0.0998	2	0.9944	-0.7351
	FGDw	79.0395	0.7910	2	0.9369	0.6450
	FF					
	FGDd					
	ESP+FGDw	44.5184	0.4459	4		
	FF+FGDd					
ESP						
	bitum	2.5084	0.0282	16		
	sub-bit	98.5847	0.9860	2		
	lig	9.9972	0.0998	2		
FGDw						
	bitum	83.1193	0.8323	4		
	sub-bit	99.1835	0.9923	2		
	lig	79.0395	0.7910	2		
FF						
	bitum	34.9337	0.3494	2		
	sub-bit	98.0099	0.9810	3		
	lig					
FGDd	bitum	99.3721	0.9948	1		
	sub-bit	-	-	0		
	lig					

Selenium (Se) 6/18/98
EPRI data
F-1: CI <DL set = avg of values < indicated (rank-specific) and EI < DI datasets NOT USED *REPEAT with all nl < 0 reset to nl = 0.*

Rank	Control Device	Unit ID	Modified EI (lb/TBtu)	Actual EI (lb/TBtu)	Modified CI (coal) (ppm)	Actual CI (coal) (ppm)	EIMain (lb/MBtu)	Ash	HHV (lb/MBtu)	FMgen (lb/MBtu)	Control Device	n	EI (lb/TBtu)	CIPMMe	CIPPM / *e^(1-n)*	n	n/n
B	ESP	110 B	46	46	0.57	0.57	0.022	0.081	11,900	7.85	ESP	99.7123	46	0.1378	47.899	3.96	0.04
B	ESP	DOE 2	62	62	0.57	< 0.6	0.019	0.12	12,900	9.30	ESP	99.7958	62	0.0903	44.786	0.00	0.00
B	ESP	114 R	150	150	0.735	< 1.1	0.016	0.089	13,300	8.89	ESP	99.7609	150	0.1321	55.263	0.00	0.00
B	ESP	114 B	240	240	0.735	< 1.2	0.025	0.087	13,500	8.44	ESP	99.6121	240	0.2112	54.444	0.00	0.00
B	ESP	12	48	48	1.9	1.9	0.1	0.094	13,700	8.86	ESP	96.5426	48	1.2766	87.591	45.20	0.48
B	ESP	122	70	70	1.6	1.6	0.12	0.093	13,370	8.96	ESP	98.2748	70	2.0645	119.671	41.51	0.42
B	ESP	110 L	130	130	2.1	2.1	0.041	0.083	12,450	8.88	ESP	99.4023	130	1.0373	173.554	25.10	0.25
B	ESP	15	77	77	2.2	2.2	0.028	0.127	13,000	9.77	ESP	99.7134	77	0.4860	169.231	54.60	0.55
B	ESP	DOE 4	80	80	2.3	2.3	0.14	0.138	14,300	9.65	ESP	98.5493	80	2.3333	160.839	50.26	0.51
B	ESP	118	31	31	2.7	2.7	0.046	0.12	12,900	9.30	ESP	99.6055	31	1.0050	209.302	65.19	0.66
B	ESP	18	170	170	3.1	3.1	0.14	0.13	13,400	9.70	ESP	98.5569	170	3.3985	231.343	25.52	0.27
B	ESP	18 L	140	140	3.7	3.7	0.12	0.095	13,850	6.88	ESP	98.2568	140	4.6737	269.116	47.73	0.48
B	ESP	DOE 3	130	130	3.7	3.7	0.11	0.12	12,900	9.30	ESP	98.8175	130	3.3917	288.822	54.68	0.55
B	ESP	16	130	130	3.8	3.8	0.21	0.1	13,750	7.30	ESP	97.1239	130	7.9800	277.372	53.13	0.55
B	ESP	19	260	260	3.9	3.9	0.016	0.091	13,530	6.74	ESP	99.4659	260	1.5423	288.683	10.00	0.10
B	ESP	DOE 5	86	86	20	20	0.043	0.114	13,850	8.26	ESP	99.4795	86	0.6754	1666.67	94.84	0.95
B	FGDw	12	13	13	1.2	1.2	0.013	0.091	13,750	6.62	FGDw	99.0043	13	0.1714	87.591	85.16	0.85
B	FGDw	21	9.9	9.9	1.2	1.2	0.011	0.087	14,000	4.79	FGDw	99.7701	9.9	0.1970	85.714	88.45	0.89
B	FGDw	DOE 4	27	27	2.3	2.3	0.014	0.138	14,300	9.65	FGDw	99.8549	27	0.2333	160.839	83.21	0.83
B	FGDw	125	320	320	4	4	0.09	0.098	13,043	7.51	FGDw	98.8022	320	3.6735	306.678	0.00	0.00
B	FF	DOE 2 FF	58	58	0.9	0.9	0.011	0.12	13,000	9.23	FF	99.8592	58	0.0826	58.560	0.00	0.01
B	FF	18 FF	72	72	3.1	3.1	0.0019	0.13	13,400	9.70	FF	99.9804	72	0.0453	231.343	98.88	0.99
B	FGDd	14	0.55	0.55	1.2	1.2	0.0073	0.093	13,700	6.79	FGDd	99.8825	0.55	0.0042	87.591	99.37	0.99
S	ESP	11	3.8	3.8	0.67	0.67	0.023	0.062	11,900	5.21	ESP	99.6586	3.8	0.2486	56.303	93.25	0.94
S	ESP	22	0.059	0.059	0.70	0.70	0.0015	0.066	11,480	5.68	ESP	99.9736	0.059	0.0172	65.109	99.92	1.00
S	FGDw	11	0.85	0.85	0.67	0.67	0.0051	0.062	11,900	5.21	FGDw	99.9021	0.85	0.0551	56.303	99.05	0.99
S	FGDw	101	1.4	1.4	2.7	2.7	0.007	0.26	10,000	25.00	FGDw	99.9720	1.4	0.0758	270.000	99.46	1.00
S	FF	115	0.36	0.36	0.82	0.82	0.0019	0.112	12,565	6.91	FF	99.9787	0.36	0.0139	65.261	99.45	0.99
S	FF	DOE 6	3.2	3.2	0.88	0.88	0.009	0.112	11,700	9.57	FF	99.9060	3.2	0.0707	75.214	95.76	0.96
S	FF	101	2.9	2.9	2.7	2.7	0.021	0.25	10,000	25.00	FF	99.9160	2.9	0.2288	270.000	99.93	0.99
L	ESP	DOE 6	8.7	8.7	1.9	< 1.3	0.02	0.17	9,970	17.05	ESP	99.8827	8.7	0.1528	130.391	93.39	0.93
L	ESP	20	780	780	4.6	4.6	0.051	0.21	10,000	21.00	ESP	99.7571	780	1.0929	450.000	0.00	0.00
L	FGDw	DOE 6	8.3	8.3	1.9	< 1.3	0.0104	0.17	9,970	17.05	FGDw	99.9390	8.3	0.0785	130.391	93.63	0.94
L	FGDw	20	160	160	4.5	4.5	0.019	0.21	10,000	21.00	FGDw	99.9096	160	0.4071	450.000	64.44	0.65

		nl	n/n	# points	*Max* n/n	*Min* n/n
	Averages					
	overall	57.5220	0.5777	34	0.9985	0.0000
	bituminous	44.2924	0.4462	23	0.9948	0.0000
	sub-bitum	97.9452	0.9805	7	0.9995	0.9866
	lignite	62.8517	0.6291	4	0.9769	0.0000
	ESP	43.9580	0.4433	20	0.9995	0.0000
	FGDw	75.8631	0.7674	8	0.9951	0.0000
	FF	72.7074	0.7284	5	0.9947	0.0099
	FGDd	99.3721	0.9948	1	-	-
	ESP+FGDw	53.2996	0.5359	28		
	FF+FGDd	77.2265	0.7728	6		
bituminous coal						
	ESP	37.0410	0.3747	10	0.9534	0.0000
	FGDw	84.2053	0.8433	4	0.8885	0.0000
	FF	34.9337	0.3494	2	0.6889	0.0099
	FGDd	99.3721	0.9948	1	-	-
	ESP+FGDw	42.4742	0.4284	20		
	FF+FGDd	58.4131	0.5845	3		
subbituminous coal						
	ESP	96.5047	0.9600	2	0.9965	0.9356
	FGDw	99.1835	0.9923	2	0.9951	0.9894
	FF	98.0399	0.9810	3	0.9947	0.9584
	FGDd	-	-	0	-	-
	ESP+FGDw	97.8741	0.9802	4		
	FF+FGDd	98.0999	0.9810	3		
lignite coal						
	ESP	46.6630	0.4672	2	0.9344	0.0000
	FGDw	79.0095	0.7910	2	0.9869	0.6450
	FF					
	FGDd					
	ESP+FGDw	62.8617	0.6291	4		
	FF+FGDd					
ESP						
	bitum	37.0410	0.3747	10		
	sub-bit	96.5047	0.9600	2		
	lig	46.6630	0.4672	2		
FGDw						
	bitum	84.2053	0.8433	4		
	sub-bit	99.1835	0.9923	2		
	lig	79.0095	0.7910	2		
FF						
	bitum	34.9337	0.3494	2		
	sub-bit	98.0399	0.9810	3		
	lig					
FGDd	bitum	99.3721	0.9948	1		
	sub-bit	-	-	0		
	lig					